



UNIVERSITÀ
DEGLI STUDI
DI PADOVA

Sede Amministrativa: Università degli Studi di Padova

Dipartimento di Scienze Chimiche

CORSO DI DOTTORATO DI RICERCA IN: SCIENZE MOLECOLARI

CURRICULO: SCIENZE CHIMICHE

CICLO XXXI

**APPROCCI ELETTROCHIMICI ALLA
POLIMERIZZAZIONE RADICALICA PER
TRASFERIMENTO DI ATOMO MEDIATA
ELETTROCHIMICAMENTE**

**ELECTROCHEMICAL APPROACHES TO ATOM
TRANSFER RADICAL POLYMERIZATION**

Tesi redatta con il contributo finanziario della Fondazione Cariparo

Coordinatore: Ch.mo Prof. Leonard Jan Prins

Supervisore: Ch.mo Prof. Armando Gennaro

Dottorando: Francesco De Bon

Contents

| | |
|--|-------------|
| Glossary of Acronyms..... | I |
| Riassunto | IV |
| Abstract | VIII |
| Chapter 1 – Atom Transfer Radical Polymerization..... | 1 |
| 1.1 General features of an RDRP..... | 2 |
| 1.2 Atom Transfer Radical Polymerization (ATRP)..... | 3 |
| 1.2.1 The mechanism of ATRP..... | 4 |
| 1.2.2 ISET vs. OSET..... | 5 |
| 1.2.3 ATRP catalytic systems..... | 6 |
| 1.3 ATRP with low catalyst loadings..... | 8 |
| 1.4 Electrochemically mediated ATRP..... | 9 |
| 1.5 Scope and organization of the PhD Thesis..... | 11 |
| References..... | 13 |
| Chapter 2 – Electrochemical characterization of common catalyst and initiators for Atom Transfer Radical Polymerization in [BMIm][OTf]..... | 15 |
| 2.1 Introduction..... | 15 |
| 2.2. Redox properties of copper complexes..... | 16 |
| 2.3 Electroreduction of initiators..... | 18 |
| 2.4 Kinetic of RX activation by $[\text{Cu}^{\text{I}}\text{TPMA}]^+$ | 20 |
| 2.5 Conclusions..... | 22 |
| References..... | 23 |
| Chapter 3 – Electrochemically mediated ATRP of methyl acrylate in [BMIm][OTf]..... | 25 |
| 3.1 Introduction..... | 25 |
| 3.2 Preliminary electrochemical characterization of the catalytic system..... | 27 |
| 3.2.1 Effect of applied potential..... | 29 |
| 3.2.2 Effect of temperature..... | 32 |

| | |
|---|----|
| 3.2.3 Galvanostatic <i>e</i> ATRP..... | 34 |
| 3.2.4 Effect of degree of polymerization and catalyst loading..... | 36 |
| 3.2.5 Livingness of the polymerization: electrochemical switch..... | 38 |
| 3.2.6 Retention of C-Br end-functionality: chain extension..... | 39 |
| 3.2.7 Recycling of IL and catalyst..... | 46 |
| 3.3 Conclusions..... | 48 |
| References..... | 49 |

Chapter 4. Electrochemically mediated ATRP for the preparation of block copolymers: from traditional approaches to catalytic halogen exchange.....52

| | |
|---|----|
| 4.1 Introduction..... | 52 |
| 4.1.1 The traditional route of synthesis: from PAN-Br to block copolymers..... | 56 |
| 4.1.1 Electrochemical characterization of $[\text{Cu}^{\text{II}}\text{TPMA}]^{2+}$ and $[\text{XCu}^{\text{II}}\text{TPMA}]^+$ | 57 |
| 4.1.2 Electrochemically mediated ATRP of acrylonitrile..... | 59 |
| 4.1.3 Preparation of PAN- <i>b</i> -PBA copolymer by <i>e</i> ATRP..... | 66 |
| 4.2 Catalytic Halogen Exchange for the preparation of well-defined block copolymers..... | 69 |
| 4.2.1 Electrochemistry of Catalytic Halogen Exchange for PBA-Br chain extension with AN..... | 69 |
| 4.2.2 Synthesis of other macronitiator by <i>e</i> ATRP..... | 73 |
| 4.2.3 Chain extension by <i>e</i> ATRP..... | 74 |
| 4.2.4 Catalytic Halogen Exchange <i>via</i> SARA ATRP..... | 77 |
| 4.2.5 Chain extension <i>via</i> SARA ATRP..... | 78 |
| 4.3 Conclusions..... | 81 |
| References..... | 82 |

Chapter 5. Electrochemically mediated ATRP of methyl methacrylate in [BMIm][OTf] and ethanol.....86

| | |
|---|----|
| 5.1 Introduction..... | 86 |
| 5.2 Switching from acrylates to methacrylates: the problem of the penultimate effect..... | 87 |
| 5.3 <i>e</i> ATRP of methyl methacrylate in [BMIm][OTf] using EBiB as initiator..... | 88 |
| 5.4 <i>e</i> ATRP of MMA in [BMIm][OTf] using BPN as initiator..... | 90 |

| | |
|--|-----|
| 5.5 Catalytic Halogen Exchange: from mechanism to more controlled polymerizations..... | 92 |
| 5.6 <i>e</i> ATRP of MMA catalyzed by [Cu ^{II} PMDETA] ²⁺ in [BMIm][OTf] | 95 |
| 5.7 From a green ionic solvent to a green molecular solvent: <i>e</i> ATRP of MMA in ethanol | 97 |
| 5.8 Tacticity..... | 98 |
| 5.9 Conclusions..... | 100 |
| References..... | 101 |

Chapter 6 – Electrochemically mediated ATRP in Ionic Liquid – Water

| | |
|--|------------|
| mixtures: green horizon in polymer synthesis | 102 |
| 6.1 Introduction | 102 |
| 6.2 The role of water in ATRP | 104 |
| 6.3 From enemies to allies | 105 |
| 6.4 Money in our head but not in our heart | 106 |
| 6.5 The choice of catalyst and monomers | 108 |
| 6.6 Electrochemical characterizations..... | 108 |
| 6.7 Electrochemically mediated ATRP in [BMIm][OTf]/H ₂ O mixtures..... | 110 |
| 6.8 Electrochemically mediated ATRP of methyl acrylate in mixture of traditional solvents and water..... | 113 |
| 6.9 Electrochemically mediated aqueous ATRP of hydrophobic monomers..... | 118 |
| 6.10 Conclusions..... | 122 |
| References..... | 123 |

Chapter 7 – From Ionic Liquids to poly(Ionic Liquids).....124

| | |
|---|-----|
| 7.1 Introduction..... | 124 |
| 7.1.1 Tunable ionic conductivity..... | 124 |
| 7.1.2 Glass Transition Temperature..... | 125 |
| 7.1.3 Polymer architecture..... | 125 |
| 7.1.4 Molecular weight..... | 126 |
| 7.1.5 Aqueous solubility..... | 126 |
| 7.1.6 Thermal stability..... | 127 |
| 7.1.7 Chemical and electrochemical stability..... | 127 |
| 7.2 Synthesis of poly(ionic liquids)..... | 128 |

| | |
|--|-----|
| 7.2.1 Synthesis and properties of methacrylate-based ILMs..... | 128 |
| 7.3 Investigation of the catalytic system..... | 131 |
| 7.4 Electrochemically mediated ATRP of [MIm][Meth]..... | 133 |
| 7.4.1 Effect of type of halide ion (Br ⁻ , Cl ⁻)..... | 133 |
| 7.4.2 pH effect..... | 134 |
| 7.4.3 Modulating the polymerization rate by tuning E_{app} and temperature | 137 |
| 7.4.4 Effect of targeted degree of polymerization (DP) | 139 |
| 7.4.5 Effect of monomer amount..... | 140 |
| 7.5 Electrochemically mediated ATRP of other ILMs..... | 141 |
| 7.6 SARA ATRP of methacrylate-based ILMs..... | 143 |
| 7.8 <i>e</i> ATRP of polyanionic ionic liquids..... | 145 |
| 7.10 Conclusions..... | 146 |
| References..... | 147 |

Chapter 8 – Electrochemically mediated Atom Transfer Radical Polymerization in a stainless-steel reactor.....150

| | |
|--|-----|
| 8.1 Introduction..... | 150 |
| 8.2 Preliminary electrochemistry and <i>e</i> ATRP..... | 151 |
| 8.3 The choice of an SS304 reactor..... | 155 |
| 8.4 Blank experiments without any applied current..... | 157 |
| 8.5 Effect of the electrolysis program..... | 158 |
| 8.6 Effect of [Cu ^I TREN] ²⁺ loadings..... | 161 |
| 8.7 Effect of solvent..... | 163 |
| 8.8 Chain extension..... | 164 |
| 8.9 ICP-MS analysis of the polymerization mixture | 166 |
| 8.10 <i>e</i> ATRP of other monomers in the reactor..... | 166 |
| 8.11 Toward the scale-up..... | 168 |
| 8.12 Conclusions..... | 171 |
| References | 171 |

Chapter 9 – Electrochemically mediated Atom Transfer Radical Polymerization of vinyl chloride.....173

| | |
|---|-----|
| 9.1 Introduction..... | 173 |
| 9.1.1 Vinyl Chloride monomer..... | 174 |
| 9.1.2 PVC polymer: the need for controlled polymerizations..... | 174 |

| | |
|--|-----|
| 9.1.3 SARA ATRP vs. SET-LRP: (never)ending controversy?..... | 175 |
| 9.1.4 SARA ATRP of vinyl chloride..... | 176 |
| 9.2 Toward <i>e</i> ATRP of vinyl chloride..... | 177 |
| 9.2.1 Kinetics of [Cu ^I TREN] ⁺ disproportionation and activation..... | 177 |
| 9.2.2 Blank tests of SARA ATRP of VC in SS304 reactor..... | 183 |
| 9.2.3 Modeling of electrolysis programs..... | 184 |
| 9.3 Electrochemically mediated ATRP of vinyl chloride..... | 186 |
| 9.4 Livingness of the polymerization: chain extension with methyl acrylate..... | 190 |
| 9.5 A comparison between SARA ATRP and <i>e</i> ATRP: synthesis of 4-arms star PVC | 194 |
| 9.5 Conclusions..... | 196 |
| References..... | 197 |

| | |
|--|------------|
| Conclusions and future perspectives | 200 |
|--|------------|

| | |
|------------------------|----------|
| Appendix A..... | I |
|------------------------|----------|

| | |
|------------------------|------------|
| Appendix B..... | VII |
|------------------------|------------|

Glossary of Acronyms

| | |
|------------------------|---|
| AN | Acrylonitrile |
| ARGET | Activator regenerated by electron transfer |
| ATRP | Atom transfer radical polymerization |
| B3 | Vitamin B3 |
| BA | Butyl Acrylate |
| BAN | Bromoacetonitrile |
| BB | Benzyl bromide |
| BC | Benzyl chloride |
| BCP | Block Copolymer(s) |
| BMI_m | 1-butyl-3-methylimidazolium |
| BPN | 2-bromopropionitrile |
| CAN | Chloroacetonitrile |
| cHE | Catalytic Halogen Exchange |
| CPN | Chloropropionitrile |
| CRP | Controlled radical polymerization |
| CTNC | Copolymer-templated nitrogen-enriched porous nanocarbons |
| CV | Cyclic voltammetry |
| <i>D</i> | Molecular weight dispersity (M_w/M_n) |
| DCPA | Dichloropropionic acid |
| DET | Dissociative electron transfer |
| DMF | Dimethylformamide |
| DMSO | Dimethyl sulfoxide |
| DP | Degree of polymerization (targeted) |
| DT | Degenerative transfer |
| <i>e</i>ATRP | Electrochemically mediated atom transfer radical polymerization |
| EBiB | Ethyl α -bromoisobutyrate |
| EBPA | α -bromophenylacetate |
| ECPA | α -chlorophenylacetate |
| En | ethylenediamine |
| ET | Electron transfer |
| EBA | Ethyl bromoacetate |

| | |
|---------------------------|--|
| ECA | Ethyl chloroacetate |
| Fc | Ferrocene |
| FRC | Free radical copolymerization |
| FRP | Free radical polymerization |
| GC | Glassy carbon electrode |
| HE | Halogen Exchange |
| ICAR | Initiators for continuous activator regeneration |
| ILM | Ionic Liquid Monomer(s) |
| ISET | Inner-sphere electron transfer |
| LCST | Lower Critical Solubility Temperature |
| LRP | Living Radical Polymerization |
| M | Monomer |
| MA | Methyl acrylate |
| MAA | Methacrylic acid |
| MBP | Methyl 2-bromopropionate |
| MCP | Methyl 2-chloropropionate |
| Me₆TREN | Tris[2-(dimethylamino)ethyl]amine |
| MIm | Methylimidazole |
| MMA | Methyl methacrylate |
| M_n | Number average molecular weight |
| M_w | Weight average molecular weight |
| MW | Molecular weight |
| NMP | Nitroxide mediated polymerization |
| OEOMA | Oligoethylene oxide methyl ether methacrylate |
| OMRP | Organometallic mediated radical polymerization |
| OSET | Outer-sphere electron transfer |
| OTf | Trifluoromethanesulfonate |
| PAN | poly(acrylonitrile) |
| PEB | 1-phenylethyl bromide |
| PEC | 1-phenylethyl chloride |
| PBA | Poly(butyl acrylate) |
| PIL | Poly(ionic liquid) |

PMA Poly(methyl acrylate)
PMDETA N,N,N',N',N''-Pentamethyldiethylenetriamine
PMMA Poly(methyl methacrylate)
PSty Polystyrene
PVC Poly(vinyl chloride)
PRE Persistent radical effect
RAFT Reversible addition fragmentation chain transfer polymerization
RDRP Reversible deactivation radical polymerization
RDE Rotating disk electrode
RP Radical polymerization
 R_p Rate of polymerization
RX Organic halide (ATRP initiator)
SARA Supplemental activator and reducing agent
SCE Saturated calomel electrode
SET Single electron transfer
SFRP Stable free-radical polymerization
SRP Standard reduction potential
SS304 Stainless steel 304
Sty Styrene
TEA Triethylamine
TEMPO 2,2,6,6-tetramethylpiperidiny-1-nitroxide
TFSI Trifluoromethanesulfonyl imide
 T_g Temperature of glass transition
TGA Thermogravimetric analysis
TPMA Tris-[(2-pyridyl)methyl]amine
TREN Tris(2-aminoethyl)amine
Vis-NIR Visible – Near-infrared
UV-Vis Ultraviolet – Visible
VC Vinyl Chloride

Riassunto

Le polimerizzazioni radicaliche controllate (CRP) sono riconosciute come i metodi più potenti per ottenere polimeri con struttura macromolecolare ben definita e alto valore commerciale. La polimerizzazione radicalica a trasferimento atomico (ATRP) è probabilmente la CRP più utilizzata, in accademia e industria, grazie alla sua versatilità e semplicità. Nell'ATRP, un complesso metallico a basso stato di ossidazione, $Mt^I L_m$ (tipicamente un sistema rame-ammina, $[Cu^I L]^+$) reagisce con una catena polimerica dormiente P_n-X (dove $X = Cl, Br$) per produrre radicali $P_n\cdot$. Questi propagando nel bulk della soluzione, crescono aggiungendo unità monomeriche. In questo processo, il complesso di rame viene ossidato e si lega a X^- , generando la specie disattivante $[X-Cu^{II} L]^+$, che intrappola la specie propagante. L'equilibrio di ATRP è fortemente spostato verso la specie dormiente P_n-X , cosicché la concentrazione di radicali sia molto bassa e la probabilità di eventi di terminazione bimolecolare sia ridotta al minimo. La crescita inizia praticamente allo stesso tempo per tutte le catene grazie a iniziatori (alogenuro alchilico) molto efficienti (RX). In tali condizioni, la crescita delle catene è omogenea ed è possibile ottenere polimeri con peso molecolare predeterminato, distribuzione stretta dei pesi molecolari e alta ritenzione della funzionalità di fine catena. L'ATRP consente di costruire dunque macromolecole con specifiche composizioni, architetture e posizionamento dei gruppi funzionali.

Lo scopo di questa tesi è di contribuire alla comprensione e allo sviluppo dell'ATRP catalizzata da complessi di rame, utilizzando metodi elettrochimici sia come strumenti analitici che come strumenti per eseguire e controllare la polimerizzazione. Il lavoro si è concentrato sulla diffusione dell'uso di tali sistemi per controllare in modo efficiente la polimerizzazione di una serie di monomeri rilevanti. I sistemi investigati per ATRP possono essere considerati anche "green" per diversi motivi: (i) la maggior parte del lavoro riguarda lo studio e lo sviluppo della reazione in solventi *green*, generalmente caratterizzati da un'elevata attività catalitica; (ii) i metodi elettrochimici per la rigenerazione del catalizzatore (ATRP mediata elettrochimicamente, *e*ATRP) permette la polimerizzazione con limitata quantità di complessi di rame; (iii) i liquidi ionici, una nuova classe di solventi non infiammabili e facilmente riciclabili, sono stati esplorati come potenziali

solventi per *e*ATRP; (iv) il meccanismo di *halogen exchange* catalitico (*c*HE) è stato studiato e sviluppato, facilitando la sintesi di copolimeri a blocchi.

I catalizzatori ATRP sono stati studiati nel liquido ionico 1-butil-3-metilimidazolio triflato. Sia la speciazione che la reattività di Cu/L sono risultate in linea per un processo di polimerizzazione ben controllato. Le polimerizzazioni sono state condotte con la (ri)generazione elettrochimica del complesso attivo $[\text{Cu}^{\text{I}}\text{L}]^+$ (*e*ATRP). L'*e*ATRP del metil acrilato è stata studiata in dettaglio variando una serie di parametri come: potenziale applicato, temperatura, grado di polimerizzazione e carico di catalizzatore di Cu/TPMA (TPMA = tris(2-piridilmetil)ammina). Un interruttore elettrochimico e l'estensione della catena con acrilonitrile (grazie al meccanismo di *halogen exchange* catalitico) hanno dimostrato la presenza della funzionalità di fine catena. Le polimerizzazioni ottenute tramite liquido ionico riciclato hanno dimostrato che *e*ATRP tollera bene anche un solvente riciclato.

I copolimeri a blocchi (BCP) hanno rilevanza in una vasta gamma di applicazioni nella vita di tutti i giorni. BCP di acrilonitrile (AN) e butil acrilato (BA) sono stati studiati come precursori di carbonio mesoporoso. Pertanto, *e*ATRP di acrilonitrile è stata introdotta e studiata nei diversi aspetti, come: effetto del potenziale applicato, del grado di polimerizzazione, della natura di C-X e della struttura dell'iniziatore. Un macroiniziatore di PAN è stato quindi esteso con BA per formare il copolimero PAN-*b*-PBA come precursore del carbonio mesoporoso. I BCP possono essere ottenuti anche via *c*HE, evitando così le procedure di purificazione e la differenza di reattività quando si passa da un monomero meno reattivo a uno più reattivo.

Il *c*HE si è dimostrato strumento efficace di polimerizzazione sia da SARA che da *e*ATRP, in una gamma di solventi incluso DMSO e acqua. Il metil metacrilato (MMA) è stato polimerizzato grazie al *c*HE in liquido ionico ed etanolo, per risolvere il problema dell'effetto del penultimo. La messa a punto delle condizioni di elettrolisi ha permesso di ottenere PMMA a bassa dispersione. Ulteriori miglioramenti sono stati ottenuti utilizzando $[\text{Cu}^{\text{II}}\text{PMDETA}]^{2+}$ come catalizzatore come alternativa economica ed efficiente a Cu/TPMA. L'analisi della tatticità del

PMMA ottenuta in [BMIm][OTf] e l'etanolo ha confermato la scarsa capacità del solvente ionico di indurre stereocontrollo durante la polimerizzazione.

I complessi piridinici, come Cu/TPMA, stabili fino a condizioni molto acide (pH ~1) hanno permesso di ottenere poli(liquidi ionici). Hanno aperto infatti una nuova strada per la polimerizzazione di monomeri liquidi ionici, una classe di molecole che può dare una pleora di nuovi materiali polimerizzati mediante ATRP. La ragione principale che impedisce l'ATRP di ILM è una reazione di ciclizzazione che coinvolge l'estremità della catena, con l'alogeno terminale come gruppo uscente, come nel caso dell'acido metacrilico. Le stesse tre strategie usate per l'acido metacrilico hanno permesso di migliorare drasticamente la conversione e il controllo sulla polimerizzazione di ILM: (i) usando la funzionalità di fine catena C-Cl, che è molto più stabile di C-Br; (ii) abbassando il pH per convertire completamente gli ioni carbossilato liberi in acido carbossilico, che è un nucleofilo molto più debole; (iii) migliorare la velocità di polimerizzazione per evitare il contributo negativo della reazione di ciclizzazione. Tali condizioni hanno permesso la sintesi di poli(liquidi ionici) (PIL) ben controllati ad alto peso molecolare fino a grado di polimerizzazione 1000. Un semplice iniziatore organico (poli)alogenato come acido 2,2-dicloropropionico è stato utilizzato per produrre un PIL lineare telechelico.

L'insieme di questi risultati può consentire una più facile implementazione e scalabilità industriale dell'*e*ATRP. Per questo motivo, è stato deciso di studiare l'*e*ATRP del cloruro di vinile, considerata finora impossibile. La polimerizzazione, effettuata in un reattore elettrochimico resistente alla pressione, è controllata, veloce e con una conversione buona in tempi ragionevoli. Oltre al classico PVC lineare, è stato anche sintetizzato un PVC a stella, evidenziando la flessibilità dell'*e*ATRP. Nell'architettura a stella, la polimerizzazione elettrochimica si è dimostrata di gran lunga superiore a quella chimica (SARA ATRP). Il successo di questa polimerizzazione ha smentito il meccanismo SET-LRP e le sue assunzioni.

Una delle proprietà dell'*e*ATRP è la tolleranza al materiale catodico utilizzato per la rigenerazione di $[Cu^I L]^+$. Si è deciso dunque di studiare la polimerizzazione di

un acrilato usando la superficie del reattore esposto alla miscela di polimerizzazione come elettrodo. In questo modo il reattore ha la duplice funzione di elettrodo e luogo fisico in cui avviene la reazione. I risultati hanno mostrato che la polimerizzazione è veloce e controllata, raggiungendo conversioni elevate in breve tempo. Inoltre, l'assenza di rilascio di ioni metallici durante la reazione (Fe, Ni, Cr) da parte dell'acciaio conferma che la polimerizzazione avviene elettrochimicamente, l'acciaio agisce solo come un serbatoio di elettroni e non è chimicamente coinvolto. Una tale impostazione elettrochimica, semplice ed economica, può rendere l'eATRP una tecnica commerciale a breve termine e aprire nuove prospettive economiche.

Abstract

Controlled radical polymerizations (CRPs) are among the most powerful methods to obtain polymers with well-defined properties and high commercial value. Atom transfer radical polymerization (ATRP) is probably the most widely used CRP, in academia and industry, thanks to its versatility and simplicity. In ATRP, a metal complex in a low oxidation state, Mt^zL_m (typically a copper-amine system, $[Cu^I L]^+$) reacts with a dormant polymeric chain P_n-X (where $X = Cl, Br$) to produce radicals P_n^\bullet that can propagate, in the bulk of the solution, by addition to monomer units. In this reaction, the copper complex is oxidized and binds to X^- , generating the deactivating species $[X-Cu^{II}L]^+$, which traps the propagating species. ATRP equilibrium is shifted towards the dormant species P_n-X , so that P_n^\bullet concentration is very low, and the probability of radical-radical termination events is minimized. Growth of all chains begins virtually at the same time, thanks to the use of alkyl halide (RX) initiators that are more reactive than the dormant species, P_n-X . In such conditions, chain growth is homogenous, and it is possible to obtain polymers with predetermined molecular weight, narrow molecular-weight distribution and high chain-end fidelity. ATRP allows to tailor macromolecules with specific compositions, architectures and position of functional groups.

The aim of this thesis is to contribute to both the understanding and development of ATRP catalyzed by copper complexes, using electrochemical methods as equally analytical tools and efficient means of triggering and controlling the polymerization. The work focused on spreading the use of such systems to efficiently control the polymerization of a series of important monomers. Moreover, the investigated ATRP systems can be considered also “green” for several reasons: (i) most of the work regards the study and development of the reaction in green solvents in which copper complexes generally have high catalytic activity; (ii) electrochemical methods for catalyst regeneration (electrochemically mediated ATRP, *e*ATRP) allowed triggering the polymerization with low loadings of copper complexes; (iii) ionic liquids, a class of non-flammable and easily recyclable solvents, were explored as potential media

for *e*ATRP; (iv) the mechanism of catalytic halogen exchange was investigated and defined, abridging the synthesis of block copolymers.

ATRP catalysts were investigated in the ionic liquid 1-butyl-3-methylimidazolium triflate ([BMIm][OTf]). Both Cu/L speciation and reactivity were found to be suitable for a well-controlled polymerization process. Polymerizations were conducted with electrochemical (re)generation of the active $[\text{Cu}^{\text{I}}\text{L}]^+$ complex (*e*ATRP). *e*ATRP of methyl acrylate was investigated in detail by varying a series of parameters such as applied potential, temperature, degree of polymerization and catalyst load ($[\text{Cu}^{\text{II}}\text{TPMA}]^{2+}$, TPMA = tris(2-pyridylmethyl)amine). Application of an electrochemical switch and chain extension with acrylonitrile via catalytic halogen exchange (*c*HE) proved the livingness of the polymerizations. Experiments triggered in recycled ionic liquid proved that *e*ATRP tolerates well the recycled solvent; polymerizations exhibited good control and high conversion.

Block copolymers (BCP) have relevance in a vast range of applications in everyday life. BCP of acrylonitrile (AN) and butyl acrylate (BA) were investigated as precursors for mesoporous carbons. Thus, *e*ATRP of acrylonitrile was studied considering several aspects, including the effect of applied potential, degree of polymerization, C-X nature and initiator structure. A macroinitiator of PAN was then extended with BA to form PAN-*b*-PBA copolymer as a precursor for mesoporous carbons. BCP can be obtained also by extension of a PBA chain with AN via *c*HE, thus avoiding purification procedures and reactivity mismatch when crossing from a less reactive monomer to a more reactive one.

*c*HE was proved to be an efficient tool of polymerization by both SARA and *e*ATRP, in a range of solvents, including water. Methyl methacrylate (MMA) was polymerized thanks to *c*HE in [BMIm][OTf] and ethanol, to solve the issue of penultimate effect. Fine tuning of the electrolysis conditions afforded PMMA with low dispersion. Further improvements were obtained by using $[\text{Cu}^{\text{II}}\text{PMDETA}]^{2+}$ as an inexpensive and efficient catalyst in alternative to $[\text{Cu}^{\text{II}}\text{TPMA}]^{2+}$. Tacticity analysis of PMMA obtained in [BMIm][OTf] and ethanol confirmed the poor ability of the ionic solvent to induce stereocontrol to the polymerization.

Pyridinic complexes such as $[\text{Cu}^{\text{II}}\text{TPMA}]^{2+}$ are stable in very acid conditions ($\text{pH} = 1$). This allowed unprecedented control over conditions of macromolecular growth in water. In addition, it opened a new avenue for the polymerization of ionic liquid monomers (ILMs), a class of building blocks that can give a plethora of new materials. The main reason preventing ATRP of ILM is a cyclization reaction involving the chain-end with the terminal halogen as a leaving group, as in the case of methacrylic acid. Application of three strategies previously developed for ATRP of methacrylic acid allowed to dramatically improve conversion and control over ILMs polymerization. (i) Using C-Cl chain end functionality, which is much more stable than C-Br, (ii) lowering further the pH to completely convert free carboxylate ions to carboxylic acid, which is a much weaker nucleophile, and (iii) enhancing the polymerization rate to avoid the negative contribution of the cyclization side reaction, allowed synthesis of well-controlled high molecular weight poly(ionic liquids), PILs, with degree of polymerization > 500 . A simple (poly)halogenated organic initiator such as 2,2-dichloropropionic acid was used to produce linear homotelechelic PILs.

Electrochemically mediated ATRP allowed exceptional control over Cu^{I} (re)generation. For this reason, it was decided to study the *e*ATRP of vinyl chloride, which was considered impossible until now. The polymerization, triggered in a pressure-resistant electrochemical reactor, was controlled, fast and afforded an acceptable conversion. In addition to linear PVC, a star PVC was also synthesized, highlighting the flexibility of *e*ATRP. In the star architecture, the electrochemical polymerization was by far superior to the chemical one (SARA ATRP). The success of this polymerization has categorically denied the SET-LRP mechanism and its assumptions.

One of the crucial properties of electrochemical *e*ATRP is the inert role played by the cathode material used for the regeneration of $[\text{Cu}^{\text{I}}\text{L}]^+$. Any electrode material with good stability in the reaction medium can be used as a cathode. It was therefore decided to study the polymerization of an acrylate using the surface of a stainless steel (SS304) reactor exposed to the polymerization mixture as a cathode. In this way, the reactor has the dual function of electrode and place where the reaction takes place. The results showed that polymerization is fast,

controlled and reaches high conversions. Moreover, the absence of release of metal ions during the reaction (Fe, Ni, Cr) confirmed that the polymerization takes place via electrochemical reduction of Cu^{II} to Cu^{I} , while SS304 acts only as an electron reservoir, not chemically involved in ATRP activation. Such simple and cheap electrochemical setup can make the scale-up of the *e*ATRP a reality in the short term and open new economic prospects.

Chapter 1

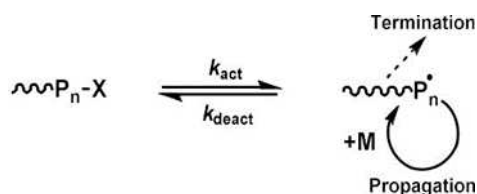
Atom Transfer Radical Polymerization

Most of the plastic commodities used worldwide are produced by free radical polymerization (FRP), a polymerization in which the chain carriers are radicals (*i.e.* the growing chain-end bears an unpaired electron). The commercial success of FRP can be attributed to the large variety of polymerizable monomers and their combination through copolymerization. The range of monomers is larger for FRP than for any other chain polymerization because radicals are tolerant to many functional groups, including acidic, hydroxyl and amino groups. FRP is not affected by water and other protic impurities and can be carried out in various media, e.g., bulk, solution, aqueous suspension, emulsion, dispersion, etc. Moreover, reaction conditions are mild (typically from room temperature to 100 °C, atmospheric pressure to 5 bar) and requirements for purification of solvents, monomers and products are minimal, making FRP a straightforward and effective synthetic technique.¹ On the other hand, radicals are extremely reactive species; therefore, unavoidable chain transfer and radical termination reactions dominate FRP, prohibiting precise tailoring of molecular structures. The inadequate level of control over chain growth has limited the application of materials prepared by FRP as commodity plastics, rubbers and fibers. In contrast, living polymerization processes (e.g. cationic and anionic polymerizations) allow finely designing macromolecular architectures. In contrast to ionic reactions, in which cations or anions do not react *via* bimolecular termination, organic radicals are short-lived species that terminate with a diffusion-controlled rate through disproportionation or coupling reactions. To achieve regular, high molecular weight polymers, terminations must be minimized. This implies that the rate of radical generation must be controlled. Since 1990s, several controlled reversible-deactivation radical polymerizations (RDRPs) have been developed, which allowed preparation of polymers with unprecedented regular, complex and predetermined design and composition. This family of polymerization techniques is often called controlled radical polymerization (CRP).²

In this chapter, we wish to focus on the characteristics of the most widely used RDRP technique: Atom Transfer Radical Polymerization (ATRP).

1.1 General features of an RDRP

FRP is dominated by the kinetics of radical chain transfer and termination. RDRP is instead governed through a fast, reversible activation-deactivation equilibrium, which dramatically enhances the lifetime of the radicals (Scheme 1.1). This equilibrium is the fundamental difference between RDRP and FRP; it is strongly shifted to the left ($k_{\text{act}}/k_{\text{deact}} \ll 1$) so that it drastically reduces the concentration of radicals, reducing the probability of termination reactions. Ideally, a propagating radical should react with a limited number of monomer units before going back to the dormant state. This equilibrium should be fast enough (both high k_{act} and k_{deact}) to ensure that all chains grow at same rate. Lifetime of radicals in FRP is in the order of magnitude of one second, implying the impossibility of any external control during such a short time. However, in RDRP periods of ~ 1 min of non-activity after each ~ 1 ms of activity, extend the lifetime of propagation from ~ 1 s to > 1 day. This is achieved with continuous alternation of reversible activation and deactivation steps.



Scheme 1.1. A schematic representation of the equilibrium between dormant and active species in RDRP. Note that the true equilibrium involves other species, omitted here for simplicity, and differs for various RDRP techniques.³

In RDRP, the amount of terminated chains drops from $\sim 100\%$ to less than 10% . Despite this, termination cannot be avoided completely; hence, RDRP is not “living” like anionic polymerizations. Nevertheless, control is often so high that controlled radical polymerizations generally exhibit the behavior of a living polymerization.

CRPs exhibit a linear increase of molecular weight with monomer conversion because all chain-ends are growing at essentially the same rate. This was

demonstrated by Gold,⁴ who showed that even if the rate of propagation is some orders of magnitude higher than that of initiation, living polymerization affords polymers with very narrow molecular weight distributions. Distributions are quantified by determining the dispersion of the molecular weight, $D = M_w/M_n$, where M_w is the weight-averaged molecular weight and M_n is the number-averaged molecular weight. When the rate of initiation is faster than or like the rate of propagation, a good control is already achieved during the early stages of the reaction.

Resuming, an RDRP reaction should exhibit the following requisites to be considered a controlled process: (i) initiation must be fast and complete, (ii) the growth of the macromolecules and monomer conversion must be in a linear relationship and (iii) D should be less than 1.5. Chain-end functionality is an important peculiarity of CRPs. Generally, RDRPs start with a functional initiator (an organic molecule, a nanoparticle, or a biomolecule), which will be covalently bonded to the polymer chain so that all chains begin with the starting fragment and terminate with this functional chain-end. One aspect to be highlighted is that propagation of radicals in RDRP and FRP is mechanistically indistinguishable: radicals exhibit high regioselectivities and add to the less substituted carbon in alkenes, but they have low stereoselectivities due to their sp^2 nature. Consequently, polymers have head-to-tail structures and are often atactic.

1.2 Atom Transfer Radical Polymerization

Atom transfer radical polymerization (ATRP) is the most preferred technique in the field of CRP. It is used by both academia and industry to achieve tailor-made macromolecules. Such polymers can be obtained with chains having high uniformity ($D < 1.5$), defined molecular weight, defined topology and selected end-groups (Figure 1.1).⁵ Single macromolecules can be prepared as stars, combs, bottlebrushes, rings or as networks with well-defined mesh size through crosslinking. The composition of individual copolymers may follow certain statistics or change either in a smooth gradient or abruptly, giving block copolymers with morphologies structured down to the nanoscale. Functionalities can be inserted into the polymer by modification of the end-group or other

reactive moieties in other specific positions, choosing the best properties for every purpose.

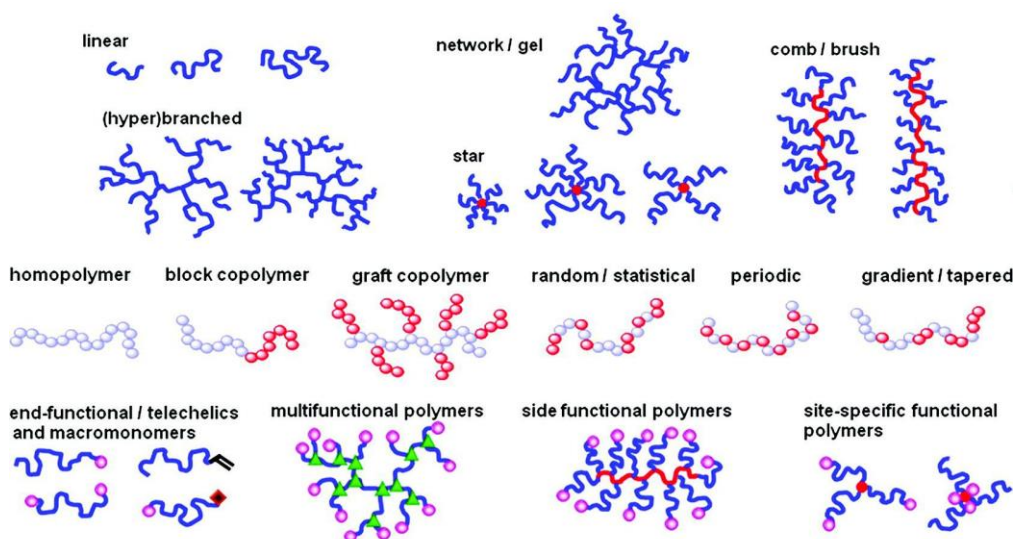
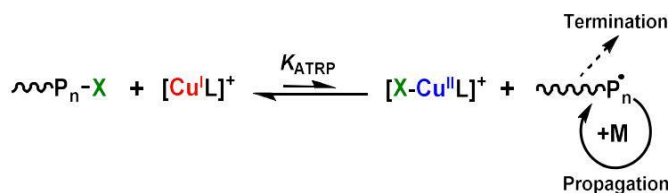


Figure 1.1. From top to bottom, examples of polymers with controlled topology, composition and position of the functional groups.

Evolution and improvements of ATRP catalysts and polymerizations that will be briefly described in this chapter, pushed ATRP to commercialization. Polymers prepared by ATRP are used in a vast range of applications like coatings, adhesives, medicine and cosmetics, environment, just to cite some of the most relevant.

1.2.1 The mechanism of ATRP

ATRP is usually catalyzed by a copper-amine complex. A reversible equilibrium involves the activator complex $[\text{Cu}^{\text{I}}\text{L}]^+$ (where L = amine ligand) and the deactivator $[\text{X-Cu}^{\text{II}}\text{L}]^+$ (where X = Cl, Br; Scheme 1.2).⁶ Normally, $K_{\text{ATRP}} \ll 1$ so that the concentration of the dormant state ($\text{P}_n\text{-X}$) is significantly higher than that of active radicals (the latter is comprised between 10^{-9} and 10^{-7} M).⁵ This minimizes termination reactions, affording the simultaneous growth of all polymer chains. When a radical is generated, it typically adds few monomer units before being quickly deactivated.



Scheme 1.2. Mechanism of ATRP.

The rate of ATRP depends on the rate constant of radical propagation (k_p) and on the concentrations of monomer and growing radicals (Eq. 1.1). The radical concentration in turn depends on the ATRP equilibrium constant and the concentrations of dormant species, activator, and deactivator. The structure of the ligand and monomer/dormant species as well as reaction conditions (solvent, temperature and pressure) can strongly influence the values of the rate constants, k_{act} and k_{deact} , and their ratio, K_{ATRP} (see Section 2.1.2).⁷ Generally, the overall rate of ATRP increases with catalyst activity (K_{ATRP}), although under certain conditions it may decrease because of radical termination leading to a decrease of the $[Cu^I L]^+ / [X-Cu^{II} L]^+$ ratio as a consequence of a buildup of the concentration of deactivator via the persistent radical effect.⁸

$$R_p = -\frac{dC_M}{dt} = k_p k_{ATRP} \frac{C_{RX} C_{Cu^I}}{C_{Cu^{II}}} C_M = k_p^{app} C_M \quad (1.1)$$

1.2.2 ISET vs. OSET

ATRP is a radical-based process and radicals can be formed from dormant species by several pathways. Mechanistically, halogen atom transfer from an alkyl halide to a Cu^I complex can occur via either outer-sphere electron transfer (OSET) or inner-sphere electron transfer (ISET), i.e., atom transfer passing through a $Cu-X-C$ transition state, which is, formally, also a single electron transfer process. Analysis of ATRP activation according to Marcus theory of electron transfer has shown that OSET has an intrinsic barrier ~ 15 kcal/mol higher than the experimentally measured value. This implies an experimental rate constant $\sim 10^{10}$ times higher than the value predicted for an OSET mechanism.⁹ The differences are much greater than any computational or experimental error, and

consequently, it has been concluded that a copper-catalyzed ATRP occurs via ISET, involving the transfer of a halogen atom from R-X to the metal center.

1.2.3 ATRP catalytic systems

Equilibrium constants in ATRP depend on the structure of catalysts, alkyl halides used as initiators, type of monomer, and reaction medium. Generally, ATRP equilibrium (K_{ATRP}) and activation (k_{act}) constants increase strongly with solvent polarity thanks to preferential stabilization of Cu^{II} species. Deactivation rate constants are usually very high and may approach diffusion-controlled limit ($k_{\text{deact}} > 10^6 \text{ M}^{-1}\text{s}^{-1}$). They are less influenced by the structure of the involved reagents than the activation rate constants.^{10,11} Figure 1.2 illustrates variation of the values of k_{act} with the ligand and alkyl halide structure, and variation of K_{ATRP} with solvent.

Copper-amine Complexes. The range of activity of ATRP catalysts spans more than six orders of magnitude. The order of Cu complex activity with ligand structure is tetradentate (cyclic-bridged) > tetradentate (branched) > tetradentate (cyclic) > tridentate > tetradentate (linear) > bidentate ligands. Complexes with tris(2-dimethylaminoethyl)-amine (Me_6TREN), tris (2-aminoethyl)amine (TREN) and tris(2-pyridylmethyl)amine (TPMA) are among the most active, while 2,2'-bipyridine (bpy) forms the least active catalyst. The nature of nitrogen atoms in the ligand also plays an important role in the activity of Cu complexes and follows the order pyridine > aliphatic amine > imine > aromatic amine. A two-carbon bridge between N atoms generates the most active complexes. The least active Cu complexes (especially those based on bpy) show excellent control for the polymerization of very reactive monomers that form stabilized propagating radicals (like methacrylates). Instead, ligands that give more active complexes are suitable for less reactive monomers, or for ATRP with low catalyst loadings¹², like vinyl chloride (see Chapter 9). The dynamics of the exchange reactions may be even more important than the absolute values of the equilibrium constants because radicals must be very quickly deactivated. Values of k_{deact} should be as large as possible.

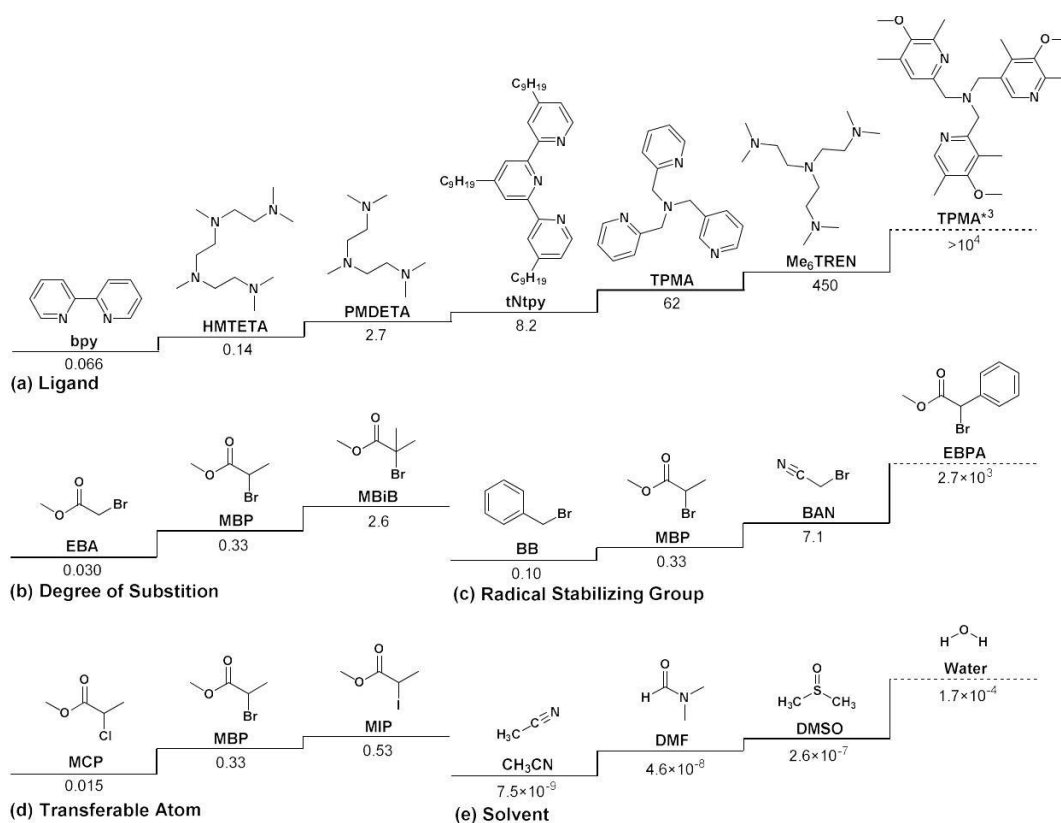


Figure 1.2. ATRP activation rate constants in CH_3CN at $35\text{ }^\circ\text{C}$: (a) for ethyl 2-bromoisobutyrate with $\text{Cu}^{\text{I}}\text{Br}$ in the presence of various ligands;¹³ (b-d) for various initiators with $\text{Cu}^{\text{I}}\text{X}/\text{PMDETA}$ ($\text{X} = \text{Br}$ or Cl).⁶ (e) ATRP equilibrium constants for the reaction between methyl 2-bromopropionate and $[\text{Cu}^{\text{I}}\text{HMTETA}]^+$.¹⁴ The dashed line indicates values obtained by extrapolation of experimental trends.

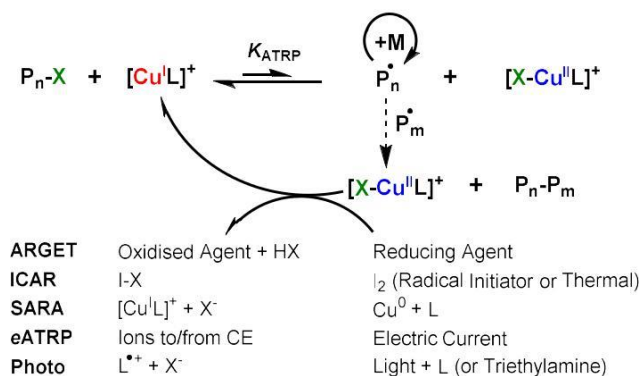
Alkyl halide-initiators. The reactivity of initiators in ATRP depends on the structure of the molecule and nature of the halogen atom. For a given monomer, it is important to select a sufficiently reactive species to ensure immediate and quantitative initiation. The order of reactivity of alkyl halides is $3^\circ > 2^\circ > 1^\circ$, in agreement with bond dissociation energy of the cleaving C-X bond. Values of K_{ATRP} increase with the presence of strong radical-stabilizing groups like aryl, carbonyl, ester and cyan moieties, attached to the carbon forming the C-X bond (Figure 1.2c). This is related to resonance stabilization as well as to polar and steric effects. To date, the most active initiator is ethyl α -bromophenylacetate (EBPA), with combined activation effects of both benzyl and ester species. Alkyl halide reactivity follows the order $\text{I} > \text{Br} > \text{Cl}$, related to the C-X bond dissociation energy.

Solvents. ATRP has been successfully carried out in a broad range of solvents, including both common organic solvents and “greener” media such as protic solvents (alcohols, water), supercritical CO₂ and ionic liquids. The properties of copper complexes in ionic liquids will be discussed in Chapter 2. Solvents have much smaller effects on radical polymerization than ionic polymerization. Nevertheless, ATRP equilibrium and rate constants are strongly influenced by the nature of the solvent. The main reason is the less polar character of Cu^I complexes (which can be considered neutral if weakly coordinated by a halide ion) with respect to the cationic Cu^{II} complexes, which are strongly stabilized in more polar solvents. In water, the difference is very marked and ATRP is characterized by very large equilibrium constants, >10⁴ times larger than in CH₃CN.

1.3 ATRP with low catalyst loadings

In traditional ATRP, relatively large amounts of catalyst, often comparable to the amount of the initiator, were used. Although very active ATRP catalysts were developed, they could not be used at very low concentrations because in ATRP, as in any other radical polymerization, radical termination occurs, leading to irreversible accumulation of the deactivator, [X-Cu^{II}L]⁺, at the expense of the activating complex, [Cu^IL]⁺, due to the persistent radical effect. Consequently, when all the activator is irreversibly transformed to deactivator, the reaction stops; this might happen at low monomer conversion.

As shown in Eq. 1.1, the rate of ATRP depends upon the ratio of activator and deactivator concentrations, not upon their absolute concentrations. If that ratio is kept constant throughout the polymerization, the ATRP rate should remain high. To reach this goal, an additional redox cycle was employed, that converted the higher-oxidation-state deactivator complex, formed during termination events, to the lower-oxidation-state activator (Scheme 1.3). In the presence of reducing agents (or Cu^I regeneration by other means), ATRP could be successfully conducted to high monomer conversion at very low amounts of catalyst.



Scheme 1.3. ATRP with low catalyst loadings.

Even zerovalent metals such as Cu, Fe, Mg and Zn can be used as reducing agents for $[XCu^{II}L]^+$.¹⁵ Besides reducing Cu^{II} to Cu^I , these metals can act as supplemental activators by direct reaction with alkyl halides. In this special case, the process is termed SARA ATRP (supplemental activators and reducing agent ATRP). ATRP with Cu^0 is particularly interesting because, in the presence of ligand, it produces in situ the efficient activating/deactivating species (Cu^I/Cu^{II}).

1.4 Electrochemically mediated ATRP

In all ARGET, SARA and ICAR processes, some side products are generated: new chains in ICAR, metal halides in SARA, dehydroascorbic acid, tin(IV) species, etc., in ARGET. These undesired products remain as impurities in the polymer and their removal often requires tedious and expensive procedures. Therefore, it would be of interest to avoid using chemicals as reducing agents and replace them with electrons, specifically electrical current. This is the idea behind electrochemically mediated ATRP (*e*ATRP), in which the ratio of the concentrations of activator and deactivator is controlled by the potential applied at the working electrode (E_{app}).¹⁶

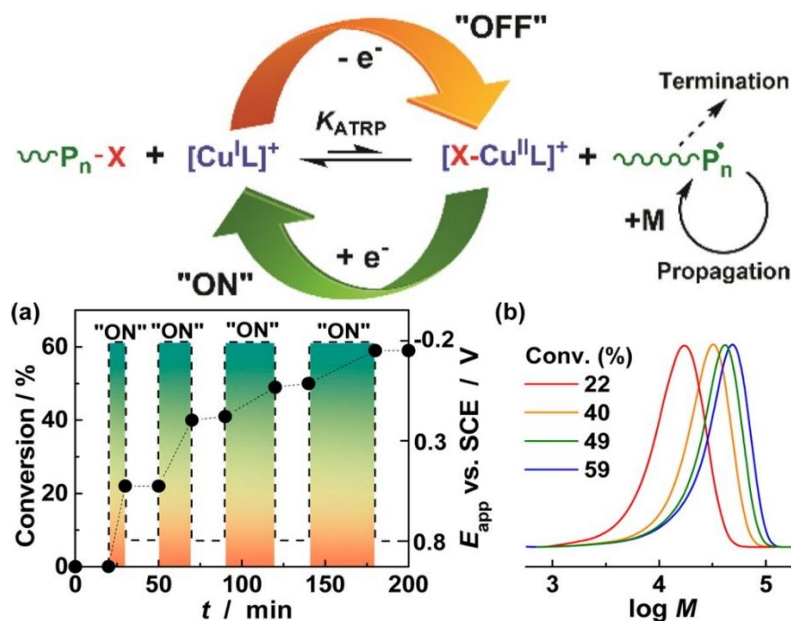


Figure 1.3. Mechanism of electrochemically mediated ATRP; (a) conversion (solid circles), applied potential (dashed line) with respect to time and b) MW distributions of polymer produced in methacrylic acid polymerization.¹⁷ (Reprinted with permission from Ref. 17, Copyright 2016, American Chemical Society).

Several parameters, such as applied current, potential, and total charge passed, can be controlled in *e*ATRP. The mechanism of ATRP mediated through electrochemical control over the ratio of $\text{Cu}^{\text{I}}/\text{Cu}^{\text{II}}$ and (re)generation of activator is shown in Figure 1.3a. A targeted amount of an air-stable $\text{Cu}^{\text{II}}/\text{L}$ catalyst complex can be electrochemically reduced to $\text{Cu}^{\text{I}}/\text{L}$ activator to start a controlled polymerization. The rate of *e*ATRP can be controlled by changing the applied potential (E_{app}). In proximity of the electrode surface, the Nernst equation is usually considered valid:

$$E_{app} = E_{1/2} + \frac{RT}{nF} \ln \frac{C_{\text{Cu}^{\text{II}}}}{C_{\text{Cu}^{\text{I}}}} \quad (1.2)$$

where $E_{1/2}$ is the half-wave potential of the copper catalyst. In the absence of mass transport limitations, the rate of reduction is directly dictated by the applied potential (E_{app}), enabling fine tuning the polymerization rate by the generated ratio of $C_{\text{Cu}^{\text{I}}}/C_{\text{Cu}^{\text{II}}}$ (a more negative potential induces an increase in the $C_{\text{Cu}^{\text{I}}}/C_{\text{Cu}^{\text{II}}}$ ratio, resulting in a faster rate of polymerization). Exploiting the same principle, electrochemistry also permits a lower oxidation state catalyst ($\text{Cu}^{\text{I}}/\text{L}$) to be reverted to its original higher oxidation state by simply shifting E_{app} to more

positive values. Therefore, the procedure provides a means to rapidly stop an ongoing polymerization and restart it if necessary; *e*ATRP offers the possibility of a quick switch between “on” and “off” polymerization states (Figure 1.3a). Monomer conversion quickly stops if an appropriate potential where fast oxidation of Cu^I to Cu^{II} occurs is applied ($E_{\text{app}} \gg E_{1/2}$). The polymerization therefore can be easily modulated, playing with E_{app} . Usually, no change in the “livingness” of the formed polymer is observed during the enforced dormant state.

1.5 Scope and organization of the Ph.D. thesis

This Ph.D. project has a dual aim: (i) to investigate the application of ionic liquids and other green solvents as valuable substitutes for the traditional organic solvents currently employed in *e*ATRP and (ii) to investigate ATRP of relevant monomers, including also vinyl chloride. Finally, one example of *e*ATRP electrochemical reactor for the scale-up is introduced. Electrochemical methods are the principal tools used. They are well suitable for the investigation of the ATRP catalytic system, which involves an electron transfer between copper species and alkyl halides. The obtained results had some important implications from both mechanistic and synthetic standpoints, and overall allowed to expand the scope of *e*ATRP polymerization.

The Ph.D. project is presented as follows:

- Chapter 2 characterizes a model ionic liquid, 1-butyl-3-methylimidazolium triflate ([BMIm][OTf]) as a new solvent for ATRP. The behavior of typical copper catalysts and alkyl halides employed as initiators for ATRP, examined by means of electrochemical techniques, is discussed.
- In Chapter 3, *e*ATRP of methyl acrylate in [BMIm][OTf] is discussed. The process was explored in detail by modifications of several experimental parameters. Chain extension of a PMA-Br macroinitiator with acrylonitrile prompted the development of a catalytic halogen exchange.
- Chapter 4 introduces *e*ATRP of acrylonitrile and the development of the mechanism of catalytic halogen exchange, introduced in chapter 3, as a simple

and outstanding tool to provide well-defined block copolymers by *e*ATRP and SARA ATRP.

- Chapter 5: *e*ATRP of methyl methacrylate was explored in [BMIm][OTf]. Several differences and issues were systematically addressed and solved by means of catalytic halogen exchange (*c*HE) and optimization of reaction; *e*ATRP of methyl methacrylate in ethanol was used to further expand the toolbox of green solvents and to provide additional information about the behavior of this monomer.
- Chapter 6: *e*ATRP of methyl acrylate was explored in mixtures of ionic liquids and water and of traditional organic solvents and water. This new ambient conjugates characteristics of organic and aqueous world by limiting negative side effects of water but fetching its benefits. This section demonstrates the feasibility of the polymerization of a hydrophobic monomer even in aqueous media.
- Chapter 7: the synthesis of poly(ionic liquids) was developed via *e*ATRP and SARA ATRP in water, expanding the concept of ionic liquids not only as solvents but also as monomers.
- Chapter 8: *e*ATRP of methyl acrylate and some other selected monomers was tested in a SS304 reactor, inspired by the work described in the previous chapters of this Ph.D. thesis. The reactor was used as cathode together with a sacrificial Al anode and the reaction was driven galvanostatically, by the (re)generation of the catalyst on the walls of the reactor. This choice dramatically reduced the complexity of the electrochemical setup.
- Chapter 9: *e*ATRP of vinyl chloride was investigated as the very first example of *e*ATRP of a gaseous monomer. The success of this polymerization greatly evidences the inconsistency of the SET-LRP mechanism.

References

1. Matyjaszewski, K. D., Thomas P., Handbook of Radical Polymerization. **2002**.
2. Gaynor, S.; Greszta, D.; Mardare, D.; Teodorescu, M.; Matyjaszewski, K., Controlled Radical Polymerization. *Journal of Macromolecular Science, Part A* **1994**, *31*, 1561-1578.
3. Braunecker, W. A.; Matyjaszewski, K., Controlled/living radical polymerization: Features, developments, and perspectives. *Prog. Polym. Sci.* **2007**, *32*, 93-146.
4. Gold, L., Statistics of Polymer Molecular Size Distribution for an Invariant Number of Propagating Chains. *The Journal of Chemical Physics* **1958**, *28*, 91-99.
5. Matyjaszewski, K.; Sumerlin, B. S.; Tsarevsky, N. V., *Progress in Controlled Radical Polymerization: Mechanisms and Techniques*. American Chemical Society: 2012; Vol. 1100.
6. De Paoli, P.; Isse, A. A.; Bortolamei, N.; Gennaro, A., New Insights into the Mechanism of Activation of Atom Transfer Radical Polymerization by Cu(I) complexes. *Chemical Communications* **2011**, *47*, 3580-3582.
7. Matyjaszewski, K.; Jakubowski, W.; Min, K.; Tang, W.; Huang, J.; Braunecker, W. A.; Tsarevsky, N. V., Diminishing catalyst concentration in atom transfer radical polymerization with reducing agents. *Proceedings of the National Academy of Sciences* **2006**, *103*, 15309-15314.
8. Fischer, H., The Persistent Radical Effect: A Principle for Selective Radical Reactions and Living Radical Polymerizations. *Chemical Reviews* **2001**, *101*, 3581-3610.
9. Lin, C. Y.; Coote, M. L.; Gennaro, A.; Matyjaszewski, K., Ab Initio Evaluation of the Thermodynamic and Electrochemical Properties of Alkyl Halides and Radicals and Their Mechanistic Implications for Atom Transfer Radical Polymerization. *Journal of the American Chemical Society* **2008**, *130*, 12762-12774.
10. Fantin, M.; Isse, A. A.; Bortolamei, N.; Matyjaszewski, K.; Gennaro, A., Electrochemical Approaches to the Determination of Rate Constants for the Activation Step in Atom Transfer Radical Polymerization. *Electrochimica Acta* **2016**, *222*, 393-401.
11. Fantin, M.; Isse, A. A.; Matyjaszewski, K.; Gennaro, A., ATRP in Water: Kinetic Analysis of Active and Super-Active Catalysts for Enhanced Polymerization Control. *Macromolecules* **2017**, *50*, 2696-2705.
12. Woodruff, S. R.; Davis, B. J.; Tsarevsky, N. V., Selecting the Optimal Reaction Conditions for Copper-Mediated Atom Transfer Radical Polymerization at Low Catalyst Concentration. In *Progress in Controlled Radical Polymerization: Mechanisms and Techniques*, American Chemical Society: 2012; Vol. 1100, 99-113.
13. Tang, W.; Matyjaszewski, K., Effects of Initiator Structure on Activation Rate Constants in ATRP. *Macromolecules* **2007**, *40*, 1858-1863.
14. Braunecker, W. A.; Tsarevsky, N. V.; Gennaro, A.; Matyjaszewski, K., Thermodynamic Components of the Atom Transfer Radical Polymerization Equilibrium: Quantifying Solvent Effects. *Macromolecules* **2009**, *42*, 6348-6360.

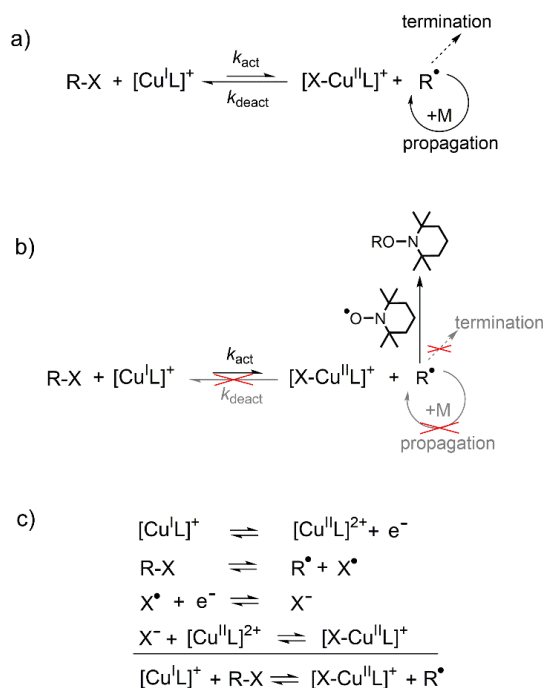
15. Zhang, Y.; Wang, Y.; Matyjaszewski, K., ATRP of Methyl Acrylate with Metallic Zinc, Magnesium, and Iron as Reducing Agents and Supplemental Activators. *Macromolecules* **2011**, *44*, 683-685.
16. Bortolamei, N.; Isse, A. A.; Magenau, A. J. D.; Gennaro, A.; Matyjaszewski, K., Controlled Aqueous Atom Transfer Radical Polymerization with Electrochemical Generation of the Active Catalyst. *Angew. Chem.* **2011**, *123*, 11593-11596.
17. Fantin, M.; Isse, A. A.; Venzo, A.; Gennaro, A.; Matyjaszewski, K., Atom Transfer Radical Polymerization of Methacrylic Acid: A Won Challenge. *Journal of the American Chemical Society* **2016**, *138*, 7216-7219.

Chapter 2

Electrochemical characterization of common catalysts and initiators for Atom Transfer Radical Polymerization in [BMIm][OTf]

2.1 Introduction

Atom transfer radical polymerization allows an extraordinary control over the polymerization process, molecular weight distribution, and macromolecular structures and compositions¹, thanks to a dynamic equilibrium between active and dormant species, which strongly favors the latter. An active catalyst, a copper complex with a polydentate amine ligand ($[\text{Cu}^{\text{I}}\text{L}]^+$), breaks the C-X bond in the initiator (RX) or in the dormant chains ($\text{P}_n\text{-X}$) to generate a radical and the oxidized complex $[\text{XCu}^{\text{II}}\text{L}]^+$ (Scheme 2.1a).² Generated radicals rapidly revert to their dormant state after adding only to few monomer units, while the rate of radical-radical termination is drastically lowered.



Scheme 2.1. a) Copper-catalyzed ATRP mechanism; b) reaction mechanism under conditions of k_{act} determination; c) splitting of the activation equilibrium into elementary steps. (Reprinted with permission, Copyright 2018 Elsevier).

Although ATRP is often performed in organic or aqueous solvents, increasing interest is devoted to the use of ionic liquids (ILs). Carmichael et al. reported the first copper-catalyzed ATRP in an IL³, showing fast polymerization of methyl methacrylate with relatively low dispersity in [BMIm][PF₆]. This pioneering study was followed by many applications of ATRP for the preparation of several homopolymers and block copolymers in ILs.^{4,5} Advanced low-ppm catalyst techniques such as ICAR⁶, ARGET⁷ and photoinduced ATRP⁸ were applied in ILs. There is also a growing interest toward ATRP in IL microemulsions.^{9,10} Last, some attempts were made to induce tacticity in polymers by using chiral ILs.¹¹ Despite such a widespread application, redox properties of common ATRP catalysts and initiators were never analyzed in ILs. Characterization of ATRP catalytic systems in ILs is highly desirable for the development of *e*ATRP. Indeed, *e*ATRP relies on selective, electrochemical generation of the active catalyst to control the [Cu^IL]⁺/[XCu^{II}L]⁺ ratio.^{12,13} Herein, the redox properties of three commonly used ATRP catalysts and ten alkyl halide initiators are reported, together with activation rate constants (k_{act}) of RX by [Cu^ITPMA]⁺ (TPMA = tris(2-pyridylmethyl)amine). The selected initiators mimic the structure of typical polymer chain-ends during ATRP. ILs are well-suited for *e*ATRP because of their exceptionally wide stability window and moderate electric conductivity without added supporting electrolytes.^{14,15} Some limitations of ILs for *e*ATRP may be high viscosity at room temperature¹⁵, entailing low mass transport rate, and the presence of possible halide ion impurities. As reported recently, residual halide ions can be easily removed through electrochemical deposition on a silver electrode.¹⁶ In addition, the viscosity of ILs significantly drops with temperature.¹⁵ Therefore, the selected solvent was 1-butyl-3-methylimidazolium trifluoromethanesulfonate, [BMIm][OTf], that exhibits the best compromise among all requested properties.

2.2. Redox properties of copper complexes

All copper complexes were prepared in situ by stepwise addition of equimolar amounts of Cu^{II} trifluoromethanesulfonate, Et₄NBr or Et₄NCl, used as X⁻ source,

and amine ligand. TPMA, tris[2-(dimethylamino)ethyl]amine (Me₆TREN), and *N,N,N',N'',N'''*-pentamethyldiethylenetriamine (PMDETA) (Figure 2.1) were used as ligands. Cu^{II} complexes with polydentate amine ligands are generally pentacoordinated, with solvent molecule(s) or X⁻ completing the coordination sphere.¹⁸

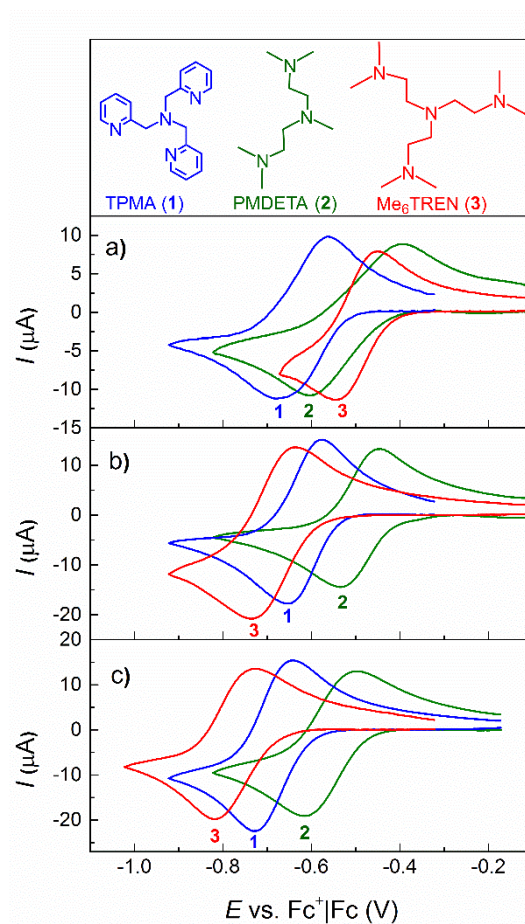


Figure 2.1. CVs of 10 mM a) [Cu^{II}L]²⁺, b) [BrCu^{II}L]⁺ and c) [ClCu^{II}L]⁺ in [BMIm][OTf] at $\nu = 0.1$ V s⁻¹ and $T = 50$ °C; L = TPMA, PMDETA or Me₆TREN. (Reprinted with permission, Copyright 2018 Elsevier).

Cyclic voltammetry (CV) of binary complexes, [Cu^{II}L]²⁺, showed a quasi-reversible peak couple for the reduction of Cu^{II} to Cu^I (Figure 2.1) and the measured redox potentials are reported in Table 2.1. E^\ominus of [Cu^{II}L]²⁺/[Cu^IL]⁺ showed a strong dependence on ligand type, decreasing in the order PMDETA \cong Me₆TREN > TPMA, which is slightly different from the trend (PMDETA > TPMA > Me₆TREN) observed in traditional solvents.^{17,19}

Table 2.1. Standard reduction potentials of $\text{Cu}^{\text{II}}/\text{L}/\text{X}^-$ complexes in [BMIm][OTf], $T = 50\text{ }^\circ\text{C}$.

| Redox couple | E^\ominus (V vs. $\text{Fc}^+ \text{Fc}$) ^a | | |
|--|---|----------|------------|
| | L = Me_6TREN | L = TPMA | L = PMDETA |
| $[\text{Cu}^{\text{II}}\text{L}]^{2+}/[\text{Cu}^{\text{I}}\text{L}]^+$ | -0.51 | -0.62 | -0.50 |
| $[\text{BrCu}^{\text{II}}\text{L}]^+ / [\text{BrCu}^{\text{I}}\text{L}]$ | -0.69 | -0.61 | -0.49 |
| $[\text{ClCu}^{\text{II}}\text{L}]^+ / [\text{ClCu}^{\text{I}}\text{L}]$ | -0.78 | -0.69 | -0.56 |

^a E^\ominus values were calculated as the average of half-wave potentials, $E_{1/2} = (E_{\text{pc}} + E_{\text{pa}})/2$, measured at different scan rates in the range $0.02 - 1\text{ V s}^{-1}$.

Addition of X^- yielded ternary complexes, $[\text{XCu}^{\text{II}}\text{L}]^+$, which exhibited similar CV pattern as $[\text{Cu}^{\text{II}}\text{L}]^{2+}$, albeit at more negative potentials (Figure 2.1), except for $[\text{BrCu}^{\text{II}}\text{TPMA}]^+$ and $[\text{BrCu}^{\text{II}}\text{PMDETA}]^+$. The shift in E^\ominus depends on the relative affinity of $[\text{Cu}^{\text{I}}\text{L}]^+$ and $[\text{Cu}^{\text{II}}\text{L}]^{2+}$ for X^- .¹³

$$E^\ominus_{[\text{XCu}^{\text{II}}\text{L}]^+ / [\text{XCu}^{\text{I}}\text{L}]} = E^\ominus_{[\text{Cu}^{\text{II}}\text{L}]^{2+} / [\text{Cu}^{\text{I}}\text{L}]^+} + \frac{RT}{F} \ln \frac{K_{\text{X}}^{\text{I}}}{K_{\text{X}}^{\text{II}}} \quad (2.1)$$

where K_{X}^{II} and K_{X}^{I} are the equilibrium constants of binding of X^- to $[\text{Cu}^{\text{II}}\text{L}]^{2+}$ and $[\text{Cu}^{\text{I}}\text{L}]^+$, respectively. In organic solvents $K_{\text{X}}^{\text{II}} > K_{\text{X}}^{\text{I}}$, hence E^\ominus of ternary complexes is more negative than that of binary complexes.^{17,19} Instead, in water a positive shift was observed,¹³ indicating higher affinity of Cu^{I} than Cu^{II} for X^- . In the IL the relative values of K_{X}^{II} and K_{X}^{I} depend on the amine ligand and X^- . In any case, each $[\text{ClCu}^{\text{II}}\text{L}]^+$ showed more negative E^\ominus than the respective $[\text{BrCu}^{\text{II}}\text{L}]^+$, accounting for the stronger affinity of these $\text{Cu}(\text{II})$ complexes (*i.e.* halidophilicity) for Cl^- than Br^- , as observed in acetonitrile.¹⁹ The reduction potentials of the ternary complexes followed the expected trend ($\text{PMDETA} > \text{TPMA} > \text{Me}_6\text{TREN}$) for both $[\text{ClCu}^{\text{II}}\text{L}]^+$ and $[\text{BrCu}^{\text{II}}\text{L}]^+$.

2.3. Electroreduction of initiators

As already observed in [BMIm][BF_4]²⁰ and acetonitrile²¹ all initiators (listed in Table 2.2) exhibited an irreversible cathodic peak attributable to a $2e^-$ reduction of RX to R^- and X^- . If RX bears a C-H group with a strong electron withdrawing

substituent (e.g. CN, COOMe) in α position, R^- can be protonated by the parent RX.² To avoid possible self-protonation reactions, all CV investigations were performed in the presence of acetic acid in slight excess over RX.

Table 2.2. Electrochemical parameters of initiators and k_{act} for the activation reaction by $Cu^I/TPMA/Br^-$ in [BMIm][OTf], $T = 50$ °C.

| Entry | RX | E_p^a (V) | α^b | k_{act} ($M^{-1}s^{-1}$) ^c |
|-------|---------------------------|-------------|------------|---|
| 1 | Ethyl bromoacetate | -1.88 | 0.37 | 5.6 |
| 2 | Benzyl bromide | -1.94 | 0.31 | 1.6×10^2 |
| 3 | Methyl 2-bromopropionate | -1.82 | 0.39 | 2.1×10^2 |
| 4 | 1-phenyl-1-bromoethane | -1.83 | 0.26 | 1.6×10^3 ^d |
| 5 | 2-bromopropionitrile | -1.71 | 0.34 | - |
| 6 | Benzyl chloride | -2.41 | 0.27 | 3.9 |
| 7 | Methyl 2-chloropropionate | -2.18 | 0.27 | 9.7 |
| 8 | 1-phenyl-1-chloroethane | -2.39 | 0.32 | 3.3×10^1 |
| 9 | Chloroacetonitrile | -2.14 | 0.34 | 2.3×10^2 |
| 10 | Chloropropionitrile | -2.17 | 0.30 | 9.0×10^2 |

^a. vs. Fc^+/Fc measured at $v = 0.1$ Vs^{-1} .

^b. Determined from the slopes ($\partial E_p / \partial \log v = -1.15RT / \alpha F$) of E_p versus $\log v$ plots.

^c. Reaction between RX and $[Cu^I TPMA]^+$ in the presence of TEMPO and X^- ($Cu^I/TEMPO/X^-$: 1/10/2). Unless otherwise stated, k_{act} accuracy was ± 5 -10%.

^d. k_{act} accuracy $\pm 20\%$.

Reductive cleavage of alkyl halides is known to follow a concerted dissociative electron transfer mechanism. Although the overall process is a $2e^-$ reduction, single electron transfer to RX is the rate-determining step and the transfer coefficient α can be calculated from the peak width and the dependence of peak potential, E_p , on scan rate^{20,21}, according to the following equations:

$$\frac{\partial E_p}{\partial \log v} = - \frac{1.151RT}{\alpha F} \quad (2.2)$$

$$E_{p/2} - E_p = \frac{1.857RT}{\alpha F} \quad (2.3)$$

where $E_{p/2}$ is the half-peak potential, and F , R and T have their usual meanings. Electrochemical data collected for all investigated alkyl halides are reported in Table 2.2. E_p depends on molecular structure of RX: in general, $E_p(RCl) <$

$E_p(\text{RBr})$, whereas, within a series of chlorides or bromides, E_p depends on the electron withdrawing power of the α -substituent, decreasing in the order $\text{CN} > \text{CO}_2\text{Me} \gg \text{Ph}$. More important, E_p of RX is more than 1.0 V more negative than E° of the copper complexes, excluding the risk of undesired RX reduction in *e*ATRP.

2.4. Kinetics of RX activation by $[\text{Cu}^{\text{I}}\text{TPMA}]^+$

A simple technique to study the kinetics of ATRP initiation is to monitor the decrease of $[\text{Cu}^{\text{I}}\text{L}]^+$ concentration at a rotating disk electrode (RDE).² Since ATRP involves a reversible reaction with a low equilibrium constant¹, a good radical scavenger is needed to trap all generated radicals and kinetically isolate the activation step (Scheme 2.1b). TEMPO was used for this purpose, after checking that it is not reduced either by Cu(I) or at the electrode within the operative potential. Moreover, the radical scavenger disabled any possible side reactions leading to organocopper species.²² Therefore, all kinetic analyses were performed in the presence of a 10-fold excess of TEMPO over $[\text{Cu}^{\text{I}}\text{L}]^+$. Halide ions were also added (Cu(I)/X⁻: 1/2) since typically ATRP is performed starting with $\text{Cu}^{\text{II}}\text{X}_2$ and therefore X⁻ is always present in the reaction medium.¹

Details of the method used to measure the activation rate constant, k_{act} , were previously reported.^{2,17} Briefly, starting with a solution of $[\text{Cu}^{\text{I}}\text{TPMA}]^+$ and TEMPO, a fixed potential ($E_{\text{app}} = -0.3$ V vs. $\text{Fc}^+|\text{Fc}$) was applied to provide diffusion-controlled oxidation of Cu(I) (Figure 2a) and the corresponding limiting current (I_L) was recorded. Immediately after, the initiator was injected, and I_L decay was monitored. All investigated initiators were sufficiently reactive to adopt a second-order kinetic regime with $C_{\text{RX}}^0 = C_{\text{Cu(I)}}^0 = 2 \cdot 10^{-3}$ M. It must be mentioned that Cu(I) species are typically involved in disproportionation equilibria, which however were proven to be much slower than RX activation.¹⁷ Considering that under the adopted experimental conditions Cu(I) concentration is proportional to I_L , the kinetic rate law is

$$\frac{1}{C_{[\text{Cu}^{\text{I}}\text{L}]^+}} - \frac{1}{C_{[\text{Cu}^{\text{I}}\text{L}]^+}^0} = \frac{I_L^0}{I_L C_{[\text{Cu}^{\text{I}}\text{L}]^+}^0} - \frac{1}{C_{[\text{Cu}^{\text{I}}\text{L}]^+}^0} = k_{\text{act}} t \quad (2.4)$$

where the superscript “0” indicates the values of I_L and $[\text{Cu}^{\text{I}}\text{TPMA}]^+$ concentration at $t = 0$. In agreement with Eq. (2.4) all systems gave straight lines (Figure 2.2b) from which k_{act} was extracted. The collected data are reported in Table 2.2. k_{act} for 2-bromopropionitrile could not be measured ($\text{Cu}(\text{I})$ lifetime < 1 s). As expected, RBr was more reactive than RCl of the same structure ($k_{\text{act}(\text{RBr})} > 10 k_{\text{act}(\text{RCl})}$), accounting for the weaker C-X bond in the initiator when $X = \text{Br}$ than Cl. The overall structure of RX also strongly affected k_{act} . Secondary RX were more reactive than primary alkyl halides of the same type. This is most likely due to the higher stability of secondary alkyl radicals than primary R^\bullet . Considering the effect of the substituent on α position of C-X, the following order of increasing k_{act} was observed: $\text{CO}_2\text{Me} < \text{Ph} < \text{CN}$. Activation rate constants in $[\text{BMIm}][\text{OTf}]$ were of the same order of magnitude of k_{act} values reported in acetonitrile or DMSO.^{2,17,23}

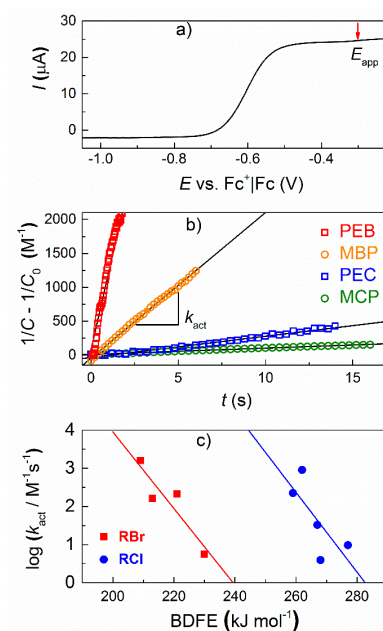


Figure 2.2 a) Linear sweep voltammetry of 5 mM $[\text{BrCu}^{\text{I}}\text{TPMA}]$ in $[\text{BMIm}][\text{OTf}]$ at RDE, $\nu = 0.005 \text{ V s}^{-1}$, $\omega = 4000 \text{ rpm}$ (the arrow indicates E_{app} during RX activation experiments). b) Kinetic analysis of RX activation by $[\text{Cu}^{\text{I}}\text{TPMA}]^+$; PEB = 1-phenyl-1-bromoethane, MBP = methyl 2-bromopropionate, PEC = 1-phenyl-1-chloroethane, MCP = methyl 2-chloropropionate. c) Correlation between k_{act} and bond dissociation free energy (BDFE) of R-X. (Reprinted with permission, Copyright 2018 Elsevier).

Seeking a useful structure-reactivity relationship, the overall activation reaction, which occurs in a single halogen transfer step^{1,2}, can be viewed as a combination of four elementary reactions (Scheme 2.1c). This is a purely thermodynamic view aimed to separate $\Delta_r G^\ominus$ of the activation reaction into distinct contributions that may be easily measured or estimated. Indeed, $\Delta_r G^\ominus$ is equal to the sum of the Gibbs free energies of the separate steps. Now, if one considers a selected catalyst and a series of RCl or RBr, three out of four reactions remain fixed: only R-X dissociation to R \cdot and X \cdot changes. Therefore, $\Delta_r G^\ominus$ depends exclusively on the bond dissociation free energy (BDFE) of RX. It follows that k_{act} can be correlated with the BDFE of the initiator (Figure 2.2c). A roughly linear plot was obtained for each series, suggesting that k_{act} of different RX should be predictable, if the relative BDFEs are known. BDFEs were not available in ILs and their solvation effects might significantly differ from traditional solvents, thus BDFE values calculated in vacuum were used.²⁴

2.5 Conclusions

Both binary and ternary copper complexes with PMDETA, TPMA, Me₆TREN and halide ions are stable in [BMIm][OTf]. E^\ominus of Cu(II)/Cu(I) depends on the nature of the ligand, decreasing in the order PMDETA \cong Me₆TREN > TPMA for [Cu^{II}L]²⁺ and PMDETA > TPMA > Me₆TREN for [XCu^{II}L]⁺. In general, E^\ominus of [XCu^{II}L]⁺ is more negative than that of [Cu^{II}L]²⁺, indicating that X⁻ stabilizes more Cu(II) than Cu(I), which is a crucial requisite of a good ATRP catalyst.

Reductive cleavage of initiators follows a concerted dissociative mechanism requiring potentials much more negative than the typical cathodic potentials used in *e*ATRP. Kinetic investigation on the activation of a series of bromides and chlorides by [Cu^ITPMA]⁺ provided k_{act} values of the same order of magnitude of values measured in molecular solvents. As well, the effect of RX molecular structure and type of halogen on k_{act} were the same as in organic solvents.

Overall, [BMIm][OTf] appears to be a suitable solvent for ATRP catalyzed by copper complexes and the collected data can be used to select the appropriate catalytic systems in ILs.

References

1. Matyjaszewski, K. Atom transfer radical polymerization (ATRP): Current status and future perspectives, *Macromolecules* **2012**, *45*, 4015-4039.
2. Isse, A.A.; Bortolamei, N.; De Paoli, P.; Gennaro, A. On the mechanism of activation of copper-catalyzed atom transfer radical polymerization, *Electrochimica Acta* **2013**, *110*, 655-662.
3. Carmichael, A.J.; Haddleton, D.M.; Bon, S.A.F.; Seddon, K.R. Copper(I) mediated living radical polymerization in an ionic liquid, *Chemical Communications* **2000**, 1237-1238.
4. Biedroń, T.; Kubisa, P. Atom transfer radical polymerization of acrylates in an ionic liquid: Synthesis of block copolymers, *J. Polym. Sci. Polym. Chem.* **2002**, *40*, 2799-2809.
5. Nguyen, V.H.; Shim, J.-J. Ionic liquid-mediated synthesis and self-assembly of poly(ethylene glycol)-block-polystyrene copolymer by ATRP method, *Colloid Polymer Science* **2015**, *293*, 617-623.
6. Wang, G.; Lu, M.; Zhong, M.; Wu, H. Preparation of poly(*n*-butyl acrylate) by ATRP using initiators for continuous activator regeneration (ICAR) in ionic liquid, *Journal of Polymer Research* **2012**, *19*, 9782.
7. Chen, H.; Wang, C.; Liu, D.; Wang, M.; Ji, C. ARGET ATRP of acrylonitrile with ionic liquid as reaction medium and FeBr₃/isophthalic acid as catalyst system, *Journal of Applied Polymer Science* **2011**, *122*, 3298-3302.
8. Wang, G.-X.; Lu, M.; Hou, Z.-H.; Yang, C.-A.; Liang, E.-X.; Liu, L.-C.; Wu, H.; Li, X.-L.; Xu, Y.-X. Photo-induced atom transfer radical polymerization in ionic liquid, *Journal of Polymer Research* **2015**, *22*, 60.
9. Wang, G.; Lu, M.; Wu, H. Preparation of poly(methyl methacrylate) by ATRP using initiators for continuous activator regeneration (ICAR) in ionic liquid/microemulsions, *Polymer* **2012**, *53*, 1093-1097.
10. Wang, G.-X.; Lu, M.; Hou, Z.-H.; Wu, H. Reactivity ratios of controlled/living copolymerization of styrene and acrylonitrile in ionic liquid microemulsion, *Journal of Polymer Research* **2013**, *20*, 80.
11. Biedroń, T.; Kubisa, P. Radical polymerization in a chiral ionic liquid: Atom transfer radical polymerization of acrylates, *Journal of Polymer Science: Polymer Chemistry* **2005**, *43*, 3454-3459.
12. Bortolamei, N.; Isse, A.A.; Magenau, A.J.D.; Gennaro, A.; Matyjaszewski, K. Controlled aqueous atom transfer radical polymerization with electrochemical generation of the active catalyst, *Angewandte Chemie International Edition* **2011**, *50*, 11391-11394.
13. Fantin, M.; Isse, A.A.; Gennaro, A.; Matyjaszewski, K. Understanding the fundamentals of aqueous ATRP and defining conditions for better control, *Macromolecules* **2015**, *48*, 6862-6875.
14. Every, H.A.; Bishop, A.G.; MacFarlane, D.R.; Oradd, G.; Forsyth, M. Transport properties in a family of dialkylimidazolium ionic liquids, *PCCP* **2004**, *6*, 1758-1765.
15. P. Hapiot, C. Lagrost, Electrochemical reactivity in room temperature ionic liquids, *Chem. Rev.* **108** **2008**, 2238-2264.

16. Arnaboldi, S.; Magni, M.; Mussini, P.R.; Gennaro, A.; Isse, A.A. "Egg of Columbus": Single-step complete removal of chloride impurities from ionic liquids by AgCl deposition on silver electrode, *Electrochemistry Communications*, **2015** *51*, 46-49.
17. Lorandi, F.; Fantin, M.; Isse, A.A.; Gennaro, A. RDRP in the presence of Cu⁰: The fate of Cu(I) proves the inconsistency of SET-LRP mechanism, *Polymer* **2015**, *72*, 238-245.
18. Pintauer, T.; Matyjaszewski, K. Structural aspects of copper catalyzed atom transfer radical polymerization, *Coordination Chemical Reviews* **2005**, *249*, 1155-1184.
19. Bortolamei, N.; Isse, A.A.; Di Marco, V.B.; Gennaro, A.; Matyjaszewski, K. Thermodynamic properties of copper complexes used as catalysts in atom transfer radical polymerization, *Macromolecules* **2010**, *43*, 9257-9267.
20. Isse, A.A.; Scarpa, L.; Durante, C.; Gennaro, A. Reductive cleavage of carbon-chlorine bonds at catalytic and non-catalytic electrodes in 1-butyl-3-methylimidazolium tetrafluoroborate, *PCCP* **2015**, *17*, 31228-31236.
21. Isse, A.A.; Berzi, G.; Falciola, L.; Rossi, M.; Mussini, P.R.; Gennaro, A. Electrocatalysis and electron transfer mechanisms in the reduction of organic halides at Ag, *Journal of Applied Electrochemistry* **2009**, *39*, 2217-2225.
22. Wehmeyer, R. M.; Rieke, R. D. Direct formation of functionalized alkylcopper reagents from alkyl halides using activated copper. Conjugate addition reactions with 2-cyclohexen-1-one, *Journal of Organic Chemistry* **1987**, *52*, 5056-5057.
23. Fantin, M.; Isse, A.A.; Bortolamei, N.; Matyjaszewski, K.; Gennaro, A. Electrochemical approaches to the determination of rate constants for the activation step in atom transfer radical polymerization, *Electrochimica Acta* **2016**, *222*, 393-401.
24. Lin, C.Y.; Coote, M.L.; Gennaro, A.; Matyjaszewski, K. Ab initio evaluation of the thermodynamic and electrochemical properties of alkyl halides and radicals and their mechanistic implications for atom transfer radical polymerization, *Journal of the American Chemical Society* **2008**, *130*, 12762-12774.

Chapter 3

Electrochemically Mediated ATRP of methyl acrylate in [BMIm][OTf]

3.1 Introduction

After the electrochemical characterizations that well supported the possibility of *e*ATRP in [BMIm][OTf], methyl acrylate (MA) was chosen as a model monomer for the first *e*ATRP in an ionic liquid.

Some limitations of *e*ATRP in molecular solvents are: i) a supporting electrolyte is required to achieve suitable conductivity in both aqueous and organic solvents; ii) employed organic solvents and copper catalysts are generally toxic¹ and iii) by-products and exhausts are expensive to recycle or dispose of.

Ionic liquids (ILs) are an attractive alternative to common organic solvents. They are non-volatile, usually non-flammable, electrically conductive, thermally stable up to > 300 °C, and easily recyclable. In addition, they are generally good solvents for inorganic, organic, and polymeric materials.^{2,3} Despite being considered green solvents, ILs are often expensive, poor biodegradable and potentially toxic.

The first attempts of ATRP in ILs explored the possibility of polymer separation and catalyst recycling. Carmichael et al.⁴ reported the first ‘normal ATRP’ of methyl methacrylate (MMA) in [BMIm][PF₆], catalyzed by Cu^IBr/N-propyl-2-pyridylmethanimine with ethyl 2-bromoisobutyrate as initiator. Polymerization rate was comparable to that in common organic solvents. Taking advantage of the immiscibility of [BMIm][PF₆] and copper complexes in toluene, the polymer was successfully separated by extraction with toluene. Afterwards, several ATRPs were conducted, with the same PF₆⁻ anion, but different cations, in a series of ILs, all able to solubilize monomers such as MMA and acrylonitrile (AN).⁵ [BMIm][PF₆] was also used for the sequential ATRP of butyl acrylate and methyl acrylate, providing block copolymers with very low dispersity ($D < 1.13$).³ This ionic liquid was also used to prepare the copolymer poly(ethylene oxide)-*b*-polystyrene.⁶ AGET ATRP of MMA and AN was performed in several ILs.^{5,7}

ILs have never been used as solvent for *e*ATRP, despite being well suitable for applications in electrochemical techniques. Indeed, ILs possess: i) a broad electrochemical window, and ii) sufficient conductivity, so that no external supporting electrolyte is necessary, leading to a cleaner polymerization system. Therefore, an *e*ATRP system in an ionic liquid is composed of only four elements: IL solvent, monomer, initiator, and a small amount of catalyst with continuous regeneration of the activator $[\text{Cu}^{\text{I}}\text{L}]^+$ by electrochemical reduction.

Nowadays, the number of possible ILs is enormous. More than 1000 ILs are described in the literature and 300 are commercially available.⁸ Selection of the appropriate IL should avoid the negative impact of solvent impurities on ATRP. For example, i) nitrogen-containing byproducts from the IL synthesis may bind to the copper complex reducing its activity or selectivity; ii) halide ions often present in ILs can decrease the rate of ATRP⁹ and reduce the available electrochemical potential window; iii) water narrows the electrochemical window and may also hydrolyze certain C-X functionalities (e.g. benzyl bromide); iv) acidic impurities can protonate alkyl amine ligands such as *N,N,N',N'',N'''*-pentamethyldiethylenetriamine (PMDETA) and tris[2-(dimethylamino)ethyl]amine (Me₆TREN), leading to decomposition of the catalyst.¹⁰ In addition, the viscosity of the IL should be low enough to allow effective mass transport to and from the electrode surface. 1-butyl-3-methylimidazolium trifluoromethanesulfonate, [BMIm][OTf], satisfies these requirements because of its adequate viscosity (2- and 5-fold lower than the viscosities of [BMIm][BF₄] and [BMIm][PF₆], respectively)² and wide electrochemical window (from -2.4 V to +1.4 V vs. Fc⁺/Fc, see Figure 3.1).

As shown in chapter 2, copper catalysts with traditional polyamine ligands (PMDETA, Me₆TREN, and tris(2-pyridylmethyl)amine (TPMA)) and halide ions are stable in [BMIm][OTf].¹¹ Moreover, activation of ATRP initiators in [BMIm][OTf] by $[\text{Cu}^{\text{I}}\text{TPMA}]^+$ showed rate constants similar to those measured in traditional molecular solvents such as acetonitrile. Also, the effect of RX molecular structure and type of halogen on the activation rate were the same as in organic solvents.^{11,12} Based on these observations, [BMIm][OTf] appears to be well-suited as a solvent for *e*ATRP.

The new electrochemical polymerization system hereafter described and studied exhibits the following characteristics: i) use of an IL as a green solvent, ii) low catalyst loading (ppm levels of $[\text{Cu}^{\text{II}}\text{TPMA}]^{2+}$), iii) electrochemical (re)generation of the active catalyst, thus avoiding chemical reducing agents and associated by-products, iv) simple extraction of the produced polymer, and v) facile catalyst and IL recycling.

Moreover, preservation of the chain-end functionality was investigated by chain extension of a poly(methyl acrylate)-Br macroinitiator with acrylonitrile. In this context, the C-Br chain end was converted to C-Cl using only a catalytic amount of Cu^{II} complex in a ‘catalytic halogen exchange’. This is a significant improvement of the traditional halogen exchange procedure, which up to now required an equimolar amount of air-sensitive Cu^{I} complex with respect to the C-Br chain-end.

3.2 Preliminary electrochemical characterization of the catalytic system

Cyclic voltammetry (CV) of the purified IL showed a wide potential window without any faradic current attributable to the oxidation or reduction of impurities (Figure 3.1). Few small peaks and a strong anticipation of the cathodic discharge is observed in the CV of the unpurified IL. The underlying redox processes may be due to residual water and other undesired impurities such as halide ions, which are typical byproducts of the synthesis of ionic liquids. After the purification procedure, most electroactive impurities were removed as confirmed by the flat baseline recorded in the CV.

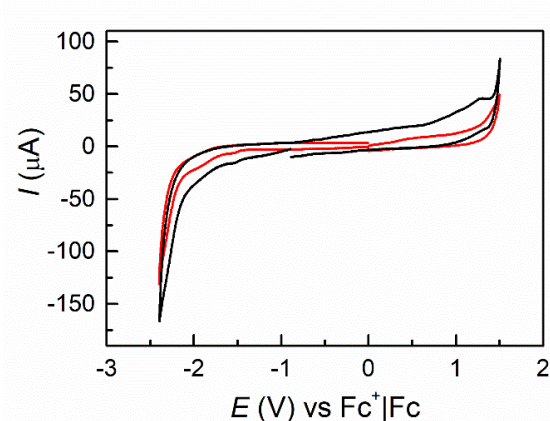


Figure 3.1. Cyclic voltammetry of pristine (—) and purified (—) $[\text{BMIm}][\text{OTf}]$, recorded at $50\text{ }^{\circ}\text{C}$ on a GC electrode at 0.2 V/s . Reproduced by permission of The Royal Society of Chemistry.

Prior to each polymerization, the stability and electrochemical properties of the catalytic system were evaluated by cyclic voltammetry (Figure 3.2a). $[\text{BrCu}^{\text{II}}\text{T-PMA}]^+$, formed in situ, exhibited a quasi-reversible peak couple, with $E_{1/2} = (E_{\text{pc}} + E_{\text{pa}})/2 = -0.62 \text{ V vs. Fc}^+|\text{Fc}$, where E_{pc} and E_{pa} are the cathodic and anodic peak potentials, respectively.



A similar voltammetric pattern was observed when methyl acrylate was added to prepare the typical IL/MA mixture (1:1, v/v) used in *e*ATRP (Figure 3.2b). The effect of the monomer is a positive shift of $E_{1/2}$ to $-0.57 \text{ V vs. Fc}^+|\text{Fc}$ and an increase of current intensity. The positive shift of $E_{1/2}$ may be attributed to the lower polarity of the mixture as compared to pure IL. Similar positive shifts of $E_{1/2}$ of copper catalysts were previously reported in molecular solvents after monomer addition.^{13,14} Instead, the current enhancement arises from the lower viscosity of the mixture as compared to the IL, despite dilution due to added monomer.

The reversibility observed in CV indicated that both Cu^{I} and Cu^{II} were stable in both IL and IL/MA (1:1, v/v). Once the initiator was added, the voltammetric pattern changed: the cathodic peak increased while the anodic one almost disappeared, indicating the occurrence of electrocatalysis (Figure 3.2c). On the electrode surface, $[\text{BrCu}^{\text{II}}\text{L}]^+$ was reduced to $[\text{BrCu}^{\text{I}}\text{L}]^+$, which partially dissociated generating the active form of the catalyst, $[\text{Cu}^{\text{I}}\text{L}]^+$.¹⁵ The latter reacted with the polymerization initiator, forming an alkyl radical and the oxidized catalyst species $[\text{BrCu}^{\text{II}}\text{L}]^+$, which diffused back to the electrode to be reduced again to $[\text{BrCu}^{\text{I}}\text{L}]^+$. Consequently, the cathodic peak became catalytic while the anodic one decreased in intensity because of the disappearance of Cu^{I} *via* reaction with RX.

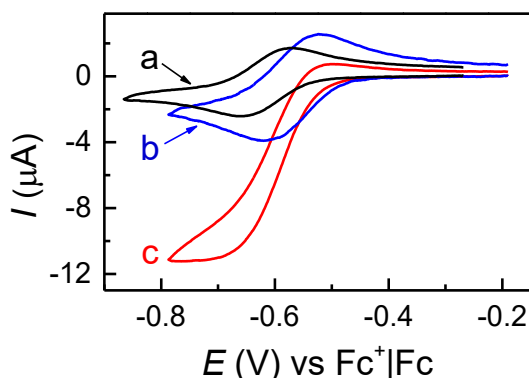


Figure 3.2. Cyclic Voltammetry of 2×10^{-3} M $[\text{BrCu}^{\text{II}}\text{TPMA}]^+$ in $[\text{BMIm}][\text{OTf}]$ (a) or 10^{-3} M $[\text{BrCu}^{\text{II}}\text{TPMA}]^+$ in $\text{MA}/[\text{BMIm}][\text{OTf}]$ (1:1, v/v) in the absence (b) and in the presence of 10^{-2} M EBiB (c), recorded at 50°C on a GC disk electrode at 0.1 V/s. Reproduced by permission of The Royal Society of Chemistry.

The standard reduction potential of the complex was estimated as $E^\ominus = E_{1/2}$, assuming similar diffusion coefficients for the oxidized (D_{O}) and reduced (D_{R}) species and activity coefficient ratio ($\gamma_{\text{O}}/\gamma_{\text{R}}$) close to unity (Eq. 3.2).

$$E_{1/2} = E^\ominus + \frac{RT}{nF} \ln \frac{\gamma_{\text{O}}}{\gamma_{\text{R}}} + \frac{RT}{nF} \ln \left(\frac{D_{\text{R}}}{D_{\text{O}}} \right)^{\frac{1}{2}} \quad (3.2)$$

where R is the gas constant and F is the Faraday constant. The values of applied potential (E_{app}) used during $e\text{ATRP}$ were chosen on the basis of $E_{1/2}$ measured for $[\text{BrCu}^{\text{II}}\text{TPMA}]^+$ reduction in $\text{MA}/[\text{BMIm}][\text{OTf}]$ (1:1, v/v).

As will be discussed in the following sections, various different parameters were examined in detail for $e\text{ATRP}$ and the stability and catalytic activity of the system were always evaluated by cyclic voltammetry.

3.2.1 Effect of applied potential

A series of $e\text{ATRP}$ s of 50% (v/v) MA in $[\text{BMIm}][\text{OTf}]$ were performed at different E_{app} values, from $E_{1/2}$ to $E_{1/2} - 0.12$ V (Table 3.1 and Figure 3.3). The ratio between Cu^{I} and Cu^{II} concentrations at the electrode surface is roughly related to E_{app} , according to the following equation:

$$E_{\text{app}} \approx E_{1/2} + \frac{RT}{F} \ln \frac{C_{\text{Cu}^{\text{II}}}}{C_{\text{Cu}^{\text{I}}}} \quad (3.3)$$

Therefore, changing E_{app} is a straightforward way to modulate the rate (R_{p}) of $e\text{ATRP}$.

$$R_p = -\frac{dC_M}{dt} = k_p K_{\text{ATRP}} \frac{C_{\text{RX}} C_{\text{Cu}^{\text{I}}}}{C_{\text{Cu}^{\text{II}}}} C_M = k_p^{\text{app}} C_M \quad (3.4)$$

where k_p is the propagation rate constant, K_{ATRP} is ATRP equilibrium constant, C_M is monomer concentration and $k_p^{\text{app}} = k_p C_{\text{R}} \cdot$ is the apparent propagation rate constant. As expected, lowering E_{app} from $E_{1/2}$ to $E_{1/2} - 0.12$ V induced faster Cu^{I} (re)generation and increased its concentration, thus enhancing polymerization rate; k_p^{app} increased from 0.17 h^{-1} to 0.79 h^{-1} .

Table 3.1. *e*ATRP of 50% (v/v) MA in [BMIm][OTf] at different E_{app} values, $T = 25 \text{ }^\circ\text{C}$.^a

| entry | $E_{\text{app}} - E_{1/2}$ (V) | $C_{\text{Cu}^{\text{II}}}/C_{\text{Cu}^{\text{I}}}$ ^b | t (h) | Conv. (%) | k_p^{app} ^c (h^{-1}) | M_n^{th} | M_n^{app} | \bar{D} |
|-------|-----------------------------------|---|------------|-----------|--|-------------------|--------------------|-----------|
| 1 | 0 | 1 | 5 | 59 | 0.17 | 28000 | 27300 | 1.08 |
| 2 | -0.03 | 0.3 | 5 | 70 | 0.27 | 33300 | 32300 | 1.10 |
| 3 | -0.06 | 0.1 | 5 | 90 | 0.47 | 42800 | 42300 | 1.10 |
| 4 | -0.09 | 0.03 | 4 | 94 | 0.61 | 44700 | 42900 | 1.24 |
| 5 | -0.12 | 0.01 | 3.5 | 96 | 0.79 | 46600 | 44100 | 1.32 |

^aConditions: $C_{\text{MA}}:C_{\text{CuBr}_2}:C_{\text{TPMA}}:C_{\text{RX}} = 552:0.1:0.1:1$, $C_{\text{CuBr}_2} = 10^{-3} \text{ M}$; $V_{\text{tot}} = 5 \text{ mL}$. ^bCalculated from Eq. (3.3). ^cThe slope of the $\ln([M]_0/[M])$ vs. t plot. Reproduced by permission of The Royal Society of Chemistry.

During *e*ATRP of MA, visible polymer formation was observed in the solution. As the conversion increases, a neat increase of the viscosity of the solution was observed.

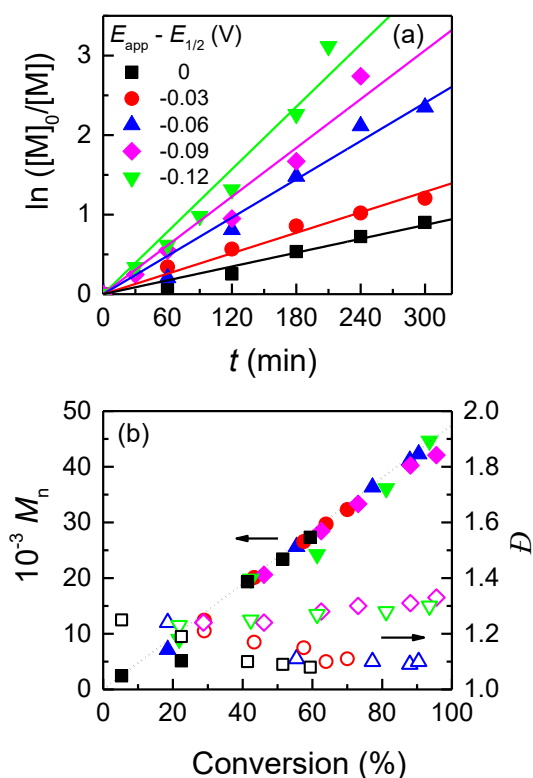


Figure 3.3. Effect of E_{app} on *e*ATRP of 50% (v/v) MA in [BMIm][OTf]. (a) First-order kinetic plots and (b) evolution of M_n and D with conversion. Conditions: $C_{MA}:C_{RX}:C_{CuBr_2}:C_{TPMA} = 552:1:0.1:0.1$. $C_{CuBr_2} = 10^{-3}$ M. The dotted line represents theoretical M_n . Reproduced by permission of The Royal Society of Chemistry.

Lowering E_{app} decreased the concentration of the deactivating Cu^{II} species and, therefore, hampered polymerization control. For example, at $E_{app} = E_{1/2} - 0.12$ V, where the target ratio between deactivating and activating species was 1/100 (see Eq. 3.3), a fast but only moderately controlled polymerization ($D = 1.32$) was observed (Table 3.1, entry 5). Despite the slight deterioration of control with decreasing E_{app} , measured M_n was always in excellent agreement with theoretical values (M_n^{th}) (Figure 3.3b).

Figure 3.4 shows the effect of E_{app} on conversion and D for *e*ATRP of MA in [BMIm][OTf]. The best conditions were found at $E_{app} = E_{1/2} - 0.06$ V: 90% conversion in 5 h, M_n in excellent agreement with M_n^{th} , and $D = 1.10$. Therefore, $E_{app} = E_{1/2} - 0.06$ V was used in further reactions.

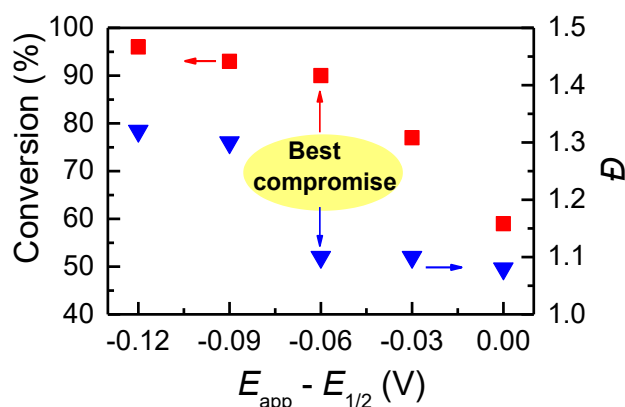


Figure 3.4. Conversion (■) and D (▼) vs. E_{app} for *e*ATRP of 50% (v/v) MA in [BMIm][OTf]. Conditions: $C_{MA}:C_{CuBr_2}:C_{TPMA}:C_{RX} = 552:0.1:0.1:1$; $t = 5$ h. Reproduced by permission of The Royal Society of Chemistry.

3.2.2 Effect of temperature

If the ionic liquid possesses a very high viscosity, thus, mass transfer problems may arise, especially when the reaction reaches high monomer conversion. The viscosity of ionic liquids strongly depends on temperature, rapidly decreasing as the temperature is raised.¹⁶ Monomer propagation rate is also significantly affected by temperature. Therefore, *e*ATRP of 50% (v/v) MA in [BMIm][OTf] was performed at different temperatures from 25 °C to 75 °C. The results are reported in Table 3.2 and Figure 3.5. The polymerization was well-controlled at all temperatures and, as expected, the reaction rate increased with T ; conversion was almost quantitative after 1 h at 75 °C as compared to 90% conversion in 5 h at 25 °C. The Cu^I catalyst, however, was a slightly weaker reducing agent at higher temperatures, in agreement with a previous report in DMF.⁹ The dispersity slightly increased with T from 1.10 to 1.19, indicating the possible occurrence of side reactions or radical-radical termination. Nevertheless, very good polymerization control and molecular weight fidelity were retained up to temperatures as high as 75 °C.

Table 3.2. *e*ATRP of 50% (v/v) MA in [BMIm][OTf] performed at $E_{\text{app}} = E_{1/2} - 0.06$ V at different temperatures.^a

| entry | T (°C) | $E_{1/2}$ vs. Fc^+/Fc (V) | t (h) | Conv. (%) | Q^b (C) | $k_p^{\text{app}c}$ (h ⁻¹) | M_n^{th} | M_n^{app} | D |
|-------|-----------------|---|------------|--------------|--------------|---|-------------------|--------------------|------|
| 1 | 25 | -0.58 | 5.00 | 90 | 3.3 | 0.17 | 42800 | 42300 | 1.10 |
| 2 | 50 | -0.56 | 1.75 | 93 | 3.0 | 1.52 | 44200 | 44200 | 1.17 |
| 3 | 75 | -0.50 | 1.00 | 98 | 0.7 | 3.91 | 46700 | 47300 | 1.19 |
| 4 | 50 ^d | -0.56 | 2.00 | 87 | 4.2 | 1.02 | 41100 | 44800 | 1.10 |

^aConditions: $C_{\text{MA}}:C_{\text{CuBr}_2}:C_{\text{TPMA}}:C_{\text{RX}} = 552:0.1:0.1:1$. $C_{\text{Cu}} = 10^{-3}$ M; $V_{\text{tot}} = 5$ mL. ^bTotal charge passed. ^cThe slope of the $\ln([M]_0/[M])$ vs. t plot. ^dExperiment at fixed current, with the following steps: 1.1 mA for 15 min, 0.95 mA for 17 min, 0.45 mA for 50 min, 0.2 mA for 73 min. Reproduced by permission of The Royal Society of Chemistry.

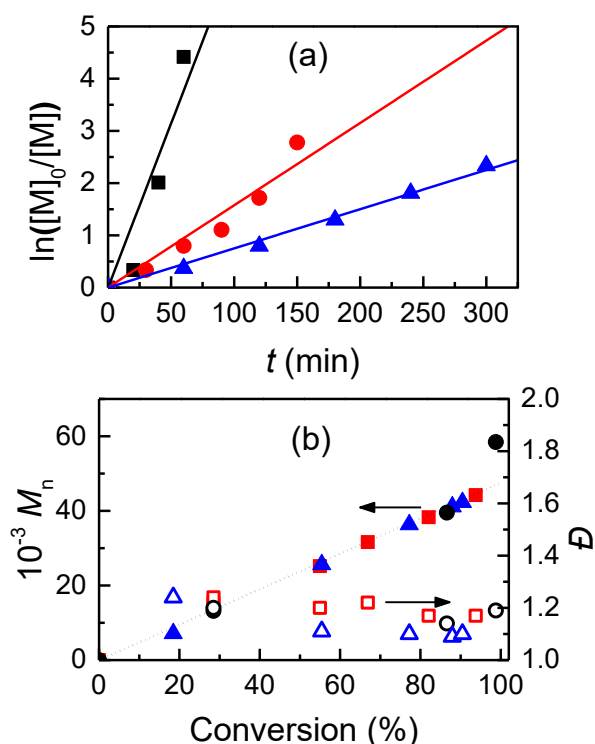


Figure 3.5. (a) First-order kinetic plots and (b) evolution of M_n and D with conversion for *e*ATRP of 50% (v/v) MA in [BMIm][OTf] performed at 25 °C (\blacktriangle), 50 °C (\bullet) or 75 °C (\blacksquare). Conditions: $C_{\text{MA}}:C_{\text{CuBr}_2}:C_{\text{TPMA}}:C_{\text{RX}} = 552:0.1:0.1:1$; $C_{\text{Cu}} = 10^{-3}$ M; $E_{\text{app}} = E_{1/2} - 0.06$ V. The dotted line represents theoretical M_n . Reproduced by permission of The Royal Society of Chemistry.

To compare IL with traditional molecular solvents, *e*ATRP was performed under the same experimental conditions in [BMIm][OTf] and in acetonitrile (MA/solvent = 1:1 (v/v), $C_{\text{MA}}:C_{\text{Cu}}:C_{\text{TPMA}}:C_{\text{RX}} = 552:0.1:0.1:1$, with $C_{\text{Cu}} = 10^{-3}$ M, Table 3.3). To

increase the electric conductivity of acetonitrile, 0.1 M Et₄NBF₄ was added as a supporting electrolyte. The chosen applied potential was $E_{\text{app}} = E_{1/2} - 0.06$ V. The results are listed in Table 3.3. Virtually the same results, in terms of molecular weights, dispersity and overall polymerization rate, were obtained in both solvents.

Table 3.3. *e*ATRP of MA in CH₃CN or IL at $E_{\text{app}} = E_{1/2} - 0.06$ V.^a

| Entry | Solvent | <i>T</i> (°C) | <i>t</i> (h) | Conv. (%) | <i>k</i> _p ^{app, b} (h ⁻¹) | <i>Q</i> (C) | <i>M</i> _n th | <i>M</i> _n ^{app} | <i>D</i> |
|-------|--------------------|---------------|--------------|-----------|--|--------------|-------------------------------------|--------------------------------------|----------|
| 1 | CH ₃ CN | 25 | 4 | 92 | 0.62 | 3.49 | 43700 | 42700 | 1.14 |
| 2 | IL | 25 | 5 | 90 | 0.17 | 1.30 | 42800 | 42300 | 1.10 |
| 3 | IL | 50 | 1.75 | 93 | 1.52 | 3.00 | 44200 | 44200 | 1.17 |
| 4 | CH ₃ CN | 50 | 2 | 93 | 1.31 | 5.39 | 47000 | 45000 | 1.09 |

^aOther experimental conditions: 0.1 M Et₄NBF₄ was used as a supporting electrolyte in CH₃CN; estimated surface area of the working electrode: 6 cm². ^bThe slope of ln([M]₀/[M]) vs. *t* plot. Reproduced by permission of The Royal Society of Chemistry.

Polymerizations of MA in [BMIm][OTf] and in acetonitrile were overall very similar in terms of molecular weights and dispersity. The polymerization rate in [BMIm][OTf] was significantly lower than in CH₃CN at 25 °C, probably due to the much higher viscosity, and thus slower mass transport, in the IL. At 50 °C similar reaction rates were observed, although the dispersity was slightly lower in CH₃CN than in the ionic liquid.

3.2.3 Galvanostatic *e*ATRP

Galvanostatic electrolysis is in general more appealing than controlled-potential electrolysis, since the required experimental setup is simpler: the reference electrode is not necessary, and a simple direct-current power supply can be used instead of a potentiostat/galvanostat. Therefore, *e*ATRP of 50% (v/v) MA in [BMIm][OTf] was carried out at 50 °C by applying a programmed constant current profile rather than a fixed potential. The appropriate profile, made of 4 current steps, was selected from the chronoamperometric curve recorded during a potentiostatic *e*ATRP experiment performed under similar conditions (Figure 3.6). Applying a fixed current,

instead of a fixed potential, causes the working electrode potential (E_{WE}) to drift with time. E_{WE} was monitored during e ATRP, and a typical trend is shown in Figure 3.6b. E_{WE} shifted to more negative values during polymerization but remained close to E_{app} used in the potentiostatic experiment ($E_{app} = E_{1/2} - 0.06$ V) in the first hour. This allowed avoiding side reactions that occur at very negative potentials, such as electrodeposition of Cu^0 on the working electrode. Figure 3.7 shows a comparison of e ATRP performed in potentiostatic or galvanostatic mode: the two experimental setup modes gave substantially the same results in terms of both polymerization rate and properties of produced polymers (Figure 3.7).

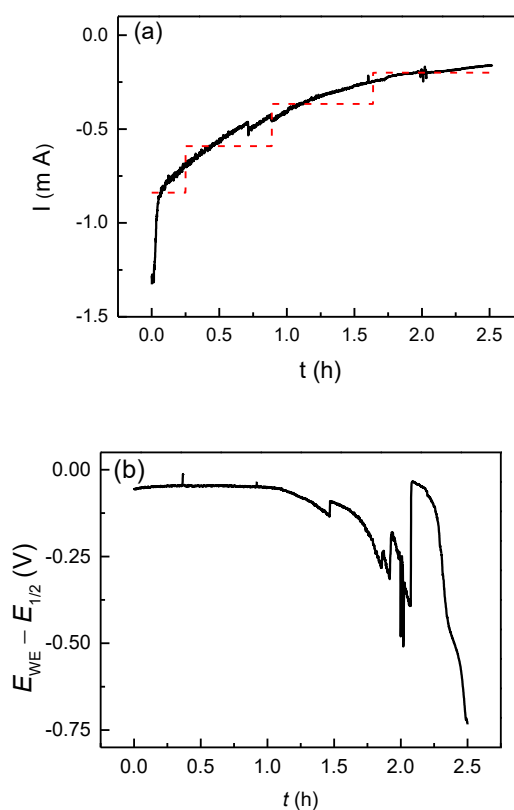


Figure 3.6. (a) Chronoamperometry recorded during potentiostatic e ATRP of MA in [BMIm][OTf] (1:1, v/v), $T = 50$ °C, $E_{app} = E_{1/2} - 0.06$ V, $C_{MA}:C_{CuBr_2}:C_{TPMA}:C_{RX} = 552:0.1:0.1:1$, $C_{CuBr_2} = 10^{-3}$ M; the dashed line shows the fixed current steps applied in the galvanostatic mode. (b) Potential (vs. $E_{1/2}$) of the working electrode during galvanostatic e ATRP. Reproduced by permission of The Royal Society of Chemistry.

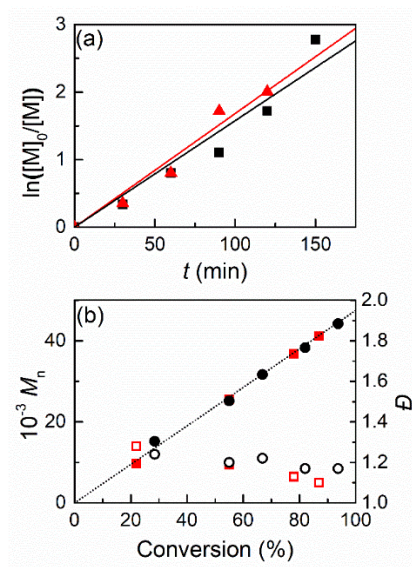


Figure 3.7. (a) Kinetic plots and (b) evolution of M_n and D as a function of conversion for potentiostatic eATRP performed at $E_{app} = E_{1/2} - 0.060$ V (\blacktriangle) and galvanostatic eATRP (\blacksquare) at $T = 50$ °C. Conditions: $C_{MA}:C_{CuBr_2}:C_{TPMA}:C_{RX} = 552:0.1:0.1:1$, $C_{CuBr_2} = 10^{-3}$ M. The dotted line represents theoretical M_n . Reproduced by permission of The Royal Society of Chemistry.

3.2.4 Effect of degree of polymerization (DP) and catalyst loading

Targeted degree of polymerization was varied by changing the monomer amount from 25 to 75 % (v/v) at constant C_{RX} . In all cases (Table 3.4, entries 1-3), reactions were fast and well-controlled, with almost quantitative conversion when 25% or 50% (v/v) of MA was used. The polymerization rate slightly decreased with increasing MA content, possibly because of a decrease in activation rate (Figure 3.8).¹³

Table 3.4. eATRP of MA in [BMIm][OTf] at different targeted degrees of polymerization and catalyst loadings, $E_{app} = E_{1/2} - 0.06$ V, $T = 50$ °C.^a

| DP_{target} | MA/IL (v/v) | C_{Cu} (mM) | t (h) | Conv. (%) | Q^b (C) | $k_p^{app\ c}$ (h ⁻¹) | M_n^{th} | M_n^{app} | D |
|------------------|----------------|------------------|------------|--------------|--------------|--------------------------------------|------------|-------------|------|
| 276 | 25/75 | 1.00 | 1.30 | 95 | 1.30 | 1.73 | 22600 | 23000 | 1.15 |
| 552 | 50/50 | 1.00 | 1.75 | 93 | 3.00 | 1.52 | 44200 | 44200 | 1.17 |
| 828 | 75/25 | 1.00 | 2.50 | 80 | 5.98 | 1.32 | 47500 | 59000 | 1.19 |
| 552 ^d | 50/50 | 0.50 | 3.00 | 94 | 1.86 | 0.89 | 44700 | 45000 | 1.19 |
| 552 ^d | 50/50 | 0.25 | 3.00 | 50 | 0.77 | 0.24 | 23800 | 21100 | 1.22 |

^a-Conditions: $C_{MA}:C_{CuBr_2}:C_{TPMA}:C_{RX} = x:0.1:0.1:1$, with $x = 276$ to 828. $V_{tot} = 5$ mL. ^bTotal consumed charge. ^cThe slope of the $\ln([M]_0/[M])$ vs. t plot. ^dConditions: $C_{MA}:C_{CuBr_2}:C_{TPMA}:C_{RX} = 552:x:x:1$ with $x = 0.05$ or 0.025. Reproduced by permission of The Royal Society of Chemistry.

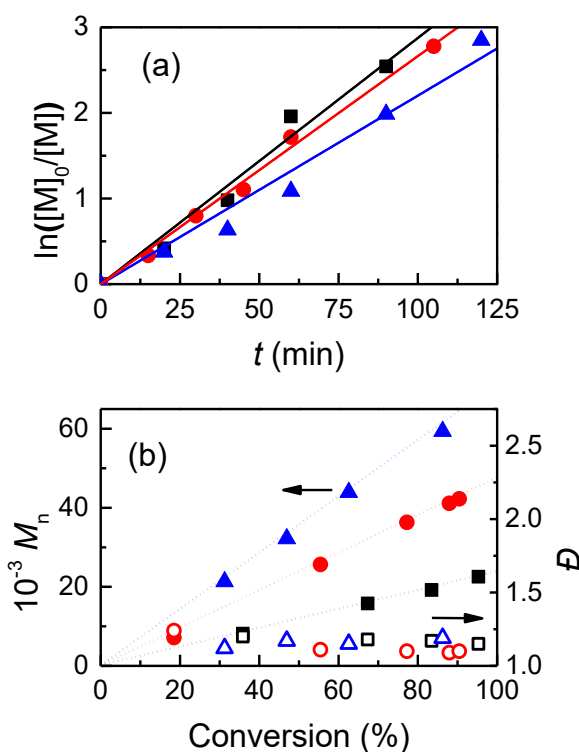


Figure 3.8. (a) First-order kinetic plots and (b) evolution of M_n and \bar{D} with conversion for e ATRP of MA in [BMIm][OTf] performed at $E_{app} = E_{1/2} - 0.06$ V and $T = 50$ °C. Other conditions: $C_{MA}:C_{CuBr_2}:C_{TPMA}:C_{RX} = x:0.1:0.1:1$, with $x = 276$ (■), 552 (●) or 828 (▲); $C_{Cu} = 10^{-3}$ M. The dotted lines represent theoretical M_n . Reproduced by permission of The Royal Society of Chemistry.

Catalyst loading for the e ATRP of 50 % (v/v) MA at 50 °C was reduced from 1 mM to 0.25 mM, which corresponds to copper/monomer molar ratio of 45 ppm. Table 3 shows that the polymerization was well-controlled with each catalyst loading. Additionally, the reaction rate increased with catalyst loading in agreement with previous reports.¹⁷ Figure 3.9 reports the kinetic plots and the trends of M_n and \bar{D} against conversion, which were linear in all cases.

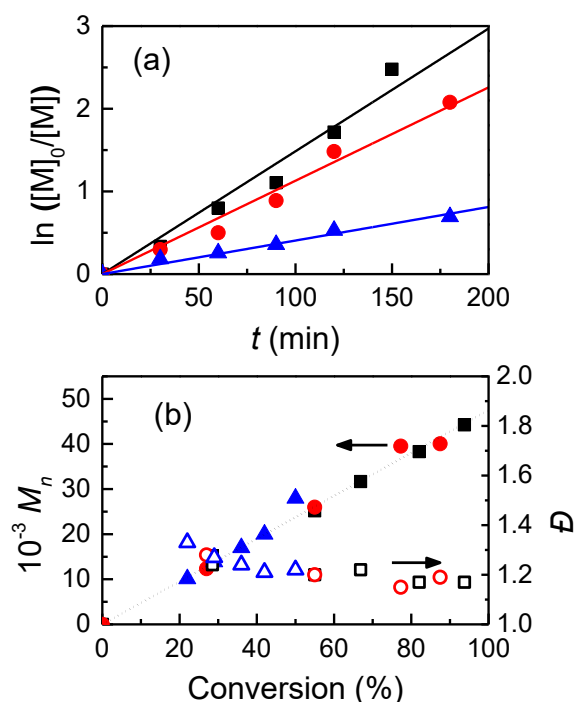


Figure 3.9. (a) First-order kinetic plots and (b) evolution of M_n and \bar{D} vs. conversion for the e ATRP of 50% (v/v) MA in [BMIm][OTf]. Conditions: $C_{MA}:C_{CuBr_2}:C_{TPMA}:C_{RX} = 552:x:x:1$, $x = 0.1$ with $C_{Cu} = 1$ mM (■), $x = 0.05$ with $C_{Cu} = 0.5$ mM (●), and $x = 0.025$ with $C_{Cu} = 0.25$ mM (▲). The dotted line represents theoretical M_n . Reproduced by permission of The Royal Society of Chemistry.

3.2.5 Livingness of the polymerization: electrochemical switch

Electrochemistry is a versatile tool to verify the living character of the process, by cycling the applied potential, repetitively, to switch the system between active and dormant states. This was achieved by modulating E_{app} between $E_{1/2} - 0.06$ V and $E_{1/2} + 0.20$ V. At $E_{app} = E_{1/2} - 0.06$ V, polymerization was activated by converting Cu^{II} to Cu^I at the electrode. In contrast, at $E_{app} = E_{1/2} + 0.20$ V, the activator was quenched by rapidly converting Cu^I to Cu^{II} and transforming the propagating radicals to dormant species (Figure 1.3a). Electrochemical oxidation of Cu^I quenched the polymerization much faster than in other ATRP techniques, such as photo ATRP¹⁸, ARGET ATRP¹⁹, or mechanically mediated ATRP²⁰. Indeed, in such polymerization methods the ON/OFF cycle is realized by simply removing the external stimulus or the feeding of reducing agents, but polymerization continues until it is slowed down by radical-radical termination and consequent build-up of Cu^{II} species. Conversely, in e ATRP negligible monomer conversion was observed during the OFF periods, due to the fast generation of Cu^{II} , despite the relative high viscosity of ILs (Figure 3.10a).

The electrochemical ON/OFF switch was applied four times, increasing the monomer conversion from 0 to 19, 39, 58, and 77 % during the active periods. M_n steadily increased during the ON periods, while no low M_n polymers were detected (Figure 3.10b). Overall, the polymer chains grew as if there were no interruptions. These observations demonstrated the living character of the polymerization: efficient re-initiation of chain ends resulted from minor termination and good preservation of chain-end functionality.

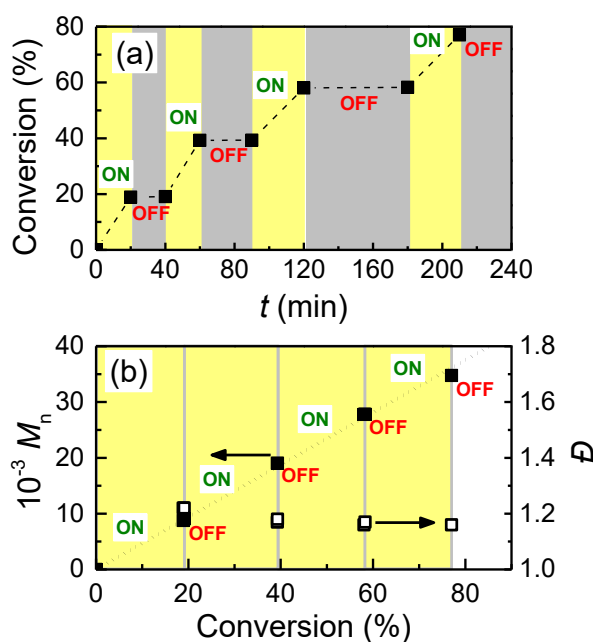
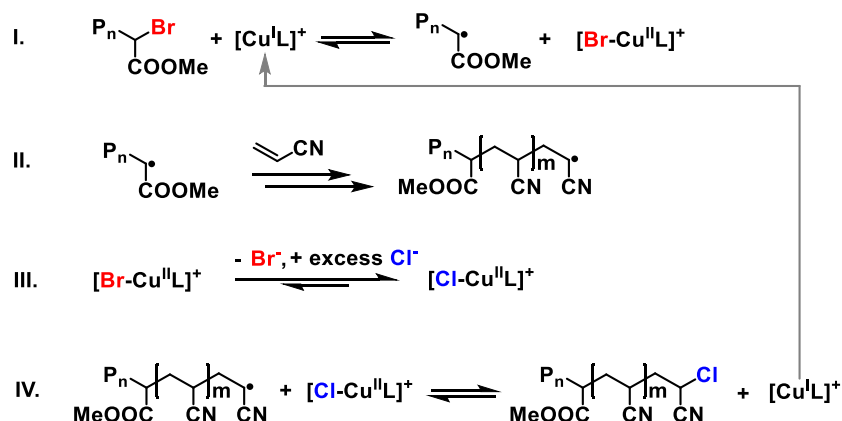


Figure 3.10. (a) Conversion vs. time plot and (b) evolution of M_n and \mathcal{D} with conversion for the potentiostatic eATRP of 50% (v/v) MA in [BMIm][OTf] under ON/OFF toggling. ON: $E_{\text{app}} = E_{1/2} - 0.06$ V; OFF: $E_{\text{app}} = E_{1/2} + 0.20$ V. The dotted line represents theoretical M_n . Reproduced by permission of The Royal Society of Chemistry.

3.2.6 Retention of C-Br functionality: chain extension

To further demonstrate the livingness of the polymerization, a poly(methyl acrylate) macroinitiator (PMA-Br) was extended with acrylonitrile (AN) to prepare a well-defined PMA-*b*-PAN copolymer. The PMA-Br macroinitiator was prepared with the same conditions as reported in Table 3.2, entry 2. Polymerization was stopped at ca. 50% conversion by applying $E_{\text{app}} = E_{1/2} + 0.20$ V to rapidly convert the Cu^{I} to Cu^{II} . Then, the residual monomer was evaporated so that the remaining mixture contained IL, $[\text{Br-Cu}^{\text{II}}\text{TPMA}]^+$, and a well-defined macroinitiator with $M_n = 2.1 \times 10^4$ Da and $\mathcal{D} = 1.16$.

Chain extension of PMA-Br with AN required halogen exchange (HE), i.e. switching from a C-Br to a C-Cl chain-end functionality (Scheme 3.1). The need for HE during chain extension is a consequence of a reactivity mismatch when crossing over from the PMA-Br chain end to the more active PAN-Br chain-end.¹² Propagation from the low fraction of initially formed PMA-*b*-PAN-Br is faster than initiation from the remaining PMA-Br, which results in low efficiency of cross-propagation. To solve this issue, the PAN-Br segment should be converted to a less reactive chain end. Both k_{act} and K_{ATRP} for alkyl chloride (macro)initiators are 1-2 orders of magnitude lower than for alkyl bromides of the same structure. PAN-Cl is activated more slowly than PMA-Br¹², thus R_p is decreased with respect to the rate of initiation from the initially added macroinitiator. This increases the initiation efficiency and enables preparation of a second block with a narrow dispersity. Up to now, preparation of block copolymers via HE was performed using high concentrations of catalyst, i.e. adding an amount of $\text{Cu}^{\text{I}}\text{Cl}/\text{L}$ equal to or higher than the amount of $\text{P}_n\text{-Br}$ chain-end²¹⁻³⁰, which ensured complete conversion of $\text{P}_n\text{-Br}$ to $\text{P}_n\text{-Cl}$. Conversely, HE was demonstrated to be inefficient under low-ppm ARGET ATRP³¹ or photo-ATRP³² conditions. Instead, we envisioned that a catalytic amount of copper complex could efficiently convert Br to Cl in all $\text{P}_n\text{-Br}$ chain ends, provided that a sufficient amount of Cl^- was available. Therefore, we performed a catalytic halogen exchange (cHE) by simply adding an equimolar amount of tetraethylammonium chloride with respect to PMA-Br, exploiting the low-ppm, catalytic amount of $\text{Cu}^{\text{II}}/\text{L}$ already present in the reaction mixture. The proposed mechanism of cHE is presented in Scheme 3.1. Once PMA-Br is activated (step I), the generated radical quickly adds one or more molecules of acrylonitrile, which is present in a large excess in the polymerization mixture (step II). In the presence of excess Cl^- , most of the deactivator complex is present as $[\text{ClCu}^{\text{II}}\text{TPMA}]^+$, due to the excess of Cl^- , but also because of the higher affinity of copper for Cl^- than Br^- ^{11,33,34} (step III). Then, the PAN chain end is preferentially deactivated by $[\text{ClCu}^{\text{II}}\text{T-PMA}]^+$, regenerating the active $[\text{Cu}^{\text{I}}\text{L}]^+$ and a Cl-capped dormant chain (step IV).



Scheme 3.1. Mechanism of catalytic halogen exchange. Reproduced by permission of The Royal Society of Chemistry.

Step IV is in principle in competition with a similar deactivation reaction involving $[\text{BrCu}^{\text{II}}\text{L}]^+$. Nevertheless, the halogen exchange reaction is strongly favored by the much higher concentration of $[\text{ClCu}^{\text{II}}\text{L}]^+$ than the bromide analogue. Indeed, we verified that addition of Cl^- to a solution of $[\text{BrCu}^{\text{II}}\text{L}]^+$ immediately and quantitatively converts the latter to $[\text{ClCu}^{\text{II}}\text{L}]^+$. Therefore, the faster activation of $\text{P}_n\text{-Br}$ than $\text{P}_n\text{-Cl}$ in combination with the faster deactivation of $\text{P}_n\cdot$ by $[\text{ClCu}^{\text{II}}\text{L}]^+$ than $[\text{BrCu}^{\text{II}}\text{L}]^+$ ensured efficient halogen exchange catalyzed by a small amount of catalyst (1/10 with respect to the initial PMA-Br).

At the end of a potentiostatic *e*ATRP of 50% (v/v) MA in $[\text{BMIm}][\text{OTf}]$ the residual monomer was evaporated with a stream of nitrogen at 75 °C. Figure 3.11 shows $^1\text{H-NMR}$ spectra of the reaction mixture before and after MA evaporation, confirming the complete removal of MA as evidenced by the disappearance of the signals of the olefinic protons of methyl acrylate ($\delta = 5.8 - 6.4$ ppm).

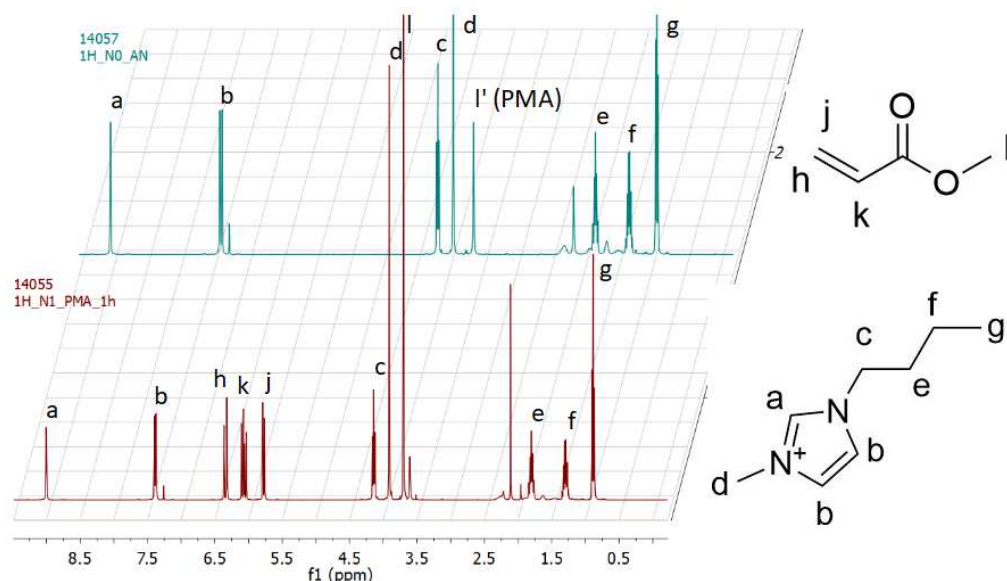


Figure 3.11. *e*ATRP of 50% (v/v) MA in [BMIm][OTf] performed at $E_{app} = E_{1/2} - 0.060$ V. Conditions: $C_{MA}:C_{CuBr_2}:C_{TPMA}:C_{RX} = 552:0.1:0.1:1$, $C_{CuBr_2} = 10^{-3}$ M; $T = 50$ °C. 1 H-NMR spectra of the reaction mixture after 50% conversion, recorded before (—) and after the residual MA evaporation (—). No signals associated to olefinic protons were detected after removal of MA. Reproduced by permission of The Royal Society of Chemistry.

After evaporating the residual monomer, a reversible peak couple was observed in cyclic voltammetry, indicating the stability of the catalyst, $[BrCu^{II}TPMA]^+$ in [BMIm][OTf]/PMA (73% w/w). A voltammogram recorded immediately after addition of Et₄NCl showed complete disappearance of the peak couple of $[BrCu^{II}TPMA]^+$, which was replaced by a new peak couple attributed to $[ClCu^{II}TPMA]^+$ (Figure 3.12). The following equilibria are established when Cl⁻ is added to a solution of $[BrCu^{II}TPMA]^+$:



If $K_{Cl} \gg K_{Br}$, as was previously observed for copper complexes of the same family in acetonitrile², $[ClCu^{II}TPMA]^+$ will be quantitatively formed by substitution of Br⁻ by Cl⁻. The observed disappearance of the peak couple of $[BrCu^{II}TPMA]^+$ confirms that the bromide complex is no longer present in solution. The clean shift of redox potential to more negative values agrees with the electrochemical behavior of Cu catalysts previously studied in [BMIm][OTf].³ Also, $E_{1/2}$ of the new species agrees well with the standard potential of $[ClCu^{II}TPMA]^+$ in [BMIm][OTf].³

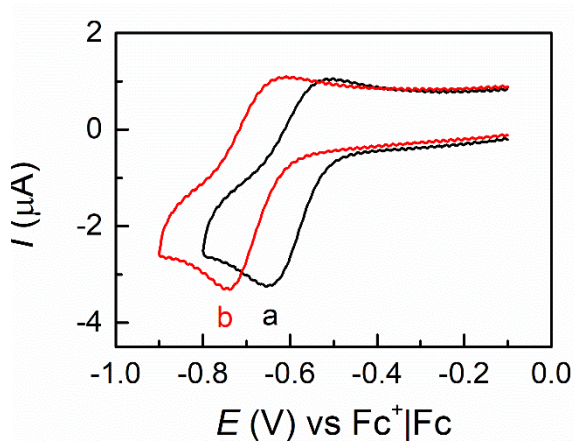


Figure 3.12. Cyclic voltammetry of 1×10^{-3} M $[\text{BrCu}^{\text{II}}\text{TPMA}]^+$ in $[\text{BMIm}][\text{OTf}] + \text{PMA-Br}$ macroinitiator (27% w/w), after *e*ATRP of 50% (v/v) MA and evaporation of residual monomer, recorded at $\nu = 0.2$ V/s in the absence (a) and presence (b) of 0.012 M Et_4NCl . Reproduced by permission of The Royal Society of Chemistry.

To confirm that equilibria (3.5) and (3.6) strongly favor $[\text{ClCu}^{\text{II}}\text{TPMA}]^+$ over the bromide complex, another exchange experiment was performed in $[\text{BMIm}][\text{OTf}]$. A solution of 1.11×10^{-3} M $[\text{ClCu}^{\text{II}}\text{TPMA}]^+$ was prepared in $[\text{BMIm}][\text{OTf}]$ by dissolving equimolar amounts of CuCl_2 and TPMA. As reported previously³, cyclic voltammetry of this solution showed a reversible peak couple due to the reversible one-electron reduction of $[\text{ClCu}^{\text{II}}\text{TPMA}]^+$ to $[\text{ClCu}^{\text{I}}\text{TPMA}]$ (Figure 3.13). Addition of 0.012 Et_4NBr did not significantly affect the voltammetric pattern of the system, which remained essentially the same as that of the $[\text{ClCu}^{\text{II}}\text{TPMA}]^+ / [\text{ClCu}^{\text{I}}\text{TPMA}]^+$ couple. If Br^- exchange with Cl^- were favored, a reversible peak couple with $E_{1/2} = -0.62$ V vs. $\text{Fc}^+|\text{Fc}$ would have appeared after bromide addition. No such a peak couple was observed in the presence of excess Br^- , clearly indicating that $[\text{ClCu}^{\text{II}}\text{TPMA}]^+$ is much more stable than $[\text{BrCu}^{\text{II}}\text{TPMA}]^+$; the arrow in Fig. 3.13 indicates the position of the missing peak couple to be attributed $[\text{BrCu}^{\text{II}}\text{TPMA}]^+$.

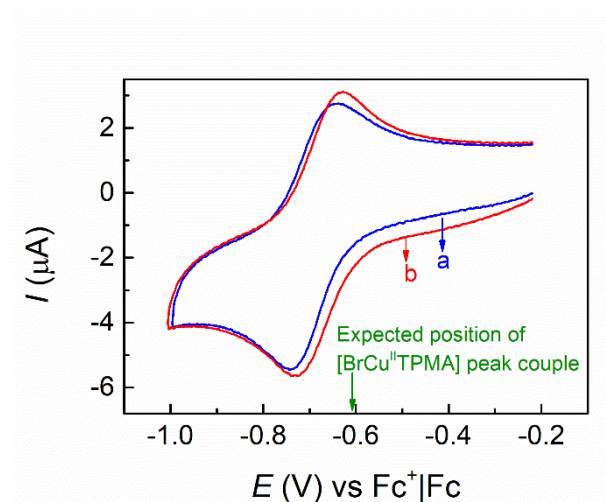


Figure 3.13. Cyclic voltammetry of 1.11×10^{-3} M $[\text{ClCu}^{\text{II}}\text{TPMA}]^+$ in pure $[\text{BMIm}][\text{OTf}]$, recorded at $\nu = 0.2$ V/s in the absence (a) and presence (b) of 0.012 M Et_4NBr . Reproduced by permission of The Royal Society of Chemistry.

Indeed, *e*ATRP of AN with PMA-Br macroinitiator led to the formation of well-defined poly(MA)-*b*-poly(AN)-Cl, with $\mathcal{D} = 1.11$ and a clean shift of the molecular weight to higher values (Figure 3.14a). There was no sign of residual unreacted macroinitiator, indicating complete cross-propagation. To further demonstrate the relevance and effectiveness of the *c*HE, a PMA-Br macroinitiator was chain-extended without adding Et_4NCl . In contrast to the previous results, a bimodal GPC distribution was obtained (Figure 3.14b), composed of the contribution of PMA-*b*-PAN-Br and unreacted PMA-Br. The faster activation of PMA-*b*-PAN-Br with respect to PMA-Br caused inefficient cross-propagation and poor control over macromolecular architecture, confirming that catalytic halogen exchange was necessary and effective.

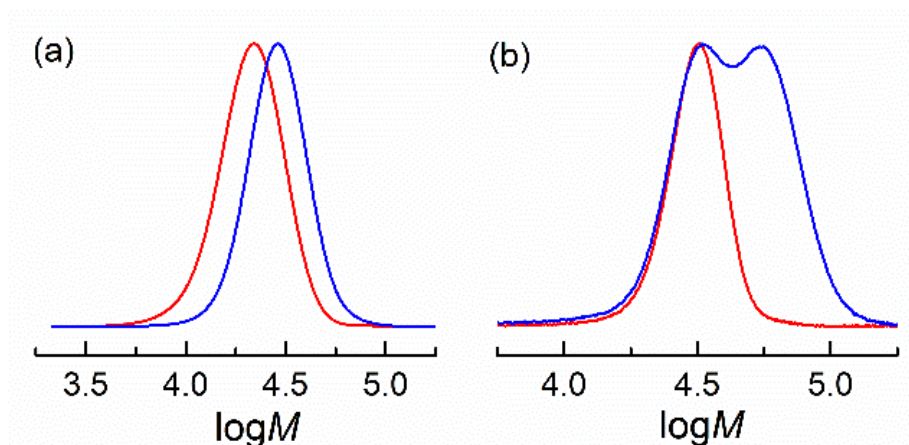


Figure 3.14. *e*ATRP of 50% (v/v) AN in [BMIm][OTf] + PMA-Br macroinitiator performed at $E_{app} = E_{1/2} - 0.06$ V; $C_{AN}:C_{PMA-Br}:C_{CuBr_2}:C_{TPMA}:C_{Et_4NCl} = 760:1:0.1:0.1:1.2$; $C_{CuBr_2} = 10^{-3}$ M. Mw distribution recorded before (—) and after (—) chain extension a) with catalytic halogen exchange or b) without catalytic halogen exchange. The amount of Et_4NCl was equimolar to Br^- present in the system (PMA-Br + $CuBr_2$). Reproduced by permission of The Royal Society of Chemistry.

At the end of the chain extension experiment, the copolymer poly(methyl acrylate)-*b*-poly(acrylonitrile)-Cl was precipitated in water, washed with methanol and dried under high vacuum for several hours. NMR analysis of the isolated polymer (Figure 3.15) confirmed the presence of both poly(methyl acrylate) and polyacrylonitrile blocks.

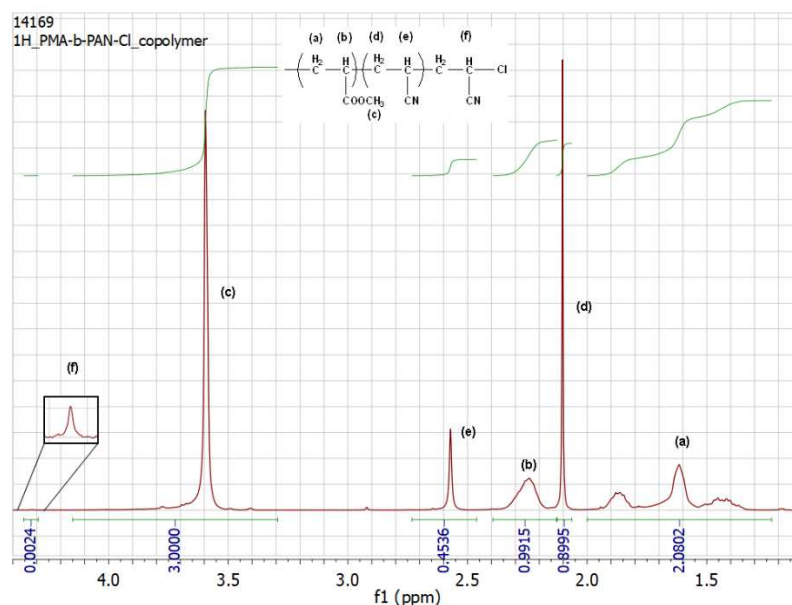


Figure 3.15. 1H -NMR spectrum of poly(methyl acrylate)-*b*-poly(acrylonitrile)-Cl, isolated after chain extension by *c*HE. Relevant peaks have been integrated and associated as indicated in the figure. Reproduced by permission of The Royal Society of Chemistry.

3.2.7 Recycling of IL and catalyst

*e*ATRP in IL can be considered an environmentally friendly process because it requires a low amount of catalyst that is continuously regenerated in the absence of chemical reducing agents. We also tested a procedure to recycle the catalyst in subsequent polymerizations. For this purpose, after a first polymerization, the residual monomer was evaporated, and the polymer was extracted with toluene. Extraction was selective and almost quantitative because toluene is immiscible with [BMIm][OTf]. In addition, [BrCu^{II}TPMA]⁺ quantitatively remained in the IL because it is a very polar catalyst³⁵ with low affinity for non-polar solvents such as toluene. The quantitative recovery of the catalyst was confirmed by cyclic voltammetry (Figure 3.16). GPC analysis of the recycled [BMIm][OTf] showed the presence of a small amount of residual polymer (< 2 mol%) (Figure 3.17). The recycling yield was 90%.

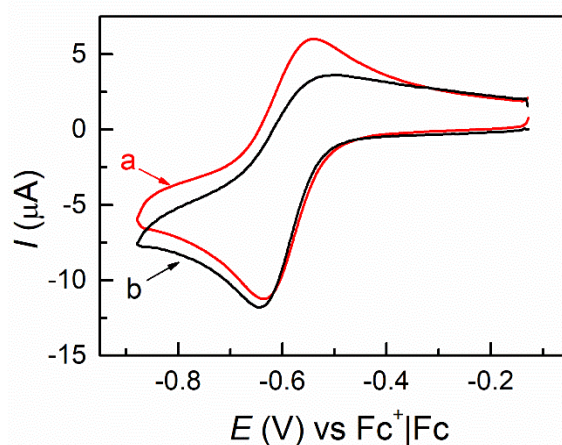


Figure 3.16. Cyclic Voltammetry of 10^{-3} M [BrCu^{II}TPMA]⁺ in 50% (v/v) MA in (a) fresh [BMIm][OTf] or (b) residual IL after *e*ATRP followed by extraction of the polymer in toluene, recorded at 25 °C on a GC electrode at 0.2 V/s. Reproduced by permission of The Royal Society of Chemistry.

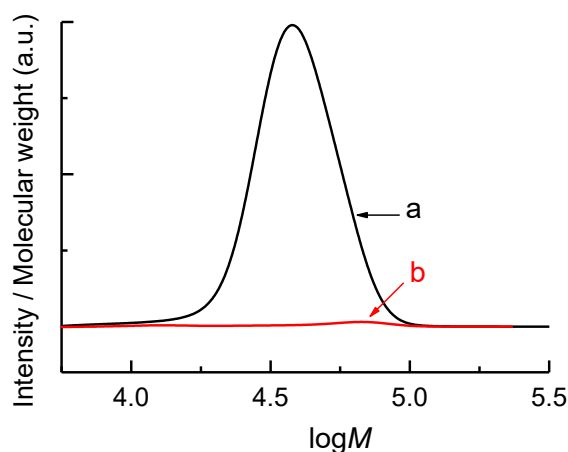


Figure 3.17. MW distribution of [BMIm][OTf] at the end of *e*ATRP of 50% (v/v) MA (a) and after IL recovery by extraction of the polymer. Reproduced by permission of The Royal Society of Chemistry.

After extraction of the polymer, the IL was reused for subsequent polymerizations. *e*ATRP of 50% (v/v) MA in recycled [BMIm][OTf] was comparable to the polymerization in fresh IL (Table 3.5). In recycled [BMIm][OTf], polymerization was fast and controlled, with first-order linear kinetics and linear evolution of M_n as a function of conversion. Actually, *e*ATRP in the recycled IL was somewhat slower but with lower dispersity. This can be due to the presence of excess bromide anions in the polymerization mixture, arising from radical-radical termination occurring during the previous polymerization; it is likely that Br^- ions, present as [BMIm][Br], are not extracted by toluene. Excess bromide anions slow down RX activation reaction^{13,15}, but, in some cases, can increase polymerization control.¹⁷ Bromide anions can be extracted from ILs by electro-oxidation on an Ag wire.³⁶

Table 3.4. *e*ATRP of 50% (v/v) MA with Pristine or Recycled [BMIm][OTf], $E_{\text{app}} = E_{1/2} - 0.06 \text{ V}$, $T = 50 \text{ }^\circ\text{C}$.^a

| IL | t (h) | Conv. (%) | $k_p^{\text{app } b}$ (h^{-1}) | Q^c (C) | M_n^{th} | M_n^{app} | D |
|----------|------------|--------------|--|--------------|-------------------|--------------------|------|
| Pristine | 1.75 | 93 | 2.6 | 3.0 | 44200 | 44200 | 1.17 |
| Recycled | 2.00 | 94 | 2.1 | 2.6 | 44700 | 55000 | 1.10 |

^a Conditions: $C_{\text{MA}}:C_{\text{CuBr}_2}:C_{\text{TPMA}}:C_{\text{RX}} = 552:0.1:0.1:1$, $C_{\text{Cu}} = 10^{-3} \text{ M}$; $V_{\text{tot}} = 5 \text{ mL}$. ^bThe slope of the $\ln([M]_0/[M])$ vs. t plot. ^cTotal consumed charge.

3.3 Conclusions

[BMIm][OTf] is an appropriate solvent for *e*ATRP. [BrCu^ITPMA]⁺ was stable in the ionic liquid as well as in its mixtures with MA and PMA. Supporting electrolytes were not necessary because of the sufficient conductivity of the IL, allowing for a cleaner polymerization media.

A wide range of reaction conditions was explored. The best applied potential was found to be $E_{app} = E_{1/2} - 0.06$ V, which established a Cu^I/Cu^{II} ratio ~10 at the electrode. A temperature range from 25 °C to 75 °C was investigated showing that polymerization was always well-controlled, although the reaction rate increased at higher temperatures owing to faster propagation rate and more efficient mass transport. Catalyst concentration could be as low as 45 ppm with respect to monomer on molar basis, whereas degree of polymerization was varied up to *ca.* 828. Good control and almost quantitative conversions in *ca.* 1 h were obtained under appropriate conditions. Finally, application of a more simplified electrochemical setup based on galvanostatic conditions gave results well matching those of potentiostatic *e*ATRP.

The polymerization can be quickly switched between active and dormant states by cycling E_{app} between $E_{app} < E_{1/2}$ and $E_{app} \gg E_{1/2}$. No polymerization occurred when $E_{app} = E_{1/2} + 0.20$ V was applied, while M_n linearly increased with conversion when polymerization was started again at $E_{app} = E_{1/2} - 0.06$ V, clearly demonstrating retention of C-X chain end. Livingness and chain end fidelity were further proved by chain extension of a PMA-Br macroinitiator with acrylonitrile. Chain extension was performed for the first time by ‘catalytic halogen exchange’, i.e. using an amount of catalyst typical of low-ppm systems together with an amount of Cl⁻ equimolar to the PMA-Br macroinitiator. The resulting PMA-*b*-PAN-Cl was well-controlled and soluble in [BMIm][OTf].

The IL and catalyst could be recycled with 90% yield of solvent and negligible catalyst loss. *e*ATRP in recycled ionic liquid proceeded to high conversion with even improved control and no impurities were detected in the isolated polymer after extraction with toluene.

Overall, *e*ATRP in [BMIm][OTf] well-matched polymerizations in traditional molecular solvents such as acetonitrile. However, ILs offer unique and desirable features that molecular solvents do not possess.

References

1. Egorova, K. S.; Ananikov, V. P. Which Metals Are Green for Catalysis? Comparison of the Toxicities of Ni, Cu, Fe, Pd, Pt, Rh, and Au Salts. *Angewandte Chemie International Edition*. **2016**, *55*, 12150–12162.
2. Zhang, S.; Sun, N.; He, X.; Lu, X.; Zhang, X. Physical Properties of Ionic Liquids: Database and Evaluation. *Journal of Physical and Chemical Reference Data*. **2006**, *35*, 1475–1517.
3. Biedron, T.; Kubisa, P. Ionic Liquids as Reaction Media for Polymerization Processes: Atom Transfer Radical Polymerization (ATRP) of Acrylates in Ionic Liquids. *Polymer International* **2003**, *52*, 1584–1588.
4. Carmichael, A. J.; Haddleton, D. M.; Bon, S. A. F.; Seddon, K. R. Copper(I) Mediated Living Radical Polymerisation in an Ionic Liquid. *Chemical Communications* **2000**, *14*, 1237–1238.
5. Chen, H.; Liang, Y.; Liu, D.; Tan, Z.; Zhang, S.; Zheng, M.; Qu, R. AGET ATRP of Acrylonitrile with Ionic Liquids as Reaction Medium without Any Additional Ligand. *Material Science and Engineering C* **2010**, *30*, 605–609.
6. Nguyen, V. H.; Shim, J.-J. Ionic Liquid-Mediated Synthesis and Self-Assembly of Poly(Ethylene Glycol)-Block-Polystyrene Copolymer by ATRP Method. *Colloid Polymer Science* **2015**, *293*, 617–623.
7. Ma, H.; Wan, X.; Chen, X.; Zhou, Q. Reverse Atom Transfer Radical Polymerization of Methyl Methacrylate in Imidazolium Ionic Liquids. *Polymer* **2003**, *44*, 5311–5316.
8. Padiuszyński, K.; Domańska, U. A New Group Contribution Method For Prediction of Density of Pure Ionic Liquids over a Wide Range of Temperature and Pressure. *Industrial & Engineering Chemistry Research* **2012**, *51*, 591–604.
9. Lanzalaco, S.; Fantin, M.; Scialdone, O.; Galia, A.; Isse, A. A.; Gennaro, A.; Matyjaszewski, K. Atom Transfer Radical Polymerization with Different Halides (F, Cl, Br, and I): Is the Process “Living” in the Presence of Fluorinated Initiators? *Macromolecules* **2016**, *50*, 192–202.
10. Tsarevsky, N. V.; Braunecker, W. A.; Vacca, A.; Gans, P.; Matyjaszewski, K. Competitive Equilibria in Atom Transfer Radical Polymerization. *Macromolecular Symposia* **2007**, *248*, 60–70.
- (11) Lorandi, F.; De Bon, F.; Fantin, M.; Isse, A. A.; Gennaro, A. Electrochemical Characterization of Common Catalysts and Initiators for Atom Transfer Radical Polymerization in [BMIm][OTf]. *Electrochemistry communications* **2017**, *77*, 116–119.
- (12) Fantin, M.; Isse, A. A.; Bortolamei, N.; Matyjaszewski, K.; Gennaro, A. Electrochemical Approaches to the Determination of Rate Constants for the Activation Step in Atom Transfer Radical Polymerization. *Electrochimica Acta* **2016**, *222*, 393–401.
- (13) Lorandi, F.; Fantin, M.; Isse, A. A.; Gennaro, A. RDRP in the Presence of Cu⁰: The Fate of Cu(I) Proves the Inconsistency of SET-LRP Mechanism.

- Polymer* **2015**, *72*, 238–245.
- (14) Fantin, M.; Isse, A. A.; Matyjaszewski, K.; Gennaro, A. ATRP in Water: Kinetic Analysis of Active and Super-Active Catalysts for Enhanced Polymerization Control. *Macromolecules* **2017**, *50*, 2696–2705.
 - (15) De Paoli, P.; Isse, A. A.; Bortolamei, N.; Gennaro, A. New Insights into the Mechanism of Activation of Atom Transfer Radical Polymerization by Cu(I) Complexes. *Chemical Communications* **2011**, *47*, 3580.
 - (16) Okoturo, O. O.; Van der Noot, T. J. Temperature Dependence of Viscosity for Room Temperature Ionic Liquids. *Journal of Electroanalytical Chemistry* **2004**, *568*, 167–181.
 - (17) Lorandi, F.; Fantin, M.; Isse, A. A.; Gennaro, A. Electrochemically Mediated Atom Transfer Radical Polymerization of n-Butyl Acrylate on Non-Platinum Cathodes. *Polymer Chemistry* **2016**, *7*, 5357–5365.
 - (18) Pan, X.; Malhotra, N.; Simakova, A.; Wang, Z.; Konkolewicz, D.; Matyjaszewski, K. Photoinduced Atom Transfer Radical Polymerization with ppm-Level Cu Catalyst by Visible Light in Aqueous Media. *Journal of the American Chemical Society* **2015**, *137*, 15430–15433.
 - (19) Simakova, A.; Averick, S. E.; Konkolewicz, D.; Matyjaszewski, K. Aqueous ARGET ATRP. *Macromolecules* **2012**, *45*, 6371–6379.
 - (20) Mohapatra, H.; Kleiman, M.; Esser-Kahn, A. P. Mechanically Controlled Radical Polymerization Initiated by Ultrasound. *Nature Chemistry* **2017**, *9*, 135–139.
 21. Siegwart, D. J.; Wu, W.; Mandalaywala, M.; Tamir, M.; Sarbu, T.; Silverstein, M. S.; Kowalewski, T.; Hollinger, J. O.; Matyjaszewski, K. Solvent Induced Morphologies of Poly(Methyl Methacrylate-*b*-Ethylene Oxide-*b*-Methyl Methacrylate) Triblock Copolymers Synthesized by Atom Transfer Radical Polymerization. *Polymer* **2007**, *48*, 7279–7290.
 22. Kadayifçioğlu, N.; Acar, H. Y. Synthesis of Poly(2-Acetamidoacrylic Acid) and its PEGMA Block Copolymer via ATRP in Water. *European Polymer Journal* **2013**, *49*, 3366–3376.
 23. Wu, L.; Glebe, U.; Böker, A. Synthesis of Hybrid Silica Nanoparticles Densely Grafted with Thermo and pH Dual-Responsive Brushes via Surface-Initiated ATRP. *Macromolecules* **2016**, *49*, 9586–9596.
 24. Simula, A.; Anastasaki, A.; Haddleton, D. M. Methacrylic Zwitterionic, Thermoresponsive, and Hydrophilic (Co)Polymers via Cu(0)-Polymerization: The Importance of Halide Salt Additives. *Macromolecular Rapid Communications* **2016**, *37*, 356–361.
 25. Dufour, B.; Koynov, K.; Pakula, T.; Matyjaszewski, K. PBA-PMMA 3-Arm Star Block Copolymer Thermoplastic Elastomers. *Macromolecular Chemistry and Physics* **2008**, *209*, 1686–1693.
 26. Höhne, S.; Uhlmann, P. Synthesis of Functional Block Copolymers and Terpolymers Containing Polyglycidyl Methacrylate Blocks. *Journal of Polymer Science Part A: Polymer Chemistry* **2015**, *53*, 675–684.
 27. Tsarevsky, N. V.; Sarbu, T.; Göbelt, B.; Matyjaszewski, K. Synthesis of Styrene–Acrylonitrile Copolymers and Related Block Copolymers by Atom Transfer Radical Polymerization. *Macromolecules* **2002**, *35*, 6142–6148.
 28. Ramakrishnan, A.; Dhamodharan, R. Facile Synthesis of ABC and CBABC Multiblock Copolymers of Styrene, Tert-Butyl Acrylate, and Methyl

- Methacrylate via Room Temperature ATRP of MMA. *Macromolecules* **2003**, *36*, 1039–1046.
29. Qin, S.; Saget, J.; Pyun, J.; Jia, S.; Kowalewski, T.; Matyjaszewski, K. Synthesis of Block, Statistical, and Gradient Copolymers from Octadecyl (Meth)Acrylates Using Atom Transfer Radical Polymerization. *Macromolecules* **2003**, *36*, 8969–8977.
 30. Dufour, B.; Tang, C.; Koynov, K.; Zhang, Y.; Pakula, T.; Matyjaszewski, K. Polar Three-Arm Star Block Copolymer Thermoplastic Elastomers Based on Polyacrylonitrile. *Macromolecules* **2008**, *41*, 2451–2458.
 31. Aitchison, T. J.; Ginic-markovic, M.; Clarke, S.; Valiyaveetil, S. Initiation Issues with Block Copolymer Formation Using ARGET ATRP. *Macromolecular Chemistry and Physics* **2012**, *213*, 79–86.
 32. Chuang, Y.; Wenn, B.; Gielen, S.; Ethirajan, A.; Junkers, T. Ligand Switch in Photoinduced Copper-Mediated Polymerization: Synthesis of Methacrylate–acrylate Block Copolymers. *Polymer Chemistry* **2015**, *6*, 6488–6497.
 33. Fantin, M.; Isse, A. A.; Gennaro, A.; Matyjaszewski, K. Understanding the Fundamentals of Aqueous ATRP and Defining Conditions for Better Control. *Macromolecules* **2015**, *48*, 6862–6875.
 34. Bortolamei, N.; Isse, A. A.; Di Marco, V. B.; Gennaro, A.; Matyjaszewski, K. Thermodynamic Properties of Copper Complexes Used as Catalysts in Atom Transfer Radical Polymerization. *Macromolecules* **2010**, *43*, 9257–9267.
 35. Fantin, M.; Park, S.; Wang, Y.; Matyjaszewski, K. Electrochemical Atom Transfer Radical Polymerization in Miniemulsion with a Dual Catalytic System. *Macromolecules* **2016**, *49*, 8838–8847.
 36. Arnaboldi, S.; Magni, M.; Mussini, P. R.; Gennaro, A.; Isse, A. A. “egg of Columbus”: Single-Step Complete Removal of Chloride Impurities from Ionic Liquids by AgCl Deposition on Silver Electrode. *Electrochemistry communications* **2015**, *51*, 46–49.

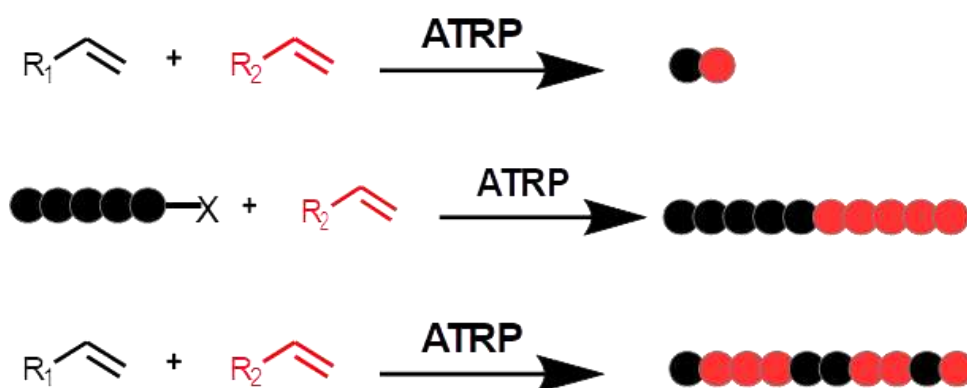
Chapter 4

Electrochemically mediated ATRP for the preparation of block copolymers: from traditional approaches to catalytic halogen exchange

4.1 Introduction

The range of polymers that can be prepared by a well-controlled ATRP nowadays includes materials with almost all desired distribution of monomers along the backbone, or within any specific segment in a copolymer. Hence, ATRP affords homopolymers, as well as random, gradient, block, graft, brush and star copolymers. Linear copolymers are a broad family of macromolecules that can be prepared *via* spontaneous or sequential ATRP of two or more monomers, with precise control of molar mass, composition and functionality.^{1,2} The use of a difunctional initiator allowed, for the first time in a radical process, the preparation of functional homotelechelic polymers with almost any desired chain end functionality.³

The reactivity ratio of the comonomers in ATRP are very similar to those of FRC (Free Radical Copolymerization) although some factors that affect CRP processes can result in different rates of consumption of comonomers.⁴

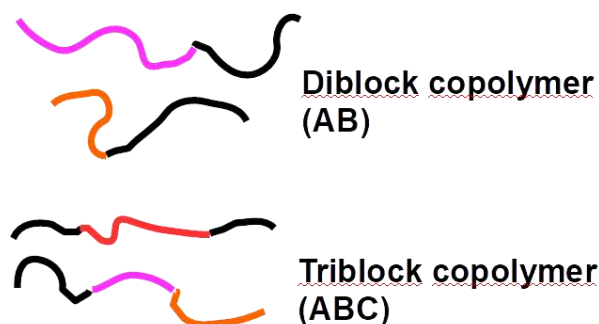


Scheme 4.1. Mechanism of radical copolymerization: statistical, block and gradient (from top to bottom).

Random (or statistical) copolymers can be prepared by ATRP of two monomers together, when there is essentially random incorporation of them into the macromolecule. This type of copolymer is formed in radical copolymerization when the reactivity ratio of the comonomers is close to one.^{5,6} The chemical composition of random copolymers prepared by ATRP is like that formed in a standard FRC.⁴ In the past, ARGET ATRP reduced catalyst-based side reactions, enabling the synthesis of high MW styrene/acrylonitrile copolymers.⁷ When the reactivity of the comonomers differs, there is preferential incorporation of one monomer. In such cases, spontaneous gradient copolymers are formed in a one-pot reaction.

Gradient copolymers are a special family of copolymers that got increasing importance with the development of ATRP. In contrast to standard FRC, as the polymerization proceeds the composition of the copolymer changes; the composition of copolymer formed at later stages of the reaction differs from that prepared at the beginning. In a CRP, variation in the rate of incorporation of the monomers into the copolymer is reflected as a change, or tapering, in composition of the monomer units along the backbone of each chain. Gradient copolymers can be prepared by copolymerization of a selected mole ratio of monomers with sufficiently different reactivity ratios or by controlled feeding of one monomer. Gradient copolymers prepared by a CRP differ from the tapered copolymers prepared by living anionic processes⁸ which can be described as multi-block copolymers with blocks of different compositions. True gradient copolymers can only be obtained in systems providing fast initiation, uniform chain growth, and easy cross-propagation.

Block copolymers are normally prepared by controlled polymerization of one monomer, followed by chain extension with a second monomer to form AB or ABC block copolymers.⁹ When ATRP is employed to form each block, the composition and molecular weight and, to some extent, the dispersity of each block can be independently controlled. Multifunctional initiators can also be used in the process to prepare ABA or AB-star multi-armed block copolymers.¹⁰



Scheme 4.2. Examples of linear block copolymers.

Macroinitiators can be prepared by any polymerization process including FRP¹¹ and controlled polymerization processes. Block copolymers (BCPs) find applications in thermoplastic elastomers¹² and as precursors for carbon nanostructures.¹³ Indeed, one material can meet the requirements of both applications.¹⁴ With the development of CRP it has been determined that the properties of the materials targeting thermoplastic elastomer applications can be significantly affected by the mode of (co)polymerization of the second block.¹² In a continuous ATRP copolymerization, the fraction of the first comonomer available for incorporation into the second block significantly modifies the properties of the final material by preparation of a gradient copolymer segment in the second block.^{15,16} The formation of gradient copolymer A-block affects phase separation.

Block copolymers containing acrylonitrile are widely used. The synthesis of polyacrylonitrile (PAN) with precisely defined morphology is essential to obtain a polymer precursor for the preparation of high-value carbon-based materials. PAN is a fundamental polymer precursor for preparing carbon-fiber composites and mesoporous carbons.¹⁷⁻¹⁸ High-molecular-weight (high-MW) PAN, with precise architecture, is necessary to produce fibers with high mechanical and chemical resistance.¹⁹⁻²⁰ Concerning porous carbons, BCPs with defined morphology, composed of PAN and a sacrificial block, serve as a template for high surface area nanocarbons, containing easily accessible redox-active N-sites. These copolymer templated nitrogen-enriched nanocarbons (CTNCs) showed exceptional efficiency as catalysts for oxygen reduction reaction (ORR)²¹ and hydrogen evolution reaction²², as sorbents of CO₂²³, Cr(VI), and U(VI)²⁴, and as electrodes for supercapacitors²⁵, and dye synthesized solar cells.²⁶ To produce high-performing

carbon materials, pre-determined MWs and microstructure must be achieved during AN polymerization, thus excluding the use of conventional radical polymerization. ATRP is the primary technique for the preparation of polymers and copolymers with defined compositions and architectures. Nevertheless, first ATRP studies on AN showed poor chain-end functionality.^{10,27} It was proposed that Cu catalysts react with growing PAN chains *via* an outer-sphere electron transfer, thus reducing radicals to carbanions, thereby broadening the molecular weight distribution and leading to loss of halide chain-end functionality. These side reactions are detrimental to the polymerization process, preventing the possibility of reaching high MWs and building block copolymers through chain extension. Low catalyst loadings dramatically decreased the extent of side reactions in ATRP of AN.²⁸ Moreover, diminishing Cu content is beneficial for CTNC production, whereby the residual metal might mask the electrocatalytic activity of the material.²⁹ Therefore, PAN homopolymers and copolymers were successfully obtained by using various radical initiators and/or reducing agents for Cu^I regeneration.²⁸⁻³³ Electrochemical stimuli (*i.e.* applied current or potential) can also be used to reduce the accumulated Cu^{II} species, with the unique advantage of avoiding the formation of by-products, because electrons are used in lieu of chemical reducing agents.³⁴⁻³⁵ Moreover, the ratio between Cu^{II} deactivator and Cu^I species is fixed by the applied potential or current, thus it can be finely tuned by modulating the electrochemical stimulus. *e*ATRP was applied to several monomers in organic solvents³⁶⁻³⁷, water (at both neutral and very acidic pH³⁸⁻³⁹), oil-in-water miniemulsion⁴⁰ and ionic liquids.⁴¹ However, the *e*ATRP of acrylonitrile has never been reported.

This chapter describes the synthesis of well-controlled PAN homopolymers, prepared *via e*ATRP catalyzed by Cu/TPMA. Second, catalytic halogen exchange (*c*HE) is introduced to build block copolymers of different compositions, in both organic and aqueous media. The versatility of *c*HE will be highlighted as a convenient and promising alternative for the preparation of well-defined block copolymers.

4.1.1 The traditional route of synthesis: from PAN-Br to block copolymers

The redox properties of the Cu complexes used as *e*ATRP catalysts were first investigated. Convenient polymerization conditions were identified by varying the applied potential, initiator nature, monomer and catalyst loading, and targeted molecular weight (MW). A short PAN was extended with butyl acrylate, forming a well-defined PAN-*b*-PBA-Br copolymer. The high activity of the catalyst enabled relatively fast polymerizations with low catalyst loadings (≤ 164 ppm on molar basis with respect to monomer). This copper complex was previously considered too active for ATRP of AN with Cu^0 as reducing agent and supplemental activator (SARA ATRP),²⁹ whereas it proved to be a good catalyst in initiators for continuous activator re-generation (ICAR) ATRP of AN, with azobis-isobutyronitrile (AIBN) as radical initiator.³² This big difference of catalyst behavior in the two ATRP techniques was attributed to different activation kinetics. The rate of ICAR ATRP depends strongly on AIBN decomposition, which is relatively slow. On the other hand, in SARA ATRP both Cu^0 and Cu^{I} , generated by relatively fast comproportionation between Cu^0 and Cu^{II} , can activate the dormant species ($\text{P}_n\text{-X}$). Thus, in SARA ATRP less active catalysts had to be employed, at the expense of the reaction rate, to avoid excessive generation of propagating radicals.²⁹ Herein, the applied potential was tuned to ensure the presence of a sufficient amount of Cu^{II} deactivator, enabling the use of such an active catalyst, and therefore shortening the reaction time. The effects of monomer loading and nature of alkyl halide initiator (RX) were investigated. High-MW PAN ($M_n = 91\text{k}$) was prepared in only 3 h. The good retention of chain-end functionality was proved by extending a PAN-Br macroinitiator with butyl acrylate (BA), obtaining PAN-*b*-PBA-Br copolymer with $D = 1.11$. *e*ATRP conditions were arranged to prepare a suitable precursor for CTNCs. Indeed, PAN-based block with ~ 40 wt% AN were demonstrated to possess a bicontinuous morphology, which is essential to avoid the collapse of the nanostructure during the pyrolysis of the copolymer.^{23,29,42}

4.1.1. Electrochemical characterization of $[\text{Cu}^{\text{II}}\text{TPMA}]^{2+}$ and $[\text{XCu}^{\text{II}}\text{TPMA}]^+$

The redox properties of the Cu complex selected as a catalyst for the *e*ATRP of AN were investigated by cyclic voltammetry. Analyzed binary and ternary complexes were generated *in situ*, by consecutive additions of a Cu salt with a non-coordinating anion, the amine ligand (TPMA), and a tetraethylammonium salt (Et_4NX) as a source of bromide or chloride ions.

$[\text{Cu}^{\text{II}}\text{TPMA}]^{2+}$ exhibited a quasi-reversible behavior in both DMF and DMSO (Figure 4.1a). Typical ATRP ligands strongly bind to Cu ions, with the formation of complexes of higher stability for Cu^{II} than Cu^{I} .⁴³⁻⁴⁴ Therefore, addition of TPMA to a solution of the Cu^{II} salt shifted the standard reduction potential of the $\text{Cu}^{\text{II}}/\text{Cu}^{\text{I}}$ couple toward more negative values. This potential shift allowed to measure the ratio between the stability constants of $[\text{Cu}^{\text{II}}\text{TPMA}]^{2+}$ and $[\text{Cu}^{\text{I}}\text{TPMA}]^+$, β^{II} and β^{I} , respectively (Table 4.1), according to the following equation:

$$E_{[\text{Cu}^{\text{II}}\text{TPMA}]^{2+}/[\text{Cu}^{\text{I}}\text{TPMA}]^+}^{\circ} = E_{\text{Cu}^{2+}/\text{Cu}^+}^{\circ} - \frac{RT}{F} \ln \frac{\beta^{\text{II}}}{\beta^{\text{I}}} \quad (4.1)$$

The standard reduction potentials in Table 4.1 were determined from the half-wave potential, as $E^{\circ} \approx E_{1/2} = (E_{\text{pa}} + E_{\text{pc}})/2$, where E_{pa} and E_{pc} are the anodic and cathodic peak potentials, respectively.

In the presence of halide ions, the ternary complexes $[\text{XCu}^{\text{II}}\text{TPMA}]^+$ ($\text{X} = \text{Cl}$ or Br) formed, exhibiting reduction potentials more negative than that of the binary complex $[\text{Cu}^{\text{II}}\text{TPMA}]^{2+}$ (Table 4.1 and Figure 4.1a), because of the greater affinity of X^- for Cu^{II} than for Cu^{I} .⁴³ The ratio between the thermodynamic association constants of X^- to Cu^{II} and Cu^{I} , *i.e.* $K_{\text{X}}^{\text{II}}/K_{\text{X}}^{\text{I}}$, was calculated from the shift of E° according to Eq. (4.2):

$$E_{[\text{XCu}^{\text{II}}\text{TPMA}]^+ / [\text{XCu}^{\text{I}}\text{TPMA}]}^{\circ} = E_{[\text{Cu}^{\text{II}}\text{TPMA}]^{2+} / [\text{Cu}^{\text{I}}\text{TPMA}]^+}^{\circ} - \frac{RT}{F} \ln \frac{K_{\text{X}}^{\text{II}}}{K_{\text{X}}^{\text{I}}} \quad (4.2)$$

$E_{[\text{ClCu}^{\text{II}}\text{TPMA}]^+ / [\text{ClCu}^{\text{I}}\text{TPMA}]}^{\circ} < E_{[\text{BrCu}^{\text{II}}\text{TPMA}]^+ / [\text{BrCu}^{\text{I}}\text{TPMA}]}^{\circ}$ because of the stronger association of Cl^- to Cu complexes, if compared to Br^- . Consequently, $K_{\text{Cl}}^{\text{II}}/K_{\text{Cl}}^{\text{I}} > K_{\text{Br}}^{\text{II}}/K_{\text{Br}}^{\text{I}}$.

In the presence of monomer (AN 20 vol%), reduction potentials of both binary and ternary complexes slightly shifted toward more positive values (Table 4.1, entries 2 and 5 and Figure 4.1b), due to the variation of solvent polarity.⁴⁵ Trends in E° values observed in pure solvents remained the same in solvent/monomer mixtures: $E^\circ_{[\text{ClCu}^{\text{II}}\text{TPMA}]^+ / [\text{ClCu}^{\text{I}}\text{TPMA}]} < E^\circ_{[\text{BrCu}^{\text{II}}\text{TPMA}]^+ / [\text{BrCu}^{\text{I}}\text{TPMA}]} < E^\circ_{[\text{Cu}^{\text{II}}\text{TPMA}]^{2+} / [\text{Cu}^{\text{I}}\text{TPMA}]^+} \ll E^\circ_{\text{Cu}^{2+} / \text{Cu}^+}$.

Standard potentials of Cu complexes were also measured under typical polymerization conditions, *i.e.* at $T = 60^\circ\text{C}$, in DMF and DMSO mixtures with 20 vol% AN (Table 4.1, entries 3 and 6, Figure 4.1c). The temperature increase generally shifted E° values to slightly more positive potentials, as previously reported.⁴⁶ To summarize, the redox properties of $[\text{XCu}^{\text{II}}\text{TPMA}]^+$ in both DMF and DMSO, and their mixtures with acrylonitrile followed the expected behavior for ATRP catalysts in organic media (Table 4.1).

Table 4.1. Thermodynamic data for the Cu/TPMA/X system measured by cyclic voltammetry in various environments.^a

| Entry | Solvent or solvent/AN (v/v) | T (°C) | Cu ²⁺ /Cu ⁺ | | [Cu ^{II} L] ²⁺ /[Cu ^I L] ⁺ | | [BrCu ^{II} L] ⁺ /[BrCu ^I L] | | [ClCu ^{II} L] ⁺ /[ClCu ^I L] | |
|-------|-----------------------------|----------|-----------------------------------|---------------|--|---------------|--|---------------|--|--|
| | | | E° (V) | E° (V) | $\beta^{\text{II}}/\beta^{\text{I}}$ | E° (V) | $K_{\text{Br}}^{\text{II}}/K_{\text{Br}}^{\text{I}}$ | E° (V) | $K_{\text{Cl}}^{\text{II}}/K_{\text{Cl}}^{\text{I}}$ | |
| 1 | DMF | 25 | -0.486 | -0.621 | 1.9×10^2 | -0.708 | 29.7 | -0.789 | 6.9×10^2 | |
| 2 | DMF/AN (4/1) | 25 | -0.260 | -0.513 | 1.9×10^4 | -0.698 | 1.3×10^3 | -0.727 | 4.1×10^3 | |
| 3 | DMF/AN (4/1) | 60 | -0.237 | -0.636 | 1.09×10^6 | -0.648 | 1.5 | - | - | |
| 4 | DMSO | 25 | -0.421 | -0.608 | 1.5×10^3 | -0.682 | 17.8 | -0.760 | 3.7×10^2 | |
| 5 | DMSO/AN(4/1) | 25 | -0.339 | -0.534 | 2.0×10^3 | -0.648 | 84.8 | -0.740 | 3.0×10^3 | |
| 6 | DMSO/AN(4/1) | 60 | -0.182 | -0.515 | 1.09×10^5 | -0.639 | 7.5×10^1 | -0.722 | 1.4×10^3 | |

^aRecorded at a GC working electrode, in the presence of 0.1 M Et₄NBF₄ as supporting electrolyte. All potentials are referred to the ferrocenium/ferrocene redox couple. Reprinted with permission, Copyright 2018 Elsevier.

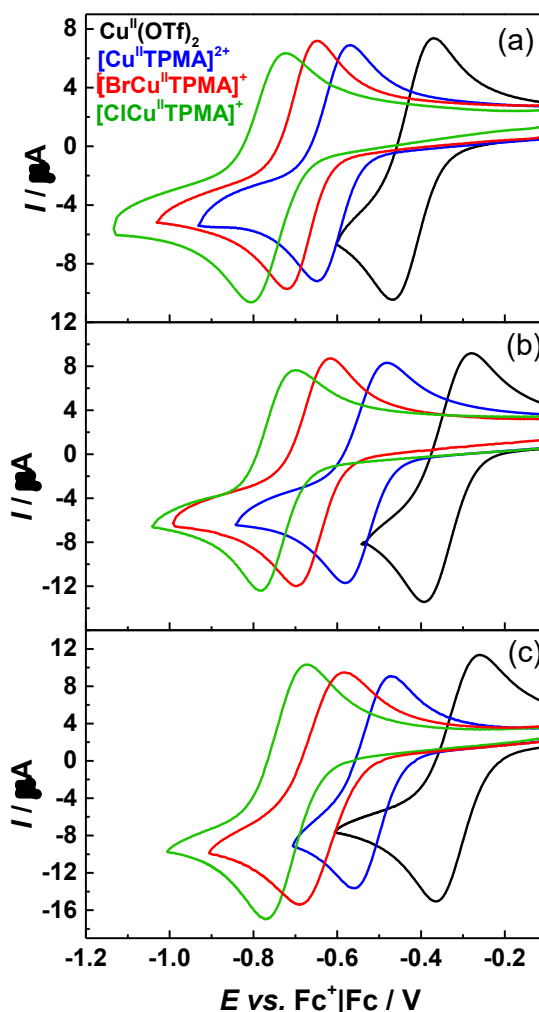


Figure 4.1. Cyclic voltammetry of 10^{-3} M $\text{Cu}^{\text{II}}(\text{OTf})_2$ in the absence and presence of 10^{-3} M TPMA, and 2×10^{-3} M Et_4NBr or Et_4NCl , in DMSO at $T = 25\text{ }^{\circ}\text{C}$ (a) and in DMSO/AN 4/1 (v/v) at $T = 25\text{ }^{\circ}\text{C}$ (b), and $T = 60\text{ }^{\circ}\text{C}$ (c). CVs were recorded on a GC disk, at $\nu = 0.2\text{ V s}^{-1}$, with 0.1 M Et_4NBF_4 as supporting electrolyte. Reprinted with permission, Copyright 2018 Elsevier.

4.1.2. Electrochemically mediated ATRP of acrylonitrile

Electrochemically mediated ATRP of AN was first attempted in DMF, under potentiostatic conditions at $T = 60\text{ }^{\circ}\text{C}$. 2-bromopropionitrile (BPN) which mimics the structure of AN monomer, was used as initiator. Regardless the E_{app} value, generated PAN showed $\bar{D} > 1.5$ and experimental molecular weights were higher than theoretical values, indicating no control over the polymerization (Table 4.2).

Table 4.2 *e*ATRP of 20 vol% AN in DMF at different applied potentials.^a

| Entry | E_{app} (V) | t (h) | Conv. (%) | k_p^{app} (h ⁻¹) | $M_n^{th} \times 10^{-3}$ | $(M_n^{app}/2.5) \times 10^{-3}$ | \bar{D} |
|-------|---------------------|------------|--------------|--------------------------------|---------------------------|----------------------------------|-----------|
| 1 | $E_{1/2}$ | 3.3 | 47 | 0.34 | 7.7 | 20.0 | 1.63 |
| 2 | $E_{1/2} +$ 0.06 | 5.3 | 47 | 0.23 | 7.7 | 15.2 | 1.55 |

^a0.1 M Et₄NBF₄, $C_{AN}/C_{BPN}/C_{Cu^{II}Br_2}/C_{TPMA} = 300/1/0.1/0.1$, $C_{Cu^{2+}} = 10^{-3}$ M; $V_{tot} = 5$ mL, $T = 60$ °C.

Reprinted with permission, Copyright 2018 Elsevier.

However, E_{app} affected the polymerization rate. A slower process was observed with $E_{app} = E_{1/2} + 0.06$ V, compared to $E_{app} = E_{1/2}$ ($k_p^{app} = 0.23$ vs. 0.34), because the concentration of active Cu^I catalyst was 10-fold smaller at the higher potential, according to Eq. (4.3):

$$E_{app} = E_{1/2} \mp \frac{RT}{F} \ln \frac{C_{[BrCu^{II}TPMA]^+}}{C_{[BrCu^{I}TPMA]}} \quad (4.3)$$

It should be noted that significantly overestimated M_n values of PAN are typically obtained by gel permeation chromatography (GPC) measurements with DMF as eluent and calibration with poly(methyl methacrylate) standards.²⁸ A more reliable estimate of the number-average molecular weight, $M_n^{app}/2.5$ was always used, as estimation of the number-average molecular weight of PAN, as previously demonstrated.^{28,30,33} One drawback of AN polymerization is the poor solubility of PAN in many solvents, and in its own monomer.¹⁰ Suitable, commonly employed solvents are ethylene carbonate and dimethyl sulfoxide (DMSO), therefore, the *e*ATRPs performed in DMF were repeated in DMSO, under otherwise identical conditions (Table 4.3, entries 1 and 2). $E_{app} = E_{1/2}$ gave a poorly controlled polymerization. However, by setting $E_{app} = E_{1/2} + 0.06$ V, PAN dispersity dramatically decreased to $\bar{D} = 1.16$. Since AN and Cu/TPMA are active monomer and ATRP catalyst, respectively, $E_{app} > E_{1/2}$ was required to keep a sufficiently high concentration of $[BrCu^{II}TPMA]^+$ deactivator in the system. The polymerization rate was unaffected by the solvent nature. M_n values deviated from M_n^{th} at relatively high conversion, possibly because of enhanced viscosity of the solution and increased importance of termination reactions.

2-Bromopropionitrile was then replaced with 2-chloropropionitrile (CPN) and ethyl α -chlorophenylacetate (ECPA) to analyze the effect of C-Cl chain-end on the activation/deactivation equilibrium (Table 4.3, entries 3 and 4). Cyclic voltammtries before the polymerizations were recorded, as shown in Figure 4.2:

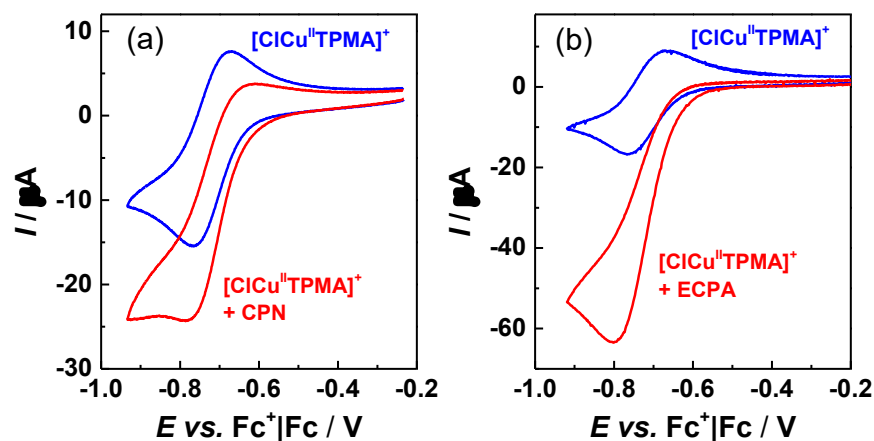


Figure 4.2. Cyclic voltammtry of 10^{-3} M $\text{Cu}^{\text{II}}\text{Cl}_2/\text{TPMA}$ in the absence (blue) and presence (red) of 0.01 M CPN (a) or 0.01 M ECPA (b), recorded on a GC disk before electrolysis in DMSO/AN 4/1 (v/v) + 0.1 M Et_4NBF_4 ; $\nu = 0.2 \text{ Vs}^{-1}$; $T = 25 \text{ }^\circ\text{C}$. Reprinted with permission, Copyright 2018 Elsevier.

The process was slightly slower, if compared to $\text{RX} = \text{BPN}$ at the same $E_{\text{app}} = E_{1/2} + 0.06 \text{ V}$ (Figure 4.3), due to the stronger chain-end functionality (C-Cl vs C-Br), which lowered the rate of re-activation of the dormant chains.⁴⁷⁻⁴⁸ Moreover, the final PAN had higher dispersity $D = 1.40$. Interestingly, when ethyl α -chlorophenylacetate (ECPA) was used as initiator, under otherwise identical conditions, the polymerization rate was similar, the reaction reaching 73% conversion in 8 h, while polymer dispersity dropped to $D = 1.17$ (Table 4.3, entry 4). Also, a better accordance between predicted and measured MWs was observed at low conversion, as in the case of $\text{RX} = \text{BPN}$ (Figure 4.3). ECPA is a more reactive ATRP initiator than CPN, thanks to the activating effect of both benzyl and acetate groups on the C-Cl bond, whereas BPN is more reactive than CPN because of the lower energy needed to break the C-Br bond.⁴⁸ This consideration suggests that highly reactive initiators enhance the control in *e*ATRP of AN.

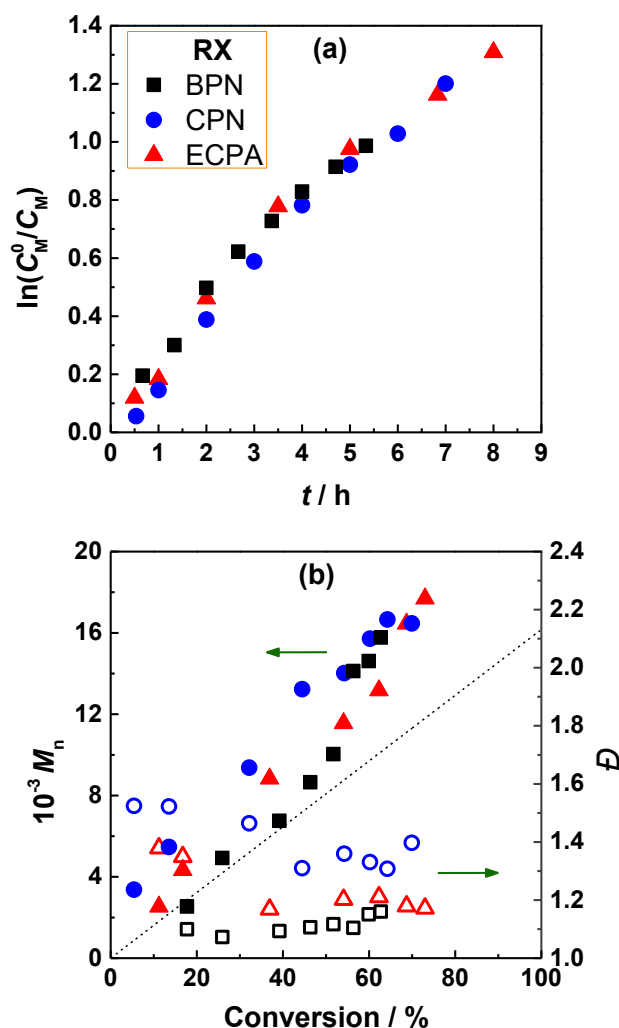


Figure 4.3. *e*ATRP of 20 vol% AN in DMSO + 0.1 M Et₄NBF₄: (a) kinetic plots and (b) evolution of MWs and dispersity with conversion. $C_{AN}/C_{RX}/C_{Cu^{II}Br_2}/C_{TPMA} = 300/1/0.1/0.1$, $C_{Cu^{2+}} = 10^{-3}$ M; $E_{app} = E_{1/2} + 0.06$ V, $V_{tot} = 5$ mL, $T = 60$ °C. The dashed line corresponds to $M_{n,th}$. Reprinted with permission, Copyright 2018 Elsevier.

The monomer loading was increased from 20 vol% to 40 vol% and the catalyst loading was decreased from 10^{-3} M to 5×10^{-4} M (from 327 ppm to 164 ppm, relative to moles of AN). These conditions would enable the production of a bigger mass of PAN, with lower contamination by Cu catalyst, thus reducing the complexity of required procedures for polymer purification. Moreover, eventual side reactions between growing chains and Cu catalyst become less important at low Cu loading.²⁸

When 5×10^{-4} M Cu^{II} was used, 69% conversion was achieved in 7 h, producing PAN with very low dispersity $D = 1.07$ (Table 4.3, entry 5 and Figure 4.4). By further decreasing the catalyst loading to 2.5×10^{-4} M (82 ppm), the polymerization was only slightly slower and remained very well-controlled (Table 4.3, entry 6,

Figure 4.4). With a Cu loading of only 41 ppm, the polymerization strongly slowed down after reaching 52% conversion, whereas the dispersity increased to about 1.2 (Table 4.3, entry 7).

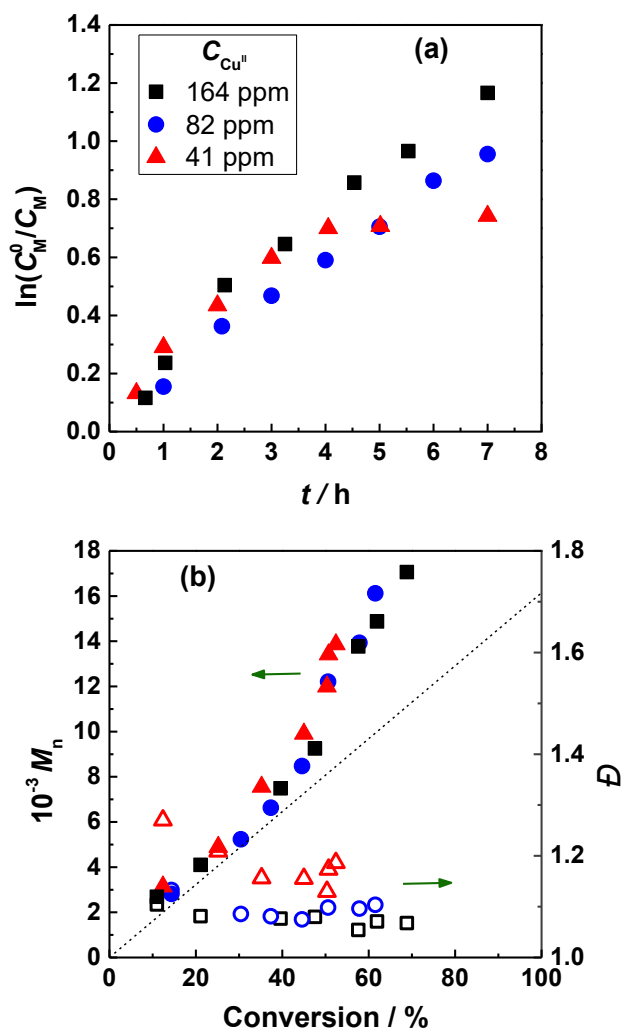


Figure 4.4. eATRP of 40 vol% AN in DMSO + 0.1 M Et₄NBF₄: (a) kinetic plots and (b) evolution of MWs and dispersity with conversion. $C_{AN}/C_{BPN} = 300/1$, $C_{BPN} = 2 \times 10^{-2}$ M, $C_{Cu^{II}Br_2}/C_{TPMA} = 1/1$; $E_{app} = E_{1/2} + 0.06$ V, $V_{tot} = 5$ mL, $T = 60$ °C. The dashed line corresponds to $M_{n,th}$. Reprinted with permission, Copyright 2018 Elsevier.

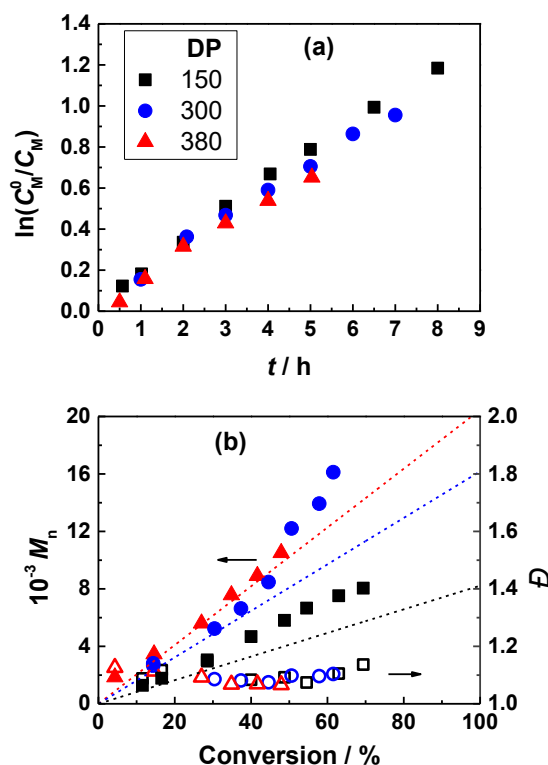


Fig. 4.5. *e*ATRP of 20 vol% (■), 40 vol% (●) and 50 vol% (▲) AN in DMSO + 0.1 M Et₄NBF₄: (a) kinetic plots and (b) evolution of MWs and dispersity with conversion. $C_{BPN}/C_{Cu^{II}Br_2}/C_{TPMA} = 1/0.025/0.025$, $C_{BPN} = 2 \times 10^{-2}$ M; $E_{app} = E_{1/2} + 0.06$ V, $V_{tot} = 5$ mL, $T = 60$ °C. Dashed lines correspond to $M_{n,th}$. Reprinted with permission, Copyright 2018 Elsevier.

The effect of target degree of polymerization (DP, defined as the ratio between initial concentrations of monomer and RX) was analyzed, by keeping constant C_{BPN} , while varying monomer loading (Table 4.3, entries 6 and 8-9, and Figure 4.5). $C_{Cu^{II}}$ was fixed at 2.5×10^{-4} M. *e*ATRPs of AN at concentrations of 20 vol%, 40 vol% and 50 vol% were well-controlled, giving PAN with $D \sim 1.1$. The polymerization rate remained almost constant while varying monomer loading. However, some problems of polymer solubility in the reaction mixture appeared at moderate conversions (>40%) together with a dramatic increase of solution viscosity during *e*ATRP of 50 vol% AN.

To prepare high-MW PAN, a relatively low monomer loading (20 vol%) was used to limit the increase in the viscosity and avoid polymer precipitation. Moreover, the syntheses were stopped at relatively low conversion. A low concentration of initiator, 10^{-3} M BPN, was used to grow long polymer chains. With these conditions, *e*ATRPs of AN were performed at $E_{app} = E_{1/2} + 0.03$ and $E_{1/2} +$

0.06 V (Table 4.3, entries 10-11). High molecular weight PAN was produced with $M_n = 79$ kDa and 91 kDa and $\bar{D} = 1.32$, within 2 h and 3 h of electrolysis, respectively. Previously reported synthesis of high-MW PAN *via* ATRP with different techniques for Cu^{I} re-generation, required much longer polymerization times, even > 2 days.^{28,31}

Table 4.3. *e*ATRP of AN in DMSO: effect of applied potential, initiator nature, catalyst loading and degree of polymerization.^a

| Entry | E_{app} (V) | RX | AN vol% | $C_{\text{AN}}/C_{\text{RX}}/C_{[\text{XCu}^{\text{II}}\text{L}]^+}$ ^b | t (h) | Conv. (%) | k_p^{app} (h^{-1}) ^c | $M_{n,\text{th}}$ $\times 10^{-3}$ | $M_{n,\text{GPC}}/2.5$ $\times 10^{-3}$ | \bar{D} |
|-----------------|----------------------|------|------------|---|---------|--------------|--|---------------------------------------|--|-----------|
| 1 | $E_{1/2}$ | BPN | 20 | 300/1/0.1 | 5.3 | 65 | 0.37 | 10.5 | 18.6 | 1.60 |
| 2 | $E_{1/2} + 0.6$ | BPN | 20 | 300/1/0.1 | 5 | 63 | 0.20 | 10.1 | 15.8 | 1.16 |
| 3 | $E_{1/2} + 0.6$ | CPN | 20 | 300/1/0.1 | 7 | 70 | 0.18 | 11.3 | 16.4 | 1.40 |
| 4 | $E_{1/2} + 0.6$ | ECPA | 20 | 300/1/0.1 | 8 | 73 | 0.19 | 11.8 | 17.7 | 1.17 |
| 5 | $E_{1/2} + 0.6$ | BPN | 40 | 300/1/0.05 | 7 | 69 | 0.18 | 11.1 | 17.1 | 1.07 |
| 6 | $E_{1/2} + 0.6$ | BPN | 40 | 300/1/0.025 | 7 | 62 | 0.16 | 9.9 | 16.1 | 1.10 |
| 7 | $E_{1/2} + 0.6$ | BPN | 40 | 300/1/0.0125 | 7 | 52 | 0.18 ^d | 8.5 | 13.9 | 1.19 |
| 8 | $E_{1/2} + 0.6$ | BPN | 20 | 150/1/0.025 | 8 | 69 | 0.17 | 5.7 | 8.0 | 1.14 |
| 9 | $E_{1/2} + 0.6$ | BPN | 50 | 380/1/0.025 | 5 | 48 | 0.15 | 9.8 | 10.5 | 1.07 |
| 10 ^e | $E_{1/2} + 0.3$ | BPN | 20 | 3053/1/0.5 | 2 | 32 | 0.55 | 51.8 | 79.1 | 1.32 |
| 11 ^e | $E_{1/2} + 0.6$ | BPN | 20 | 3053/1/0.5 | 3 | 40 | 0.30 | 64.7 | 90.9 | 1.32 |

^a 0.1 M Et_4NBF_4 ; $T = 60$ °C; unless otherwise stated, $V_{\text{tot}} = 5$ mL.

^b L = TPMA, $[\text{XCu}^{\text{II}}\text{L}]^+$ was prepared in situ by mixing equimolar amounts of $\text{Cu}^{\text{II}}\text{X}_2$ and TPMA, with X = Br for RX = BPN, and X = Cl for RX = CPN, ECPA.

^c Defined as the slope of $\ln(C_M^0/C_M)$ vs. time.

^d For the interval 0-4 h, then the polymerization strongly slowed down.

^e $V_{\text{tot}} = 10$ mL.

Reprinted with permission, Copyright 2018 Elsevier.

4.1.3. Preparation of PAN-*b*-PBA copolymer *via* eATRP

Two different strategies can be used to produce block copolymers of poly(acrylonitrile) and poly(butyl acrylate): i) preparation of PAN-Br macroinitiator and its chain extension with BA, ii) synthesis of PBA-Br macroinitiator and subsequent chain extension with AN. The latter implies the polymerization of an active monomer (AN), starting from a less active macroinitiator (PBA-Br), thus first generated PBA-*b*-PAN-Br chains will be activated faster than the remaining PBA-Br macroinitiator chains, leading to uneven growth of chains. In conventional ATRP (*i.e.* >1000 ppm of Cu), this issue can be solved with the halogen exchange technique: a copper chloride catalyst is used to convert the macroinitiator to PBA-*b*-PAN-Cl chains that are more difficult to activate than PBA-Br molecules, ensuring high initiation efficiency.⁴⁹ However, this method is less effective with low Cu loadings. In fact, in Chapter 3, a well-defined poly(methyl acrylate)-*b*-poly(acrylonitrile) was prepared *via* eATRP in an ionic liquid, with halogen exchange under low Cu catalyst loading.⁴¹

On the other hand, the first strategy requires to produce PAN with high chain end functionality and to find suitable conditions to overcome the poor solubility of PAN in BA monomer.²⁹ The fraction of dead chains (DCF) in ATRP can be estimated by using Eq. (4.4); it depends on the rate of propagation and termination of the monomer (k_p and k_t , respectively), targeted degree of polymerization (DP_T), initial monomer concentration (C_M^0), and monomer conversion (p) at the time t .⁴⁹ Considering $k_p = 7 \times 10^3 \text{ M}^{-1}\text{s}^{-1}$ and $k_t = 10^8 \text{ M}^{-1}\text{s}^{-1}$ for AN at $T = 60 \text{ }^\circ\text{C}$,⁵⁰ the estimated fraction of dead chains for eATRPs in Table 4.3 is very low (*e.g.* for entry 5, DCF = 1.1%), and becomes slightly higher when targeting higher DP (*e.g.* for entry 10, DCF = 8.4%), in accordance with the broader MWs distribution observed for high-MW PAN. Therefore, it is reasonable to expect high chain-end functionality in PAN produced under the conditions employed in this study.

$$DCF = \frac{2DP_T k_t [\ln(1-p)]^2}{[M]_0 k_p^2 t} \quad (4.4)$$

eATRP of AN was therefore performed on a larger volumetric scale, aiming to obtain enough PAN-Br macroinitiator to produce a block copolymer that could be

subjected to pyrolysis and further characterizations. The polymerization was stopped after 8 h, at 53% conversion (Table 4.4): the fraction of dead chains was estimated to be < 1%.

Table 4.4 *e*ATRP of AN and chain extension of produced PAN-Br with BA.^a

| Entry | M | Solvent | RX | DP | <i>t</i> | Conv. | k_p^{app} | M_n^{th} | $M_n^{\text{app}/2.5}$ | M_n^{NMR} | <i>D</i> |
|-------|----|---------|------------------------|-----|----------|-------|--------------------|--------------------|------------------------|--------------------|----------|
| | | | | | (h) | (%) | (h ⁻¹) | × 10 ⁻³ | × 10 ⁻³ | × 10 ⁻³ | |
| 1 | AN | DMSO | BPN | 204 | 8 | 53 | 0.07 | 5.7 | 5.0 | 5.7 | 1.11 |
| 2 | BA | DMF | PAN ₁₀₈ -Br | 130 | 5 | 59 | 0.10 | 15.5 | 13.7 | 15.9 | 1.11 |

^a0.1 M Et₄NBF₄, $E_{\text{app}} = E_{1/2} + 0.06$ V, $C_{\text{Cu}^{\text{II}}\text{Br}_2/\text{TPMA}} = 5 \times 10^{-4}$ M. Entry 1: $C_{\text{AN}} = 6.1$ M, $V_{\text{tot}} = 40$ mL, $T = 60$ °C. Entry 2: $C_{\text{BA}} = 1.7$ M, $V_{\text{tot}} = 15$ mL, $T = 50$ °C. Reprinted with permission, Copyright 2018 Elsevier.

PAN-Br was isolated by precipitation into methanol/water and dried under vacuum. The polymer (white powder, 5.90 g) was characterized *via* NMR (Figure 4.7) and GPC, obtaining $M_n^{\text{NMR}} = 5677$ and $D = 1.11$. PAN-Br (DP = 107) was then extended with BA (25 vol%) in DMF, at $T = 50$ °C. The *e*ATRP was stopped after 5 h, at 59% conversion (Table 4.4). GPC traces in Fig. 4.4 proved high retention of chain-end functionality. The copolymer was precipitated into a water/methanol solution, dried under vacuum and characterized (Figure 4.8), obtaining 2.78 g of PAN-*b*-PBA (DP_{BA} = 80) with $M_n^{\text{NMR}} = 15900$ and $D = 1.11$ (Figure 4.6).

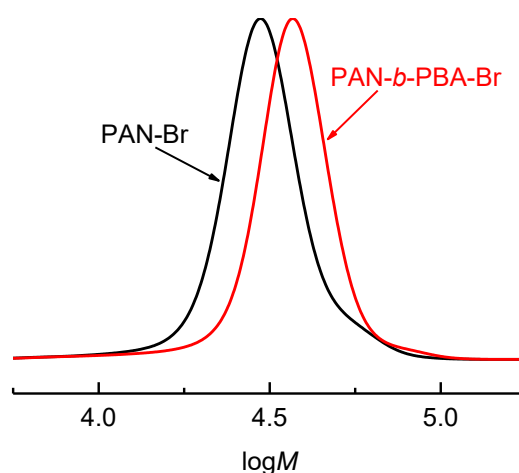


Figure 4.6. GPC traces of PAN-Br macroinitiator ($M_{n,\text{NMR}} = 5677$, $D = 1.11$) and PAN-*b*-PBA-Br ($M_{n,\text{NMR}} = 15900$, $D = 1.11$). Reprinted with permission, Copyright 2018 Elsevier.

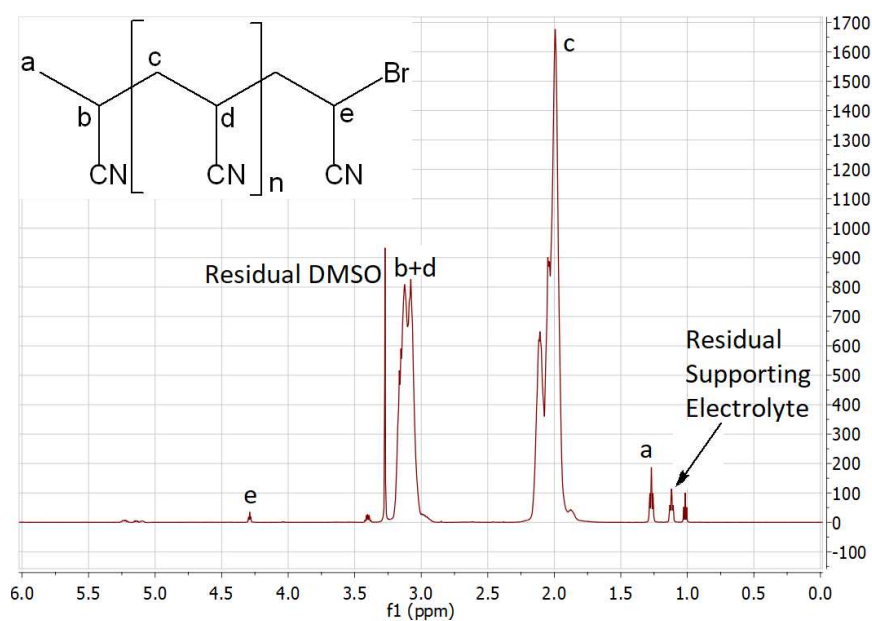


Figure 4.7. 600 MHz $^1\text{H-NMR}$ of PAN-Br macroinitiator in $\text{DMSO-}d_6$. Reprinted with permission, Copyright 2018 Elsevier.

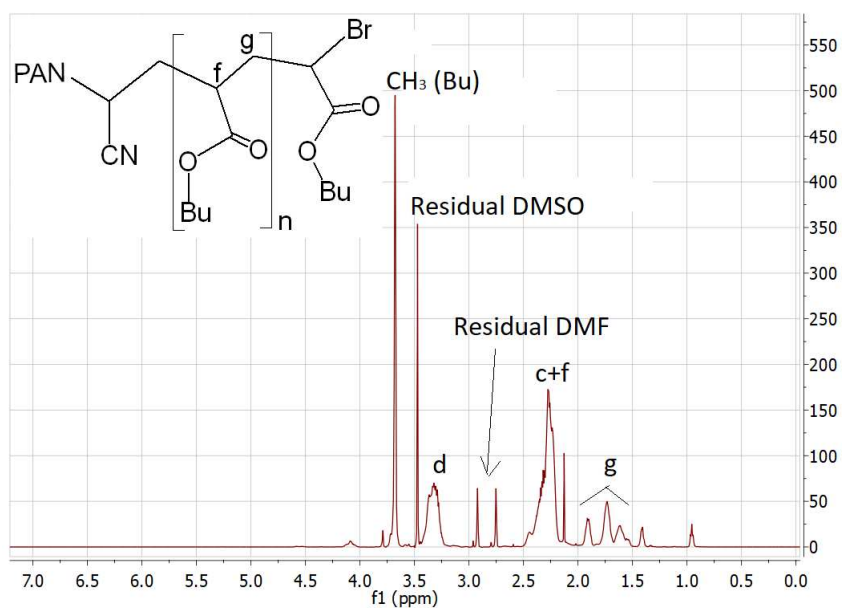


Figure 4.8. 600 MHz $^1\text{H-NMR}$ of PAN-*b*-PBA-Br in $\text{DMF-}d_7$ ($M_{n,\text{NMR}} = 15900$, $D = 1.11$). Reprinted with permission, Copyright 2018 Elsevier.

4.2 Catalytic halogen exchange for the preparation of well-defined block copolymers

In the previous sections it was shown that *e*ATRP of AN required prolonged reaction time (> 5 h) and precautions for a successful polymerization. Moreover, to obtain a high molecular weight macroinitiator it was necessary to increase the reaction volume to 40 mL, limiting the conversion with non-negligible waste of reagent. In contrast, acrylates can be polymerized faster with less stringent conditions and the macroinitiator can be recovered with a higher yield.⁵¹ Starting from the previous results of *e*ATRP of AN, catalytic halogen exchange was implemented to produce PBA-*b*-PAN-Cl copolymer by using PBA-Br as macroinitiator.

4.2.1 Electrochemistry of Catalytic Halogen Exchange for PBA-Br chain extension with AN

Electrochemistry is an outstanding tool to understand the mechanism of *c*HE. Detailed electrochemical analysis of *c*HE in [BMIm][OTf] was already shown in chapter 3. In DMSO, chloride anions have a detrimental effect on the stability of Cu^I active catalyst as shown by cyclic voltammetry of [Cu^{II}TPMA]²⁺ in the presence of Cl⁻ (Figure 4.9); the anodic peak progressively decreases in height until it disappears when $C_{Cl^-} \gg C_{Cu}$. Note that the required excess for *c*HE should be at least $C_{Cl^-} = 2C_{Cu} + C_{Pn-X}$ to allow quantitative exchange all brominated species with Cl.

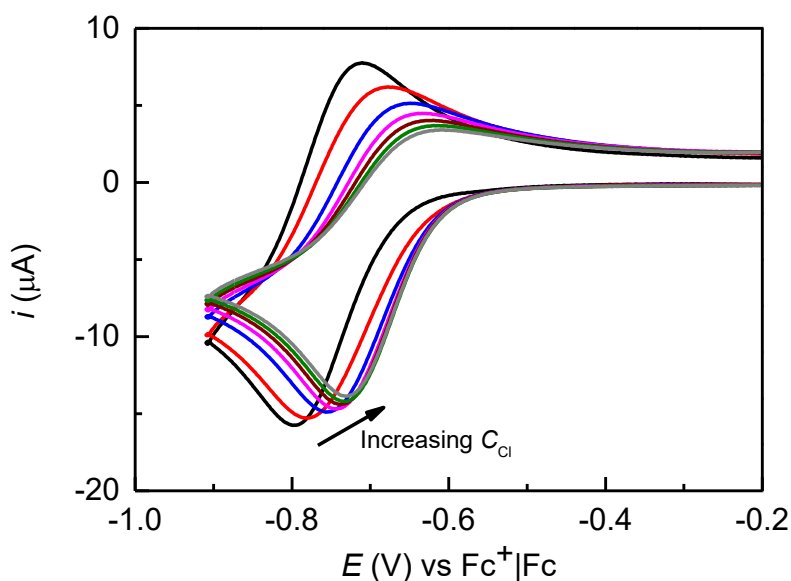


Figure 4.9. Cyclic voltammetry of 10^{-3} M $[\text{ClCu}^{\text{II}}\text{TPMA}]^+$ (—), in the presence of increasing amounts of Et_4NCl from 1×10^{-3} M to 1.2×10^{-2} M in $\text{DMSO} + 0.1$ M Et_4NBF_4 at $T = 60$ °C. CVs were recorded on a GC disk, $\nu = 0.2$ V s^{-1} .

Yet, $[\text{Cu}^{\text{I}}\text{TPMA}]^+$ tolerates a certain amount of chloride ions, still exhibiting a reversible voltammogram, confirming that it is somewhat stable enough to activate dormant $\text{P}_n\text{-X}$.

After synthesizing a PBA-Br macroinitiator ($M_n = 11600$, $D = 1.13$), new electrochemical characterization was performed to examine the possibility of extending PBA-Br with AN, using $[\text{Cu}^{\text{II}}\text{TPMA}]^{2+}$ as catalyst. The electrochemical characterization is shown in Figure 4.10.

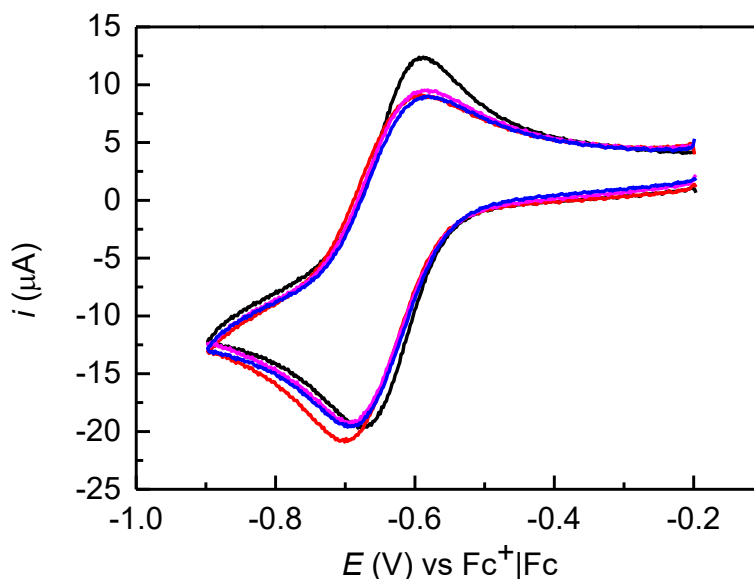


Figure 4.10. Cyclic voltammetry of 10^{-3} M $[\text{ClCu}^{\text{II}}\text{TPMA}]^+$ (—), in the presence of 5×10^{-3} Et_4NCl (—), 20% (v/v) AN (—), and 2×10^{-3} PBA-Br (—) in DMSO + 0.1 M Et_4NBF_4 ; $T = 60$ °C. CVs were recorded on a GC disk, $\nu = 0.2$ V s^{-1} .

Addition of AN and PBA-Br did not modify appreciably the voltammetric pattern of $[\text{ClCu}^{\text{II}}\text{TPMA}]^+$. Reaction conditions for *c*HE include $E_{\text{app}} > E_{1/2}$ to avoid excessive (re)generation of acrylonitrile radicals in addition to the general optimized conditions previously found for AN polymerization. Potentiostatic *e*ATRP was triggered at $E_{\text{app}} = E_{1/2} + 0.06$ V with $C_{\text{AN}}/C_{\text{PBA-Br}} = 305/0.2$, $C_{\text{PBA-Br}} = 2 \times 10^{-3}$ M, $C_{\text{Cu}^{\text{II}}\text{Br}_2} = C_{\text{TPMA}} = 10^{-3}$ M, $C_{\text{Cl}^-} = 5 \times 10^{-3}$ M; $V_{\text{tot}} = 10$ mL and $T = 60$ °C. The results are summarized in Table 4.5.

Table 4.5. *e*ATRP of AN in DMSO starting from PBA-Br macroinitiator with catalytic halogen exchange.^a

| Entry | t (h) | Conv. (%) | $M_n^{\text{th}} \times 10^{-3}$ | $M_n^{\text{app}/2.5} \times 10^{-3}$ | D |
|-----------------------|---------|-----------|----------------------------------|---------------------------------------|------|
| PBA-Br | 0 | - | 11.0 | 2.6 | 1.11 |
| PBA- <i>b</i> -PAN-Cl | 1 | 9 | 18.3 | 10.8 | 1.30 |
| PBA- <i>b</i> -PAN-Cl | 2 | 19 | 24.8 | 17.5 | 1.21 |

^a 0.1 M Et_4NBF_4 ; $T = 60$ °C, $\text{DP} = 1526$, $V_{\text{tot}} = 10$ mL.

The chain extension reaction was stopped after 2 h due to high viscosity. The conversion was quite low (< 20%) but a well-controlled PBA-*b*-PAN-Cl of $M_n = 24800$ and $D = 1.21$ was obtained. MW distributions of PBA-Br and PBA-*b*-PAN-Cl show a clear shift to higher MW as PAN is incorporated (Figure 4.11).

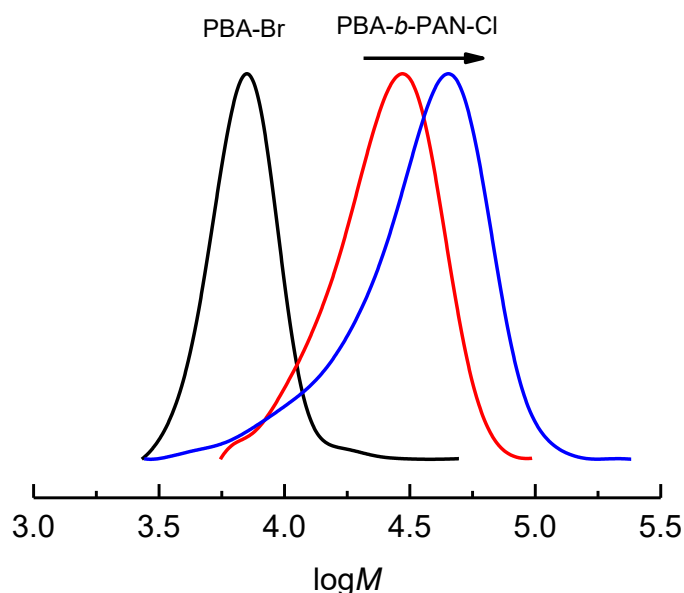
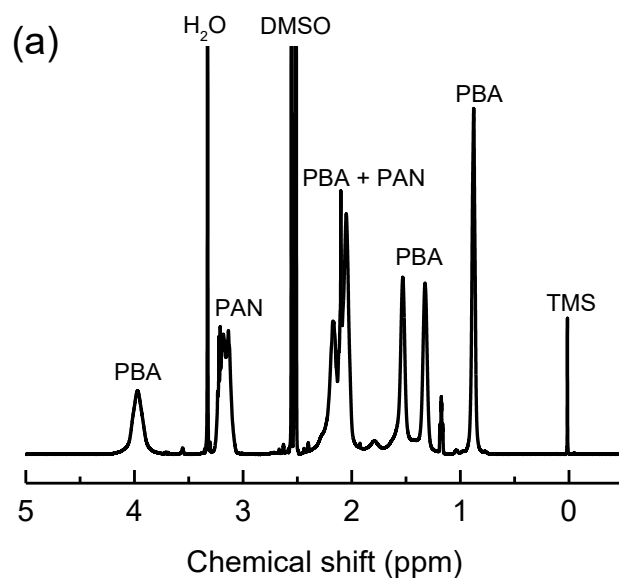


Figure 4.11. MW distribution of PAN-Br macroinitiator (—, $M_{n,NMR} = 11000$, $D = 1.11$) and PBA-*b*-PAN-Cl after 1 hour (—, $M_{n,NMR} = 18300$, $D = 1.30$) and 2 hours (—, $M_{n,NMR} = 24800$, $D = 1.21$) of chain extension.

NMR analysis of the block copolymer shows that acrylonitrile incorporation (PAN block = 13800, Figure 4.12) is close to double that of BA in mol.



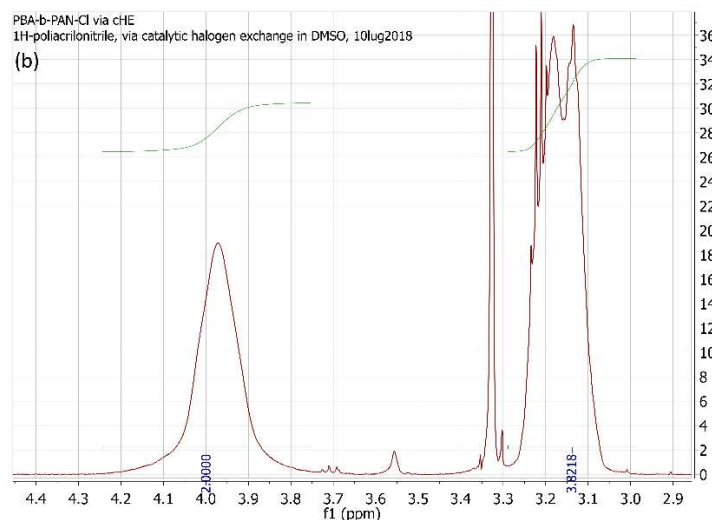


Figure 4.12. a) 600 MHz $^1\text{H-NMR}$ of PBA-*b*-PAN-Cl in $\text{DMSO-}d_6$ ($M_{n,\text{NMR}} = 24800$, $D = 1.21$), b) integration of relevant PBA and PAN signals of the copolymer (PBA: $-\text{CH}_2-$ side chain and PAN: $-\text{CH}-$).

In contrast to the conventional approach, there are important improvements. First, PBA-Br macroinitiator can be synthesized with a high yield and in high amounts in a short time (< 2 h for at least 5 g of PBA). Second, DMSO can replace DMF for both macroinitiator synthesis and chain extension, with positive impacts on a green chemistry basis. Third, PBA-*b*-PAN-Cl with a high AN content can be prepared by catalytic chain extension starting from PBA-Br.

Encouraged by the positive results of PBA-*b*-PAN-Cl, application of *c*HE extended to the synthesis of new BCPs, exploring new monomers and solvents. It will be shown *c*HE is a valuable, universal tool for the preparation of BCPs.

4.2.2 Synthesis of other macroinitiators by *e*ATRP

A series of new macroinitiators was prepared by *e*ATRP catalyzed by copper complexes with TPMA or Me_6TREN as ligands. Polystyrene-Br was synthesized in ethanol at $80\text{ }^\circ\text{C}$ using $[\text{Cu}^{\text{II}}\text{TPMA}]^{2+}$; poly(methyl acrylate)-Br was synthesized in DMSO at $50\text{ }^\circ\text{C}$ using $[\text{Cu}^{\text{II}}\text{Me}_6\text{TREN}]^{2+}$ and poly(oligoethylene oxide methyl ether acrylate)-Br macroinitiator was synthesized in water at $25\text{ }^\circ\text{C}$ using $[\text{Cu}^{\text{II}}\text{TPMA}]^{2+}$. The appropriate reaction time and other conditions were chosen to ensure high chain-end functionality even if this had implied low conversion. The results are reported in Table 4.6.

Table 4.6. Synthesis of macroinitiators for cHE by electrochemically mediated ATRP.^a

| Entry | Solvent | E_{app} | t (h) | Conv. (%) | M_n^{th} | M_n^{app} | D |
|----------|------------------|--------------------|---------|-----------|------------|-------------|------|
| PS-Br | EtOH | $E_{1/2}$ | 5 | 23 | 7000 | 7800 | 1.10 |
| PMA-Br | DMSO | $E_{1/2} - 0.06$ | 0.25 | 60 | 25000 | 26200 | 1.05 |
| POEOA-Br | H ₂ O | $E_{1/2}$ | 1 | 21 | 10700 | 11400 | 1.09 |
| PAN-Br | DMSO | $E_{1/2} + 0.06$ V | 4 | 57 | 9200 | 30600 | 1.04 |

^aSupporting electrolyte: 0.1 M Et₄NBF₄ for DMSO, 0.1 M Na₂SO₄ for H₂O. Conditions for PMA-Br: $C_{MA}:C_{Me6TREN}:C_{CuBr_2}:C_{EBiB} = 552:0.1:0.1:1$, MA/DMSO = 50% v/v; for PS-Br: $C_{Sty}:C_{TPMA}:C_{CuBr_2}:C_{EBiB} = 436:0.1:0.1:1.5$, Sty/EtOH = 50% v/v; for POEOA-Br: $C_{OEOA}:C_{TPMA}:C_{CuBr_2}:C_{EBiB} = 176:0.1:0.1:0.5$, OEOA/H₂O = 20% v/v; $V = 20$ mL; $C_{CuBr_2} = 10^{-3}$ M. Estimated geometrical surface of the Pt electrode = 6 cm².

All three macroinitiators were synthesized successfully, with very low dispersity; they were suitable for chain extension with other monomers.

4.2.3 Chain extension by eATRP

To verify the living character of each macroinitiator, chain extension with monomers more reactive than those of the macroinitiators was triggered by eATRP. cHE was mediated by [Cu^{II}TPMA]²⁺. PMA-Br and PAN-Br were extended with methyl methacrylate in DMSO, PS-Br was extended with methyl acrylate in AcOEt + 20% (v/v) [BMIm][OTf] and POEOA-Br was extended with OEOMA in H₂O. PMA-Br was also self-extended to double-check the livingness (Table 4.7).

Table 4.7. Chain extension of macroinitiators with different monomers by *e*ATRP, through *c*HE, using $[\text{Cu}^{\text{II}}\text{TPMA}]^{2+}$ as catalyst at $E_{\text{app}} = E_{1/2}$.^a

| Copolymer | Solvent | <i>t</i> (h) | Conv. (%) | M_n^{th} | M_n^{app} | \bar{D} |
|--------------------------------|------------------------------------|--------------|-----------|-------------------|--------------------|-------------------|
| PMA- <i>b</i> -PMA-Br | DMSO | 1 | 27 | 89400 | 91800 | 1.15 |
| PMA- <i>b</i> -PMMA-Cl | DMSO | 2 | 18 | 67200 | 110100 | 1.22 ^b |
| PS- <i>b</i> -PMA-Cl | AcOEt + 20% [BMIIm] [OTf] | 2 | 5 | 19700 | 22000 | 1.16 |
| PAN- <i>b</i> -PMMA-Cl | DMSO | 2 | 60 | 149300 | 154300 | 1.33 |
| POEOA- <i>b</i> - POEOMA-Cl | H ₂ O | 3 | 24 | 30900 | 46800 | 1.39 |

^aSupporting electrolyte: 0.1 M Et₄NBF₄ for DMSO, 0.1 M Na₂SO₄ for H₂O. Other conditions: MMA: $C_{\text{MMA}}:C_{\text{TPMA}}:C_{\text{CuBr}_2}:C_{\text{PMA-Br}} = 467:0.1:0.1:0.2$, MMA/DMSO = 50 % v/v; MA: $C_{\text{MA}}:C_{\text{TPMA}}:C_{\text{CuBr}_2}:C_{\text{PS-Br}} = 552:0.1:0.1:0.2$, MA/DMSO = 50% v/v; OEOMA: $C_{\text{MA}}:C_{\text{TPMA}}:C_{\text{CuBr}_2}:C_{\text{POEOA-Br}} = 108:0.1:0.1:0.2$, OEOMA/DMSO = 20% v/v. $V = 10$ mL; $C_{\text{CuBr}_2} = 10^{-3}$ M. Estimated geometrical surface of the Pt electrode = 6 cm². ^b Dispersity of copolymer obtained by extension of a small fraction of macroinitiator chains.

When PMA-Br was extended with itself, a clear shift to higher MW with no detectable dead chains was observed (Figure 4.13a). The reaction was well-controlled resulting in a new homopolymer with a MW of $\sim 10^5$, corresponding to a 2.5-fold increase of chain length. This provided a clear evidence of high chain-end fidelity in the macroinitiator. Nevertheless, when *c*HE was triggered with MMA from the same macroinitiator, the MW distribution was split in two, clearly indicating inefficient cross-propagation. Despite this, the newly formed block copolymer exhibited narrow dispersity (Figure 4.13b).

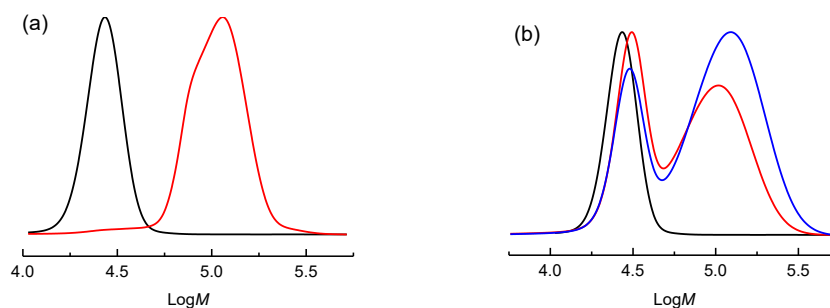


Figure 4.13. Chain extension of PMA-Br by *e*ATRP in DMSO at 50 °C. a) MW distribution of PMA-Br macroinitiator (—) and PMA-*b*-PMA-Br (—); b) PMA-Br (—) and PMA-*b*-PMMA-Cl after 1 h (—) and 2 h (—).

Since the self-chain extension experiment confirmed high C-Br functionality in the macroinitiator, the observed inefficient cross-propagation must be attributed to k_{act} mismatch. To improve cross-propagation, the concentration of chloride ions was increased 4 times. Unfortunately, this did not give the expected result; there was no polymerization at all. This was caused by the detrimental effect of the high amount of chloride ions, previously discussed (Section 4.2.1). As chloride ions displace the ligand forming other species like $[Cu^I Cl_2]^-$, the *e*ATRP process could not be established.

To prove that *c*HE is possible with methacrylates, a PAN-Br macroinitiator was chosen. The terminal unit, represented by the model compound 2-bromopropionitrile, has higher k_{act} than methyl 2-bromopropionate, representative of PMA-Br. As expected, with PAN-Br a clear shift to higher MW was observed, without the characteristic peak splitting of inefficient cross-propagation (Figure 4.14).

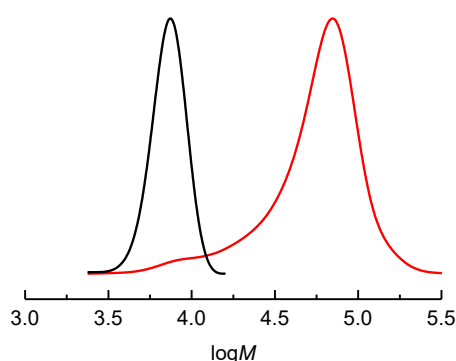


Figure 4.14. Chain extension of PAN-Br by *e*ATRP in DMSO at 50 °C. MW distribution of PAN-Br macroinitiator (—) and of PAN-*b*-PMMA-Cl after 2 h (—) of reaction time.

When PS-Br was extended with MA in AcOEt + 20% [BMIm][OTf], a well-defined PS-*b*-PMA-Cl copolymer was obtained with a clear shift of the distribution to higher MW (Figure 4.15).

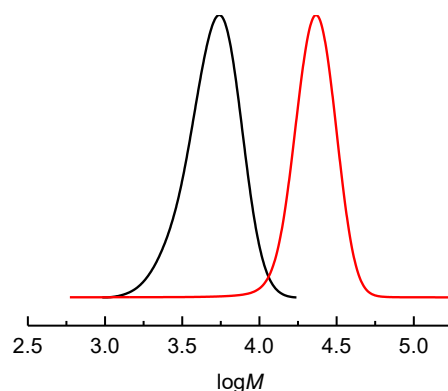


Figure 4.15. Chain extension of PS-Br by *e*ATRP in AcOEt + 20% [BMIm][OTf] at 80 °C. MW distribution of PS-Br (—) and PS-*b*-PMA-Cl (—) after 1 h of reaction time, produced by *e*ATRP.

Similarly, when POEOA-Br was extended with OEOMA in H₂O, the block copolymer POEOA-*b*-POEOMA-Cl was formed, with a clear shift to higher MW (Figure 4.16).

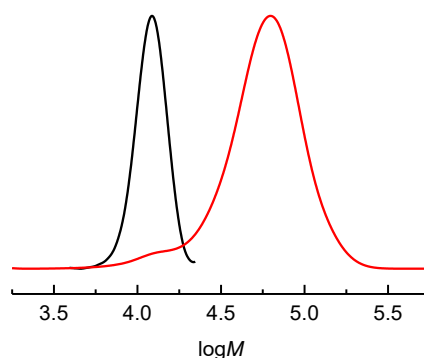


Figure 4.16. Chain extension of POEOA-Br by *e*ATRP in H₂O at 25 °C. MW distribution of POEOA-Br (—) and POEOA-*b*-POEOMA-Cl (—) after 3 h of reaction time.

Overall, *e*ATRP performed well in both the synthesis of macroinitiators and chain extensions with *c*HE.

4.2.4 Catalytic Halogen Exchange *via* SARA ATRP

As electrochemistry is only one of the possible solutions to regenerate the active catalyst, experiments were performed again by using SARA ATRP, which exploits comproportionation between Cu⁰ and Cu^{II} to (re)generate Cu^I. Metallic Cu also acts as a supplemental activator. The three macroinitiators were prepared by SARA ATRP, with properties reported in Table 4.8.

Table 4.8. Properties of macroinitiators prepared by SARA ATRP.^a

| Entry | Solvent | <i>t</i> (h) | Conv. (%) | M_n^{th} | M_n^{app} | \bar{D} |
|----------|------------------|--------------|-----------|-------------------|--------------------|-----------|
| PS-Br | AcOEt | 5 | 30 | 9100 | 9400 | 1.16 |
| PMA-Br | DMSO | 0.75 | 51 | 24200 | 25200 | 1.06 |
| POEOA-Br | H ₂ O | 3 | 83 | 42300 | 43400 | 1.21 |

^aConditions for PS-Br: $C_{\text{Sty}}:C_{\text{PMDETA}}:C_{\text{CuBr}_2}:C_{\text{EBiB}} = 436:0.1:0.1:1.5$; for PMA-Br: $C_{\text{MA}}:C_{\text{Me6TREN}}:C_{\text{CuBr}_2}:C_{\text{EBiB}} = 552:0.1:0.1:1$; for POEOA-Br: $C_{\text{OEOA}}:C_{\text{TPMA}}:C_{\text{CuBr}_2}:C_{\text{HEBiB}} = 176:0.1:0.1:0.5$, $V = 20$ mL; $C_{\text{CuBr}_2} = 10^{-3}$ M, Cu⁰ wire: $l = 5$ cm, $d = 1$ mm.

As in *e*ATRP, all macroinitiators were successfully obtained with low dispersity.

4.2.5 Chain extension *via* SARA ATRP

The chain extension was triggered by replacing the driving force from electrons to metallic copper and adding a source of chlorides. In SARA ATRP, Cu⁰ acts as both supplemental activator and reducing agent (SARA). Cu⁰ can activate alkyl halide directly but slowly. Cu⁰ can also reduce Cu^{II} to Cu^I. Both processes help to regenerate Cu^I activator, which drives the polymerization. The results of the chain extension are shown in Table 4.9:

Table 4.9. Chain extension of macroinitiators with different monomers, by SARA ATRP using $[\text{Cu}^{\text{II}}\text{TPMA}]^{2+}$ as catalyst at $T = 50\text{ }^{\circ}\text{C}$.^a

| Macroinitiator | Copolymer | Solvent | t (h) | Conv. (%) | M_n^{th} | M_n^{app} | \mathcal{D} |
|--------------------|--------------------------------|-----------------------------------|------------|--------------|-------------------|--------------------|---------------|
| PMA-Br | PMA- <i>b</i> - PMMA-Cl | DMSO | 2 | 90 | 235300 | 477000 | 1.21 |
| PAN-Br | PAN- <i>b</i> - PMMA-Cl | DMSO | 2 | 48 | 122400 | 121500 | 1.23 |
| PS-Br ^b | PS- <i>b</i> -PMA-Cl | AcOEt + 20% [BMIm][OTf] | 3 | 7 | 25700 | 27500 | 1.19 |
| POEOA | POEOA- <i>b</i> - POEOMA-Cl | H ₂ O | 3 | 92 | 280300 | 325300 | 1.65 |

^aConditions for MMA: $C_{\text{MMA}}:C_{\text{TPMA}}:C_{\text{CuBr}_2}:C_{\text{PMA-Br/PAN-Br}} = 467:0.1:0.1:0.2$; for MA: $C_{\text{MA}}:C_{\text{TPMA}}:C_{\text{CuBr}_2}:C_{\text{PS-Br}} = 552:0.1:0.1:0.2$; for OEOMA: $C_{\text{OEOMA}}:C_{\text{TPMA}}:C_{\text{CuBr}_2}:C_{\text{POEOA-Br}} = 108:0.1:0.1:0.2$. $V = 10\text{ mL}$; $C_{\text{CuBr}_2} = 10^{-3}\text{ M}$, Cu^0 wire: $l = 5\text{ cm}$, $d = 1\text{ mm}$. ^b $T = 80\text{ }^{\circ}\text{C}$.

Chain extension with *c*HE was successful also with SARA ATRP. Well-defined block copolymers with narrow dispersity were obtained in a few hours. As found in the case of *e*ATRP, also in SARA ATRP complete reactivation of PMA-Br macroinitiator was not possible when MMA was used for chain extension. However, the fraction of generated PMA-*b*-PMMA-Cl copolymer was controlled ($\mathcal{D} = 1.21$).

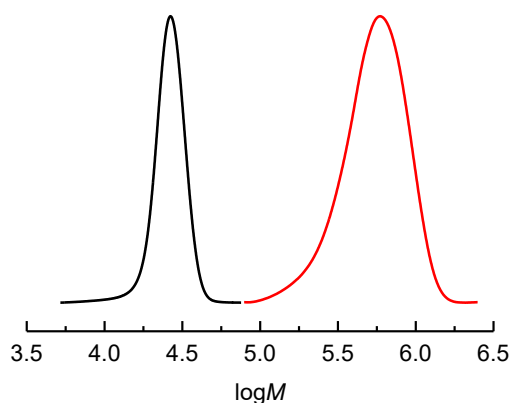


Figure 4.17. Chain extension of PMA-Br by SARA ATRP in DMSO at $50\text{ }^{\circ}\text{C}$. MW distribution of PMA-Br macroinitiator (—), and of PMA-*b*-PMMA-Cl (—) after 2 h of reaction time.

Like *e*ATRP, when PAN-Br was extended with MMA, the copolymer was formed with no unreacted macroinitiator (Figure 4.18).

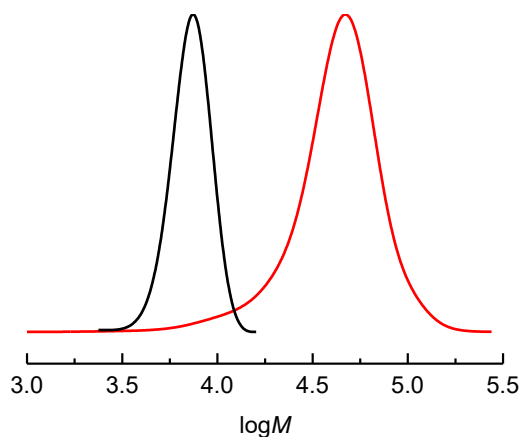


Figure 4.18. Chain extension of PAN-Br by SARA ATRP in DMSO at 50 °C. MW distribution of PAN-Br macroinitiator (—), and of PAN-*b*-PMMA-Cl (—) after 2 h of reaction time.

The chain extension performed well also for PS-Br and POEOA-Br in EtOAc + 20% [BMIm][OTf] and H₂O, respectively (Figures 4.19 and 4.20).

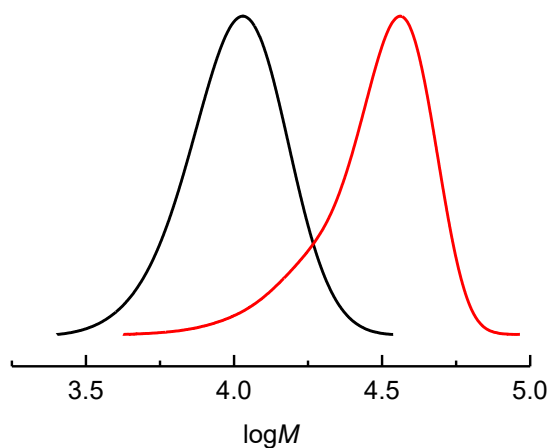


Figure 4.19. Chain extension of PS-Br by SARA ATRP in AcOEt + 20% (v/v) [BMIm][OTf] at 80 °C. Molecular weight distribution of PS-Br macroinitiator (—), and of PS-*b*-PMA-Cl (—) after 2 h of reaction time.

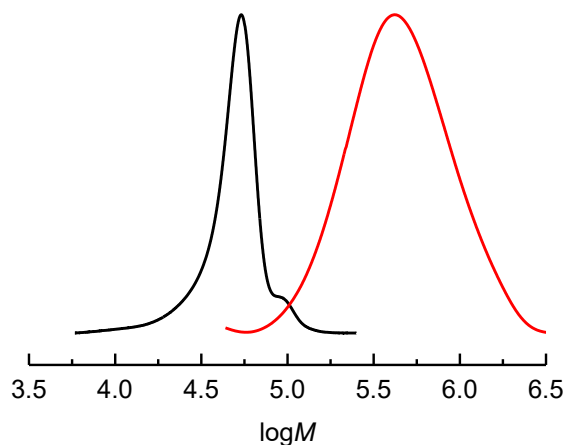


Figure 4.20. Chain extension of POEOA-Br by SARA ATRP in H₂O at 25 °C. MW distribution of POEOA-Br macroinitiator (—), and of POEOA-*b*-POEOMA-Cl (—) after 2 h of reaction time.

4.3 Conclusions

Well-defined PAN was prepared via *e*ATRP, catalyzed by CuX₂/TPMA. The redox properties of the Cu complexes were characterized by cyclic voltammetry, exhibiting typical features of common ATRP catalysts in organic solvents and their mixtures with monomers. Controlled polymerizations were triggered by applying a potential more positive than the standard reduction potential of the catalyst, so to ensure the presence of enough Cu^{II} species, which effectively deactivated the propagating chains. Moreover, highly reactive ATRP initiators showed better performances than less reactive ones. The catalyst loading was successfully decreased from 327 to 41 ppm. PAN with very low dispersity, $D < 1.1$, was prepared even at high AN loading (up to 50 vol%). High-MW PAN ($M_n = 79\text{k}$ and 91k) was prepared *via e*ATRP in ≤ 3 h. The good retention of chain end functionality was proved by extending a PAN-Br macroinitiator with butyl acrylate, thus forming a PAN-*b*-PBA copolymer, with $D = 1.11$.

On the other hand, catalytic halogen exchange proved to be a very valuable tool to build well-defined block copolymers by extending bromine-capped macroinitiators from styrene, methyl acrylate and OEOA with more active monomers in the presence of chloride ions. *c*HE was shown to be independent of

the mechanism of Cu^{I} regeneration, both *e*ATRP and SARA ATRP yielding excellent results. Different copolymers with high molecular weight and narrow dispersity were obtained in different solvents with different couples of monomers, showing that *c*HE is suitable for a wide range of polymerization mixtures. So far it is rather difficult to envisage which Cu(I) regeneration method is better for *c*HE, however controlled potential electrolysis should be preferred as a unique and outstanding way to precisely modulate the amount of generated active catalyst and avoid side-reactions.

References

1. Beers, K. L.; Gaynor, S. G.; Matyjaszewski, K.; Sheiko, S. S.; Möller, M., The Synthesis of Densely Grafted Copolymers by Atom Transfer Radical Polymerization. *Macromolecules* **1998**, *31*, 9413-9415.
2. Qin, S.; Saget, J.; Pyun, J.; Jia, S.; Kowalewski, T., Synthesis of Block, Statistical, and Gradient Copolymers from Octadecyl (Meth)acrylates Using Atom Transfer Radical Polymerization. *Macromolecules* **2003**, *36*, 8969-8977.
3. Shipp, D. A.; Wang, J.-L.; Matyjaszewski, K., Synthesis of Acrylate and Methacrylate Block Copolymers Using Atom Transfer Radical Polymerization. *Macromolecules* **1998**, *31*, 8005-8008.
4. Matyjaszewski, K., Factors Affecting Rates of Comonomer Consumption in Copolymerization Processes with Intermittent Activation. *Macromolecules* **2002**, *35*, 6773-6781.
5. Arita, T.; Kayama, Y.; Ohno, K.; Tsujii, Y.; Fukuda, T., High-pressure atom transfer radical polymerization of methyl methacrylate for well-defined ultrahigh molecular-weight polymers. *Polymer* **2008**, *49*, 2426-2429.
6. Davis, K. A.; Matyjaszewski, K., Statistical, Gradient, Block, and Graft Copolymers by Controlled/Living Radical Polymerizations. In *Statistical, Gradient, Block and Graft Copolymers by Controlled/Living Radical Polymerizations*, Springer Berlin Heidelberg: Berlin, Heidelberg, 2002; pp 1-13.
7. Pietrasik, J.; Dong, H.; Matyjaszewski, K., Synthesis of High Molecular Weight Poly(styrene-*co*-acrylonitrile) Copolymers with Controlled Architecture. *Macromolecules* **2006**, *39*, 6384-6390.
8. Hashimoto, T.; Tsukahara, Y.; Tachi, K.; Kawai, H., Structure and properties of tapered block polymers. 4. "Domain-boundary mixing" and "mixing-in-domain" effects on microdomain morphology and linear dynamic mechanical response. *Macromolecules* **1983**, *16*, 648-657.
9. Matyjaszewski, K.; Tsarevsky, N. V., Nanostructured functional materials prepared by atom transfer radical polymerization. *Nature Chemistry* **2009**, *1*, 276.
10. Matyjaszewski, K.; Mu Jo, S.; Paik, H.-J.; Gaynor, S. G., Synthesis of Well-Defined Polyacrylonitrile by Atom Transfer Radical Polymerization. *Macromolecules* **1997**, *30*, 6398-6400.

11. Xia, J.; Paik, H.-J.; Matyjaszewski, K., Polymerization of Vinyl Acetate Promoted by Iron Complexes. *Macromolecules* **1999**, *32*, 8310-8314.
12. Krzysztof, M.; A., S. D.; P., M. G.; G., G. S.; Tadeusz, P., Simple and effective one-pot synthesis of (meth)acrylic block copolymers through atom transfer radical polymerization. *Journal of Polymer Science Part A: Polymer Chemistry* **2000**, *38*, 2023-2031.
13. Kowalewski, T.; Tsarevsky, N. V.; Matyjaszewski, K., Nanostructured Carbon Arrays from Block Copolymers of Polyacrylonitrile. *Journal of the American Chemical Society* **2002**, *124*, 10632-10633.
14. Dufour, B.; Koynov, K.; Pakula, T.; Matyjaszewski, K., PBA–PMMA 3-Arm Star Block Copolymer Thermoplastic Elastomers. *Macromol. Chem. Phys.* **2008**, *209*, 1686-1693.
15. Krzysztof, M.; J., Z. M.; V., A. S.; Dorota, G.; Tadeusz, P., Gradient copolymers by atom transfer radical copolymerization. *Journal of Physical Organic Chemistry* **2000**, *13*, 775-786.
16. Angot, S.; Murthy, K. S.; Taton, D.; Gnanou, Y., Atom transfer radical polymerization of styrene using a novel octafunctional initiator: Synthesis of well-defined polystyrene stars. *Macromolecules* **1998**, *31*, 7218-7225.
17. Frank, E.; Steudle, L. M.; Ingildeev, D.; Spörl, J. M.; Buchmeiser, M. R., Carbon fibers: precursor systems, processing, structure, and properties. *Angewandte Chemie International Edition* **2014**, *53*, 5262-5298.
18. Xin, W.; Song, Y., Mesoporous carbons: recent advances in synthesis and typical applications. *Rsc Advances* **2015**, *5*, 83239-83285.
19. Pitto, V.; Voit, B. I.; Loontjens, T. J.; van Benthem, R. A., New Star-Branched Poly(acrylonitrile) Architectures: ATRP Synthesis and Solution Properties. *Macromolecular Chemistry and Physics* **2004**, *205*, 2346-2355.
20. Hou, C.; Qu, R.; Liu, J.; Ying, L.; Wang, C., High-molecular-weight polyacrylonitrile by atom transfer radical polymerization. *Journal of applied polymer science* **2006**, *100*, 3372-3376.
21. Zhong, M.; Jiang, S.; Tang, Y.; Gottlieb, E.; Kim, E. K.; Star, A.; Matyjaszewski, K.; Kowalewski, T., Block copolymer-templated nitrogen-enriched nanocarbons with morphology-dependent electrocatalytic activity for oxygen reduction. *Chemical Science* **2014**, *5*, 3315-3319.
22. Gottlieb, E.; Kopeć, M.; Banerjee, M.; Mohin, J.; Yaron, D.; Matyjaszewski, K.; Kowalewski, T., In-situ platinum deposition on nitrogen-doped carbon films as a source of catalytic activity in a hydrogen evolution reaction. *ACS applied materials & interfaces* **2016**, *8*, 21531-21538.
23. Zhong, M.; Natesakhawat, S.; Baltrus, J. P.; Luebke, D.; Nulwala, H.; Matyjaszewski, K.; Kowalewski, T., Copolymer-templated nitrogen-enriched porous nanocarbons for CO₂ capture. *Chemical Communications* **2012**, *48*, 11516-11518.
24. Song, Y.; Wei, G.; Kopeć, M.; Rao, L.; Zhang, Z.; Gottlieb, E.; Wang, Z.; Yuan, R.; Ye, G.; Wang, J., Copolymer-Templated Synthesis of Nitrogen-Doped Mesoporous Carbons for Enhanced Adsorption of Hexavalent Chromium and Uranium. *ACS Applied Nano Materials* **2018**.
26. Ju, M. J.; Choi, I. T.; Zhong, M.; Lim, K.; Ko, J.; Mohin, J.; Lamson, M.; Kowalewski, T.; Matyjaszewski, K.; Kim, H. K., Copolymer-templated nitrogen-enriched nanocarbons as a low charge-transfer resistance and highly stable

alternative to platinum cathodes in dye-sensitized solar cells. *Journal of Materials Chemistry A* **2015**, *3*, 4413-4419.

27. Matyjaszewski, K.; Jo, S. M.; Paik, H.-j.; Shipp, D. A., An investigation into the CuX/2,2'-bipyridine (X= Br or Cl) mediated atom transfer radical polymerization of acrylonitrile. *Macromolecules* **1999**, *32*, 6431-6438.

28. Dong, H.; Tang, W.; Matyjaszewski, K., Well-defined high-molecular-weight polyacrylonitrile via activators regenerated by electron transfer ATRP. *Macromolecules* **2007**, *40*, 2974-2977.

29. Kopeć, M.; Yuan, R.; Gottlieb, E.; Abreu, C. M.; Song, Y.; Wang, Z.; Coelho, J. F.; Matyjaszewski, K.; Kowalewski, T., Polyacrylonitrile-*b*-poly (butyl acrylate) block copolymers as precursors to mesoporous nitrogen-doped carbons: synthesis and nanostructure. *Macromolecules* **2017**, *50*, 2759-2767.

30. Chen, Q.; Zhang, Z.; Zhou, N.; Cheng, Z.; Tu, Y.; Zhu, X., Copper (0)-mediated living radical polymerization of acrylonitrile at room temperature. *Journal of Polymer Science Part A: Polymer Chemistry* **2011**, *49*, 1183-1189.

31. Liu, X. H.; Zhang, G. B.; Li, B. X.; Bai, Y. G.; Li, Y. S., Copper (0)-mediated living radical polymerization of acrylonitrile: SET-LRP or AGET-ATRP. *Journal of Polymer Science Part A: Polymer Chemistry* **2010**, *48*, 5439-5445.

32. Lamson, M.; Kopeć, M.; Ding, H.; Zhong, M.; Matyjaszewski, K., Synthesis of well-defined polyacrylonitrile by ICAR ATRP with low concentrations of catalyst. *Journal of Polymer Science Part A: Polymer Chemistry* **2016**, *54*, 1961-1968.

33. Huang, Z.; Chen, J.; Zhang, L.; Cheng, Z.; Zhu, X., ICAR ATRP of acrylonitrile under ambient and high pressure. *Polymers* **2016**, *8*, 59.

34. Chmielarz, P.; Fantin, M.; Park, S.; Isse, A. A.; Gennaro, A.; Magenau, A. J.; Sobkowiak, A.; Matyjaszewski, K., Electrochemically mediated atom transfer radical polymerization (*e*ATRP). *Progress in Polymer Science* **2017**, *69*, 47-78.

35. Lorandi, F.; Fantin, M.; Isse, A. A.; Gennaro, A., Electrochemical triggering and control of atom transfer radical polymerization. *Current Opinion in Electrochemistry* **2018**, *8*, 1-7.

36. Magenau, A. J.; Strandwitz, N. C.; Gennaro, A.; Matyjaszewski, K., Electrochemically mediated atom transfer radical polymerization. *Science* **2011**, *332*, 81-84.

37. Magenau, A. J.; Bortolamei, N.; Frick, E.; Park, S.; Gennaro, A.; Matyjaszewski, K., Investigation of electrochemically mediated atom transfer radical polymerization. *Macromolecules* **2013**, *46*, 4346-4353.

38. Fantin, M.; Isse, A. A.; Gennaro, A.; Matyjaszewski, K., Understanding the fundamentals of aqueous ATRP and defining conditions for better control. *Macromolecules* **2015**, *48*, 6862-6875.

39. Fantin, M.; Isse, A. A.; Venzo, A.; Gennaro, A.; Matyjaszewski, K., Atom transfer radical polymerization of methacrylic acid: a won challenge. *Journal of the American Chemical Society* **2016**, *138*, 7216-7219.

40. Fantin, M.; Chmielarz, P.; Wang, Y.; Lorandi, F.; Isse, A. A.; Gennaro, A.; Matyjaszewski, K., Harnessing the Interaction between Surfactant and Hydrophilic Catalyst To Control *e*ATRP in Miniemulsion. *Macromolecules* **2017**, *50*, 3726-3732.

41. De Bon, F.; Fantin, M.; Isse, A. A.; Gennaro, A., Electrochemically mediated ATRP in ionic liquids: Controlled polymerization of methyl acrylate in [BMIm][OTf]. *Polymer Chemistry* **2018**.
42. Zhong, M.; Kim, E. K.; McGann, J. P.; Chun, S.-E.; Whitacre, J. F.; Jaroniec, M.; Matyjaszewski, K.; Kowalewski, T., Electrochemically active nitrogen-enriched nanocarbons with well-defined morphology synthesized by pyrolysis of self-assembled block copolymer. *Journal of the American Chemical Society* **2012**, *134*, 14846-14857.
43. Bortolamei, N.; Isse, A. A.; Di Marco, V. B.; Gennaro, A.; Matyjaszewski, K., Thermodynamic properties of copper complexes used as catalysts in atom transfer radical polymerization. *Macromolecules* **2010**, *43*, 9257-9267.
44. Fantin, M.; Lorandi, F.; Gennaro, A.; Isse, A. A.; Matyjaszewski, K., Electron transfer reactions in atom transfer radical polymerization. *Synthesis* **2017**, *49*, 3311-3322.
45. Lorandi, F.; Fantin, M.; Isse, A. A.; Gennaro, A., RDRP in the presence of Cu⁰: The fate of Cu(I) proves the inconsistency of SET-LRP mechanism. *Polymer* **2015**, *72*, 238-245.
46. Lanzalaco, S.; Fantin, M.; Scialdone, O.; Galia, A.; Isse, A. A.; Gennaro, A.; Matyjaszewski, K., Atom Transfer Radical Polymerization with Different Halides (F, Cl, Br, and I): Is the Process “Living” in the Presence of Fluorinated Initiators? *Macromolecules* **2016**, *50*, 192-202.
47. Lorandi, F.; Fantin, M.; Isse, A. A.; Gennaro, A.; Matyjaszewski, K., New protocol to determine the equilibrium constant of atom transfer radical polymerization. *Electrochimica Acta* **2018**, *260*, 648-655.
48. Fantin, M.; Isse, A. A.; Bortolamei, N.; Matyjaszewski, K.; Gennaro, A., Electrochemical approaches to the determination of rate constants for the activation step in atom transfer radical polymerization. *Electrochimica Acta* **2016**, *222*, 393-401.
49. Krys, P.; Matyjaszewski, K., Kinetics of atom transfer radical polymerization. *European Polymer Journal* **2017**, *89*, 482-523.
50. Junkers, T.; Koo, S. P.; Barner-Kowollik, C., Determination of the propagation rate coefficient of acrylonitrile. *Polymer Chemistry* **2010**, *1*, 438-441.
51. Lorandi, F.; Fantin, M.; Isse, A. A.; Gennaro, A., Electrochemically mediated atom transfer radical polymerization of *n*-butyl acrylate on non-platinum cathodes. *Polymer Chemistry* **2016**, *7*, 5357-5365.

Chapter 5

Electrochemically mediated ATRP of methyl methacrylate in [BMIm][OTf] and ethanol

5.1 Introduction

In Chapter 3, *e*ATRP of methyl acrylate was analyzed in detail and the effects of several reaction parameters were evaluated. The first successful utilization of [BMIm][OTf] in *e*ATRP prompted us to explore its application as solvent and supporting electrolyte also for methacrylic monomers. Methacrylates are widely used and have a quite important market. As of 2015, the U.S. methacrylate market (as PMMA) was estimated as 4.06 billion \$, with PMMA applications in many fields, mainly based on its high thermal and chemical resistance, durability, low smoke emission (if burned or when processed) and excellent abrasion resistance.¹ Among the many applications of PMMA, its use as a shatterproof alternative to glass in public illuminations, aircraft canopies and windows for domestic applications is worth mentioning.² Optical fibers made from PMMA are utilized in telecommunications, and in various applications such as electronic screens and endoscopy, thanks to the unusual property of this material to retain a beam of reflected light within surfaces.³

Methyl methacrylate (MMA), the simplest and the most widely used monomer of this family, was never polymerized in [BMIm][OTf] and only one single polymerization by *e*ATRP in DMF was reported.⁴ For this reason and for its enormous applications in everyday life, its *e*ATRP was studied in detail in two green solvents, namely [BMIm][OTf] and ethanol. The structures of methyl acrylate and methyl methacrylate are very similar but the additional -CH₃ group on the olefinic unit drastically modifies the reactivity of the monomer. Consequently, MMA polymerization is completely different from that of MA in terms of activation rate constant, polymer structure and viscosity.

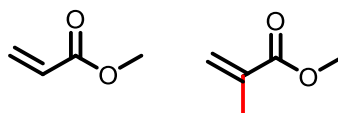


Figure 5.1. Chemical structures of methyl acrylate and methyl methacrylate. The -CH₃ group is evidenced in red on MMA structure.

This chapter shows how sensible is *e*ATRP to structural variations of monomers and highlights the impact of catalytic halogen exchange not only as a tool for block copolymer synthesis but also as a tool to gain extra control on methacrylate polymerizations in [BMIm][OTf] and in ethanol. Tacticity was determined to check if the ionic liquid could induce some stereocontrol in contrast to classic molecular solvents.

5.2 Switching from acrylates to methacrylates: the problem of the penultimate effect

The best polymerization conditions found for *e*ATRP of methyl acrylate in [BMIm][OTf] were:

1. [Cu^{II}TPMA]²⁺ as catalyst at 10⁻³ M concentration, formed in situ by equimolar amounts of CuBr₂ and tris(2-pyridylmethyl)amine;
2. 10⁻² M ethyl 2-bromoisobutyrate initiator, which well mimics (meth)acrylate structures;
3. $E_{app} = E_{1/2} - 0.06$ V to impose $C_{Cu^I} / C_{Cu^{II}} = 10$ at the surface of the working electrode;
4. $T = 50$ °C.

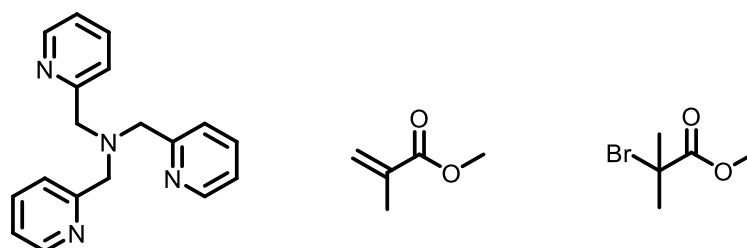


Figure 5.2. Chemical structures of the components involved in *e*ATRP of methyl methacrylate, from left to right: tris(2-pyridylmethyl)amine (TPMA), methyl methacrylate (MMA) and ethyl 2-bromoisobutyrate (EBiB).

The possibility of maintaining these conditions for *e*ATRP of methyl methacrylate in [BMIm][OTf] was first explored. As described in Chapter 3, electrochemical characterizations were performed prior to the electrolysis. Figure 5.3 shows cyclic voltammetry of $[\text{BrCu}^{\text{II}}\text{TPMA}]^{2+}$ in [BMIm][OTf] and in [BMIm][OTf]/MMA (1:1, v/v); the reversible voltammetric pattern observed in the presence of the monomer indicates that both $[\text{BrCu}^{\text{II}}\text{TPMA}]^{2+}$ and $[\text{BrCu}^{\text{I}}\text{TPMA}]^+$ are stable. The monomer causes a drift of $E_{1/2}$ to more positive values due to lower polarity of the mixture. The increase of the current is due to the reduced viscosity in the presence of MMA (Figure 5.3).

Addition of 10^{-2} M EBiB caused an impressive modification of the voltammetric pattern, indicating the establishment of a considerably high catalysis (Figure 5.3).

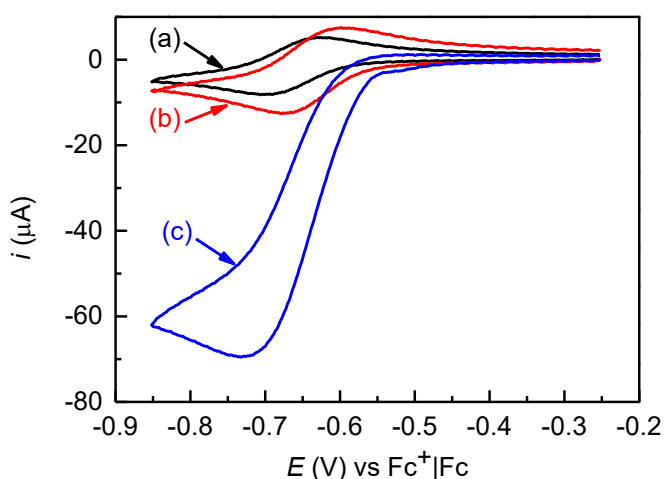


Figure 5.3. Cyclic Voltammetry of 2×10^{-3} M $[\text{BrCu}^{\text{II}}\text{TPMA}]^+$ in [BMIm][OTf] (a) or 10^{-3} M $[\text{BrCu}^{\text{II}}\text{TPMA}]^+$ in MMA/[BMIm][OTf] (1:1, v/v) in the absence (b) and in the presence of 10^{-2} M EBiB (c), recorded at 50°C on a GC disk electrode at 0.2 V/s.

5.3 *e*ATRP of methyl methacrylate in [BMIm][OTf] using EBiB as initiator

A very high catalysis may result in a high polymerization rate and hence high conversion in a short time, with charge saving benefits and low termination events. However, the results summarized in Table 5.1 show a very poorly controlled polymerization with low to moderate conversion.

Table 5.1. *e*ATRP of 50 % (v/v) MMA in [BMIm][OTf] catalyzed by [Cu^{II}TPMA]²⁺ at 50 °C using EBiB as initiator, at different applied potentials and different concentrations of [Br⁻].

| Entry | <i>t</i> (h) | <i>E</i> _{app} | <i>C</i> _{Br⁻} (mM) | Conv. (%) | <i>M</i> _n th | <i>M</i> _n ^{app} | <i>D</i> | <i>I</i> _{eff} | <i>Q</i> (C) |
|-------|--------------|-----------------------------------|--|--------------|-------------------------------------|--------------------------------------|----------|-------------------------|--------------|
| 1 | 3 | <i>E</i> _{1/2} - 0.06 | 2 | 43 | 20200 | 18900 | 2.6 | 1.07 | 2.24 |
| 2 | 3 | <i>E</i> _{1/2} + 0.06 | 2 | 57 | 26800 | 49000 | 4.5 | 0.55 | 4.76 |
| 3 | 3 | <i>E</i> _{1/2} + 0.06 | 10 | 31 | 14570 | 42000 | 4.1 | 0.35 | 3.25 |

^a*C*_{MMA}:*C*_{Cu}:*C*_{TPMA}:*C*_{EBiB} = 467:0.1:0.1:1. *V*_{tot} = 5 mL. WE = Pt mesh (estimated surface area = 6 cm²), CE = graphite in a separate compartment. DP = 467.

The polymerization triggered with the same conditions of methyl acrylate (Entry 1) produced PMMA-Br of broad dispersity. Clearly the polymerization was too fast at *E*_{1/2} - 0.06 V: in the early stages, the catalyst rapidly activates the initiator and the small oligomers produced, causing a burst of radicals that propagate without control and terminate by coupling or disproportionation. To avoid this, the applied potential was switched to *E*_{1/2} + 0.06 V to reduce the rate of Cu^I regeneration. According to eq. 3.3, shifting *E*_{app} from *E*_{1/2} - 0.06 V to *E*_{1/2} + 0.06 V should decrease *C*_{Cu^I} / *C*_{Cu^{II}} at the electrode surface from 10 to 0.1. Surprisingly, polymerization was faster with worsened control, when *E*_{app} was shifted to *E*_{1/2} + 0.06 V. Excluding the applied potential as the origin of poor control, other mechanisms should be considered, for example, decomposition of the dormant species by solvolysis or other means, interactions with the solvent or other side-reactions. To improve chain-end fidelity and suppress undesired side-reactions of the C-Br end-group, an excess of bromide ions was added to the polymerization solution (Entry 3). No improvements were observed: polymers were still of very broad dispersity and the mismatch between theoretical and apparent MWs was further marked. Therefore, poor control is not related to the end-functionality.

We therefore moved to investigate if the problems were related to a known phenomenon of methyl methacrylate, termed the *penultimate effect*. It is reported that inefficient initiation provided by EBiB causes *penultimate effect* in conventional solvents.⁵ In general, the reactivity of tertiary alkyl halides is higher than that of secondary ones, due to better stabilization of the radicals derived from the former species and a lower C-Br cleavage energy. The MMA-Br terminal unit is very sensitive to the structure of the penultimate unit. Reactivity of monomeric and dimeric acrylate dormant species (MA or BA for instance) is essentially identical, meaning that both species are good initiators for ATRP of the corresponding monomers. In contrast, dimeric methacrylate dormant species are more reactive than MMA-Br. The bulky MMA penultimate unit destabilizes the dormant alkyl bromide, lowering the C-Br bond dissociation energy, and presumably stabilizes the resulting sp²-hybridized radical species. Because of this back-strain effect, H-MMA-MA-Br is ~5 times more active than H-MA-MA-Br. The rate of activation of a dormant chain-end with an MMA-Br terminal unit is ~20 times faster than with a MA terminal unit with the same penultimate unit. This is attributed to the formation of thermodynamically more stable tertiary radical from the former species when compared to the less stable secondary radical from the latter species. The combined effects of back-strain and generation of stable tertiary radical result in a ~100-fold increase of k_{act} for H-MMA-MMA-Br with respect to H-MA-MA-Br.⁶ Even though EBiB mimics well the growing PMMA, it fails to initiate quantitatively the polymerization. One of the most important ATRP prerequisites is that the activity of the initiator should be higher or equal to that of the growing polymer to avoid poor initiation. Therefore, we changed the initiator to 2-bromopropionitrile (BPN), which is more active than EBiB and dormant species from MMA polymerization.⁷

5.4 *e*ATRP of MMA in [BMIm][OTf] using BPN as initiator

As shown in Figure 5.4, addition of BPN to a solution of [BrCu^{II}TPMA]²⁺ in 50 % (v/v) MMA in [BMIm][OTf] resulted in a very large catalytic current enhancement (~8-fold increase of I_{pc}). As expected, electrogenerated Cu^I reacts faster with BPN than EBiB, yielding a higher catalytic current.

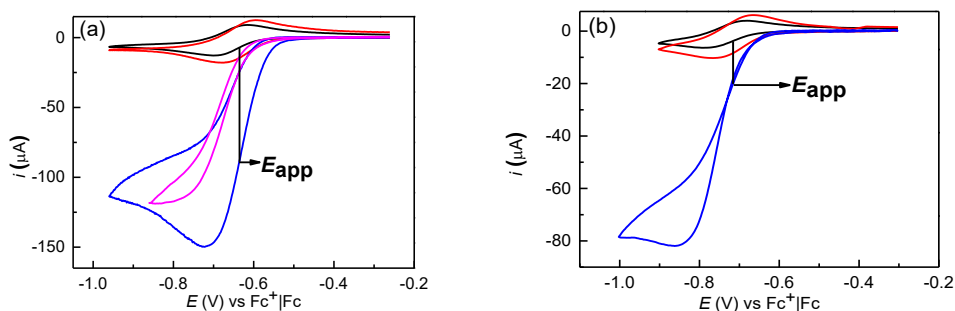


Figure 5.4. (a) CV of 2×10^{-3} M $[\text{BrCu}^{\text{II}}\text{TPMA}]^+$ in $[\text{BMIm}][\text{OTf}]$ (—), in presence of 50% v/v MMA (—), in presence of 10 mM BPN (—) and in presence of 10 mM BPN + 10 mM TEABr (—); (b) CV of 2×10^{-3} M $[\text{ClCu}^{\text{II}}\text{TPMA}]^+$ in $[\text{BMIm}][\text{OTf}]$ (—), in presence of 50% v/v MMA (—) and in presence of 10 mM BPN + 10 mM TEACl (—), recorded at 50 °C on GC electrode at 0.2 V/s.

Starting with conditions like those of MA polymerization, *e*ATRP was electrochemically triggered using BPN as initiator. The effect of applied potential was first investigated (Table 5.2). It appeared immediately that BPN was by far a better initiator than EBiB as $D < 1.5$. However, initiation efficiency was still poor ($< 20\%$). Apparent MWs were significantly higher than the theoretical values. To address the poor initiation, the application of a more positive potential as $E_{\text{app}} > E_{1/2}$ may be helpful. According to Eq. 5.1:

$$R_p = k_p K_{\text{ATRP}} \frac{C_{\text{RX}} C_{\text{Cu}^{\text{I}} L_n}}{C_{\text{X-Cu}^{\text{II}} L_n}} C_M, \quad (5.1)$$

which describes the rate of polymerization as a function of concentrations of monomer, initiator and catalyst in its two forms, and Eq. 5.2:

$$E_{\text{app}} = E^{o'} + \frac{RT}{F} \ln \frac{C_{\text{Cu}^{\text{II}}}}{C_{\text{Cu}^{\text{I}}}} \quad (5.2)$$

R_p can be modulated by E_{app} through the ratio between Cu^{I} and Cu^{II} concentrations. When $E_{\text{app}} = E_{1/2}$ the ratio at the surface of the electrode is unitary, while $C_{\text{Cu}^{\text{II}}} > C_{\text{Cu}^{\text{I}}}$ if $E_{\text{app}} > E_{1/2}$ and vice versa.⁸ We tuned the applied potential to obtain $C_{\text{Cu}^{\text{II}}}/C_{\text{Cu}^{\text{I}}}$ ratios close to 5 - 10, to regenerate more slowly Cu^{I} and hopefully improve initiation efficiency. This strategy was not helpful: at $E_{\text{app}} = E_{1/2} + 0.03$ V or $E_{\text{app}} = E_{1/2} + 0.06$ V no improvements were observed on D , M_n

and I_{eff} . Charge consumption was high in all these experiments, indicating high termination in the early stages of polymerization.

Thus, BPN proved to be inadequate as initiator for *e*ATRP of MMA. There may be at least two different hypotheses for the inefficient polymerizations using BPN: the first is again the *penultimate effect* and the second could be an enhanced propagation of MMA in ILs. The latter is a well-known behavior and was reported by Harrison et al.⁹ Although application of potentials higher than $E_{1/2}$ did not appreciably improve polymerization, in terms of M_n and I_{eff} , \bar{D} was slightly reduced (from 1.46 to 1.40, which is almost comparable with the experimental errors).

Table 5.2. *e*ATRP of 50% v/v MMA in [BMIm][OTf] catalyzed by $[\text{Cu}^{\text{II}}\text{TPMA}]^{2+}$ at 50 °C using BPN as initiator.^a

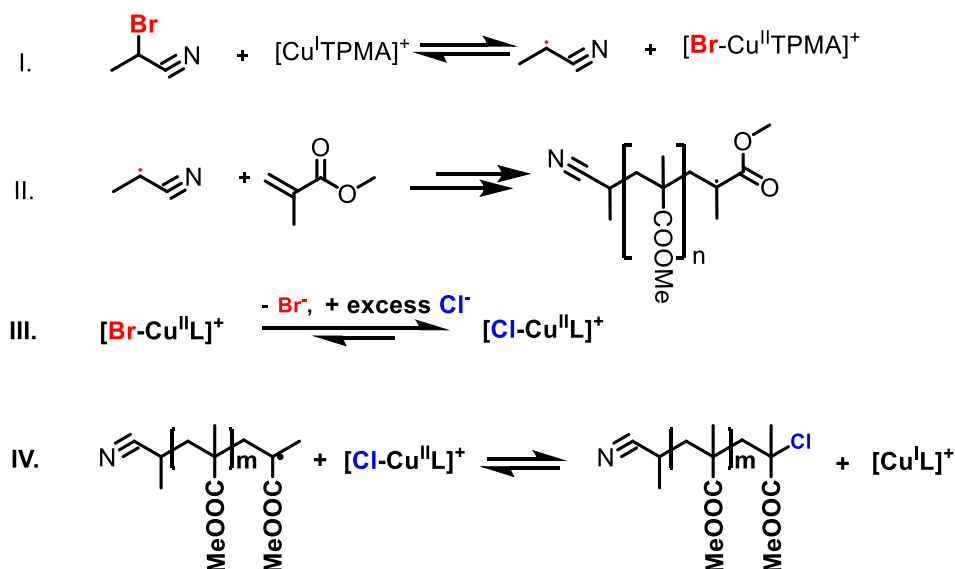
| Entry | t (h) | E_{app} (V) | Conv. (%) | M_n^{th} | M_n^{app} | \bar{D} | I_{eff} | k_{app} | Q (C) |
|-------|---------|----------------------|-----------|-------------------|--------------------|-----------|------------------|------------------|---------|
| 1 | 3 | $E_{1/2}$ | 34 | 16000 | 86500 | 1.46 | 0.19 | 0.127 | 6.08 |
| 2 | 3 | $E_{1/2} + 0.03$ | 30 | 14100 | 70100 | 1.40 | 0.20 | 0.112 | 5.66 |
| 3 | 5 | $E_{1/2} + 0.06$ | 25 | 11750 | 60600 | 1.40 | 0.19 | 0.049 | 5.20 |

^aOther conditions: $C_{\text{MMA}}:C_{\text{Cu}}:C_{\text{TPMA}}:C_{\text{BPN}} = 467:0.1:0.1:1$. $V_{\text{tot}} = 5$ mL. WE = Pt mesh (estimated surface area = 6 cm²), CE = graphite in separate compartment. DP = 467.

5.5 Catalytic halogen exchange: from mechanism to more controlled polymerizations

The importance of catalytic halogen exchange (*c*HE) is due to its ability to suppress the reactivity mismatch between a macroinitiator and the newly generated block copolymer chains when the latter are more reactive than the formed (see Chapter 4). Ideally, imagine the first block as a single molecule of initiator such as BPN and MMA the second monomer with which to build the second block. The dormant species of the new chain, $\text{CH}_3\text{-CH}(\text{CN})\text{-MMA-Br}$ is more reactive than the initiator and this reactivity mismatch will result in a poor initiation efficiency. The addition of a source of chloride ions to the

polymerization mixture can suppress the reactivity mismatch between BPN and PMMA-Br, by switching catalytically C-Br to C-Cl, according to Scheme 5.1:



Scheme 5.1. Mechanism of catalytic halogen exchange. Evidenced in bold are steps III and IV that are crucial for cHE.

Table 5.3 shows the results of a new set of polymerizations, performed in the presence of Et₄NCl and initiated by BPN. For the sake of comparison *e*ATRP experiments performed in similar conditions without chloride ions are also reported in the Table.

Table 5.3. *e*ATRP of 50% (v/v) MMA in [BMIm][OTf] catalyzed by [Cu^{II}TPMA]²⁺ at 50 °C, using BPN as initiator in the presence of an excess of halide ions.^a

| Entry | <i>t</i> (h) | X ⁻ | C _X - (mM) | Conv (%) | <i>M</i> _n , th | <i>M</i> _n , ^{app} | <i>D</i> | <i>I</i> _{eff} | <i>k</i> _{app} | <i>Q</i> (C) |
|-------|--------------|----------------|--------------------------|-------------|---------------------------------------|--|----------|-------------------------|-------------------------|--------------|
| 1 | 3 | Br | 2 | 28 | 13160 | 125000 | 1.45 | 0.11 | 0.110 | 7.01 |
| 2 | 1.25 | Br | 12 | 33 | 15510 | 88700 | 1.40 | 0.17 | 0.262 | 6.60 |
| 3 | 1.25 | Cl | 12 | 52 | 24440 | 50100 | 1.19 | 0.49 | 0.541 | 2.24 |
| 4 | 1.25 | Cl | 22 | 49 | 22900 | 30600 | 1.21 | 0.75 | 0.551 | 4.00 |

^a. Other conditions: C_{MMA}:C_{Cu}:C_{TPMA}:C_{RX} = 467:0.1:0.1:1. *V*_{tot} = 5 mL. WE = Pt mesh (estimated surface area = 6 cm²), CE = graphite in separate compartment. *E*_{app} = *E*_{1/2}. DP = 467.

At $E_{app} = E_{1/2}$, first the effect of an excess of bromide ions was studied. An excess of halide ions lowers the rate of activation by decreasing the concentration of reactive Cu^I , *i.e.*, $[\text{Cu}^I\text{L}]^+$. It might also affect the deactivation rate by increasing the concentration of the deactivator complex, $[\text{XCu}^{II}\text{L}]^+$. Overall, the expected effect of excess X^- improved polymerization control. In effect, slight improvements were observed on \bar{D} , conversion and M_n when the concentration of bromide ions was increased from 2 mM to 12 mM (Table 5.3, entries 1 and 2). Clearly bromide ions could not suppress the reactivity mismatch, so I_{eff} remained very low. When chloride ions were added, a strong improvement was obtained. According to Scheme 5.1, at the beginning of polymerization, after BPN activation by $[\text{Cu}^I\text{TPMA}]^+$, $\text{CH}_3(\text{CH}^\bullet)\text{CN}$ reacts with MMA and the new radical propagates until it is deactivated. Deactivation occurs with the transfer of a chlorine atom rather than bromine atom because the deactivator complex is exclusively present as $[\text{ClCu}^{II}\text{TPMA}]^+$. Obviously, the C-Cl bond in the dormant species, $\text{P}_n\text{-MMA-Cl}$, is stronger than the C-Br bond in BPN and requires more energy to be cleaved. In other words, activation of $\text{P}_n\text{-MMA-Cl}$ is slower than BPN activation to generate new chains. With these conditions, the initiation efficiency increases. As shown Table 5.3 (entry 3), when *e*ATRP was repeated in the presence of 12 mM Et_4NCl , not only \bar{D} fell from 1.40 to 1.19 but also the theoretical and apparent MWs became closer and I_{eff} improved from 17% to 49%. This very simple strategy greatly improved the polymerization. Progresses in this sense are shown in Figure 5.5:

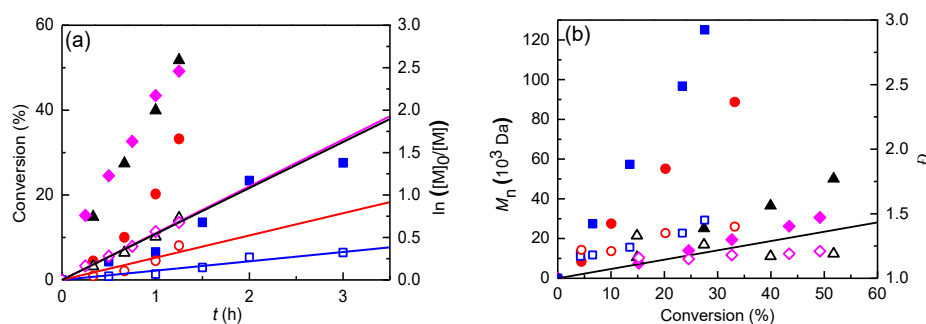


Figure 5.5. (a) Kinetic plots and (b) evolution of M_n and \bar{D} with conversion for potentiostatic *e*ATRP of 50% (v/v) MMA in [BMIm][OTf] performed at $E_{app} = E_{1/2}$ in the presence of halide ions. Conditions: $C_{\text{MMA}}:C_{\text{Cu}}:C_{\text{TPMA}}:C_{\text{RX}} = 467:0.1:0.1:1$. $C_{\text{Cu}} = 10^{-3}$ M. Halide ions: (▲) 12 mM Cl⁻, (◆) 22 mM Cl⁻, (■) 2 mM Br⁻, (●) 12 mM Br⁻. Black straight line represents theoretical molecular weight. Empty symbols refer to the right ordinate in the figures.

Increase of C_{Cl^-} to 22 mM further improved the polymerization control, giving experimental M_n closely following the theoretical values and initiation efficiency of 75%, while conversion and dispersity remained essentially unaffected. Despite these improvements, the reaction medium became considerably viscous at 49% conversion, which forced to stop polymerization. Viscosity bears a great relevance in this process because of the very high viscosity of PMMA solutions in general and the high viscosity of the ionic liquid used as a solvent. Moreover, at 50 °C PMMA is well below its glass transition temperature ($T_g = 101$ °C) and mobility of the polymer is further impeded.

5.6 *e*ATRP of MMA catalyzed by $[Cu^{II}PMDETA]^{2+}$ in $[BMIm][OTf]$

Given that methacrylates are very reactive monomers, *e*ATRP can be triggered with a less active catalyst. For instance, K_{ATRP} of $[Cu^I PMDETA]^+$ with EBiB is twice smaller than that of $[Cu^I TPMA]^+$ with the same initiator in CH_3CN .⁷ Moreover, PMDETA is inexpensive compared to TPMA.¹⁰ Thus, optimization of *e*ATRP of MMA with $[Cu^{II}PMDETA]^{2+}$ appeared to be very appealing. The reaction could be achieved using $RX =$ ethyl α -bromophenylacetate (EBPA), currently the most active initiator, which does not cause the penultimate effect, permitting the best initiation efficiency. As usual, voltammetric characterization of the catalytic system was performed, showing that Cu^I reacts rapidly with EBPA.

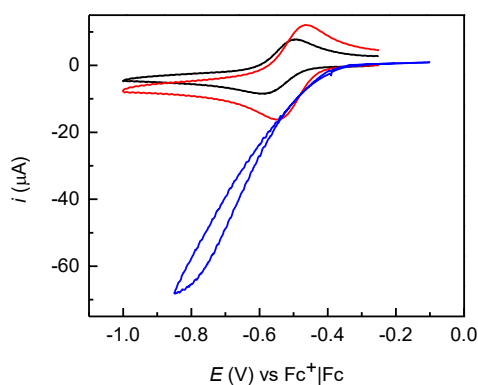


Figure 5.6. CV of 2×10^{-3} M $[BrCu^{II}PMDETA]^+$ in $[BMIm][OTf]$ (—), in presence of 50% v/v MMA (—), in presence of 1×10^{-2} M EBPA (—), recorded at 50 °C on GC electrode at 0.2 V/s.

In Table 5.4 and Figure 5.7 the results of *e*ATRP using $[\text{Cu}^{\text{II}}\text{PMDETA}]^{2+}$ as catalyst and EBPA as initiator are shown. The electrolysis was done at $E_{\text{app}} = E_{1/2}$ at two different concentrations of bromide ions.

Table 5.4. *e*ATRP of 50% (v/v) MMA in [BMIm][OTf] catalyzed by $[\text{Cu}^{\text{II}}\text{PMDETA}]^{2+}$ at 50 °C using EBPA as initiator.^a

| Entry | t (h) | C_{Br^-} (mM) | Conv. (%) | M_n^{th} | M_n^{app} | \bar{D} | I_{eff} | Q (C) |
|-------|---------|------------------------|-----------|-------------------|--------------------|-----------|------------------|---------|
| 1 | 1.16 | 2 | 31 | 14500 | 19600 | 1.12 | 0.74 | 1.05 |
| 2 | 1.33 | 12 | 50 | 23400 | 28100 | 1.19 | 0.84 | 1.78 |

^aApplied potential = $E_{\text{app}} = E_{1/2}$. Other conditions: $C_{\text{MMA}}:C_{\text{Cu}}:C_{\text{TPMA}}:C_{\text{EBPA}} = 467:0.1:0.1:1$. $V_{\text{tot}} = 5$ mL. WE = Pt mesh (estimated surface area = 6 cm²), CE = graphite in separate compartment. DP = 467.

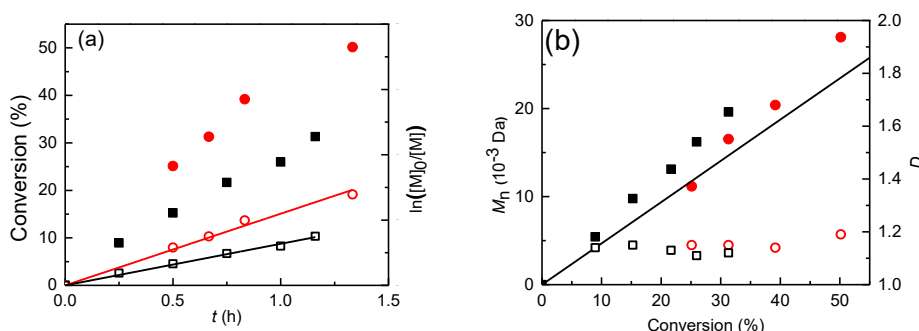


Figure 5.7. (a) Kinetic plots and (b) evolution of M_n and \bar{D} with conversion for potentiostatic *e*ATRP of 50% v/v MMA in [BMIm][OTf]; $E_{\text{app}} = E_{1/2}$. Conditions: $C_{\text{MMA}}:C_{\text{Cu}}:C_{\text{PMDETA}}:C_{\text{RX}}:C_{\text{Br}^-} = 467:1:1:10:x$. $C_{\text{Cu}} = 10^{-3}$ M. x : (■) 2 and (●) 12. The black straight line represents theoretical molecular weights. Empty symbols refer to the right ordinate in the figures.

Reactions were very well controlled using $[\text{Cu}^{\text{II}}\text{PMDETA}]^{2+}$ as catalyst, affording PMMA-Br of narrow dispersity. As expected, excessive viscosity limited conversion to $\leq 50\%$. When a 12 mM excess Br⁻ was added, initiation efficiency as well as conversion increased, while \bar{D} slightly increased. Entry 2 of Table 5.4 may be compared with entry 2 of Table 5.3. The two experiments were conducted in similar conditions, except the catalyst and initiator, but much better results were obtained with $[\text{Cu}^{\text{II}}\text{PMDETA}]^{2+}$. As $[\text{Cu}^{\text{I}}\text{PMDETA}]^+$ is less active than $[\text{Cu}^{\text{I}}\text{TPMA}]^+$, excessive generation of radicals in the early stages of the polymerization was avoided even though a more reactive initiator was used.

Indeed, EBPA is ~ 2 orders of magnitude more active than BPN (in CH_3CN).⁷ $[\text{Cu}^{\text{II}}\text{PMDETA}]^{2+}$ proved to be a very efficient catalyst in ionic liquids and its use might be recommended for very reactive monomers, which usually undergo quite fast polymerization, as it is ~ 160 times less expensive than $[\text{Cu}^{\text{II}}\text{TPMA}]^{2+}$.¹⁰

5.7 From a green ionic solvent to a green molecular solvent: *e*ATRP of MMA in ethanol

The improved conditions for *e*ATRP of MMA catalyzed by $[\text{Cu}^{\text{II}}\text{TPMA}]^{2+}$ in $[\text{BMIm}][\text{OTf}]$ were adopted for a further extension of this specific polymerization to ethanol, a biodegradable molecule considered to be a green solvent. Ethanol dissolves (meth)acrylic polymers,¹¹ and exhibits lower critical solubility temperature (LCST) in the case of PMMA above $60\text{ }^\circ\text{C}$.¹² Despite these good characteristics, ethanol needs a supporting electrolyte, typically a 0.1 M tetraalkylammonium salt, to have a suitable conductivity for electrosynthesis. Obviously, the supporting electrolyte represents an additional cost and, therefore, lowering its concentration would be desirable, also on a green chemistry basis. The reduction of supporting electrolyte is a key aspect for *e*ATRP as the only purpose of supporting electrolyte is achieving enough electrical conductivity in the polymerization medium. To date, however, the effect of its concentration has never been investigated. Electrochemically-mediated polymerizations of MMA in ethanol were performed with catalytic halogen exchange conditions at $E_{\text{app}} = E_{1/2} + 0.06\text{ V}$. The overall concentration of salts, Bu_4NBF_4 and Bu_4NCl , the latter used as a source of Cl^- , was lowered from 0.12 to 0.05 M. The results are summarized in Table 5.5. Interestingly, it was found that the best compromise, in terms of control and conversion, was achieved by using only Bu_4NCl as supporting electrolyte at a relatively low concentration (Table 5.5, entry 4).

Table 5.5. *e*ATRP of 50% (v/v) MMA in ethanol catalyzed by [Cu^{II}TPMA]²⁺ at 50 °C using BPN as initiator.^a

| Entry | <i>t</i> (h) | [Bu ₄ NBF ₄] (M) | [Bu ₄ NCl] (M) | Conv. (%) | <i>M_n</i> th | <i>M_n</i> ^{app} | <i>D</i> | <i>I_{eff}</i> | <i>Q</i> (C) |
|----------------|-----------------|--|------------------------------|--------------|------------------------------------|-------------------------------------|----------|------------------------|-----------------|
| 1 ^b | 1 | 0.10 | 0.02 | 55 | 25700 | 117000 | 1.67 | 0.22 | 9.06 |
| 2 | 4 | 0.10 | 0.02 | 62 | 29000 | 38600 | 1.34 | 0.75 | 5.09 |
| 3 | 4 | 0.02 | 0.05 | 71 | 33200 | 33800 | 1.26 | 0.98 | 3.35 |
| 4 | 4 | 0 | 0.05 | 77 | 36000 | 37800 | 1.21 | 0.95 | 2.20 |

^aUnless otherwise stated, $E_{app} = E_{1/2} + 0.06$ V. Other conditions: $C_{MMA}:C_{Cu}:C_{TPMA}:C_{BPN} = 467:0.1:0.1:1$. $V_{tot} = 10$ mL. WE = Pt mesh (estimated surface area = 6 cm²), CE = graphite in a separate compartment. DP = 467. ^bApplied potential = $E_{app} = E_{1/2}$.

5.8 Tacticity

Polymers are categorized also in terms of tacticity. IUPAC definition of tacticity is “*the orderliness of the succession of configurational repeating units in the main chain of a regular macromolecule, a regular oligomer molecule, a regular block, or a regular chain*”.¹³ The practical significance of tacticity is on its effects on the physical properties of the polymer. The regularity of the macromolecular structure influences the degree to which it has rigid, crystalline long-range order or flexible, amorphous long-range disorder. Precise knowledge of tacticity of a polymer also helps understanding at what temperature a polymer melts, how soluble it is in a solvent and its mechanical properties. Tacticity is described and quantified per diads, triads, tetrads and pentads, which are consecutive units in the backbone of a polymer. Polymers can be (a) isotactic when all substituents are located on the same side of the macromolecular backbone; (b) syndiotactic when the substituents have alternate positions along the chain or (c) atactic when substituents are placed randomly along the chain. Tacticity may be measured directly using ¹H or ¹³C-NMR. This technique enables quantification of the tacticity distribution by comparison of peak areas or integral ranges corresponding to known diads (*r*, *m*), triads (*mm*, *rm* + *mr*, *rr*) and/or higher order arrangements. It has been proposed

that ionic liquids may induce some stereocontrol during chemical reactions while common organic solvents do not have any influence.¹⁴ Hence, a comparison between a PMMA obtained in [BMIm][OTf] (a model ionic liquid) and ethanol (a model organic solvent) was made, considering the ¹H-NMR signal of the protons of the α -methyl group of the stereocenter. The ¹H-NMR spectrum of PMMA produced by *e*ATRP in [BMIm][OTf] (Table 5.3, entry 4) is shown in Figure 5.8.

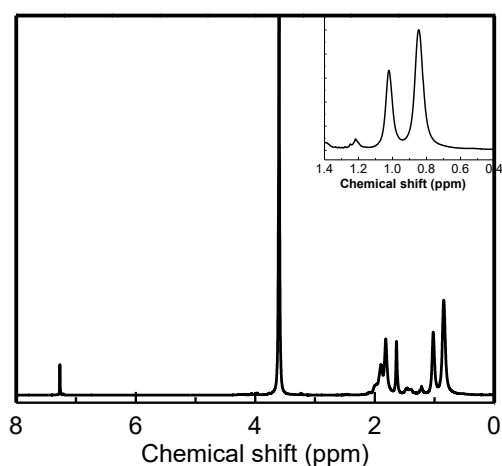


Figure 5.8. Full ¹H-NMR spectrum of PMMA ($M_n = 30600$, $D = 1.21$) in $CDCl_3$ at ambient temperature produced by *e*ATRP in [BMIm][OTf]. The inset highlights the zone used for tacticity evaluation.

The signal at 1.21 ppm corresponds to the meso triad (*mm*), the signal at 1.02 ppm corresponds to the atactic triad (*mr*) and the signal at 0.84 ppm to the syndiotactic triad (*rr*). Lorentzian fitting of the multiplet gives the tacticity of the polymer: syndiotactic 63%, atactic 32% and isotactic 5%. The same procedure gives the tacticity of a PMMA obtained by *e*ATRP in ethanol, with full spectrum reported in Figure 5.9.

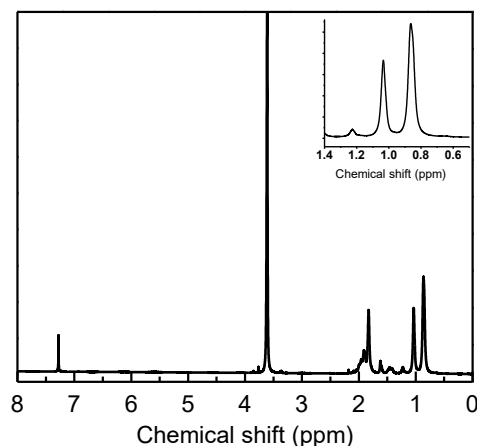


Figure 5.9. Full ¹H-NMR spectrum of PMMA ($M_n = 37800$, $D = 1.21$) in $CDCl_3$ at ambient temperature obtained by *e*ATRP in ethanol. The inset highlights the zone used for tacticity evaluation.

The polymer obtained in ethanol is 61% syndiotactic, 31% atactic and 8% isotactic. It is rather difficult to envisage any significant difference between the two samples; there is no apparent induction of tacticity by the ionic liquid. The absence of relevant effect was already reported by Biedron *et al.*²⁶ and Carmichael *et al.*²⁷ This further confirms the similarity of behavior as a reaction medium between common organic solvents and this ionic liquid.

5.9 Conclusions

The main conclusion of this chapter is that the ionic liquid [BMIm][OTf] proved to be an excellent candidate to replace organic solvents. *e*ATRP of MMA was successful providing well-defined PMMA ($M_n > 20000$ and $D < 1.2$), thanks to catalytic halogen exchange. Low catalyst loading and use of inexpensive ligands such as PMDETA further reduced polymerization cost. Ethanol, a solvent not taken much into consideration in ATRP, strikingly proved to be a green alternative to many commonly used toxic solvents; its LCST has been deftly exploited to isolate the polymer at the end of polymerization by just cooling the reaction mixture and washing the separated PMMA. The supporting electrolyte could as well be reduced with additional cost reduction. Tacticity analysis showed that mainly syndiotactic PMMA is produced in ethanol and [BMIm][OTf] ionic liquids, essentially without solvent effect. The lack of any influence on tacticity is

a further indication that this ionic liquid behaves just as “common” organic solvents as far as ATRP is concerned.

References

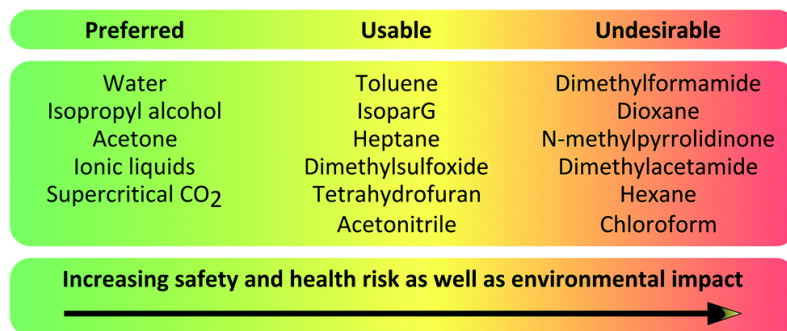
1. ICIS, Methyl methacrylate prices, markets & analysis. **2018**.
2. Ali, U.; Karim, K. J. B. A.; Buang, N. A., A Review of the Properties and Applications of Poly (Methyl Methacrylate) (PMMA). *Polymer Reviews* **2015**, *55*, 678-705.
3. Wu, Y.; Rao, Y.-J.; Chen, Y.-h.; Gong, Y., Miniature fiber-optic temperature sensors based on silica/polymer microfiber knot resonators. *Optics Express* **2009**, *17*, 18142-18147.
4. Carmo dos Santos, N. A.; Lorandi, F.; Badetti, E.; Wurst, K.; Isse, A. A.; Gennaro, A.; Licini, G.; Zonta, C., Tuning the reactivity and efficiency of copper catalysts for atom transfer radical polymerization by synthetic modification of tris(2-methylpyridyl)amine. *Polymer* **2017**, *128*, 169-176.
5. Yohann, G.; Didier, G.; A., M. S. R.; Paul, T.; Denis, B., Nitroxide-Mediated Polymerization of Methyl Methacrylate Using an SG1-Based Alkoxyamine: How the Penultimate Effect Could Lead to Uncontrolled and Unliving Polymerization. *Macromolecular Chemistry and Physics* **2006**, *207*, 1278-1288.
6. Nanda, A. K.; Matyjaszewski, K., Effect of Penultimate Unit on the Activation Process in ATRP. *Macromolecules* **2003**, *36*, 8222-8224.
7. Tang, W.; Matyjaszewski, K., Effects of Initiator Structure on Activation Rate Constants in ATRP. *Macromolecules* **2007**, *40*, 1858-1863.
8. Bortolamei, N.; Isse, A. A.; Magenau, A. J. D.; Gennaro, A.; Matyjaszewski, K., Controlled Aqueous Atom Transfer Radical Polymerization with Electrochemical Generation of the Active Catalyst. *Angewandte Chemie* **2011**, *123*, 11593-11596.
9. Harrisson, S.; Mackenzie, S. R.; Haddleton, D. M., Pulsed Laser Polymerization in an Ionic Liquid: Strong Solvent Effects on Propagation and Termination of Methyl Methacrylate. *Macromolecules* **2003**, *36*, 5072-5075.
10. Kwak, Y.; Magenau, A. J. D.; Matyjaszewski, K., ARGET ATRP of Methyl Acrylate with Inexpensive Ligands and ppm Concentrations of Catalyst. *Macromolecules* **2011**, *44*, 811-819.
11. Capello, C.; Fischer, U.; Hungerbuhler, K., What is a green solvent? A comprehensive framework for the environmental assessment of solvents. *Green Chemistry* **2007**, *9*, 927-934.
12. Cowie, J. M. G.; Mohsin, M. A.; McEwen, I. J., Alcohol-water cosolvent systems for poly(methyl methacrylate). *Polymer* **1987**, *28*, 1569-1572.
13. Suter, J., Glossary of basic terms in polymer science (IUPAC Recommendations 1996). *Pure and Applied Chemistry* **2009**, *68*, 2287-2311.
14. Strehmel, V.; Laschewsky, A.; Wetzel, H.; Görnitz, E., Free Radical Polymerization of *n*-Butyl Methacrylate in Ionic Liquids. *Macromolecules* **2006**, *39*, 923-930.

Chapter 6

Electrochemically mediated ATRP in Ionic Liquid – Water mixtures: green horizons in polymer synthesis

6.1 Introduction

Since its discovery in 1995, ATRP has been widely carried out in non-green, toxic and harmful solvents such as dimethylformamide, benzene, toluene, acetonitrile, *N*-methyl-2-pyrrolidone, anisole and others. Yet, stringent regulations introduced for the protection of our planet, atmosphere and oceans, leave less and less space for the use of these solvents. Processes in which they are involved are now mainly limited to studies in academia. For a commercialization step, it is necessary to choose greener substitutes. Recently, efforts to change ATRP media to non-harmful solvents such as water and ionic liquids have been successful.¹ Scheme 6.1 shows the current view about some solvents in terms of safety, health and environmental risk.



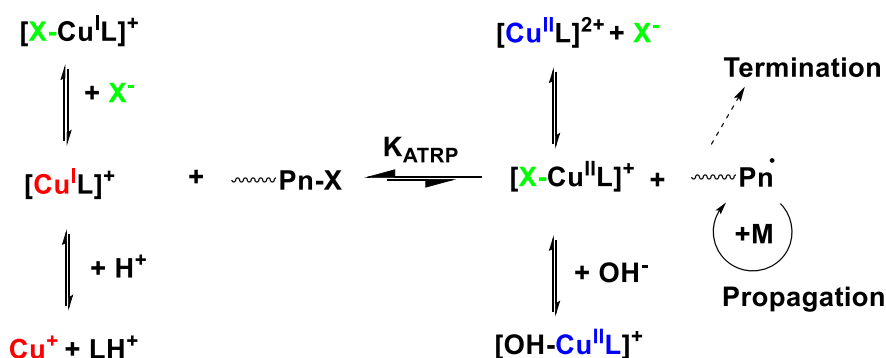
Scheme 6.1. Current opinion about a selection of solvents for chemical synthesis.² Reproduced by permission of The Royal Society of Chemistry.

According to this study, ionic liquids, water and supercritical carbon dioxide perfectly match the goal of sustainability. Dimethyl sulfoxide and acetonitrile are considered usable but there are some studies already reporting the latter as undesirable.³ Chlorinated solvents, aromatics, amides and alkanes are already inadequate for synthesis, due to toxicity and high disposal costs. Ionic liquids

remove all volatile compounds from an exhaust reaction, especially if combined with vacuum drying and other treatments. Another strength of ionic liquids is the preservation of catalyst: in the case of *e*ATRP, during recycling procedures, it remains inside the ionic liquid avoiding losses and further costs of recovery and replacement.⁵ According to this perspective, further implementation of technology in the field of RDRP should consider the use of water and/or ionic liquids or their combination, from both environmental and economic facets. This chapter indeed focuses on *e*ATRP in ionic liquid – water mixtures.

6.2 The role of water in ATRP

In Chapter 2 it was highlighted that ATRP equilibrium and rate constants are strongly influenced by the choice of the medium, especially water. Too high K_{ATRP} can lead to excessive radical concentration and difficulties in controlling the polymerization.^{6,7} Water is an inexpensive, environmentally friendly solvent with high thermal capacity. Any relevant polymerization involving a biocompatible moiety, such as formation of protein–polymer conjugates or other bio-hybrids requires conducting the polymerization in an aqueous environment with a very limited monomer/catalyst content. The introduction of water as a co-solvent is of primary importance. Conditions should be adjusted from those applied in traditional organic solvents to account for higher k_{act} and K_{ATRP} , lower catalyst stability that may lead to disproportionation and/or deactivator dissociation, and potential hydrolysis of $\text{Cu}^{\text{II}}\text{-X}$ and $\text{P}_n\text{-X}$ bonds, as shown in Scheme 6.3.



Scheme 6.3. ATRP equilibrium and relevant side reactions in water.

In terms of ATRP performance, the main difference between a pure aqueous system and one composed by an ionic liquid and water arises from the changes of the thermodynamic and kinetic constants. Reasonable trends can be formulated, based on the well-established behavior of aqueous ATRP.⁷ By passing from a pure water medium to a mixed one:

1. halidophilicity constants, K_X , will increase;
2. activation rate constants and K_{ATRP} will decrease;
3. solubility of hydrophobic polymers and monomers will increase;
4. stability of the catalyst will increase, while the relevance of all side-reactions will decrease.

Hence, ionic liquid – water mixtures are promising, conjugating properties from both organic solvents and water, thus broadening the horizon for the polymerization of hydrophobic monomers in aqueous media.

6.3 From enemies to allies

Some ILs are very hydrophilic and absorb moisture from the environment. Since the beginning of studies on ionic liquids, their tendency to absorb moisture was considered undesirable for various reasons. For example, [BMIm][PF₆] reacts with water forming HF as the anion slowly hydrolyzes.⁸ Therefore, efforts were oriented to develop ILs based on other anions such as triflate or bistriflimide to avoid this side-reaction. These novel ionic liquids show a wide electrochemical window (up to 5 V), when water has only 1.23 V.⁹ [BMIm][OTf], the ionic liquid of our interest, is hydrophilic and tends to absorb moisture. Water modifies deeply the properties of [BMIm][OTf] and in general of ionic liquids.¹⁰ Miscibility is very important when considering the properties of mixtures. Indeed, it strongly depends on the nature the anionic species present in the IL: generally, highly-fluorinated, charge-delocalizing anions such as NTf₂⁻ and PF₆⁻ tend to form hydrophobic ILs that are immiscible with water. These hydrophobic IL-water mixtures easily form liquid/liquid biphasic systems. On the other hand, ILs with hydrophilic anions such as halides, phosphates, carboxylates, *etc.* are mostly miscible with water.¹¹ Cationic species also affect the miscibility of ILs with water. Long alkyl chains on the cations dramatically decrease the miscibility of

the ILs with water. For instance, in the case of ILs composed of 1-alkyl-3-methylimidazolium cations and BF_4^- , ILs with short alkyl chains such as [EMIm][BF_4] and [BMIm][BF_4] mix homogeneously with water (with hydrolysis of the anion), whereas longer alkyl chains ($n = 6 - 10$) lead to phase-separation.¹²

Even a small amount of water can dramatically influence the liquid properties of ILs without any reaction. For example, mass transport in ILs, as well as their viscosity, polarity, and surface tension vary considerably upon adding water. Incorporation of water into ILs increases the diffusion coefficients of dissolved species, because of a decrease in viscosity arising from reduction of electrostatic interactions between ions. To facilitate the use of ILs in industrial processes, it is essential to assemble a body of knowledge about these changes taking place in the physicochemical properties of IL-water mixtures.

6.4 Money in our head but not in our heart

As it is at the heart of green chemistry to recycle ionic liquids, 10 - 20 recycles gives them the same cost per cycle as conventional organic solvents, and over 50 recycles makes them significantly cheaper.¹³ Their application in industrial processes is increasing every year. The major hurdle faced at academic scale is cost: commercially available ionic liquids, depending on the composition and purity, can easily reach 1000 €/kg. Nevertheless, benefits of ILs were already described in Chapter 3. Clearly, for academic purposes even a pilot reactor, involving 1 kg of ionic liquid, is for the beginners unaffordable. A simple strategy to reduce significantly the cost is the introduction of co-solvents. Their role is to replace a very expensive moiety with an inexpensive one, allowing the reduction of expenses. Nevertheless, most organic solvents are harmful for humans, animals and environment. DMF, acetonitrile, DMSO and others are good solvents for polymerization processes; however, their disposal is expensive. Furthermore, it is counter-productive to replace partially a green solvent with a non-green one. Industries are spending time and money to replace common organic solvents and improve their green scores; that is why using ionic liquids to replace much cheaper but much hazardous solvents should be encouraged. The greenest, non-toxic, non-harmful, easy on call and recyclable solvent is water. The biggest

advantage of water is its negligible cost compared to all the other chemicals involved. Neglecting the cost of deionizing or double distilling, the first euro is spent using 25 m³ (25,000 liters) of water.¹⁴ The replacement of expensive ionic liquids with water is greatly attractive. Table 6.1 shows the cost of some reagents used in a typical *e*ATRP of MA in pure [BMIm][OTf]:

Table 6.1. Price of *e*ATRP reagents for a 5 mL polymerization in [BMIm][OTf].^a

| Reagent | Price (€/g) | Mass (g) | Cost (€) |
|--------------------------------|-------------|-----------------------|--------------------|
| [BMIm][OTf] | 0.87 | 2.50 | 2.18 |
| Water | ~0 | 0 | 0 |
| Methyl Acrylate | 0.04 | 2.50 | 0.10 |
| TPMA ^b | 122.5 | 1.45×10 ⁻³ | 0.18 |
| PMDETA ^b | 0.54 | 9×10 ⁻⁴ | < 10 ⁻³ |
| CuBr ₂ ^b | 0.45 | 1.12×10 ⁻³ | < 10 ⁻³ |

^a $V_{\text{tot}} = 5$ mL; source: all reagents from Sigma-Aldrich except [BMIm][OTf] from Iolitec. ^b 1.0 mM.

Examination of our polymerization system, in Table 6.2, shows how the cost changes as water replaces [BMIm][OTf].

Table 6.2. Price of *e*ATRPs at different water/IL mixtures.^a

| Water (% v/v) | [BMIm][OTf] (% v/v) | Price (€) | %Save ^b |
|---------------|------------------------|-----------|--------------------|
| 0 | 50 | 2.461 | 0 |
| 10 | 40 | 2.238 | 9 |
| 20 | 30 | 2.021 | 10 |
| 30 | 20 | 1.803 | 27 |

^aSource: Sigma-Aldrich and Iolitec. ^b Based from entry 1. Using [Cu^ITPMA]²⁺ 10⁻³ M as catalyst.

Replacing only 10% (v/v) of [BMIm][OTf] with water means ~10% saving. At 30% of water, the cost is ~30% less, guaranteeing a justifiable innovation in the world of CRP.

6.5 The choice of catalyst and monomers

The successful *e*ATRP of methyl acrylate catalyzed by $[\text{Cu}^{\text{II}}\text{TPMA}]^{2+}$ in $[\text{BMIm}][\text{OTf}]$ was previously reported in Chapter 4. It was shown that, in a wide range of conditions, the polymerization is well-controlled and proceeds rapidly in both potentiostatic and galvanostatic *e*ATRP. This successful polymerization is the primary candidate for a further development of water/ionic liquid mixtures. The purpose is the systematic replacement of $[\text{BMIm}][\text{OTf}]$ with water to highlight the benefits of this novel approach.

6.6 Electrochemical characterizations

Prior to *e*ATRP syntheses, a series of voltammetric characterizations, shown in Figure 6.1, has been performed to understand the effect of water on the catalytic system in $[\text{BMIm}][\text{OTf}]$, in the presence of MA and EBiB:

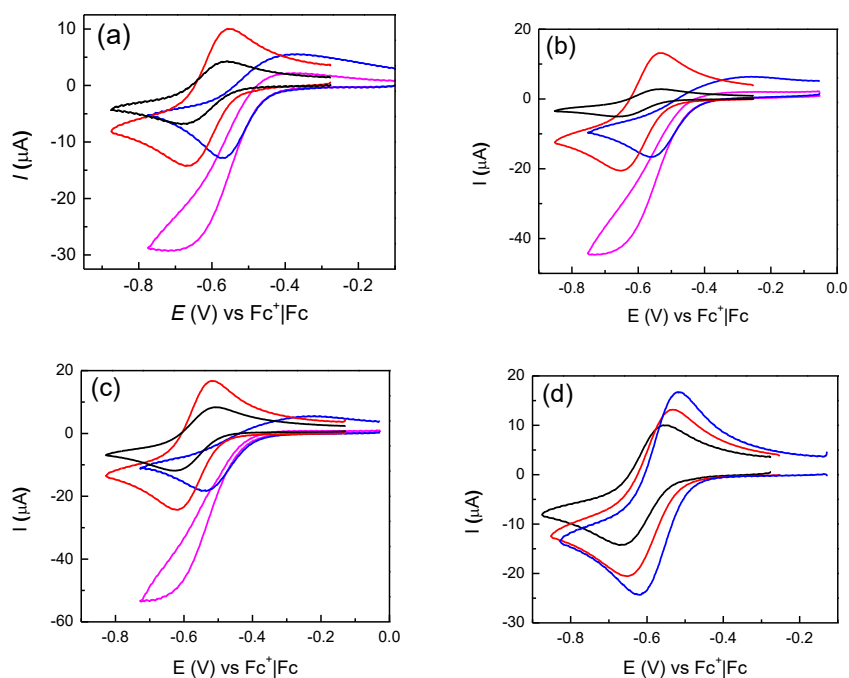


Figure 6.1. CV of 1 mM $[\text{BrCu}^{\text{II}}\text{TPMA}]^+$ in $[\text{BMIm}][\text{OTf}]$, recorded at 50 °C on GC at 0.2 V/s in the absence (—) and presence of water (—) and 10 mM EBiB (—) (H_2O : 10% (a), 20% (b) and 30% (c)); CV recorded after addition of 50% (v/v) MA (—). (d) Effect of 10% (—), 20% (—) and 30% (—) of water on $[\text{BrCu}^{\text{II}}\text{TPMA}]^+$.

As already reported, $[\text{Cu}^{\text{II}}\text{TPMA}]^{2+}$ in $[\text{BMIm}][\text{OTf}]$ exhibits a reversible pattern with $E_{1/2} = -0.61$ V vs. Fc^+/Fc . In the presence of water (Figure 6.1d) the current

intensity increases because of a sensible drop in viscosity. Addition of methyl acrylate further modifies the voltammetric response. The anodic peak becomes strongly stretched, while the cathodic peak slightly decreases in height. These changes are highlighted in Figure 6.2:

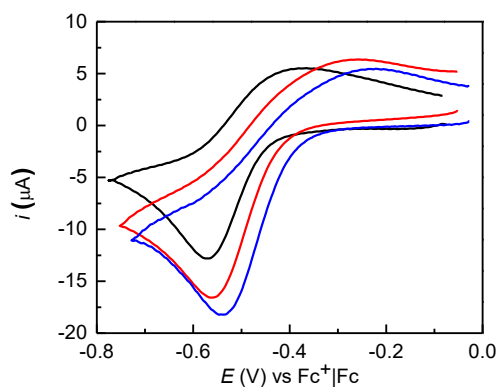


Figure 6.2. CV of $[\text{BrCu}^{\text{II}}\text{TPMA}]^+$ in $[\text{BMIm}][\text{OTf}]/\text{MA}$ (1/1, v/v) + H_2O (— 10%, — 20% and — 30%) recorded at 50 °C on GC at 0.2 V/s.

When the initiator EBiB is added another dramatic modification in the shape appears confirming the onset of catalysis. The cathodic peak increases sensibly in intensity while the anodic one disappears. The increase of the cathodic peak, up to 3 times its height without initiator, follows the increase of water, confirming that k_{act} is influenced by water concentration. In Table 6.3 the standard redox potential of $[\text{BrCu}^{\text{II}}\text{TPMA}]^+$ in $[\text{BMIm}][\text{OTf}] + \text{H}_2\text{O}$ is reported; since it is not possible to calculate $E_{1/2}$ in the presence of the monomer, E_{pc} is reported:

Table 6.3. Standard redox potential ($E_{1/2}$) of $[\text{BrCu}^{\text{II}}\text{TPMA}]^+$ in $[\text{BMIm}][\text{OTf}]$ and in presence of different uptakes of H_2O .^a

| Entry | $E_{1/2}^b$ (V) | E_{pc}^c (V) |
|-----------------------------|-----------------|-----------------------|
| $[\text{BMIm}][\text{OTf}]$ | -0.61 | -0.66 |
| 10% H_2O | -0.61 | -0.57 |
| 20% H_2O | -0.59 | -0.56 |
| 30% H_2O | -0.57 | -0.54 |

^aAll potentials are vs. Fc^+/Fc . ^bIn $[\text{BMIm}][\text{OTf}] + \text{H}_2\text{O}$. ^cIn presence of 50% (v/v) MA.

In presence of 10% H_2O a negligible change of $E_{1/2}$ (< 5 mV) was observed. Up to 20 and 30% instead, the standard redox potential shifted to more positive values.

The addition of 50% MA caused a further shift to more positive values in all cases, due to lower polarity.

6.7 Electrochemically mediated ATRP in [BMIm][OTf]/H₂O mixtures

Methyl acrylate is slightly soluble in water (50 g/L at 25 °C). A systematic replacement of [BMIm][OTf] with water provides different systems as the H₂O/IL ratio changes and there will be a limit at which the components, at a given temperature, are not miscible, thus a biphasic system is expected. At 50 °C, a reaction mixture made of 50% (v/v) methyl acrylate in [BMIm][OTf] remains miscible with water up to 25% (v/v); at 30% H₂O the system begins to split into two phases. Therefore, qualitatively the zone in which *e*ATRP of MA in water and ionic liquid mixtures is expected to occur in a homogenous phase is comprised between 0 and 30% H₂O. Various polymerizations were performed in 50% (v/v) MA in [BMIm][OTf] with different concentrations of H₂O and the results are reported in Table 6.4:

Table 6.4. *e*ATRP of 50% v/v MA in [BMIm][OTf] with different H₂O uptakes (% v/v of the total volume).^a

| Entry | H ₂ O ^b | <i>t</i> (h) | Conv. (%) | <i>M_n</i> ^{app} | <i>M_n</i> th | <i>D</i> | <i>Q</i> (C) | <i>I</i> _{eff} | <i>k</i> _{app} |
|----------------|-------------------------------|--------------|-----------|-------------------------------------|------------------------------------|----------|--------------|-------------------------|-------------------------|
| 1 | 0 | 1.75 | 93 | 44200 | 44200 | 1.18 | 5.39 | 0.99 | 0.95 |
| 2 | 10 | 1.25 | 95 | 45000 | 45100 | 1.12 | 2.51 | 0.99 | 2.26 |
| 3 | 20 | 0.75 | 95 | 48900 | 46500 | 1.18 | 2.50 | 1.05 | 3.58 |
| 4 | 30 | 0.67 | 47 | 21000 | 22300 | 1.18 | 4.39 | 0.94 | 0.98 |
| 5 ^c | 10 | 1.25 | 74 | 36500 | 35200 | 1.14 | - | 0.96 | 0.93 |
| 6 ^d | 0 | 3 | 99 | 45000 | 47000 | 1.09 | 5.39 | 0.94 | 0.96 |

^aApplied potential, $E_{app} = E_{pc}$. ^bVol% in the mixture. ^c“User friendly” galvanostatic *e*ATRP based on entry 2; fixed $i_{app} = 0.58$ mA. ^dIn CH₃CN + 0.1 M Et₄NBF₄. $C_{MA}: C_{Cu}: C_{TPMA}: C_{EBiB} = 552:0.1:0.1:1$. $V_{tot} = 5$ mL. WE = Pt mesh (estimated surface area = 6 cm²), CE = graphite in separate compartment. DP = 552.

Figure 6.3 shows the effect of H₂O concentration on the polymerizations:

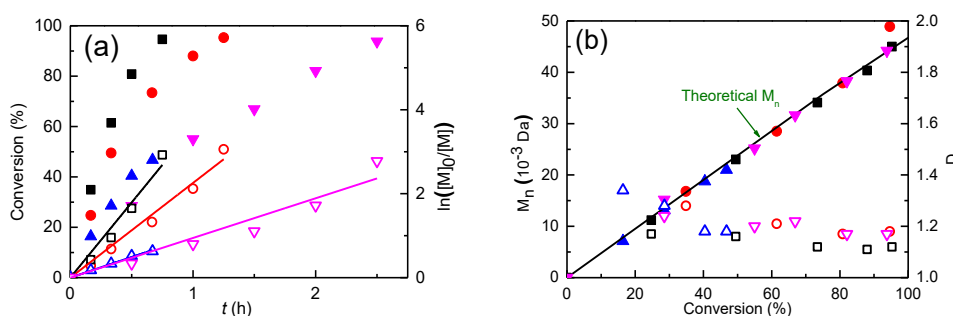


Figure 6.3. (a) Kinetic plots and (b) evolution of M_n and \bar{D} with conversion for potentiostatic *e*ATRP of 50% v/v MA in [BMIm][OTf] + H₂O. Conditions: $C_{MA}:C_{Cu}:C_{TPMA}:C_{EBiB} = 552:0.1:0.1:1$. $C_{Cu} = 10^{-3}$ M. $E_{app} \approx E_{pc}$. H₂O% (v/v): (▼) 0, (●) 10 (■) 20, (▲) 30. Empty symbols refer to the right ordinate in the figures.

When 10% H₂O was added, all parameters improved dramatically: \bar{D} was reduced to 1.12, charge consumption (Q) was halved and k_{app} more than doubled, while conversion remained unchanged (Table 6.4, entries 1 and 2). Increasing water concentration to 20% further enhanced k_{app} although the dispersity slightly worsened, reaching however the same value observed in pure [BMIm][OTf] ($\bar{D} = 1.18$). At 30% H₂O, the limit of solubility for MA, the system behaved almost like an emulsion rather than a solution. Indeed, after 30% conversion, the transparency of the reaction mixture gave way to a slightly milky ambient with visible droplets of monomer, which collapsed and formed a separate phase when the stirrer was set off. Since the polymerization was performed under vigorous stirring, the reaction continued in an emulsion-like fashion. The reaction proceeded at a rate lower than in the presence of 10 or 20% water, but comparable to pure [BMIm][OTf]. Such polymerization slowing might be attributable to the break-up of the homogeneous phase and PMA precipitation. Hence, at 50% conversion, PMA precipitation completely stopped the reaction. Interestingly, \bar{D} was the same as that of polymerizations in pure [BMIm][OTf] or in the presence of 20% H₂O. It should be mentioned that even if the Cu^{II}/Cu^I ratio at the surface of the electrode is fixed by E_{app} (the same value was used in all experiments), the effective concentration of the deactivator is lower in the presence of H₂O, due to the instability of [BrCu^{II}TPMA]⁺ towards dissociation to [Cu^{II}TPMA]²⁺ and Br⁻.

Despite the limited conversion, *e*ATRP in 30% H₂O in [BMIm][OTf] runs effectively as an aqueous system. It is worthwhile to mention that in the presence of 30% H₂O the same dispersity as in the pure ionic liquid was obtained. Furthermore, unreacted monomer can be removed and recycled.

*e*ATRP in [BMIm][OTf] + 10% H₂O was performed under galvanostatic conditions (Table 6.4, entry 5). The aim of the “*user friendly*” galvanostatic *e*ATRP is to drive the reaction with a single fixed current step in an easy and intuitive manner. The applied current was calculated as the average value ($i = 0.58$ mA) required to pass in 1.25 h the same charge consumed in the corresponding potentiostatic *e*ATRP (Table 6.4, entry 2). A comparison between the results of potentiostatic and galvanostatic experiments is shown in Figure 6.4:

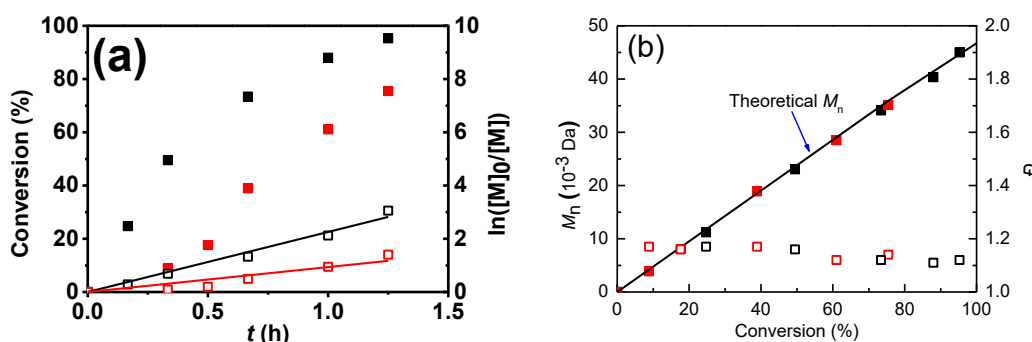


Figure 6.4. (a) Kinetic plots and (b) evolution of M_n and D with conversion for the potentiostatic (■) and galvanostatic (■) *e*ATRP of 50% (v/v) MA in [BMIm][OTf] + 10 vol% H₂O. Conditions: $C_{MA}:C_{Cu}:C_{TPMA}:C_{EBiB} = 552:1:1:10$. $C_{Cu} = 10^{-3}$ M. $E_{app} = E_{1/2} - 0.06$ V. Empty symbols refer to the right ordinate in the figures.

The galvanostatic polymerization was slower than *e*ATRP under potentiostatic mode. This is probably due to the uncontrolled potential during galvanostatic *e*ATRP. The uncompleted conversion is consistent with the rapid fall of E_{app} at high conversion. As the system is not able to sustain the imposed current, the potential shifts to more negative values, which probably involves other reactions, penalizing the *e*ATRP equilibrium. Even though the passage to the galvanostatic mode may appear a regression, it underscores the extraordinary ease of control with this setup, suggesting possible scale-up in future.

6.8 Electrochemically mediated ATRP of methyl acrylate in mixtures of traditional solvents and water

The effect of water addition was investigated also in some traditional solvents, namely, acetonitrile, DMF, DMSO and EtOH. These solvents are all able to dissolve MA and PMA and have been already used for ATRP. Among all, only ethanol is considered a green solvent and its mixtures with water are of considerable interest. As usual, voltammetric analyses were performed to evaluate the effect of water on both binary and ternary complexes (Fig. 6.5-6.7):

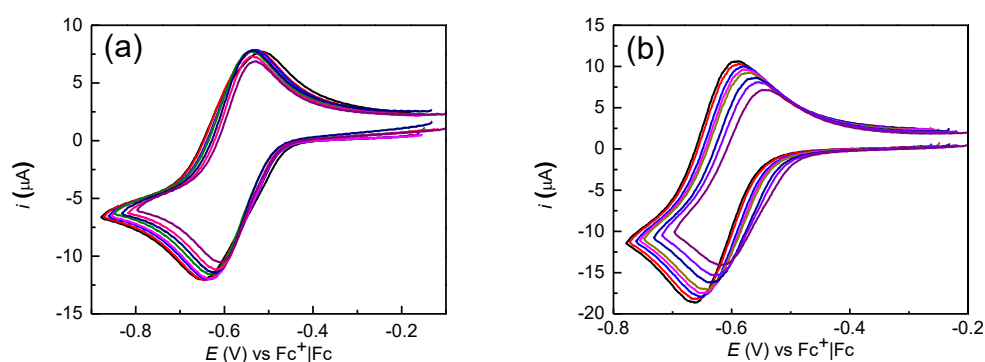


Figure 6.5. a) CV of a) $[\text{Cu}^{\text{II}}\text{TPMA}]^{2+}$ and b) $[\text{BrCu}^{\text{II}}\text{TPMA}]^{+}$ in EtOH + 0.1 M Bu_4NBF_4 in the presence of water (1, 2, 3, 4, 5, 7.5, 10 and 15%) recorded at 25 °C on GC at 0.2 V/s.

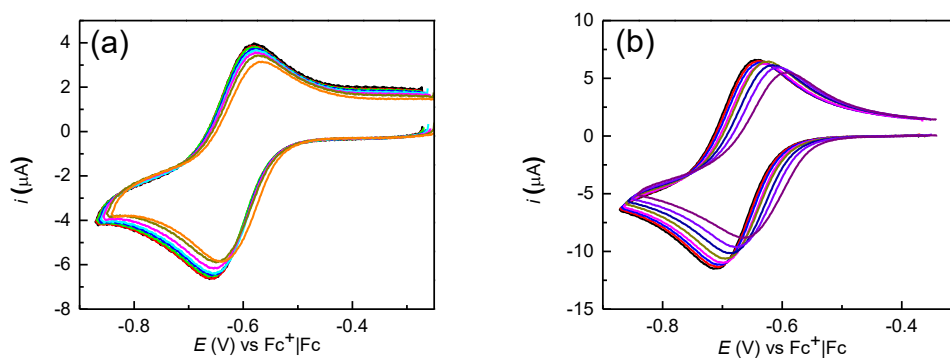


Figure 6.6. a) CV of a) $[\text{Cu}^{\text{II}}\text{TPMA}]^{2+}$ and b) $[\text{BrCu}^{\text{II}}\text{TPMA}]^{+}$ in DMSO + 0.1 M Et_4NBF_4 in the presence of water (1, 2, 3, 4, 5, 7.5, 10 and 15%) recorded at 25°C on GC at 0.2 V/s.

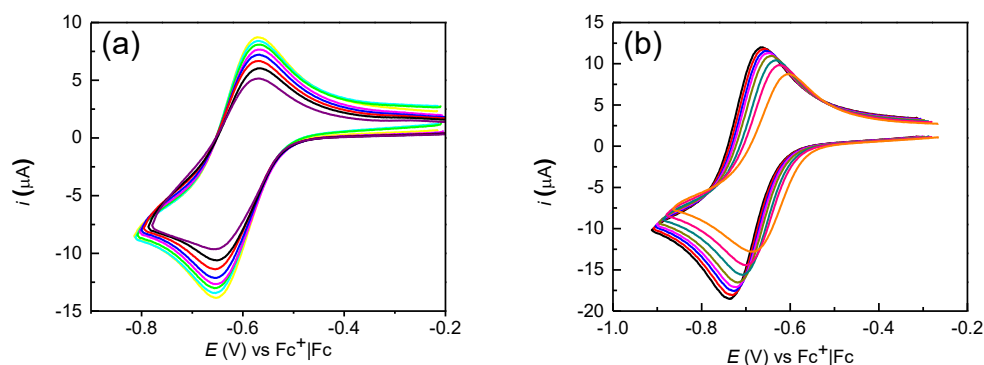


Figure 6.7. CV of a) [Cu^{II}TPMA]²⁺ and b) [BrCu^{II}TPMA]⁺ in DMF + 0.1 M Et₄NBF₄ in the presence of water (1, 2, 3, 4, 5, 7.5, 10 and 15%) recorded at 25 °C on GC at 0.2 V/s.

Addition of water shifts $E_{1/2}$ of the ternary complex [BrCu^{II}TPMA]⁺ to more positive values (Fig. 6.7). The effect of H₂O on $E_{1/2}$ of the binary complex [Cu^{II}TPMA]²⁺ is much less defined; it shifts to more negative potentials in CH₃CN (Figure 6.9), whereas a slight anodic shift can be observed in other solvents.

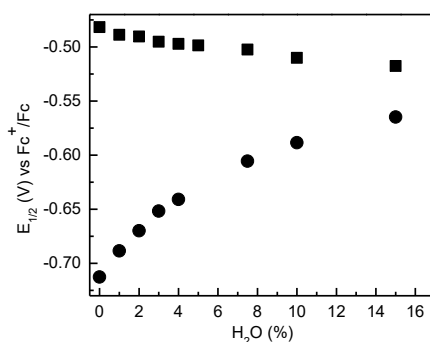


Figure 6.9. Evolution of $E_{1/2}$ of ■ [Cu^{II}TPMA]²⁺ and ● [BrCu^{II}TPMA]⁺ in CH₃CN + 0.1 M Et₄NBF₄ in the presence of water at 25 °C.

Regarding catalytic efficiency, it was found that cathodic peak current increases significantly with increasing water concentration, clearly indicating a significant increase of k_{act} . Figure 6.10 shows the catalytic enhancement as a function of H₂O concentration from 0 to 3%.

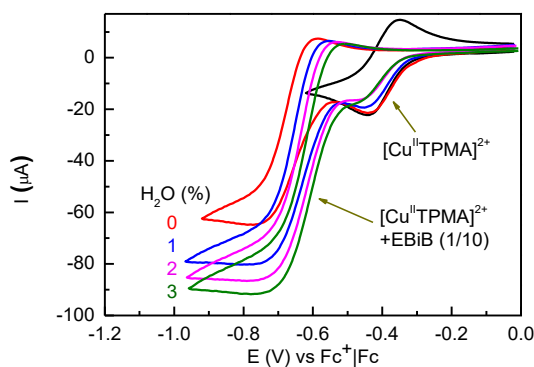


Figure 6.10. CV of 1.0 mM $[\text{Cu}^{\text{II}}\text{TPMA}]^{2+}$ in $\text{CH}_3\text{CN} + 0.1 \text{ M Et}_4\text{NBF}_4$, recorded at 25 °C on GC at 0.2 V/s.

Before *e*ATRP, voltammetric analysis was always performed in the actual reaction medium at 50 °C (Fig. 6.11-6.14):

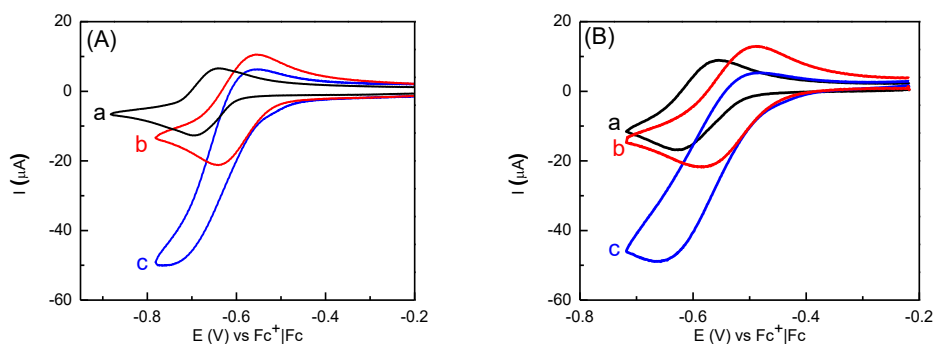


Figure 6.11. CV of 1.0 mM $[\text{BrCu}^{\text{II}}\text{TPMA}]^+$ in ethanol (A) or ethanol + 10% water (B), recorded at 50 °C on GC at 0.2 V/s: (a) $[\text{BrCu}^{\text{II}}\text{TPMA}]^+$ in EtOH or EtOH + H_2O ; (b) as (a) + 50% MA (v/v); (c) as (b) + 10 mM EBiB.

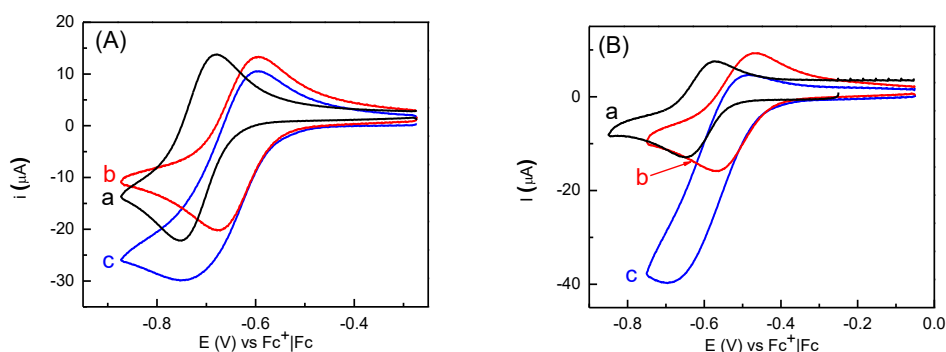


Figure 6.12. CV of 1.0 mM $[\text{BrCu}^{\text{II}}\text{TPMA}]^+$ in DMSO (A) or DMSO + 10% water (B), recorded at 50 °C on GC at 0.2 V/s: (a) $[\text{BrCu}^{\text{II}}\text{TPMA}]^+$ in DMSO or DMSO + H_2O ; (b) as (a) + 50% MA (v/v); (c) as (b) + 10 mM EBiB.

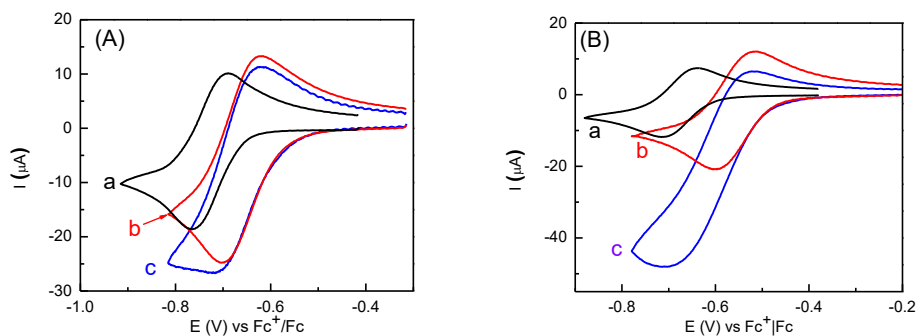


Figure 6.13. CV of 1.0 mM $[\text{BrCu}^{\text{II}}\text{TPMA}]^+$ in DMF (A) or DMF + 10% water (B), recorded at 50 °C on GC at 0.2 V/s: (a) $[\text{BrCu}^{\text{II}}\text{TPMA}]^+$ in DMSO or DMSO + H_2O ; (b) as (a) + 50% MA (v/v); (c) as (b) + 10 mM EBiB.

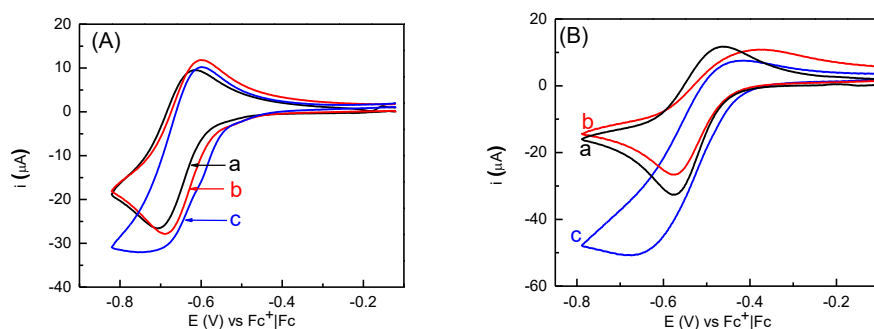


Figure 6.14. CV of 1.0 mM $[\text{BrCu}^{\text{II}}\text{TPMA}]^+$ in CH_3CN (A) or CH_3CN + 10% water (B), recorded at 50 °C on GC at 0.2 V/s: (a) $[\text{BrCu}^{\text{II}}\text{TPMA}]^+$ in DMSO or DMSO + H_2O ; (b) as (a) + 50% MA (v/v); (c) as (b) + 10 mM EBiB.

Table 6.5 summarizes the electrochemical properties of $[\text{BrCuTPMA}]^+$ in different solvents.

Table 6.5. Electrochemical properties of $[\text{BrCuTPMA}]^+$ in different solvents in the absence and presence of 10% H_2O (v/v) at 50 °C.^a

| Solvent | E° (V) | E° (+10% H_2O v/v) (V) | E° (+10% H_2O + 50% MA v/v) (V) |
|------------------------|------------------|--|--|
| [BMIm][OTf] | -0.61 | -0.61 ^b | -0.57 |
| DMF | -0.70 | -0.66 | -0.58 |
| DMSO | -0.68 | -0.64 | -0.52 |
| CH_3CN | -0.66 | -0.66 | -0.64 |
| EtOH | -0.58 | -0.58 | -0.58 |

^aAll potentials are vs. Fc^+/Fc .

The results of electrochemically mediated polymerizations performed in different solvents both in the absence and presence of H₂O are summarized in Table 6.6.

Table 6.6. *e*ATRP of 50% v/v MA in different solvents with or without 10% v/v H₂O.^a

| Entry | Solvent | H ₂ O (v/v) | <i>t</i> (h) | Conv. (%) | <i>M_n</i> ^{app} | <i>M_n</i> th | <i>D</i> | <i>Q</i> (C) | <i>I</i> _{eff} | <i>k</i> _{app} |
|-------|--------------------|---------------------------|-----------------|--------------|-------------------------------------|------------------------------------|----------|-----------------|-------------------------|-------------------------|
| 1 | DMF | 0 | 4 | 56 | 25900 | 26600 | 1.18 | 2.28 | 1.02 | 0.26 |
| 2 | DMF | 10 | 4 | 62 | 29400 | 29500 | 1.15 | 2.81 | 0.99 | 0.29 |
| 3 | CH ₃ CN | 0 | 4 | 70 | 32300 | 33300 | 1.10 | 2.83 | 0.98 | 0.37 |
| 4 | CH ₃ CN | 10 | 4 | 78 | 36700 | 37200 | 1.09 | 2.92 | 0.99 | 0.42 |
| 5 | DMSO | 0 | 2.5 | 57 | 26100 | 27100 | 1.19 | 1.44 | 0.96 | 0.50 |
| 6 | DMSO | 10 | 1.5 | 65 | 30200 | 30900 | 1.14 | 1.33 | 0.98 | 0.75 |
| 7 | EtOH | 0 | 3 | 45 | 20600 | 21400 | 1.21 | 2.92 | 0.96 | 0.23 |
| 8 | EtOH | 10 | 3 | 51 | 23700 | 24200 | 1.19 | 3.70 | 0.98 | 0.31 |

^a Applied potential = $E_{app} = E_{1/2}$. Other conditions: $C_{MA}:C_{Cu}:C_{TPMA}:C_{EBiB} = 552:0.1:0.1:1$. $V_{tot} = 10$ mL. WE = Pt mesh (estimated surface area = 6 cm²), CE = graphite in separate compartment. DP = 552. Supporting electrolyte: 0.1 M Et₄NBF₄ except for ethanol where Bu₄NBF₄ was used. $T = 50$ °C.

In all investigated solvents, the addition of 10% (v/v) of H₂O was beneficial in terms of conversion of the monomer, lower dispersion of the polymer, reaction rate and cost. Water represents an attractive solution to improve cleanness and reduce costs even when added to traditional solvents. EtOH/H₂O was found to be a benign ambient up to 15% H₂O. Ethanol is not widely used in ATRP, but we believe its use should be preferred because at moderate temperatures (50 °C) it dissolves many monomers and polymers.

Table 6.7 reports few *e*ATRPs of MA performed in ethanol at increasing water amounts. Noteworthy, mixtures of ethanol and water are totally green solvents. Increasing the amount of water in the mixture, the reaction becomes faster with higher monomer conversion after 3 h, but the dispersity of the polymer increases. The observed decrease of control is consistent with a decrease in the equilibrium concentration of the deactivator [BrCu^{II}TPMA]⁺ because of the lower halidophilicity of bromide ions for copper in the presence of water. The imposition of a more positive potential is somehow beneficial, as dispersity is

lower and conversion higher with respect to the synthesis at $E_{\text{app}} = E_{1/2} - 0.06$ V. However, water concentrations higher than 10% (v/v) are not recommendable due to deterioration of control of the polymerization.

Table 6.7. *e*ATRP of 50% (v/v) MA in EtOH/H₂O mixtures at different H₂O uptakes (% v/v of the total volume).^a

| Entry | H ₂ O (v/v) | <i>t</i> (h) | Conv. (%) | M_n^{app} | M_n^{th} | <i>D</i> | <i>Q</i> (C) | <i>I</i> _{eff} | <i>k</i> _{app} |
|----------------|------------------------|--------------|-----------|--------------------|-------------------|----------|--------------|-------------------------|-------------------------|
| 1 | 0 | 3 | 45 | 20600 | 21400 | 1.21 | 2.92 | 0.96 | 0.23 |
| 2 | 10 | 3 | 51 | 23700 | 24200 | 1.19 | 3.70 | 0.98 | 0.31 |
| 3 | 20 | 3 | 58 | 27700 | 27500 | 1.36 | 3.99 | 0.99 | 0.29 |
| 4 ^b | 20 | 4 | 65 | 31100 | 30900 | 1.30 | 4.20 | 0.99 | 0.26 |

^aApplied potential, $E_{\text{app}} = E_{1/2} - 0.06$ V $\sim E_{\text{pc}}$, unless otherwise indicated. ^b $E_{\text{app}} = E_{1/2}$. Other conditions: $C_{\text{MA}}:C_{\text{Cu}}:C_{\text{TPMA}}:C_{\text{EBiB}} = 552:0.1:0.1:1$. $V_{\text{tot}} = 5$ mL. WE = Pt mesh (estimated surface area = 6 cm²). DP = 552.

6.9 Electrochemically mediated aqueous ATRP of hydrophobic monomers

For drug delivery applications, organic solvents may represent a problem. Hence, special and expensive purification steps that are often time-consuming should be adopted. Water represents an attractive alternative to improve the cleanness of the products. In aqueous *e*ATRP of 10% (v/v) oligoethylene glycol methyl ether methacrylate (OEOMA), there are no solubility limitations for both monomer and polymer. Considering instead hydrophobic monomers, there are severe limitations caused by insolubility of polymer and often very low solubility of monomer. It is possible to overcome this limitation by replacing a certain amount of water with [BMIm][OTf]. The systematical replacement of water has a limit at which the system will lose its cost-effective advantage and cleanness, due to the increase of the organic fraction. Here we report the first example of *e*ATRP of a hydrophobic monomer in a true aqueous system (with [H₂O] > 33 M) with perfect control and good conversion. At 50 °C a system composed of 60% H₂O, 20% MA and 20 % [BMIm][OTf] (v/v) gives a homogeneous solution.

In Fig. 6.15, as an example, the voltammetric characterization of the polymerization reported in Table 6.8 entry 3 is shown.

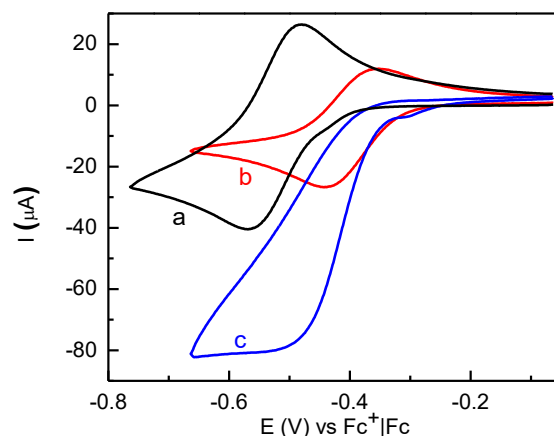


Figure 6.15. CV of 1.0 mM $[\text{BrCu}^{\text{II}}\text{TPMA}]^+$ in $\text{H}_2\text{O} + 20\%$ $[\text{BMIm}][\text{OTf}]$, recorded at $80\text{ }^\circ\text{C}$ on GC at 0.2 V/s before (a) and after addition of 20% (v/v) MA (b) and after further addition of 10 mM EBiB (c).

The catalyst exhibits a reversible peak couple in $\text{H}_2\text{O} + [\text{BMIm}][\text{OTf}]$ as well as in $\text{H}_2\text{O} + [\text{BMIm}][\text{OTf}] + \text{MA}$. It is worthy to notice the significant shift of $E_{1/2}$ to more positive potentials after monomer addition. This behavior has been widely observed in other aqueous systems; it is related to the relative stability $[\text{Cu}^{\text{II}}\text{L}]^{2+}$ and $[\text{Cu}^{\text{I}}\text{L}]^+$, which is strongly affected by the polarity of the reaction medium. The decrease of current intensity after MA addition is mainly due to a dilution effect. As expected, a strong catalytic current is observed when EBiB is added.

A series of potentiostatic polymerizations was carried out in $\text{H}_2\text{O}/\text{IL}/\text{MA}$ (60:20:20, v/v) at different temperatures (Table 6.8). At $50\text{ }^\circ\text{C}$, conversion was less than 10%, as precipitation of PMA occurred after only 12 min. This confirms the very low solubility of hydrophobic polymers in aqueous ambient even at $50\text{ }^\circ\text{C}$. The increase of the temperature to $80\text{ }^\circ\text{C}$ improved polymer solubility, allowing better results, with conversions close to 50%. It is important to note that all polymerizations were well controlled with very low D values, regardless of conversion. In entry 4, NaBr was used instead of Et_4NBr to improve the cleanness of the system.

Table 6.8. Aqueous *e*ATRP of 20% (v/v) MA in H₂O/[BMIm][OTf] (3:1, v/v) at different temperatures.^a

| Entry | <i>T</i> (°C) | <i>t</i> (h) | Conv. (%) | <i>M_n^{app}</i> | <i>M_nth</i> | <i>D</i> | <i>Q</i> (C) | <i>I_{eff}</i> | <i>k_{app}</i> |
|----------------|------------------|--------------|--------------|------------------------------------|-----------------------------------|----------|-----------------|------------------------|------------------------|
| 1 | 50 | 0.17 | 8 | 1300 | 1500 | 1.11 | 0.44 | 1.16 | 0.49 |
| 2 | 65 | 0.35 | 28 | 4700 | 5300 | 1.13 | 1.12 | 1.13 | 0.88 |
| 3 | 80 | 0.47 | 46 | 8400 | 8700 | 1.09 | 1.54 | 1.01 | 1.40 |
| 4 ^b | 80 | 0.48 | 47 | 8300 | 8700 | 1.09 | 1.52 | 1.02 | 1.38 |
| 5 ^c | 80 | 0.75 | 93 | 8500 | 8900 | 1.08 | 1.79 | 1.08 | 2.51 |

^aApplied potential, $E_{app} = E_{1/2}$. Other conditions: Unless otherwise stated, all experiments were performed in the presence of 0.1 M Et₄NBr. $C_{MA}:C_{Cu}:C_{TPMA}:C_{EBiB} = 221:1:1:100:10$. $V_{tot} = 5$ mL. WE = Pt mesh (estimated surface area = 6 cm²), CE = graphite in separate compartment. DP = 221. ^b0.1 M NaBr was used instead of Et₄NBr. ^cDP = 110; MA = 10% v/v.

Figure 6.16 shows representative examples of kinetic analyses of *e*ATRP of 20% (v/v) MA in H₂O/[BMIm][OTf] (3:1, v/v).

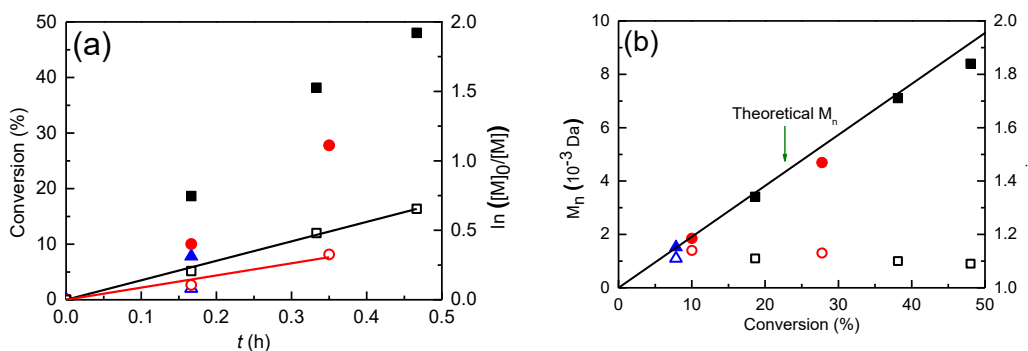


Figure 6.16. (a) Kinetic plots and (b) evolution of *M_n* and *D* with conversion for *e*ATRP of 20% v/v MA in H₂O/[BMIm][OTf] (3:1, v/v). Polymerization conditions: $C_{MA}:C_{Cu}:C_{TPMA}:C_{RX}:C_{Br} = 221:0.1:0.1:1:10$. $C_{Cu} = 10^{-3}$ M. $E_{app} = E_{1/2} - 60$ mV. 50 °C (▲), 65 °C (●) and 80 °C (■).

To increase the yield of polymer, the amount of both monomer and I Empty symbols refer to the right ordinate in the figures. L in the reaction mixture was increased, each of them from 20 to 25 to 30% (v/v).

Table 6.9. Aqueous *e*ATRP of MA in H₂O containing equal volumetric amounts of MA and [BMIm][OTf] (20, 25 and 30%, v/v) at 80 °C.^a

| Entry | H ₂ O/IL/MA (v/v) | <i>t</i> (min) | Conv. (%) | M_n^{app} | M_n^{th} | \bar{D} | Q (C) | I_{eff} | k_{app} |
|----------------|---------------------------------|-------------------|--------------|-------------|------------|-----------|------------|-----------|-----------|
| 1 | 3/1/1 | 12 | 46 | 8400 | 8700 | 1.09 | 1.54 | 1.03 | 1.40 |
| 2 | 2/1/1 | 40 | 40 | 9800 | 8100 | 1.10 | 2.49 | 0.83 | 0.82 |
| 3 | 1.33/1/1 | 60 | 42 | 10800 | 8900 | 1.09 | 3.30 | 0.83 | 0.59 |
| 4 ^b | 1.33/1/1 | 60 | 45 | 11000 | 9400 | 1.10 | 2.99 | 0.85 | 0.84 |

^a $E_{app} = E_{1/2}$. Other conditions: $C_{MA}:C_{Cu}:C_{TPMA}:C_{EBIB}:C_{NaBr} = x:0.1:0.1:1:10$ with $x = 221$ (entry 1), 234 (entry 2), 247 (entry 3) and 123 (entry 4); $C_{Cu} = 10^{-3}$ M. $V_{tot} = 5$ mL. ^b DP = 113. WE = Pt mesh (estimated surface area = 6 cm²).

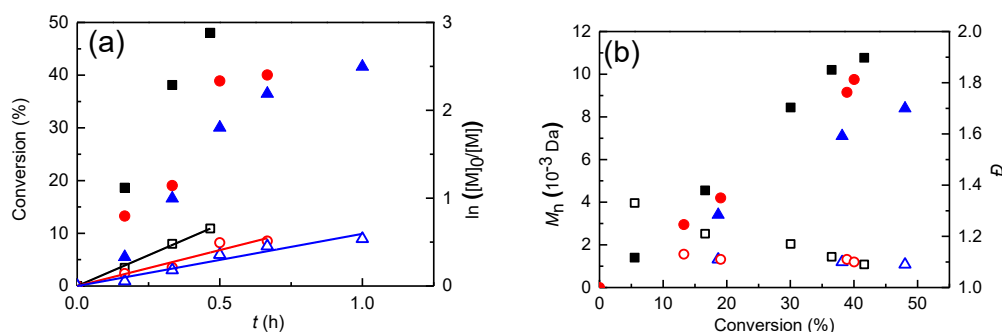


Figure 6.17. (a) Kinetic plots and (b) evolution of M_n and \bar{D} with conversion for the aqueous *e*ATRP of MA. $C_{Cu} = 10^{-3}$ M. $E_{app} = E_{1/2}$. H₂O/IL/MA (v/v): 3/1/1 (■), 2/1/1 (●) and 1.33/1/1 (▲). Empty symbols refer to the right ordinate in the figures.

As the organic fraction in the reaction mixture is increased the polymerization becomes slower, whereas the molecular weight of the produced polymer increases. Mixing IL with water appears an interesting strategy allowing the polymerization of hydrophobic monomers such as methyl acrylate in an environmentally friendly medium. Of course, production of high molecular weight polymers requires enriching the system with the organic component (IL + monomer) to avoid polymer precipitation. It is not, however, convenient for economic reasons and cleanness of the system to increase the organic fraction to >60%. It is possible to maintain and improve, for some aspects, the characteristics of the polymerization performed in common organic solvents by exploiting the benefits of water and ionic liquids, creating eco-friendly, inexpensive and clean systems.

6.10 Conclusions

The main conclusion of this work is straightforward: in *e*ATRP it is possible to use mixtures of [BMIm][OTf] and water, which is an inexpensive solvent. The abatement of cost goes close to 30% when water is 30% (v/v). Using up to 20% (v/v) water increases significantly the rate of polymerization without negatively affecting molecular weight control; a well-defined PMA with $M_n > 40000$ and $D < 1.2$ was obtained. These benefits are also present when the polymerization is triggered in organic solvents with small amounts of water. *e*ATRP of methyl acrylate was further studied in an aqueous environment: ionic liquids are powerful allies in the polymerization of hydrophobic monomers, enhancing the solubility of both monomer and polymer. The role of temperature in this case is very important: high temperatures (80 °C) are necessary to delay the precipitation of polymer towards high conversions. In these aqueous systems, polymerizations are fast with fair conversions in less than 60 min and perfect control ($D \leq 1.10$) before precipitation of the polymer starts. It was found also that a decrease of water reduces the rate of polymerization improving conversion, delaying the precipitation.

All polymers can be isolated by either precipitation with water or by cooling at ambient temperature, followed by filtration and washing with water. This work anticipates the successful introduction of water/ionic liquid mixtures without any other species. A more widespread use of this polymerization technique, thanks to the improved costs for the scale-up of the process would allow the possibility to polymerize several other monomers by tuning the amount of ionic liquid to promote solubility of even hydrophobic monomers. It is necessary to emphasize the use of water whenever possible in *e*ATRP, even with traditional solvents, as no adverse effects have been found.

References

1. Fantin, M.; Isse, A. A.; Venzo, A.; Gennaro, A.; Matyjaszewski, K., Atom Transfer Radical Polymerization of Methacrylic Acid: A Won Challenge. *Journal of the American Chemical Society* **2016**, *138*, 7216-7219.
2. Szekely, G.; Jimenez-Solomon, M. F.; Marchetti, P.; Kim, J. F.; Livingston, A. G., Sustainability assessment of organic solvent nanofiltration: from fabrication to application. *Green Chemistry* **2014**, *16*, 4440-4473.
3. Capello, C.; Fischer, U.; Hungerbuhler, K., What is a green solvent? A comprehensive framework for the environmental assessment of solvents. *Green Chemistry* **2007**, *9*, 927-934.
4. Solvent Use and Waste Issues. In *Green Chemistry in the Pharmaceutical Industry*.
5. De Bon, F.; Fantin, M.; Isse, A. A.; Gennaro, A., Electrochemically mediated ATRP in ionic liquids: controlled polymerization of methyl acrylate in [BMIm][OTf]. *Polymer Chemistry* **2018**, *9*, 646-655.
6. Fantin, M.; Isse, A. A.; Gennaro, A.; Matyjaszewski, K., Understanding the Fundamentals of Aqueous ATRP and Defining Conditions for Better Control. *Macromolecules* **2015**, *48*, 6862-6875.
7. Fantin, M.; Isse, A. A.; Matyjaszewski, K.; Gennaro, A., ATRP in Water: Kinetic Analysis of Active and Super-Active Catalysts for Enhanced Polymerization Control. *Macromolecules* **2017**, *50*, 2696-2705.
8. Freire, M. G.; Neves, C. M. S. S.; Marrucho, I. M.; Coutinho, J. A. P.; Fernandes, A. M., Hydrolysis of Tetrafluoroborate and Hexafluorophosphate Counter Ions in Imidazolium-Based Ionic Liquids. *Journal of Physical Chemistry A* **2010**, *114*, 3744-3749.
9. Bonhôte, P.; Dias, A.P.; Papageorgiou, N.; Kalyanasundaram, K.; Grätzel, M., Hydrophobic, Highly Conductive Ambient-Temperature Molten Salts. *Inorganic Chemistry* **1996**, *35*, 1168-1178.
10. Ge, M.-L.; Zhao, R.-S.; Yi, Y.-F.; Zhang, Q.; Wang, L.-S., Densities and Viscosities of 1-Butyl-3-methylimidazolium Trifluoromethanesulfonate + H₂O Binary Mixtures at $T = (303.15 \text{ to } 343.15) \text{ K}$. *Journal of Chemical & Engineering Data* **2008**, *53*, 2408-2411.
11. Rodríguez, H.; Brennecke, J. F., Temperature and Composition Dependence of the Density and Viscosity of Binary Mixtures of Water + Ionic Liquid. *Journal of Chemical & Engineering Data* **2006**, *51*, 2145-2155.
12. Seddon, K. R.; Stark, A.; Torres, M.-J., Viscosity and Density of 1-Alkyl-3-methylimidazolium Ionic Liquids. In *Clean Solvents*, American Chemical Society: 2002; Vol. 819, 34-49.
13. Plechkova, N. V.; Seddon, K. R., Applications of ionic liquids in the chemical industry. *Chemical Society Reviews* **2008**, *37*, 123-150.
14. Etra SpA, Price Chart, **2018**.

Chapter 7

From Ionic liquids to poly(Ionic Liquids)

7.1 Introduction

Poly(ionic liquids) or polymerizable ionic liquids (PILs) are polyelectrolytes. They comprise a polymeric backbone and an ionic liquid species in the repeating unit. Many properties of the starting ionic liquid such as negligible vapor pressure, thermal and electrochemical stability, non-flammability and good ionic conductivity are transferred to the polymer upon polymerization. PILs permit to achieve structures and morphologies that monomeric ionic liquids cannot provide, and the design of the monomeric unit considerably enriches and tailors the PIL to the specific application.^{1,2,3} PILs represent a rapidly growing sector of macromolecular engineering. This exponential growth is, in part, a consequence of an ever-growing interest in Ionic Liquid Monomers (ILMs). The controlled synthesis of (co)polymers containing carboxylic ionic groups, like (meth)acrylates, can lead to a plethora of applications. Such polymers are hydrophilic, often pH responsive, and generally biocompatible. They exhibit also unique complexing properties. Besides these properties, the ionic conductivity, hydrophilicity/hydrophobicity, (electro)chemical and thermal stability, and structure of PILs promoted interest and research in these materials. Some of the most relevant properties of PILs will be summarized hereafter. However, focusing on all of them is beyond the scope of this chapter.

7.1.1 Tunable ionic conductivity

Ionic conductivity is one of the most important properties in solid state applications and electrochemical devices. Ions of PILs are constrained because they are part of the macromolecule. Typically, the conductivity of a given PIL is lower than that of the parent ILM, due to the significant increase of glass transition temperature (T_g). Besides this, other factors such as temperature, polymer architecture, molecular

weight, and chemical nature of polymer chains and IL moieties may affect ionic conductivity.

7.1.2 Glass Transition Temperature

Low T_g promotes a high ionic conductivity.⁴ In contrast to conventional polyelectrolytes, PILs have weakly bound counter ions with bulky sizes and lower mobilities. Counter ions affect the T_g : one way to reduce it is to substitute one mobile ion with another, *via* ion exchange. However, both the anionic and cationic moieties of PILs affect T_g . A PIL with a T_g of 57 °C was synthesized through FRP of an acrylate ILM (2-acrylamido-2-methyl-1-propanesulfonate anion) and tris(2-[2-methoxyethoxy]ethyl)ammonium cation.^{5,6} It exhibited a low T_g by structurally shielding coulombic interactions. Recently, the synthesis of a low glass transition temperature PIL prepared from a quaternary ammonium cationic monomer, poly(vinylbenzyltriethylammonium bis(trifluoromethanesulfonyl)imide) P[VBTA][TFSI], was reported. The synthesis was performed *via* atom transfer radical polymerization (ATRP), producing a polymer with well-defined molecular weights and narrow molecular weight distributions ($D = 1.1-1.3$).⁷

7.1.3 Polymer architecture

Most polycations with small anions exhibit higher conductivities than do the same polycations with more bulky counter anions: the negative charge is more mobile with smaller anions. A comparison of various polyanions bearing pyrrolidinium cation, $C_4H_{10}N^+$, as counter-ion suggests that the conductivity is determined by the delocalization of the charge on the anion. The position of substituents on imidazolium cation, spacer structure and length, and anion species have influences on the ionic conductivity.^{8,9} It is important to maintain the flexibility of the imidazolium cation to obtain higher ionic conductivities for PILs. Both translational and rotational mobilities affect ionic conductivity. The effects of varying the spacer length between the backbone and the imidazolium cation on the static dielectric constant have been demonstrated. The ionic conductivities increase considerably with the extension of the spacer in the side chains of both polycations and polyanions. Moving chemically bonded cations or anions farther from the polymer backbone increases their range of motion and facilitates mobile ion transport.

Similarly, with increasing spacer length between ions hosted in the PIL backbone, the number density of ions decreases, and conductivity decreases. Colby et al. synthesized a series of PILs based on imidazolium cation and methacrylate anions with different pendant structures containing a combination of alkylene ($[\text{CH}_2]_n$, $n = 5$ or 10) and oxyethylene ($[\text{OCH}_2\text{CH}_2]_n$, ($n = 4$ or 7) units as spacers between the imidazolium cations and the backbone.¹⁰ An increase in spacer length is accompanied by a marked reduction in T_g . The incorporation of imidazolium cations with longer non-ionic spacer lengths makes ions responding more easily to an applied electric field due to decreased electrostatic shielding.

7.1.4 Molecular weight

Molecular weight of PILs can also influence several properties such as T_g , viscosity, elastic modulus, and ionic conductivity. In the case of PILs based on imidazolium polycations, the ionic conductivity decreases with increasing molecular weight and reaches a plateau at a molecular weight of about 10^5 Da. T_g increases with increasing molecular weight, reaching a plateau at degrees of polymerization greater than 70, just as for regular flexible non-charged polymers.

7.1.5 Aqueous solubility

Structures and properties of PILs can be easily modulated by changing the type of counter-ion.¹¹ PILs can be tuned from being hydrophilic to hydrophobic through simple counter-ion exchange. By replacing a halide ion with bis(trifluoromethanesulfonyl)imide (TFSI) or PF_6^- , PILs may be made hydrophobic and precipitated out of aqueous solutions. Many ILs are moisture-retentive and assimilate water from the atmosphere, and their solubility in water increases with increasing temperature. Hydrogen bonding, intermolecular interactions between water hydrogens and electron lone pairs of IL heteroatoms, are considered an important factor in modifying miscibility. Cammarata et al. suggested that IL hydrophilicity could be employed as an indicator for the intensity of H-bonding interactions. It was noted that water molecules are inclined to interact with the H-2, H-4, and H-5 protons of the imidazolium ring (see Fig. 7.2).¹²

7.1.6 Thermal stability

The thermal stability of PILs is a relevant parameter: many applications of polymers operate at high temperatures; thus, thermal stability is of primary interest. The massive structural variety of PILs contributes to a wide interval of stability, from 150 °C to more than 400 °C. The onset temperature of decomposition (T_{onset}) in TGA (thermo-gravimetric analysis) experiments is usually controlled through the nature of the PIL backbone chemical structure. Aromatic PILs usually possess a higher T_{onset} than PILs with aliphatic backbone structures. The thermal stability of a PIL increases with the length of substituent in the cation. Lengthening the spacer between a polymer backbone chain and the ionic substituent group results in decreasing thermal stability. The chemical structures of anions also affect the T_{onset} values of PILs.^{13,14}

7.1.7 Chemical and electrochemical stability

PILs are resistant to chemical and electrochemical degradation. In any case, side reactions (structural rearrangement or degradation) might occur under extreme circumstances in a device or reaction. These effects must be studied in practical applications. A hydroxide anion in PILs may trigger chemical instability because of its highly nucleophilic nature. At highly alkaline concentrations and high temperatures, covalently connected cations in anion exchange membranes are prone to degradation through OH^- attack. The electrochemical stability window of ILs is in the range from 2.5 V to 5.0 V. Like ILs, the electrochemical-stability windows of PILs vary widely, depending on the PIL cation–anion pair. The electrochemical stability of PILs (up to 5 V) is usually comparable with that of structurally similar ILs and, in some cases, it even surpasses them. Pyrrolidinium-based PILs have been reported to have electrochemical stabilities superior to imidazolium-based PILs. Pyrrolidinium cations also present more negative cathodic decomposition potentials than noncyclic and unsaturated cyclic quaternary ammonium cations.^{15,16,17}

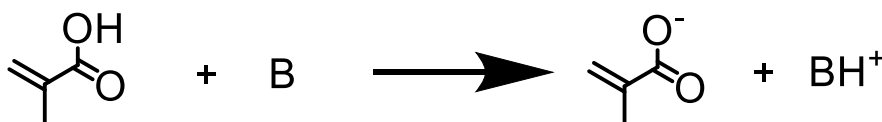
7.2 Synthesis of poly(ionic liquids)

The broad applications of PILs as polymer electrolytes in electrochemical devices, smart materials, catalyst supports, and for the construction of porous polymers and antibacterial materials, require different structures and properties. The common synthetic approaches are of three types: (i) direct sequential chain growth polymerization of ILs with and without non-ionic monomers; (ii) step growth polymerization of ILMs; (iii) post-modification of polymer chains with ILMs. To date, a large number of polymerization techniques have been applied: free radical polymerization, mini-,¹⁸ micro-¹⁹ and emulsion polymerization, suspension,²⁰ dispersion²¹ and cationic polymerization, ring opening metathesis,²² ATRP,^{23,24,25,26} RAFT^{27,28} and CMRP.²⁹

The neutralization of organic acids with organic bases having at least one vinyl functionality, in aqueous medium, leads to the corresponding organic salt, which is an ionic liquid (Scheme 7.1). Often, ILMs comprise an alkylimidazolium (or alkylammonium) cation and a (meth)acrylate anion, which can be polymerized *via* ATRP. In this chapter the polymerization of ILMs containing different organic cations and methacrylate anion was investigated.

7.2.1 Synthesis and properties of methacrylate-based ILMs

The syntheses of ILMs based on unsaturated carboxylates require precautions due to the use of methacrylic acid without inhibitor. Methacrylic acid (MAA) is prone to polymerize without inhibitor and therefore MAA-derived ILMs may polymerize upon heating or exposure to UV radiation (even laboratory neon lights). Thus, operating and storing in the dark (or without neon lights) at low temperatures (ice bath or dry-ice bath) is recommended. The synthesis of these monomers can be carried out conveniently *in situ*, by mixing equimolar amounts of MAA and the desired cation precursor. In this way, undesired polymerization is avoided.



Scheme 7.1. General route of synthesis of ILMs *via* aqueous neutralization.

1-methylimidazolium methacrylate [MIm][Meth] is an ionic liquid of yellowish color. [MIm][Meth] is soluble in a range of solvents spanning from water to chloroform to ethyl acetate. Aqueous solutions of up to 10% (v/v) [MIm][Meth] are neutral, with pH comprised between 6 and 7. To confirm the synthesis of [MIm][Meth] *in situ*, NMR analysis was performed (Fig. 7.1):

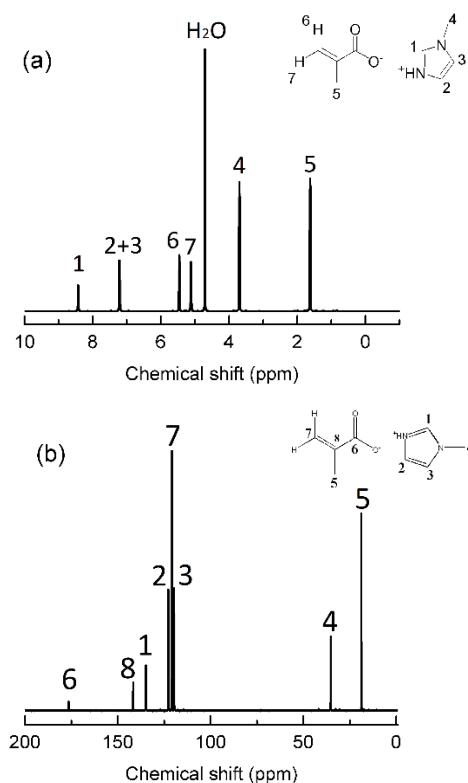


Figure 7.1. a) 600 MHz ^1H -NMR and b) 150 MHz ^{13}C -NMR of 1-methylimidazolium methacrylate, recorded at 25 °C in D_2O .

ILMs containing amino acids and vitamins were also synthesized, affording nicotinium acid methacrylate [B3][Meth], and L-Valinium methacrylate [L-Val][Meth]. More complex ILMs have been obtained by neutralizing two or four times a polyamine such as ethylenediamine and tris(2-aminoethyl)amine, respectively, with methacrylic acid. The resulting liquid monomers are composed by one cation and two or four methacrylate anions: $[\text{H}_2\text{en}][\text{Meth}]_2$ and $[\text{H}_4\text{TREN}][\text{Meth}]_4$ (Figure 7.2).

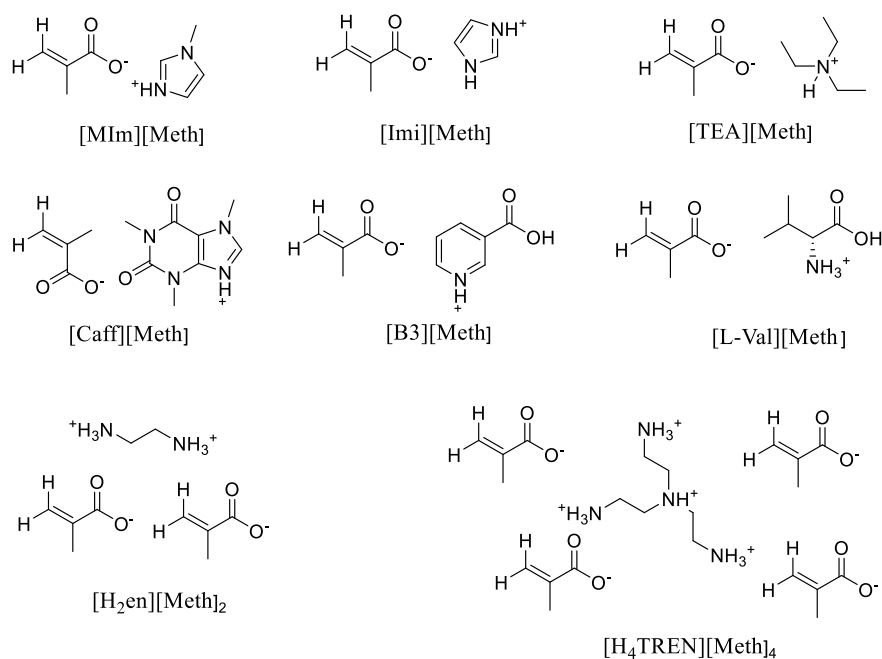


Figure 7.2. Structures of investigated ionic liquid monomers.

Some properties of these ILMs are summarized in Table 7.1.

Table 7.1. Properties of investigated ionic liquid monomers.^a

| ILM | MW (g/mol) | Assay | Color | pH ^b | Storing |
|--|------------|-------|--------------------------|-----------------|------------|
| [MIm][Meth] | 168.16 | >99% | Yellowish liquid | 5-6 | Dark/-20°C |
| [Imi][Meth] | 154.14 | >99% | Slight yellow liquid | 6-7 | Dark/-20°C |
| [TEA][Meth] | 187.25 | >99% | Colorless liquid | 6-7 | Dark/-20°C |
| [Caff][Meth] | 280.25 | >99% | White solid | 6-7 | Dark/-20°C |
| [L-Val][Meth] | 203.21 | >99% | Colorless liquid | 3-4 | Dark/-20°C |
| [Vit. B3][Meth] | 209.17 | >99% | White solid ^d | 3-4 | Dark/-20°C |
| [H ₂ En][Meth] ₂ | 232.22 | >99% | Colorless liquid | 5-6 | Dark/-20°C |
| [H ₄ TREN][Meth] ₄ | 490.60 | >99% | Colorless liquid | 4-5 | Dark/-20°C |

^aMeasured at 25°C. ^bThe pH of an aqueous solution of 10% (v/v) of monomer.

7.3 Investigation of the catalytic system

Electrochemical analysis was carried out before the polymerization. The catalyst $[\text{Cu}^{\text{II}}\text{TPMA}]^{2+}$ was used as internal probe to monitor the steps of synthesis of ILM *in situ* (Figure 7.3).

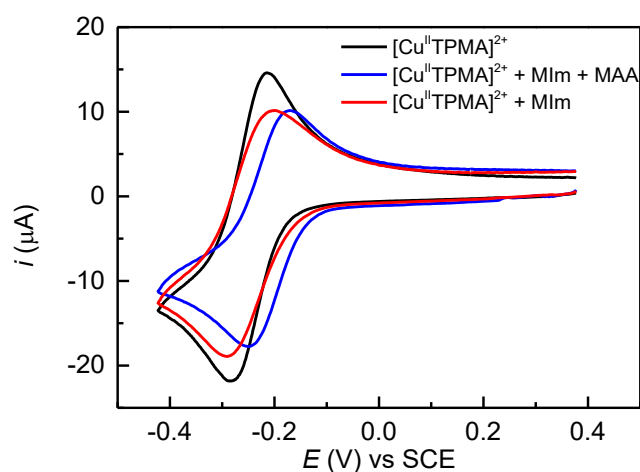


Figure 7.3. CV of 10^{-3} M $[\text{Cu}^{\text{II}}\text{TPMA}]^{2+}$ in water + 0.1 M NaBr, recorded at 25 °C on a GC electrode at $v = 0.2$ V/s in the absence (—) and presence of 10% (v/v) MIm (—) or MIm + MAA (—) (10% v/v of each, respectively).

The catalyst in water + 0.1 M NaBr exhibits a distinct reversible cyclic voltammogram at $E_{1/2} = -0.250$ V vs. SCE. Upon the addition of MIm the solution turned from almost colorless to blue as MIm, coordinated the metal *via* N-atom, displacing the bromide ion to give the complex $[\text{Cu}^{\text{II}}\text{TPMA}(\text{MIm})]^{2+}$. Further addition of MAA protonated MIm. Neutralization of MIm with MAA destroyed $[\text{Cu}^{\text{II}}\text{TPMA}(\text{MIm})]^{2+}$, which was converted back to $[\text{BrCu}^{\text{II}}\text{TPMA}]^+$. In these conditions, $E_{1/2}$ of the complex shifts to -0.209 V vs. SCE, reflecting the decreased polarity of the reaction medium.

The polymerization of $[\text{MIm}][\text{Meth}]$ is conveniently triggered in water because it ensures the complete solubility of all reagents and products. Water is an inexpensive and readily available green solvent with high thermal capacity and low viscosity. Electrochemically mediated ATRP of 10% v/v OEOMA in water provides excellent control under a wide range of pH conditions. Typically, with $[\text{Cu}^{\text{II}}\text{TPMA}]^{2+}$ as catalyst, 98% conversion was achieved within 4 h in a well-controlled process

yielding polymers with $D = 1.10$ - 1.15 .³⁰ Therefore, an *e*ATRP of [MIm][Meth] was performed, replicating the experimental conditions that were successful for OEOMA.

Only 4% of [MIm][Meth] was converted after 20 min, after which the reaction completely stopped, yielding a polymer of $M_n = 9800$ and of broad dispersity ($D = 1.76$). Cyclic voltammetry of $[\text{Cu}^{\text{II}}\text{TPMA}]^{2+}$ in 10% (v/v) [MIm][Meth] in $\text{H}_2\text{O} + 0.1 \text{ M NaBr}$ exhibits a reversible peak couple, with $E^\circ = -0.209 \text{ V vs. SCE}$ (black solid line in Figure 7.4a). For comparison, E° of $[\text{Cu}^{\text{II}}\text{TPMA}]^{2+}$ in 10% (v/v) OEOMA in water + 0.1 M Et_4NBr is -0.260 V vs. SCE .³⁰ This difference in the redox potentials ($\sim 0.05 \text{ V}$) suggests that the complex is a slightly weaker reducing agent and therefore less active in the presence of [MIm][Meth] than OEOMA. To check the stability of $[\text{Cu}^{\text{II}}\text{TPMA}]^+$ during electrolysis, the typical conditions of a polymerization experiment were simulated by vigorously stirring under open circuit a cell containing all components needed for *e*ATRP for 2 h. The shape of the voltammetric curve of $[\text{Cu}^{\text{II}}\text{TPMA}]^{2+}$ was still reversible. Since no other peak appeared in the CV, the initial complex did not dissociate, or, in other words, [MIm][Meth] does not compete with TPMA for Cu^{2+} ions (Figure 7.4 a-b).

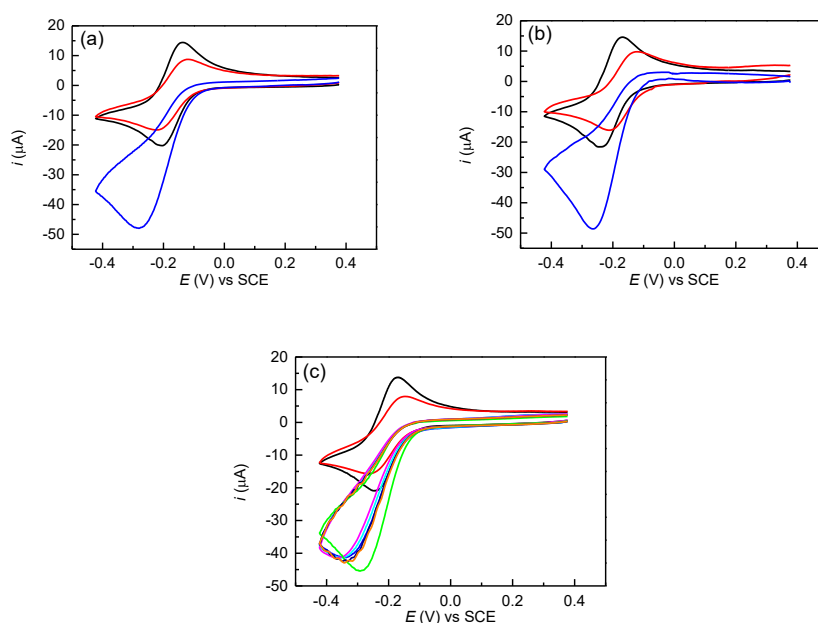


Figure 7.4. CV of $10^{-3} \text{ M } [\text{Cu}^{\text{II}}\text{TPMA}]^{2+}$ in water (—) or + 10% v/v [MIm][Meth] (—) and + 10^{-2} M HEBiB (—) (a) in the presence of 0.1 M NaBr or (b) 0.1 M NaCl. CV were recorded immediately after addition of the reagents. (c) CV of $10^{-3} \text{ M } [\text{Cu}^{\text{II}}\text{TPMA}]^{2+}$ in water (—) or + 10% v/v [MIm][Meth] (—) and + 10^{-2} M HEBiB (different colors). CV were recorded in presence of 0.1 M NaBr, times from 0 to 2 h. All CV were recorded on GC electrode, at $v = 0.2 \text{ V/s}$.

A similar situation was observed in the presence of initiator HEBiB (Figure 7.4c). As expected, the CV was irreversible, confirming the catalytic behavior of the system. The electrogenerated $[\text{Cu}^{\text{I}}\text{L}]^+$ quickly disappears by reaction with the initiator. This reaction regenerates Cu^{II} , which is subsequently reduced at the electrode, causing the enhancement of the cathodic current (I_{pc}). As in the previous case, the voltammetric pattern was essentially unchanged after two hours of stirring at open circuit in the presence of $[\text{MIm}][\text{Meth}]$. This indicated that the initiator was stable and did not undergo hydrolysis, while its catalytic activity remained unchanged. This proved that the complex was stable also in the presence of the PIL, which could act as a stronger polydentate ligand, using multiple carboxylic groups to bind Cu^{2+} ions.

7.4 Electrochemically mediated ATRP of $[\text{MIm}][\text{Meth}]$

7.4.1 Effect of type of halide ion (Br^- , Cl^-)

*e*ATRP in water is performed with a relatively high concentration (0.1–0.3 M) of halide ions to prevent the dissociation of the ternary deactivator complex $[\text{X}-\text{Cu}^{\text{II}}\text{L}]^+$.³⁰ As mentioned previously *e*ATRP of 10% (v/v) $[\text{MIm}][\text{Meth}]$ in water containing 10^{-3} M $[\text{Cu}^{\text{II}}\text{TPMA}]^{2+}$ + 0.1 M NaBr was unsuccessful (Table 7.2, entry 1). No appreciable improvement was observed when NaCl was used in place of NaBr, with conversion still below 10% (Table 7.2, entries 2-3). With high Cl^- concentration, catalytic halogen exchange from the starting HEBiB initiator was immediately achieved at the beginning of the reaction. Changing the halide ions and their concentration can also affect other important ATRP parameters, such as $[\text{X}-\text{Cu}^{\text{II}}\text{L}]^+$ association constant and ATRP equilibrium constants. Nevertheless, only a very slight improvement was observed with Cl^- (up to 0.3 M), mainly due to the better stability of the C-Cl chain-end functionality than C-Br.

Table 7.2. *e*ATRP of 10% (v/v) [MIm][Meth] in water at $E_{\text{app}} = E_{1/2}$ and $T = 25$ °C.^a

| Entry | X ⁻ | [X ⁻] (M) | <i>t</i> (h) | Conv. (%) | M_n^{app} | M_n^{th} | \bar{D} | k_p^{app} | Q (C) | I_{eff} |
|-------|-----------------|-----------------------|--------------|-----------|--------------------|-------------------|-----------|--------------------|---------|------------------|
| 1 | Br ⁻ | 0.1 | 0.33 | 4 | 9800 | 2100 | 1.75 | - | 1.43 | 0.21 |
| 2 | Cl ⁻ | 0.1 | 0.66 | 5 | 5500 | 2700 | 1.69 | - | 1.66 | 0.49 |
| 3 | Cl ⁻ | 0.3 | 1 | 8 | 9900 | 4800 | 1.67 | - | 1.69 | 0.43 |

^aMeasured pH = 5.9. Conditions: $C_M:C_{\text{HEBiB}}:C_{\text{Cu(OTf)}_2}:C_{\text{TPMA}} = 63:2:0.1:0.1$. $C_{\text{Cu}} = 10^{-3}$ M. $V_{\text{total}} = 10$ mL.

In any case these results prompted us to consider the effects of pH and chain-end structure. In particular, we adopted three strategies that were reported to be successful for *e*ATRP of MAA.³¹ First, the C-Br chain end was switched to C-Cl. Then, the pH was lowered to reduce the concentration of free carboxylate anions. Finally, appropriate conditions were selected to accelerate the polymerization. The idea behind these measures was to suppress the cyclization side reaction responsible for the failure of aqueous ATRP of MAA.³¹

7.4.2 pH effect

The fate of the polymerization depends strongly on the pH. Free carboxylate anions are powerful nucleophiles and intramolecular cyclization reactions occur, as in the case of methacrylic acid.³¹ To avoid cyclization and dramatically improve conversion and dispersity, *e*ATRP of [MIm][Meth] was triggered by lowering pH from 5.9 to 0.1 by using perchloric acid, a value at which the methacrylate anions should be almost quantitatively protonated.

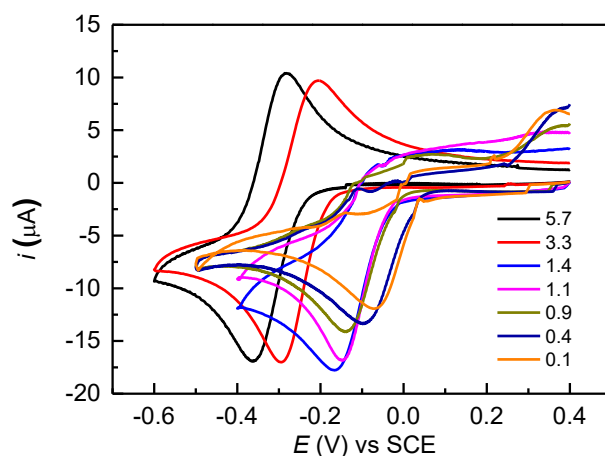


Figure 7.5. CV of 10^{-3} M $[\text{Cu}^{\text{II}}\text{TPMA}]^{2+}$ in 10% (v/v) $[\text{MIm}][\text{Meth}]$ in water + 0.1 M NaCl at different pH (values labeled in the Figure). CV are recorded at 25 °C on a glassy carbon electrode at $v = 0.2$ V/s at increasing HClO_4 loadings.

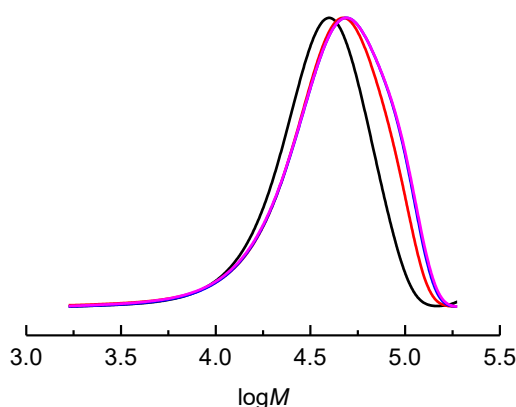
A series of strategies was employed in combination with pH lowering. A four-fold TPMA excess was added to promote a better complexation of Cu^+ at low pH. Modification of Cu/TPMA structure with pH could cause a shift in the standard reduction potential of the catalyst (Figure 7.5). At acid pH, partial protonation of the ligand may occur, which can result in the dissociation of one or more arms of the tetradentate ligand. Excess TPMA can assist complex formation by binding to vacant coordination sites. Another important strategy is the use of polychlorinated initiators to produce a symmetrical polymer architecture. 2,2-dichloropropionic acid (DCPA) generates two chains per initiator molecule, producing therefore homotelechelic polymers. Symmetry of the growing chain guarantees the perfectly symmetrical growth from both sides. It should be mentioned however that at pH = 1 the polymerization may be intended as the polymerization of non-ionized methacrylic acid (MAA) in the perchlorate salt of the cation (e.g. $[\text{MIm}][\text{ClO}_4]$). Regardless this aspect, at the end of the polymerization, the restoration of neutral pH affords the PIL of interest, as seen by NMR analysis (Figure 7.7). The results of *e*ATRPs are summarized in Table 7.3:

Table 7.3. *e*ATRP of 10 % (v/v) [MIm][Meth] in water at different pH and $T = 25$ °C at $E_{app} = E_{pc}$.^a

| Entry | pH | t (h) | Conv. (%) | M_n^{app} | M_n^{th} | \bar{D} | k_{app} | Q (C) | I_{eff} |
|------------------|------------------|---------|-----------|-------------|------------|-----------|-----------|---------|-----------|
| 1 ^b | 5.9 ^c | 0.66 | 5 | 5500 | 2700 | 1.69 | 0.08 | 1.69 | 0.49 |
| 2 ^b | 3.0 | 1.33 | 49 | 30100 | 26000 | 1.69 | 0.51 | 1.99 | 0.86 |
| 3 ^{d,e} | 1.0 | 2 | 83 | 45900 | 44000 | 1.42 | 0.89 | 3.36 | 0.96 |
| 4 ^{d,e} | 0.1 | - | 3 | - | 1600 | - | - | 1.25 | - |

^apH was adjusted by addition of HClO₄; NaCl was added to have a constant total 0.3 M C_{Cl}. Conditions: C_M:C_{RX}:C_{Cu(OTf)₂}:C_{TPMA} = 63:0.2:0.1:0.1. C_{Cu} = 10⁻³ M. V_{total} = 10 mL. ^bHEBiB was used as initiator. ^cpH of 10% (v/v) [MIm][Meth] in water. ^dC_M:C_{RX}:C_{CuCl₂}:C_{TPMA} = 63:0.2:0.1:0.4. ^eDCEPA used as initiator.

Conversion dramatically increased by lowering pH. At pH = 1, 83% conversion was reached after 2 h with good control and apparent molecular weights matching the theoretical values. At pH = 0.1, no polymerization happened probably because, at this extremely acid ambient, [Cu^IL]⁺ was not stable enough to promote activation. Evolution of molecular weight distribution during the polymerization at pH = 1 (Table 7.3, entry 3) and ¹H-NMR of the isolated PIL are shown in Figures 7.6 and 7.7.

**Figure 7.6.** MW distribution recorded during *e*ATRP of 10% (v/v) [MIm][Meth] at pH = 1, catalyzed by [Cu^{II}TPMA]²⁺ at $T = 25$ °C.

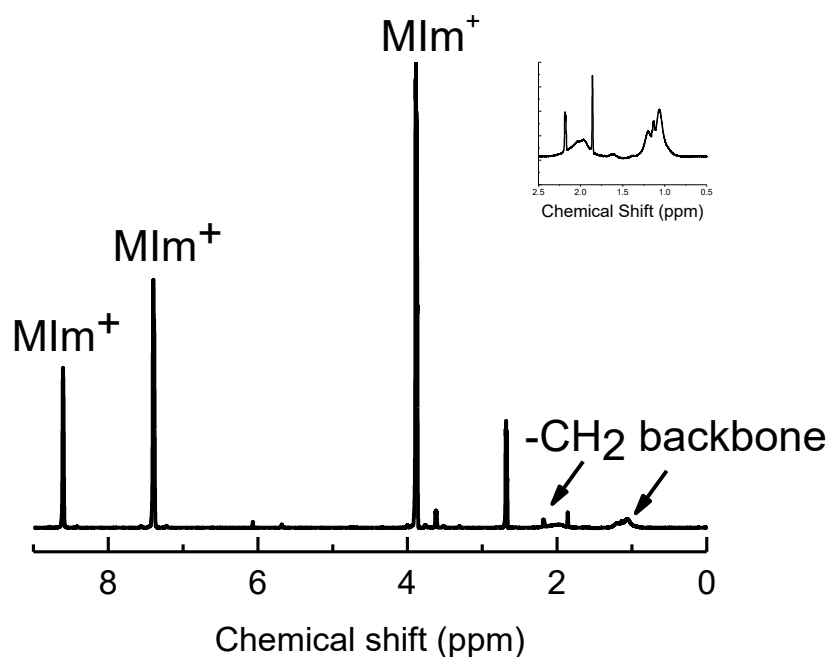


Figure 7.7. 600 MHz ^1H -NMR of poly(1-methylimidazolium methacrylate), $M_n = 45900$ Da, recorded at 25 °C in D_2O .

7.4.3 Modulating the polymerization rate by tuning E_{app} and temperature

Modulating E_{app} is an easy way to modify the overall rate of $e\text{ATRP}$. For example, in the case of 50% (v/v) MA in $[\text{BMIm}][\text{OTf}]$, the reaction rate reached its maximum value when $E_{\text{app}} = E_{1/2} - 0.12$ V was imposed (see Chapter 3). This limiting rate is dictated by the mass transport of reagents and products to and from the electrode surface. In the $e\text{ATRP}$ of $[\text{MIm}][\text{Meth}]$ at pH 1, $E_{1/2}$ could not be measured. Therefore, the applied potential was chosen with reference to the peak potential, E_{pc} , which is usually at least 0.03 V more negative than $E_{1/2}$. At $E_{\text{app}} = E_{\text{pc}}$, the rate of Cu^{II} reduction should be close to the limit of mass transport and therefore the polymerization proceeded at a rate close to the highest possible value. Consequently, the contribution of cyclization was minimized (Table 7.4, entry 1).

Table 7.4. *e*ATRP of 10 % (v/v) [MIm][Meth] in water at different E_{app} and $T = 0, 25$ and 50 °C at pH = 1, RX = DCPA.^a

| Entry | T (°C) | $E_{\text{app}} - E_{\text{pc}}$ | | Conv. (%) | M_n^{app} | M_n^{th} | D | k_p^{app} | Q (C) | I_{eff} |
|-------|-------------|----------------------------------|---------|--------------|--------------------|-------------------|------|--------------------|------------|------------------|
| | | E_{pc} (V) | t (h) | | | | | | | |
| 1 | 25 | 0 | 2 | 83 | 45900 | 44000 | 1.42 | 0.89 | 3.36 | 0.96 |
| 2 | 25 | 0.06 | 2 | 78 | 43800 | 40000 | 1.43 | 0.76 | 2.36 | 0.91 |
| 3 | 50 | 0 | 0.25 | 43 | 25800 | 23000 | 1.95 | 2.24 | 1.09 | 0.89 |
| 4 | 0 | 0 | 4 | 77 | 40100 | 39500 | 1.42 | 0.37 | 2.13 | 0.99 |

^apH was adjusted by addition of HClO₄; NaCl was added to have a constant total 0.3 M C_{Cl} . Conditions: $C_M:C_{\text{RX}}:C_{\text{Cu(OTf)}_2}:C_{\text{TPMA}} = 63:0.2:0.1:0.4$. $C_{\text{Cu}} = 10^{-3}$ M. $V_{\text{total}} = 10$ mL.

Applying a more positive potential $E_{\text{app}} - E_{\text{pc}} = 0.06$ V may result in a more controlled polymerization. It was found that the two reactions were practically identical (Figure 7.8), but initiation efficiency was higher with $E_{\text{app}} - E_{\text{pc}} = 0$ V. Thus, $E_{\text{app}} = E_{\text{pc}}$ was chosen for all further polymerizations.

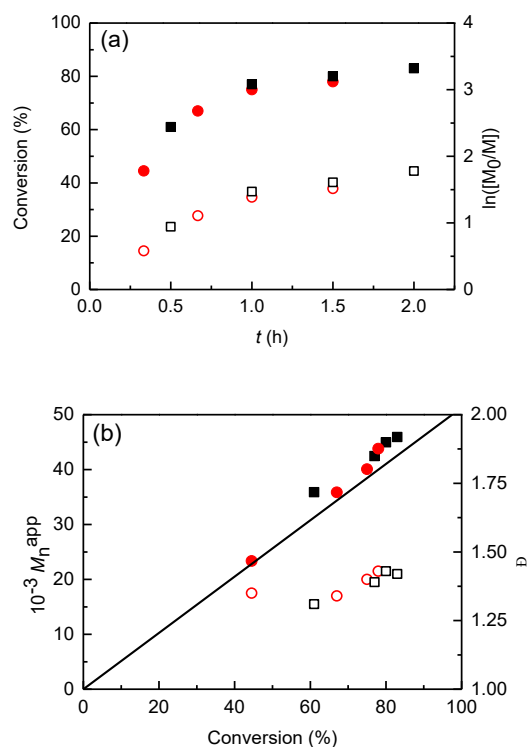


Figure 7.8. a) Kinetic plots and b) evolution of M_n and D of *e*ATRP of 10% (v/v) [MIm][Meth] in H₂O + 0.1 M NaCl, catalyzed by $[\text{Cu}^{\text{II}}\text{TPMA}]^{2+}$ at $E_{\text{app}} = E_{\text{pc}}$ (squares) or $E_{\text{app}} = E_{\text{pc}} + 0.06$ V (circles) at $T = 25$ °C and pH = 1. Empty symbols refer to the right ordinate in the figures.

Raising the temperature was detrimental: at 50 °C, the reaction was uncontrolled and much faster than at 25 °C, stopping just after 15 min with 47% conversion (Figure 7.9). A possible rationalization of the effect of T may be that at 50 °C the rate of intramolecular cyclization was enhanced more than the polymerization rate. Nevertheless, when the reaction was repeated at 0 °C, the overall rate decreased significantly but control over molecular remained essentially unaffected.

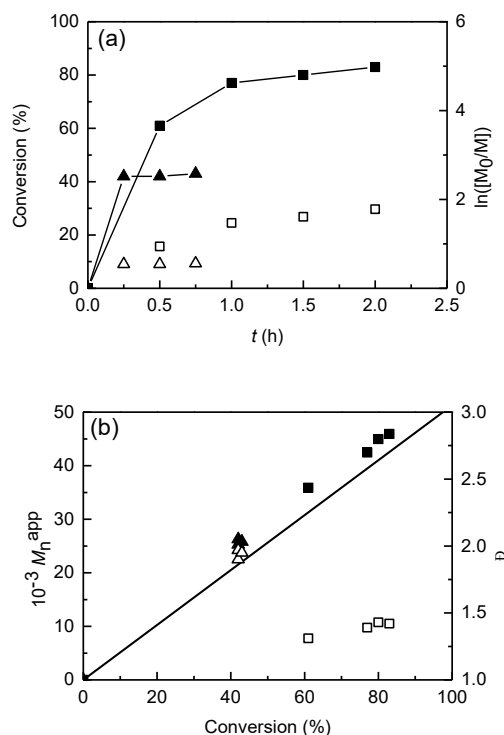


Figure 7.9. a) Kinetic plots and b) evolution of M_n and D of eATRP of 10% (v/v) [MIm][Meth] in $H_2O + 0.1 M NaCl$, catalyzed by $[Cu^{II}TPMA]^{2+}$ at $E_{app} = E_{pc}$, at pH = 1 and $T = 25$ °C (■) or at $T = 50$ °C (▲). Empty symbols refer to the right ordinate in the figures.

7.4.4 Effect of targeted degree of polymerization (DP)

To modify DP, eATRP of 10% (v/v) [MIm][Meth] was carried out at different initiator concentrations, from 2 mM down to 0.5 mM. The selected experimental conditions (Table 7.5) allowed to prepare polymers with tunable and high M_n . Figure 7.10 shows that molecular weights increased linearly with conversion and the final M_n closely matched the theoretical value (with $D \leq 1.5$). [MIm][Meth] was polymerized from DP 305 to 1220, affording PILs of molecular weight from 10^4 to $\sim 10^5$ (Table 7.5).

Table 7.5. *e*ATRP of 10% (v/v) [MIm][Meth] in water targeting different DPs at pH = 1 and $T = 25\text{ }^{\circ}\text{C}$.^a

| Entry | C_{DCPA} (mM) | t (h) | DP | Conv. (%) | M_n^{app} | M_n^{th} | \bar{D} | k_{app} | Q (C) | I_{eff} |
|-------|---------------------------|------------|------|--------------|--------------------|-------------------|-----------|------------------|------------|------------------|
| 1 | 2 | 2 | 305 | 83 | 45900 | 44000 | 1.42 | 1.06 | 3.36 | 0.96 |
| 2 | 1 | 2 | 610 | 60 | 59800 | 61400 | 1.40 | 0.52 | 2.26 | 1.03 |
| 3 | 0.5 | 2 | 1220 | 34 | 85600 | 69800 | 1.31 | 0.25 | 1.55 | 0.82 |

^apH was adjusted by addition of HClO₄; NaCl was added to have a constant total 0.3 M C_{Cl} . Conditions: $C_{\text{M}}:C_{\text{Cu}(\text{OTf})_2}:C_{\text{TPMA}} = 63:0.1:0.4$. $C_{\text{Cu}} = 10^{-3}$ M. $V_{\text{total}} = 10$ mL.

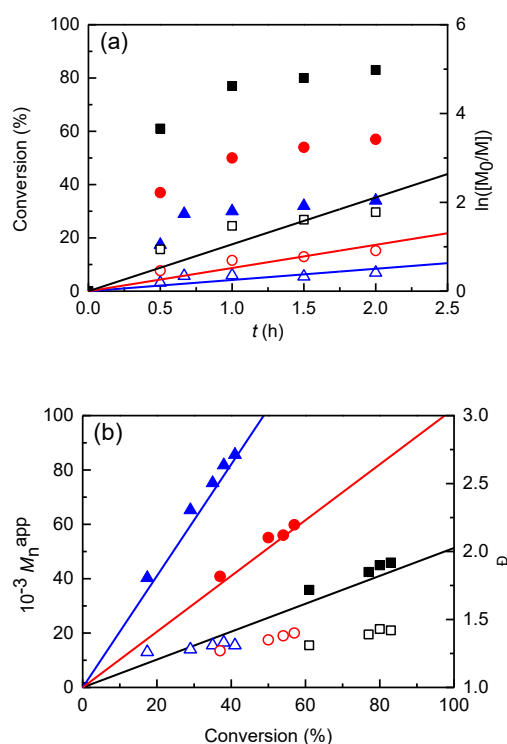


Figure 7.10. a) Kinetic plots and b) evolution of M_n and \bar{D} of *e*ATRP of 10% (v/v) [MIm][Meth] in H₂O + 0.1 M NaCl, catalyzed by $[\text{Cu}^{\text{II}}\text{TPMA}]^{2+}$ at DP = 305 (■), DP = 610 (●) or DP = 1220 (▲) at $T = 25\text{ }^{\circ}\text{C}$. Empty symbols refer to the right ordinate in the figures.

7.4.5 Effect of monomer amount

A synthesis with high monomer loading is interesting because a high amount of polymer can be produced by a single batch, which helps to reduce the cost of PIL production, especially the high cost of the ligand, used in a four-fold excess. *e*ATRPs were performed by increasing [MIm][Meth] from 10% to 25% and 50% (v/v). To maintain DP at 305, the concentration of the initiator DCPA was appropriately changed. The results are summarized in Table 7.6. Overall, increasing

monomer loading yielded virtually the same results of *e*ATRP with 10% (v/v) [MIm][Meth], in terms of conversion, molecular weight and dispersity, but the quantity of produced polymer was up to 5 times higher.

Table 7.6. *e*ATRP of [MIm][Meth] in water at different monomer concentrations, at pH 1 and $T = 25\text{ }^{\circ}\text{C}$.^a

| Entry | M (%) v/v) | t (h) | Conv. (%) | M_n^{app} | M_n^{th} | \mathcal{D} | k_{app} | Q (C) | I_{eff} |
|-------|---------------|------------|--------------|--------------------|-------------------|---------------|------------------|------------|------------------|
| 1 | 10 | 2 | 83 | 45900 | 44000 | 1.42 | 1.06 | 3.36 | 0.96 |
| 2 | 25 | 1.5 | 91 | 48900 | 46700 | 1.44 | 1.71 | 4.23 | 0.96 |
| 3 | 50 | 1.5 | 81 | 43200 | 41500 | 1.45 | 1.16 | 3.29 | 0.96 |

^apH was adjusted by addition of HClO₄; NaCl was added to have a constant total 0.3 M C_{Cl}. Conditions: C_M:C_{D CPA}:C_{Cu(OTf)₂}:C_{TPMA} = x:y:0.1:0.4, where x = 63, 157, 315; y = 0.2, 0.5, 1. C_{Cu} = 10⁻³ M. V_{total} = 10 mL.

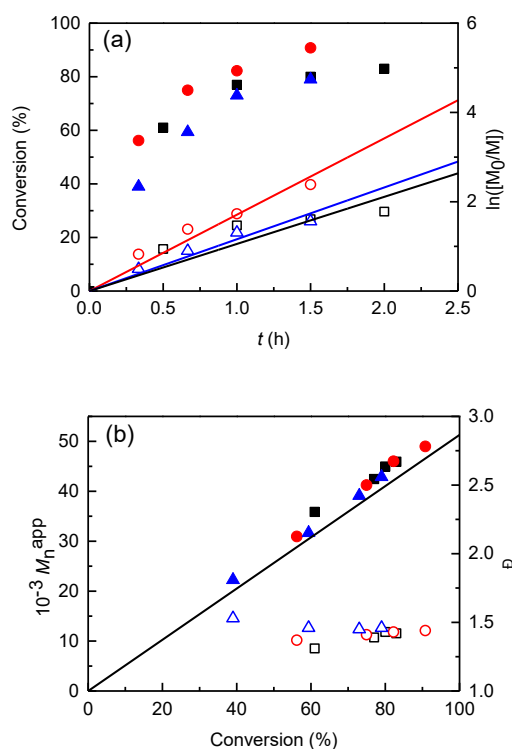


Figure 7.11. a) Kinetic plots and b) evolution of M_n and \mathcal{D} of *e*ATRP of [MIm][Meth] in H₂O + 0.1 M NaCl, catalyzed by [Cu^{II}TPMA]²⁺ at C_M = 10 vol% (■), 25 vol% (●) or 50 vol% (▲) at $T = 25\text{ }^{\circ}\text{C}$. Empty symbols refer to the right ordinate in the figures.

7.5 Electrochemically mediated ATRP of other ILMs

The successful ATRP of methylimidazolium methacrylate prompted the investigation of other ILMs. It was chosen to keep constant the vinylic functionality

(methacrylic) and change the cation, to study how its structure affects the polymerization. Imidazole, triethylamine, caffeine and vitamin B3 were chosen as sources of cation, affording imidazolium methacrylate [Imi][Meth], triethylammonium methacrylate [TEA][Meth], nicotinium acid methacrylate [B3][Meth] and caffeinium methacrylate [Caff][Meth]. Nevertheless, it was found that the latter two were ionic solids rather than liquids at neutral pH. They become liquid only at pH = 1. All polymerizations were carried out with the optimized conditions found for [MIm][Meth].

Table 7.6. *e*ATRP of 10% (v/v) ILMs in water at pH = 1, $E_{app} = E_{pc}$ and $T = 25$ °C.^a

| Entry | Cation | <i>t</i> (h) | Conv. (%) | M_n^{app} | M_n^{th} | \bar{D} | k_{app} | Q (C) | I_{eff} |
|-------|---------|-----------------|-----------------|-------------|------------|-----------|-----------|------------|-----------|
| 1 | MIm | 2 | 82 | 45900 | 42100 | 1.42 | 1.05 | 3.36 | 0.92 |
| 2 | Imi | 1.5 | 87 | 42400 | 40900 | 1.44 | 1.41 | 2.64 | 0.96 |
| 3 | TEA | 2 | 80 | 42900 | 45700 | 1.42 | 1.03 | 2.83 | 1.07 |
| 4 | Caff | 0.3 | 15 ^b | 14400 | 12800 | 1.23 | 0.49 | 0.70 | 0.89 |
| 5 | L-Val | 2 | 80 | 48200 | 49600 | 1.34 | 0.88 | 1.81 | 1.03 |
| 6 | Vit. B3 | 2 | 70 | 45600 | 46700 | 1.44 | 0.78 | 2.26 | 1.02 |

^apH was adjusted by addition of HClO₄; NaCl was added to have a constant total 0.3 M C_{Cl}. Conditions: C_M:C_{RX}:C_{Cu(OTf)₂}:C_{TPMA} = 63:0.2:0.1:0.4. C_{Cu} = 10⁻³ M. RX = DCPA, V_{total} = 10 mL.

^bThe polymer precipitated.

All PILs were obtained with low dispersion and high conversion in limited time, except for poly(caffeinium methacrylate), which precipitated at low monomer conversion (Table 7.6, entry 4). It is noteworthy to mention that despite the low conversion, *e*ATRP of caffeinium methacrylate was well-controlled yielding a polymer with very low dispersity.

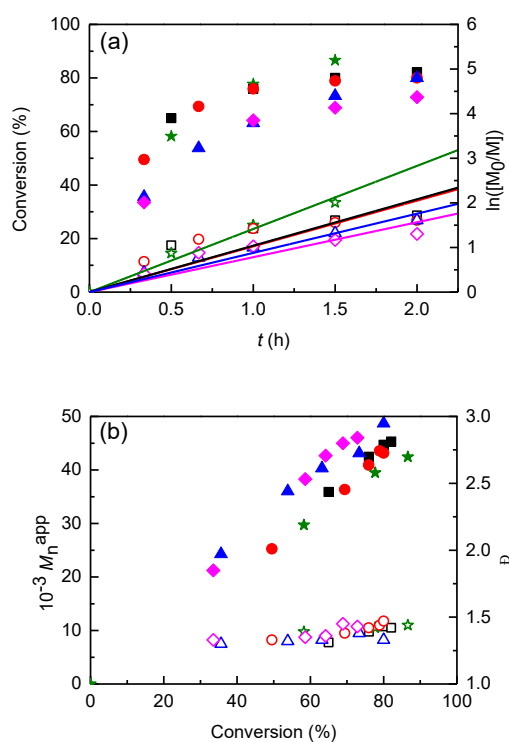


Figure 7.12. a) Kinetic plots and b) evolution of M_n and D of *e*ATRP of 10% (v/v) [Cat][Meth] (Cat = cation) in $H_2O + 0.1$ M NaCl, catalyzed by $[Cu^{II}TPMA]^{2+}$ at $T = 25$ °C and pH = 1. Symbols: Imi (★), MIm (■), TEA (●), L-Val (▲), B3 (◆). Empty symbols refer to the right ordinate in the figures.

7.6 SARA ATRP of methacrylate-based ILMs

With the aim of testing a different ATRP method, a series of experiments was conducted by (re)generating the active Cu^I complex through comproportionation, in the presence of a Cu^0 wire (SARA ATRP). Cu^0 was both a reducing agent of Cu^{II} and a supplemental activator of the C-X bond.³² SARA ATRP setup is simpler than *e*ATRP, which requires electrochemical instrumentation. The presence of a high load of halide ions and the higher reduction potential of the catalyst favor the fast comproportionation of Cu^0 and Cu^{II} species. SARA ATRP was triggered for a series of ILMs:

Table 7.7. SARA ATRP of 10% (v/v) ILMs in water at pH = 1, $T = 25\text{ }^{\circ}\text{C}$.^a

| Entry | Cation | t (h) | Conv. (%) | M_n^{th} | M_n^{app} | \bar{D} | k_{app} | I_{eff} |
|-------|---------|---------|-----------------|-------------------|--------------------|-----------|------------------|------------------|
| 1 | MIm | 2 | 78 | 43600 | 42100 | 1.42 | 0.88 | 0.97 |
| 2 | Imi | 2 | 81 | 38100 | 37300 | 1.52 | 0.84 | 0.98 |
| 3 | TEA | 1.5 | 88 | 50300 | 37700 | 1.38 | 0.52 | 0.75 |
| 4 | Caff | 0.3 | 13 ^b | 10300 | 10800 | 1.24 | 0.46 | 1.05 |
| 5 | Vit. B3 | 2 | 56 | 38300 | 32300 | 1.50 | 0.44 | 0.84 |

^apH was adjusted by addition of HClO₄; NaCl was added to have a constant total 0.3 M C_{Cl}. Conditions: $C_M:C_{RX}:C_{Cu(OTf)_2}:C_{TPMA} = 305:0.2:0.1:0.4$. $C_{Cu} = 10^{-3}$ M; RX = DCPA; 5 cm Cu wire ($d = 1$ mm). Total $V = 10$ mL. ^bPolymer precipitation.

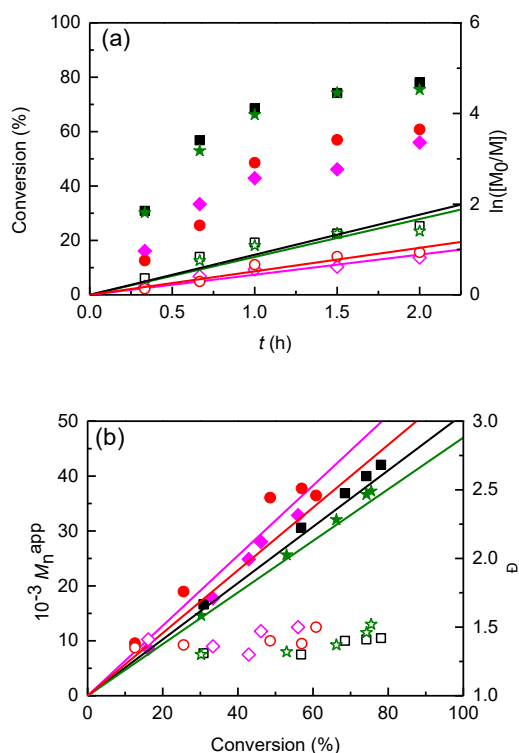


Figure 7.13. a) Kinetic plots and b) evolution of M_n and \bar{D} of eATRP of 10% [Cat][Meth] (v/v) (Cat = cation) in H₂O + 0.1 M NaCl, catalyzed by [Cu^{II}TPMA]²⁺ at $T = 25\text{ }^{\circ}\text{C}$. Symbols for cations: Imi (★), MIm (■), TEA (●), B3 (◆). Empty symbols refer to the right ordinate in the figures.

A copper wire (5 cm, $d = 1$ mm) could promote a fast and sufficiently controlled ATRP of 10% (v/v) ILMs in water for all four monomers (Table 7.7). Good levels of control over molecular-weight distributions ($\bar{D} \leq 1.5$) were observed. SARA ATRPs were slower than the corresponding eATRPs but reached moderate-to-high conversions in ~ 2 h, except in the case of [Caff][Meth] for limited polymer solubility. Agreement between experimental and theoretical M_n values was

satisfactory. This result proved that synthesis of PILs in aqueous conditions is flexible and versatile because similar successful results were obtained using two different low-ppm polymerization methods (*e*ATRP and SARA ATRP). Examples of MW evolution are shown in Figure 7.14:

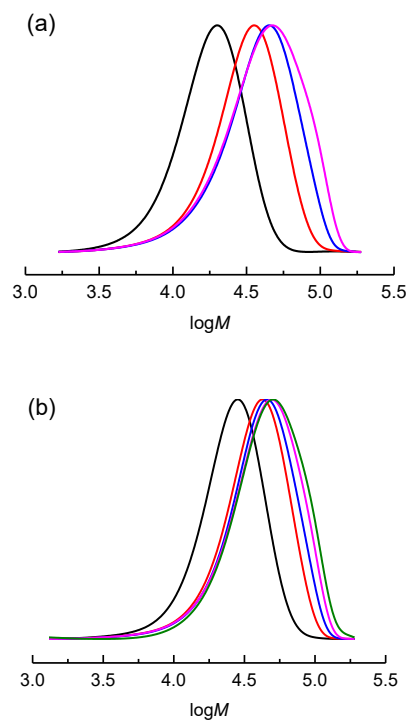


Figure 7.14. MW distribution recorded during SARA ATRP of 10% (v/v) a) [MIm][Meth] and b) [B3][Meth], catalyzed by $[\text{Cu}^{\text{II}}\text{TPMA}]^{2+}$ at $T = 25\text{ }^{\circ}\text{C}$, at $\text{pH} = 1$. Cu^0 wire length = 5 cm.

7.8 *e*ATRP of polyanionic ionic liquid monomers

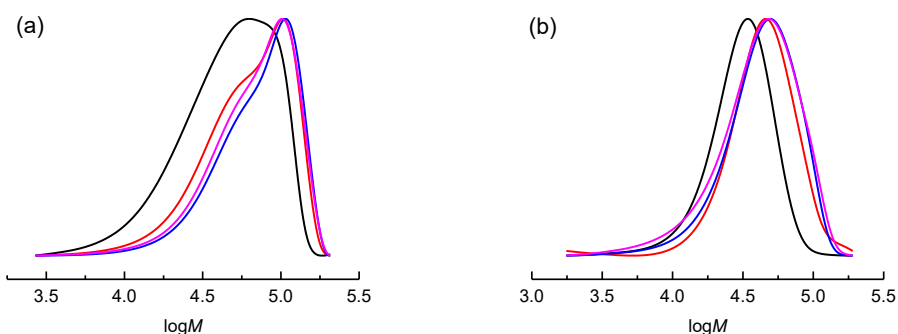
Polyanionic ionic liquid monomers can further broaden the spectrum of polymerizable monomers via ATRP. These are composed of one cation and at least two anions. Simple polyamines such as ethylenediamine (en) and tris(2-aminoethyl)amine (TREN) were neutralized completely with methacrylic acid. The polymerizations were carried out in the same conditions of [MIm][Meth] (Table 7.9).

Table 7.9. *e*ATRP of 10% (v/v) [Cat][Meth]_n (n = 2 or 4) in water at pH = 1, $E_{app} = E_{pc}$ and $T = 25$ °C.^a

| Entry | Cation | <i>t</i> (h) | Conv. (%) | M_n^{app} | M_n^{th} | \bar{D} | k_{app} | Q (C) | I_{eff} |
|-------|-----------------------------------|-----------------|--------------|-------------|------------|-----------|-----------|------------|-----------|
| 1 | H ₂ en ²⁺ | 2 | 67 | 75900 | 94900 | 1.29 | 0.55 | 2.89 | 1.25 |
| 2 | H ₄ TREN ⁴⁺ | 1.3 | 48 | 41200 | 70300 | 1.51 | 0.49 | 2.60 | 1.71 |

^apH was adjusted by addition of HClO₄; NaCl was added to have a constant total 0.3 M C_{Cl}. Conditions: C_M:C_{RX}:C_{Cu(OTf)₂}:C_{TPMA} = 305:2:0.1:0.4; RX = DCPA; C_{Cu} = 10⁻³ M. Total V = 10 mL.

*e*ATRP of these polyamine-based ILMs afforded well-defined complex PILs with dispersion as low as 1.29 for H₂en²⁺ cation. However, a strong deviation of apparent MW obtained by GPC analysis from the theoretical values was observed, suggesting that PMAA standards are not suitable for these polymers due to the sensibly different hydrodynamic volumes.

**Figure 7.15.** MW distribution recorded during *e*ATRP of 10% (v/v) a) [H₂en²⁺][Meth]₂ and b) [H₄TREN⁴⁺][Meth]₄, catalyzed by [Cu^{II}TPMA]²⁺ at $T = 25$ °C, pH = 1 and $E_{app} = E_{pc}$.

7.10 Conclusions

Broadening the spectrum of monomers polymerizable *via* ATRP is a key aspect of current research, with the goal of making ATRP a universal polymerization tool. The catalytic system composed of the complex Cu/TPMA and the initiator HEBiB was investigated in aqueous methylimidazolium methacrylate [MIm][Meth]. Simple electrochemical methods (cyclic voltammetry) confirmed the stability of both the copper complex and initiator in the presence of both ILM and PIL. Different approaches allowed to increase conversion and improve control over PIL growth: (i) working in acid conditions at pH = 1, (ii) using Cl as chain-end halogen,

(iii) using high Cl⁻ content, and (iv) increasing the polymerization rate. ILMs were polymerized by *e*ATRP or SARA ATRP with relatively low copper concentration (<250 ppm), with adequate control over molecular weight dispersity ($D < 1.5$) and M_n in very good agreement with theoretical values. Both *e*ATRP and SARA ATRP, with inexpensive and non-toxic reagents (NaCl and water), could efficiently control the reaction, which proceeded with fast kinetics at ambient temperature (>80% conversion in < 3 h). These processes led to the successful synthesis of a new unexplored class of polyelectrolytes of narrow dispersion and controlled molecular weight.

References

1. Welton, T., Room-Temperature Ionic Liquids. Solvents for Synthesis and Catalysis. *Chemical Reviews* **1999**, *99*, 2071-2084.
2. Lu, J.; Yan, F.; Texter, J., Advanced applications of ionic liquids in polymer science. *Progress in Polymerization Science* **2009**, *34*, 431-448.
3. MacFarlane, D. R.; Forsyth, M.; Howlett, P. C.; Kar, M.; Passerini, S.; Pringle, J. M.; Ohno, H.; Watanabe, M.; Yan, F.; Zheng, W.; Zhang, S.; Zhang, J., Ionic liquids and their solid-state analogues as materials for energy generation and storage. *Nature Reviews Materials* **2016**, *1*, 15005.
4. Green, O.; Grubjesic, S.; Lee, S.; Firestone, M. A., The Design of Polymeric Ionic Liquids for the Preparation of Functional Materials. *Polymer Reviews* **2009**, *49*, 339-360.
5. Ricks-Laskoski, H. L.; Snow, A. W., Synthesis and Electric Field Actuation of an Ionic Liquid Polymer. *Journal of the American Chemical Society* **2006**, *128*, 12402-12403.
6. Prescher, S.; Polzer, F.; Yang, Y.; Siebenbürger, M.; Ballauff, M.; Yuan, J., Polyelectrolyte as Solvent and Reaction Medium. *Journal of the American Chemical Society* **2014**, *136*, 12-15.
7. He, H.; Chung, H.; Roth, E.; Luebke, D.; Hopkinson, D.; Nulwala, H.; Matyjaszewski, K., Low glass transition temperature poly(ionic liquid) prepared from a new quaternary ammonium cationic monomer. *Polymer Advanced Technology* **2015**, *26*, 823-828.
8. Masahiro, Y.; Hiroyuki, O., Molecular Brush Having Molten Salt Domain for Fast Ion Conduction. *Chemical Letters* **1999**, *28*, 889-890.
9. Hirao, M.; Ito, K.; Ohno, H., Preparation and polymerization of new organic molten salts; N-alkylimidazolium salt derivatives. *Electrochimica Acta* **2000**, *45*, 1291-1294.
10. Choi, U. H.; Mittal, A.; Price, T. L.; Gibson, H. W.; Runt, J.; Colby, R. H., Polymerized Ionic Liquids with Enhanced Static Dielectric Constants. *Macromolecules* **2013**, *46*, 1175-1186.

11. João, K. G.; Tomé, L. C.; Isik, M.; Mecerreyes, D.; Marrucho, I. M., Poly(ionic liquid)s as phase splitting promoters in aqueous biphasic systems. *PCCP* **2015**, *17*, 27462-27472.
12. Mele, A.; Tran, C. D.; De Paoli Lacerda, S. H., The Structure of a Room-Temperature Ionic Liquid with and without Trace Amounts of Water: The Role of C-H...O and C-H...F Interactions in 1-*n*-Butyl-3-Methylimidazolium Tetrafluoroborate. *Angewandte Chemie* **2003**, *115*, 4500-4502.
13. Shaplov, A. S.; Ponkratov, D. O.; Vygodskii, Y. S., Poly(ionic liquid)s: Synthesis, properties, and application. *Polymer Science Series B* **2016**, *58*, 73-142.
14. Marcilla, R.; Blazquez, J. A.; Fernandez, R.; Grande, H.; Pomposo, J. A.; Mecerreyes, D., Synthesis of Novel Polycations Using the Chemistry of Ionic Liquids. *Macromolecular Chemistry and Physics* **2005**, *206*, 299-304.
15. Ye, Y.; Elabd, Y. A., Relative Chemical Stability of Imidazolium-Based Alkaline Anion Exchange Polymerized Ionic Liquids. *Macromolecules* **2011**, *44*, 8494-8503.
16. Appetecchi, G. B.; Kim, G. T.; Montanino, M.; Carewska, M.; Marcilla, R.; Mecerreyes, D.; De Meazza, I., Ternary polymer electrolytes containing pyrrolidinium-based polymeric ionic liquids for lithium batteries. *Journal of Power Sources* **2010**, *195*, 3668-3675.
17. Zhou, Z.-B.; Matsumoto, H.; Tatsumi, K., Cyclic Quaternary Ammonium Ionic Liquids with Perfluoroalkyltrifluoroborates: Synthesis, Characterization, and Properties. *Chemistry – A European Journal* **2006**, *12*, 2196-2212.
18. Tokuda, M.; Thickett, S. C.; Minami, H.; Zetterlund, P. B., Preparation of Polymer Particles Containing Reduced Graphene Oxide Nanosheets Using Ionic Liquid Monomer. *Macromolecules* **2016**, *49*, 1222-1228.
19. Chen, Z.; Yan, F.; Qiu, L.; Lu, J.; Zhou, Y.; Chen, J.; Tang, Y.; Texter, J., Sustainable Polymerizations in Recoverable Microemulsions. *Langmuir* **2010**, *26*, 3803-3806.
20. Nakamura, R.; Tokuda, M.; Suzuki, T.; Minami, H., Preparation of Poly(ionic liquid) Hollow Particles with Switchable Permeability. *Langmuir* **2016**, *32*, 2331-2337.
21. Yuan, J.; Antonietti, M., Poly(ionic liquid) Latexes Prepared by Dispersion Polymerization of Ionic Liquid Monomers. *Macromolecules* **2011**, *44*, 744-750.
22. Wiesenauer, E. F.; Edwards, J. P.; Scalfani, V. F.; Bailey, T. S.; Gin, D. L., Synthesis and Ordered Phase Separation of Imidazolium-Based Alkyl-Ionic Diblock Copolymers Made via ROMP. *Macromolecules* **2011**, *44*, 5075-5078.
23. Texter, J.; Vasantha, V. A.; Crombez, R.; Maniglia, R.; Slater, L.; Mourey, T., Triblock Copolymer Based on Poly(propylene oxide) and Poly(1-[11-acryloylundecyl]-3-methyl-imidazolium bromide). *Macromolecular Rapid Communications* **2012**, *33*, 69-74.
24. He, H.; Luebke, D.; Nulwala, H.; Matyjaszewski, K., Synthesis of Poly(ionic liquid)s by Atom Transfer Radical Polymerization with ppm of Cu Catalyst. *Macromolecules* **2014**, *47*, 6601-6609.
25. von Werne, T.; Patten, T. E., Preparation of Structurally Well-Defined Polymer-Nanoparticle Hybrids with Controlled/Living Radical Polymerizations. *Journal of the American Chemical Society* **1999**, *121*, 7409-7410.

26. Wang, P.; Zhou, Y.-N.; Luo, J.-S.; Luo, Z.-H., Poly(ionic liquid)s-based nanocomposite polyelectrolytes with tunable ionic conductivity prepared via SI-ATRP. *Polymer Chemistry* **2014**, *5*, 882-891.
27. Zhang, B.; Yan, X.; Alcouffe, P.; Charlot, A.; Fleury, E.; Bernard, J., Aqueous RAFT Polymerization of Imidazolium-Type Ionic Liquid Monomers: En Route to Poly(ionic liquid)-Based Nanoparticles through RAFT Polymerization-Induced Self-Assembly. *ACS Macro Letters* **2015**, *4*, 1008-1011.
28. Chen, Q.; Peng, C.; Xie, H.; Zhao, Z. k.; Bao, M., Cellulosic poly(ionic liquid)s: synthesis, characterization and application in the cycloaddition of CO₂ to epoxides. *RSC Advances* **2015**, *5*, 44598-44603.
29. Obadia, M. M.; Colliat-Dangus, G.; Debuigne, A.; Serghei, A.; Detrembleur, C.; Drockenmuller, E., Poly(vinyl ester 1,2,3-triazolium)s: a new member of the poly(ionic liquid)s family. *Chemical Communication* **2015**, *51*, 3332-3335.
30. Fantin, M.; Isse, A. A.; Gennaro, A.; Matyjaszewski, K., Understanding the Fundamentals of Aqueous ATRP and Defining Conditions for Better Control. *Macromolecules* **2015**, *48*, 6862-6875.
31. Fantin, M.; Isse, A. A.; Venzo, A.; Gennaro, A.; Matyjaszewski, K., Atom Transfer Radical Polymerization of Methacrylic Acid: A Won Challenge. *Journal of the American Chemical Society* **2016**, *138*, 7216-7219.
32. Konkolewicz, D.; Krys, P.; Góis, J. R.; Mendonça, P. V.; Zhong, M.; Wang, Y.; Gennaro, A.; Isse, A. A.; Fantin, M.; Matyjaszewski, K., Aqueous RDRP in the Presence of Cu⁰: The Exceptional Activity of Cu^I Confirms the SARA ATRP Mechanism. *Macromolecules* **2014**, *47*, 560-570.

Chapter 8

Electrochemically mediated Atom Transfer Radical Polymerization in a stainless-steel reactor

8.1 Introduction

Among controlled radical polymerization techniques, Atom Transfer Radical Polymerization (ATRP) so far is probably the most used method, widely exploited to synthesize polymers with precise architectures, predetermined molecular weights (MWs) and low dispersity ($D \leq 1.3$).¹

*e*ATRP showed over the years several very interesting features, including: a) superior ability of tuning reaction rate, compared to other low ppm catalyst techniques, b) low charge consumption, c) the possibility of using undivided cells with sacrificial anodes, d) use of inexpensive, non-noble metals as cathodic materials (and anodic materials in divided cells), e) the possibility of working in galvanostatic mode, and f) absence of harmful by-products.² Electrochemistry also provides a very simple tool to investigate the system before and after the polymerization, *e.g.*, by cyclic voltammetry.

Hence, *e*ATRP is probably the best low-ppm candidate for a scale-up. We focused on two recent advances: galvanostatic *e*ATRP and the simplified setup with a sacrificial anode. Galvanostatic electrolysis is a simple, elegant and versatile solution to avoid the use of a three-electrode system with a reference electrode. A substantial cost reduction can be achieved if galvanostatic *e*ATRP is implemented with inexpensive metals as electrode materials, both cathode and anode. Use of sacrificial anodes is another simplification that avoids separation of electrolysis compartments and is certainly convenient in a large-scale applications.³ We envisaged the possibility to merge the cathode and the vessel where the reaction is carried out, with a simple but outstanding improvement of the overall *e*ATRP configuration, making it versatile and more user-friendly.

Therefore, a homemade SS304 reactor was used to test the possibility of triggering *e*ATRP, using the scaffold of the reactor as cathode. This further

simplifies the overall equipment and becomes a crucial step towards the scale-up of *e*ATRP.

8.2 Preliminary electrochemistry and *e*ATRP

Before testing the SS304 reactor, a screening of possible catalytic systems was performed, considering also the cost of reagents and ligand for a future extension to higher production (> 100 g of polymer).

A variety of catalysts, monomers and solvents may be used, but for simplicity we focused on *e*ATRP of MA catalyzed by $[\text{Cu}^{\text{II}}\text{TPMA}]^{2+}$, $[\text{Cu}^{\text{II}}\text{TREN}]^{2+}$ and $[\text{Cu}^{\text{II}}\text{Me}_6\text{TREN}]^{2+}$ in DMSO initiated by EBiB. Yet, to the best of our knowledge, no previous electrochemical reports were published regarding the voltammetric behavior of $[\text{Cu}^{\text{II}}\text{TREN}]^{2+}$. Electrochemical characterization was carried out to gather information about the catalysts in DMSO (Figure 8.1).

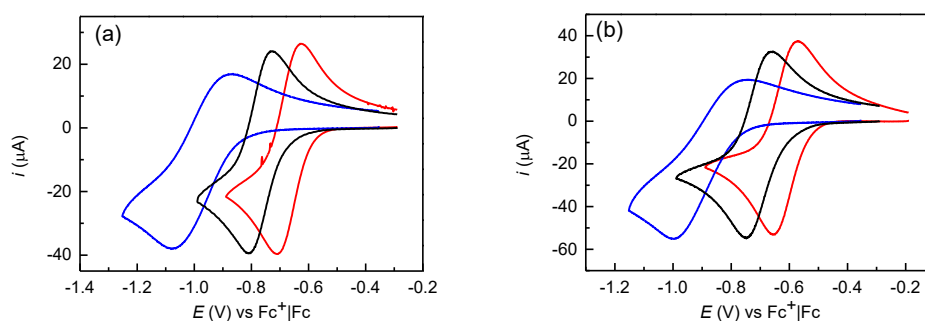


Figure 8.1. Cyclic voltammetry of $[\text{BrCu}^{\text{II}}\text{TPMA}]^+$ (—), $[\text{BrCu}^{\text{II}}\text{TREN}]^+$ (—), and $[\text{BrCu}^{\text{II}}\text{Me}_6\text{TREN}]^+$ (—) in a) pure DMSO + 0.1 M Et_4NBF_4 or b) DMSO + 50% (v/v) MA + 0.1 M Et_4NBF_4 , recorded on GC electrode at 0.2 V s^{-1} .

The voltammetric analysis shows a quasi-reversible electron transfer ascribed to the $[\text{BrCu}^{\text{II}}\text{L}]^+|[\text{BrCu}^{\text{I}}\text{L}]^+$ couple in both DMSO and DMSO + 50% (v/v) MA. Focusing on TREN, detailed electrochemical analysis was performed in DMSO (Figures 8.2 and 8.3).

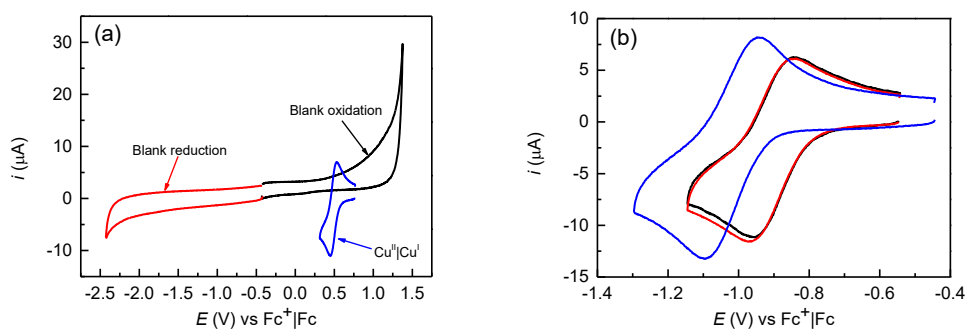


Figure 8.2. a) Cyclic voltammetry of pure DMSO + 0.1 M Et_4NBF_4 (— ox, — red) and in presence of 10^{-3} M $\text{Cu}(\text{OTf})_2$ (—); b) Cyclic voltammetry of $[\text{Cu}^{\text{II}}\text{TREN}]^{2+}$ (—), $[\text{BrCu}^{\text{II}}\text{TREN}]^+$ (—) and $[\text{ClCu}^{\text{II}}\text{TREN}]^+$ (—) in DMSO, recorded at 25 °C on a GC electrode at 0.2 V s^{-1} .

Addition of EBiB in a 10-fold excess with respect to the catalyst drastically changed the voltammetric response: the cathodic peak increased, while the anodic one disappeared. On the electrode surface, $[\text{BrCu}^{\text{II}}\text{TREN}]^+$ was reduced to $[\text{BrCu}^{\text{I}}\text{TREN}]$, which partially dissociated generating the active form of the catalyst, $[\text{Cu}^{\text{I}}\text{TREN}]^+$. The latter reacted with the polymerization initiator, forming an alkyl radical and the oxidized catalyst species $[\text{BrCu}^{\text{II}}\text{TREN}]^+$, which diffuses back to the electrode to be reduced again to $[\text{BrCu}^{\text{I}}\text{TREN}]$. Consequently, the cathodic peak became catalytic while the anodic one decreased because of the disappearance of $[\text{BrCu}^{\text{I}}\text{TREN}]^+$ via reaction with RX.

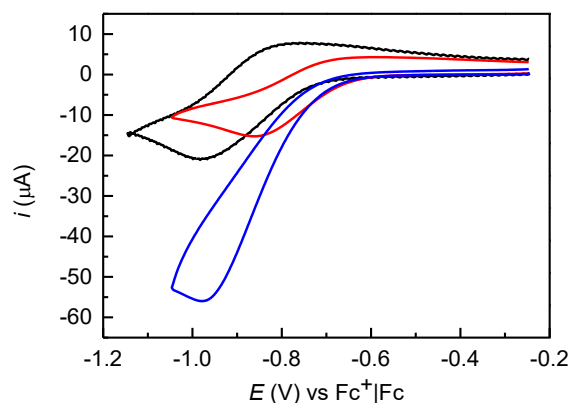


Figure 8.3. Cyclic voltammetry of $[\text{BrCu}^{\text{II}}\text{TREN}]^+$ in DMSO + 0.1 M Et_4NBF_4 before (—) and after addition of 50 vol% MA (—) and after further addition of 10^{-2} M EBiB (—), recorded at 50 °C on a GC electrode at 0.2 V s^{-1} .

Table 8.1 resumes the redox properties of Cu/TREN binary and ternary complexes in DMSO at $T = 25 \text{ }^\circ\text{C}$.

Table 8.1. Electrochemical properties of Cu/TREN complexes in DMSO + 0.1 M Et₄NBF₄ at $T = 25$ °C.

| Cu ^{II} species | E° (V) vs. Fc ⁺ /Fc | $D \times 10^7$ (cm ² s ⁻¹) | k^0 (cm s ⁻¹) |
|--|---|---|-----------------------------|
| Cu ²⁺ | +0.492 | - | - |
| [Cu ^{II} TREN] ²⁺ | -0.900 | 7.85 | 1.66×10^{-3} |
| [BrCu ^{II} TREN] ⁺ | -0.913 | 8.61 | 1.35×10^{-3} |
| [ClCu ^{II} TREN] ⁺ | -1.018 | 10.1 | 1.02×10^{-3} |

Some precautions are needed when a sacrificial Al anode is used in Cu-catalyzed *e*ATRP. An excess of ligand must be added and in the case of TREN it is known that the ligand reacts with monomers *via* Michael reaction, forming TREN-monomer derivatives that are, however, able to form complexes with Cu.⁴ The use of an aluminum anode allows the polymerization to be carried out in a single-compartment cell (undivided cell) in which both the cathode and anode are immersed in the same reaction medium. Such a setup greatly suppresses ohmic drop due to compartment separation.³ Despite these advantages, Al³⁺ interferes with the catalyst, limiting the stability and its activity *via* competing equilibria involving copper and aluminum ions and the ligand.⁵⁻⁶ In general, when Al anode is used, the quantity of ligand must be high enough to ensure full complexation of both Cu catalyst and all Al³⁺ ions released during the electrolysis. *e*ATRP of MA was triggered with all selected catalysts, in the presence of Al sacrificial anode. The results are reported in Table 8.2.

Table 8.2. *e*ATRP of 50% (v/v) MA in DMSO catalyzed by Cu complexes with amine ligands (L) at $T = 50\text{ }^{\circ}\text{C}$.^a

| Ligand | t (h) | Conv. (%) | M_n^{th} | M_n^{app} | \bar{D} | I_{eff} | Q (C) |
|----------------------|---------|-----------|-------------------|--------------------|-----------|------------------|---------|
| TPMA | 4 | 95 | 45100 | 45500 | 1.12 | 0.99 | 2.88 |
| TREN | 2 | 85 | 40400 | 41000 | 1.09 | 0.99 | 1.65 |
| Me ₆ TREN | 1 | 85 | 40400 | 39700 | 1.08 | 1.02 | 1.32 |

^a. Supporting electrolyte: 0.1 M Et₄NBF₄. Conditions: $C_{\text{MA}}:C_{\text{L}}:C_{\text{Cu}}:C_{\text{EBiB}} = 552:0.2:0.1:1$. $V = 10\text{ mL}$; $C_{\text{CuBr}_2} = 10^{-3}\text{ M}$; DP = 552. Geometrical surface exposed to the solution = 6 cm². $E_{\text{app}} = E_{1/2} - 0.06\text{ V}$.

Kinetic plots and evolutions of M_n and \bar{D} with conversion are shown in Figure 8.4:

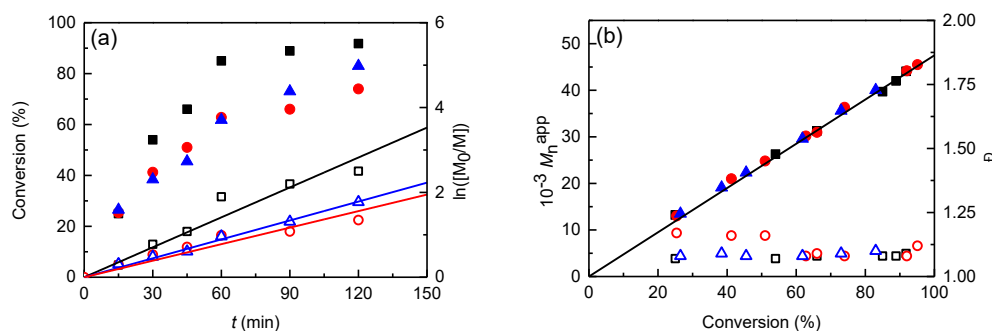


Figure 8.4. a) Kinetic plots and b) evolution of M_n and \bar{D} of *e*ATRP of 50% (v/v) MA in DMSO catalyzed by [Cu^{II}TPMA]²⁺ (●) or [Cu^{II}TREN]²⁺ (▲) or [Cu^{II}Me₆TREN]²⁺ (■) at $T = 50\text{ }^{\circ}\text{C}$. Empty symbols refer to the right ordinate in the figures.

All polymerizations reached high conversions in a short time, affording PMA-Br with very low dispersity and MWs matching closely the theoretical values.

To prove that use of excess ligand is necessary, *e*ATRP catalyzed by [Cu^{II}TREN]²⁺ was repeated without an excess of ligand. The results are reported in Table 8.3 and Figure 8.5.

Table 8.3. *e*ATRP of 50% (v/v) MA in DMSO catalyzed by $[\text{Cu}^{\text{II}}\text{TREN}]^{2+}$ at $T = 50\text{ }^{\circ}\text{C}$.^a

| Entry | TREN | t (h) | Conv. (%) | M_n^{th} | M_n^{app} | D | I_{eff} | Q (C) |
|-------|------|---------|-----------|-------------------|--------------------|------|------------------|---------|
| 1 | 1 eq | 1 | 37 | 17600 | 15900 | 1.10 | 1.11 | 1.30 |
| 2 | 2 eq | 2 | 85 | 40400 | 41000 | 1.09 | 0.99 | 1.65 |

^aSupporting electrolyte: 0.1 M Et_4NBF_4 . Conditions: $C_{\text{MA}}:C_{\text{TREN}}:C_{\text{Cu}}:C_{\text{EBiB}} = 552:x:0.1:1$. $V = 10\text{ mL}$; $x = 0.1$ (entry 1) or 0.2 (entry 2); $C_{\text{CuBr}_2} = 10^{-3}\text{ M}$; $\text{DP} = 552$. Geometrical cathode surface exposed to the solution = 22 cm^2 .

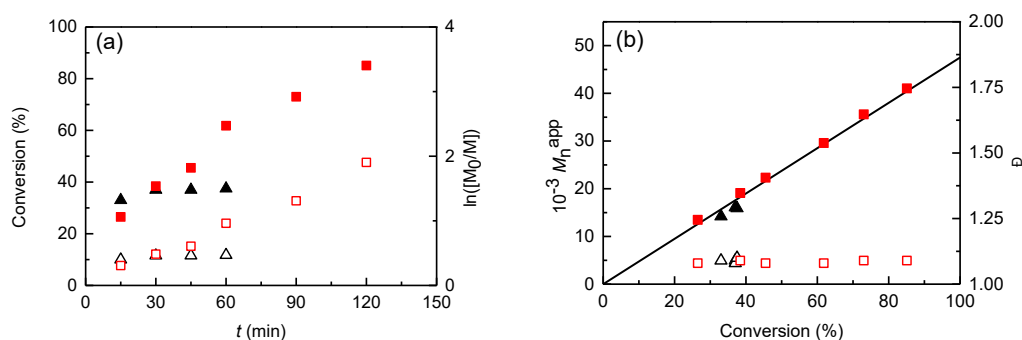
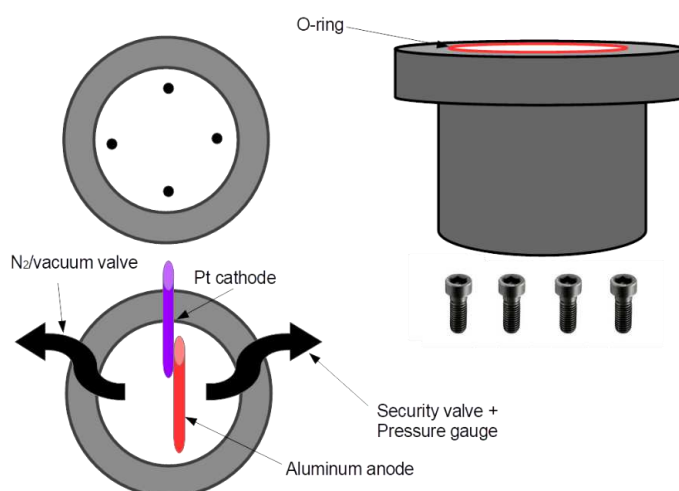


Figure 8.5. a) Kinetic plots and b) evolution of M_n and D of *e*ATRP of 50% (v/v) MA in DMSO catalyzed by $[\text{Cu}^{\text{II}}\text{TREN}]^{2+}$ at $T = 50\text{ }^{\circ}\text{C}$; $C_{\text{CuII}}:C_{\text{TREN}} = 1$ (\blacktriangle) or 2 (\blacksquare). Empty symbols refer to the right ordinate in the figures.

Catalysts based on all three ligands proved to be very efficient. Since, however, TREN is much less expensive than both Me_6TREN and TPMA, further investigations in the SS304 reactor were performed using only $[\text{Cu}^{\text{II}}\text{TREN}]^{2+}$ as catalyst.

8.3 The choice of an SS304 reactor

The use of an SS304 reactor removes completely all noble metals from the setup and physically merges the cathode and the vessel where polymerization takes place. The homemade SS304 reactor is the first electrochemical reactor for *e*ATRP and can also be considered the first step towards the scale-up of the technique. Scheme 8.1 shows the concept of the reactor:



Scheme 8.1. Schematic representation of the SS304 reactor used for *e*ATRP.

The SS304 stainless steel vessel is a reactor designed and built to host reactions with both liquid and gaseous monomers (e.g. methyl acrylate and vinyl chloride, respectively) and for high temperature polymerizations. It is divided in two parts: body and head. The body, a single piece, was obtained by a single rod of steel by working the metal at a lathe to avoid welding joints. Also, the head was obtained by sectioning the same rod with the desired specifications. A 50-mL reaction cup was lathed inside the body, where the reaction takes place. On the top of the body there is a circular rut where an O-ring of fluorinated rubber is housed. The head is furnished with two pipes: one used for degassing has an open/close valve, the other has a 0-25 bar pressure gauge and a security valve to avoid overpressure. An optional open-close valve can selectively exclude both security valve and pressure gauge. On the head there are housings for an optional platinum (or any other electronic conductor) working electrode (serving as a cathode) and an aluminum rod anode. The slot for the optional working electrode can serve also as sampling point, simply by using a silicone rubber cap. Electric and chemical insulation at the anode slot is ensured by a symmetric double joint of PEEK, reinforced by a fluorinated O-ring. Under operative conditions, the body and the head are held together by four SS304 threaded screws, positioned each other orthogonally. The stirring of the polymerization mixture is achieved by using a rare-earth octahedral magnetic stirring bar. A picture of the assembled reactor is shown Figure 8.6.



Figure 8.6. The SS304 reactor used for *e*ATRP of MA in the mechanical facility of the Department of Chemical Sciences.

8.4 Blank experiments without any applied current

Before performing *e*ATRP experiments in the reactor, we checked whether the vessel itself (SS304) could activate ATRP by dissociative electron transfer to the alkyl halide initiator or reduction of Cu^{II} to Cu^{I} , without any applied current (at open circuit).⁶ To this end, we ran blank experiments in the absence of i_{app} (Table 8.4).

Table 8.4. Blank tests of SARA ATRP of MA at $T = 50\text{ }^{\circ}\text{C}$ in DMSO in the SS304 reactor.^a

| Entry | t (h) | TREN (eq) | Conv. (%) | M_n^{th} | M_n^{app} | \bar{D} | I_{eff} |
|-------|---------|--------------|--------------|-------------------|--------------------|-----------|------------------|
| 1 | 2 | 2 | <1 | 200 | - | - | - |
| 2 | 2 | 3 | 1 | 400 | - | - | - |
| 3 | 3 | 3 | 1 | 400 | - | - | - |

^aOther experimental conditions: $C_{\text{MA}}:C_{\text{TREN}}:C_{\text{Cu}}:C_{\text{EBIB}} = 552:x:0.1:0.1$, where $x = 0.2$ (entry 1) and 0.3 (entries 2 and 3). $V = 10\text{ mL}$.

In all three attempts, negligible conversion was found. Moreover, the GPC traces did not evidence any polymer formation. This points out that the scaffold of the reactor is not chemically involved in ATRP mechanism and, therefore, it could be used as a cathode for *e*ATRP.

8.5 Effect of the electrolysis program

Six different electrolysis programs were tested. The program is the current-time steps that the galvanostat applies to the reactor. They are composed as follows:

1. Program I: 1 mA for 3600 s (single step), total charge $Q = 3.600$ C, Al^{3+} released = 12.43×10^{-6} mol;
2. Program II: 0.7 mA for 3600 s (single step), total charge $Q = 2.520$ C, Al^{3+} released = 8.71×10^{-6} mol;
3. Program III: 0.4 mA for 3600 s (single step), total charge $Q = 1.440$ C, Al^{3+} released = 4.97×10^{-6} mol;
4. Program IV: 0.15 mA for 3600 s (single step), total charge $Q = 0.540$ C, Al^{3+} released = 1.87×10^{-6} mol;
5. Program V: 0.4 mA for 30 s, 0.3 mA for 180 s, 0.25 mA for 600 s and 0.15 mA for 2790 s for a total reaction time of 3600 s (multistep), total charge $Q = 0.635$ C, Al^{3+} released = 2.22×10^{-6} mol.
6. Program VI: 0.8 mA for 30 s, 0.6 mA for 180 s, 0.5 mA for 600 s and 0.30 mA for 2790 s for a total reaction time of 3600 s (multistep), total charge $Q = 1.270$ C, Al^{3+} released = 4.44×10^{-6} mol.

Figure 8.7 visualizes the electrolysis programs:

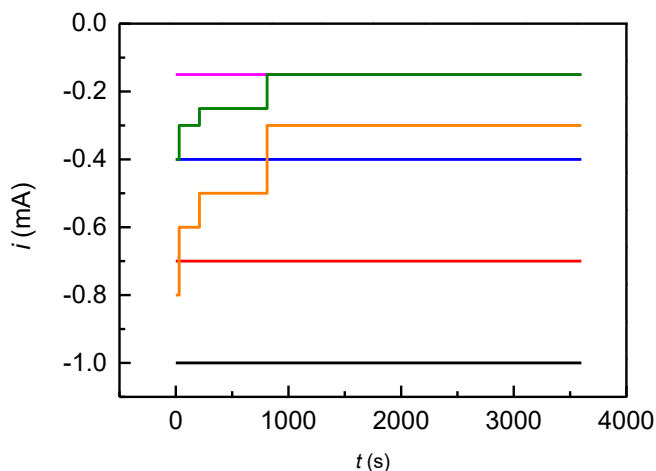


Figure 8.7. Electrolysis programs I (—), II (—), III (—), IV (—), V (—) and VI (—) applied to eATRP of methyl acrylate in DMSO at $T = 50$ °C.

According to the electrolysis programs, the concentration of TREN was maintained constant to 3 mM (Program I) or 2 mM (all others), to complex all the aluminum ions released in solution and avoid any interference, according to the charge fed to the reactor. The effect of the electrolysis program on *e*ATRP is shown in Table 8.5.

Table 8.5. *e*ATRP of 50% (v/v) MA in DMSO at $T = 50$ °C with different electrolysis programs.^a

| Entry | Program | t (h) | Conv. (%) | M_n^{th} | M_n^{app} | \bar{D} | I_{eff} | Q (C) |
|----------------|---------|---------|-----------|-------------------|--------------------|-----------|------------------|---------|
| 1 | I | 1 | 45 | 21600 | 28200 | 1.23 | 0.77 | 3.600 |
| 2 | II | 1 | 44 | 21100 | 25600 | 1.22 | 0.82 | 2.520 |
| 3 | III | 1 | 58 | 27800 | 28800 | 1.17 | 0.96 | 1.440 |
| 4 | IV | 1 | 51 | 24500 | 25300 | 1.17 | 0.97 | 0.540 |
| 5 | V | 1 | 85 | 40600 | 37400 | 1.10 | 1.09 | 0.635 |
| 6 | VI | 1 | 60 | 28600 | 29600 | 1.11 | 0.97 | 1.270 |
| 7 ^b | V | 1 | 67 | 32100 | 36000 | 1.09 | 0.89 | 0.635 |

^aSupporting electrolyte: 0.1 M Et₄NBF₄. Conditions: $C_{\text{MA}}:C_{\text{TREN}}:C_{\text{Cu}}:C_{\text{EBiB}} = 552:0.x:0.1:1$; $x = 0.3$ for Program I, $x = 0.2$ for the other programs. $V = 10$ mL; $C_{\text{CuBr}_2} = 10^{-3}$ M; DP = 552. Geometrical electrode surface exposed to the solution = 22 cm². ^b Pt cathode ($A = 6$ cm²).

The MW distributions of PMA-Br obtained at the end of each program are shown in Figure 8.8:

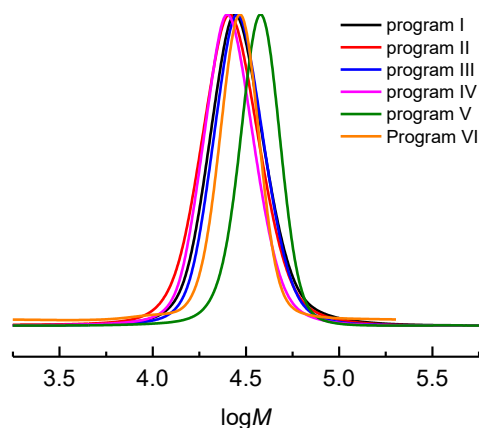


Figure 8.8. MW distribution of PMA-Br produced by galvanostatic *e*ATRP of 50% (v/v) MA in DMSO + 0.1 M Et₄NBF₄ at *T* = 50 °C.

All electrolyses with single step programs afforded polymers with $M_n < 30000$ and $D \geq 1.17$, with conversion $< 60\%$. The incomplete conversion is ascribed to the electrolysis program, which did not allow to modulate properly the Cu^{II}/Cu^I ratio at the walls of the reactor. Indeed, during galvanostatic electrolysis, this ratio changes with time, following the unavoidable drift of the potential difference required to match the applied current. If the effective potential difference becomes sensibly high, other processes may start, including the reduction of Cu^I to Cu⁰, which destroys the catalyst.

A multistep approach (program V), instead, permitted higher conversion (up to 85%) and lower dispersity ($D = 1.10$). In this case, the chosen current-time profile mimicked the evolution of current with time during a virtual potentiostatic electrolysis. Therefore, program V was maintained for all following experiments. A two-fold increase of the applied currents (program VI) did not perform as well as program V. Although the advantage of the multistep approach was maintained, the higher charge fed to the system probably triggered undesired processes that interfered with *e*ATRP and limited the conversion. A comparison between SS304 and Pt (Table 8.5, entries 5 and 7) showed marginal differences between the cathodic materials. While dispersity was almost the same, conversion was slightly lower on Pt, as seen from MW distribution (Figure 8.9). The geometrical surface area of Pt exposed to the solution was $\sim 6 \text{ cm}^2$ whereas that of SS304 was $\sim 22 \text{ cm}^2$.

The bigger area may promote a higher propagation rate as $[\text{Cu}^{\text{I}}\text{TREN}]^+$ is regenerated on a bigger surface.

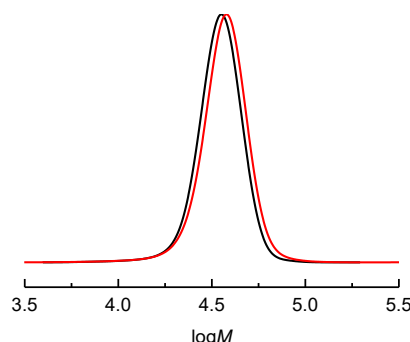


Figure 8.9. MW distribution of PMA-Br produced by galvanostatic *e*ATRP of 50% (v/v) MA in DMSO + Et_4NBF_4 at $T = 50\text{ }^\circ\text{C}$, using Pt (—) or SS304 (—) as cathode.

8.6 Effect of $[\text{Cu}^{\text{II}}\text{TREN}]^{2+}$ loadings

It is well-established in the literature that copper complexes used as catalysts in ATRP may color the polymer and, in particular, their presence in the final product is undesirable for (bio)medical applications.⁷⁻⁸ Therefore, the effect of Cu concentration on the synthesis was investigated to evaluate the minimum amount of catalyst required to obtain a controlled, efficient process. Electrolysis program V was used, and the results are shown in Table 8.6:

Table 8.6. *e*ATRP of 50% (v/v) MA in DMSO at different catalyst concentrations and $T = 50\text{ }^\circ\text{C}$.^a

| Entry | C_{Cu} (mM) | Conv. (%) | t (h) | M_n^{th} | M_n^{app} | \mathcal{D} | I_{eff} |
|-------|-------------------------|--------------|---------|-------------------|--------------------|---------------|------------------|
| 1 | 1 | 85 | 1 | 40600 | 37400 | 1.10 | 1.09 |
| 2 | 0.5 | 90 | 1 | 43000 | 39600 | 1.14 | 1.09 |
| 3 | 0.25 | 55 | 1 | 26300 | 25700 | 1.39 | 1.02 |
| 4 | 0.25 ^b | 87 | 2 | 41500 | 42900 | 1.42 | 0.97 |
| 5 | 0.5 ^c | 26 | 1 | 12500 | 11400 | 1.28 | 1.10 |

^aSupporting electrolyte: 0.1 M Et_4NBF_4 ; electrolysis program V. Conditions: $C_{\text{MA}}:C_{\text{TREN}}:C_{\text{Cu}}:C_{\text{EBIB}} = 552:0.2:x:1$, with $x = 0.1$ (entry 1), 0.05 (entry 2), 0.025 (entries 3 and 4). $V = 10\text{ mL}$. Geometrical electrode surface exposed to the solution = 22 cm^2 . ^bModified program V: 0.2 mA for 30 s, 0.15 mA for 180 s, 0.125 mA for 600 s and 0.075 mA for 2790 s. ^c $C_{\text{MA}}:C_{\text{TREN}}:C_{\text{Cu}}:C_{\text{EBIB}} = 552:0.1:0.5:1$.

The polymerizations were controlled and fast with catalyst concentration down to 0.5 mM. Further reduction to 0.25 mM afforded a lower conversion and polymer with higher dispersity (Fig. 8.10a). It is likely that a low amount of catalyst, combined with an electrolysis program involving high regeneration rate of activator is not fully able to mediate a well-controlled polymerization (Figure 8.10a). Interestingly, when the currents of program V were halved, and the reaction time was extended to 2 h to maintain the same charge consumption, higher conversion was obtained but the molecular weight distribution remained broad ($D > 1.3$). Molecular weight analysis however did not evidence any shoulder; all GPC traces exhibited a monomodal distribution of PMA-Br for all catalyst concentrations.

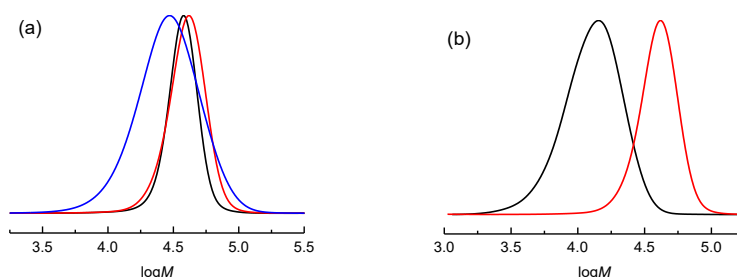


Figure 8.10. Galvanostatic *e*ATRP (program V) of 50% (v/v) MA catalyzed by $[\text{Cu}^{\text{II}}\text{TREN}]^{2+}$ in DMSO + 0.1 M Et_4NBF_4 at $T = 50\text{ }^\circ\text{C}$. MW distribution of a) PMA-Br produced using $[\text{Cu}^{\text{II}}] = 10^{-3}\text{ M}$ (—) or 5×10^{-4} (—) or $2.5 \times 10^{-4}\text{ M}$ (—); b) PMA-Br produced using $[\text{Cu}^{\text{II}}] = 5 \times 10^{-4}\text{ M}$ and $[\text{TREN}] = 10^{-3}\text{ M}$ (—) or $2 \times 10^{-3}\text{ M}$ (—).

We attempted to trigger a polymerization based on entry 2, with TREN concentration reduced to 1 mM. In this case, the polymerization became slower and less controlled (Table 8.6, entry 5 and Figure 8.10b). Indeed, as the electrolysis program is fixed, the charge fed to the reactor is always 0.635 C (corresponding to a release of 2.2×10^{-6} mol of Al^{3+}). It is known that aluminum release in solution is detrimental for catalyst stability and *e*ATRP and its effects were already highlighted.⁶ Therefore, the minimum amount of TREN required to avoid interference of Al^{3+} with $[\text{Cu}^{\text{II}}\text{TREN}]^{2+}$ is 2 mM when program V is used and this was maintained in all experiments.

8.7 Effect of Solvent

To evaluate the effect of the solvent on the polymerization, the same experiment was repeated in DMF and CH₃CN. Table 8.7 summarizes the results obtained in different solvents.

Table 8.7. *e*ATRP of 50% (v/v) MA in different solvents at $T = 50\text{ }^{\circ}\text{C}$.^a

| Entry | Solvent | t (h) | Conv. (%) | M_n^{th} | M_n^{app} | \bar{D} | I_{eff} |
|-------|--------------------|---------|-----------|-------------------|--------------------|-----------|------------------|
| 1 | DMSO | 1 | 85 | 40600 | 37400 | 1.10 | 1.09 |
| 2 | DMF | 1 | 42 | 20000 | 18100 | 1.12 | 1.11 |
| 3 | CH ₃ CN | 1 | 26 | 12400 | 11100 | 1.17 | 1.12 |

^aConditions: $C_{\text{MA}}:C_{\text{TREN}}:C_{\text{Cu}}:C_{\text{EBiB}} = 552:0.2:0.1:1$; galvanostatic electrolysis with program V; $V = 10\text{ mL}$; $C_{\text{CuBr}_2} = 10^{-3}\text{ M}$; $\text{DP} = 552$.

The effect of the solvent is well represented by the set of experiments reported in Table 8.7. The kinetics of ATRP activation by Cu complexes depends on the nature of the solvent, with the activation rate constant (k_{act}) increasing in the following order: $k_{\text{act}}(\text{CH}_3\text{CN}) < k_{\text{act}}\text{ DMF} < k_{\text{act}}\text{ DMSO}$.⁹ As k_{act} diminishes while k_{deact} is only slightly influenced by the solvent, the polymerization becomes slower. Although polymerization was well-controlled in all three solvents, the highest conversion was obtained in DMSO, whereas conversion in CH₃CN was unsatisfactory. We may anticipate that, if the reaction time is appropriately extended, polymerizations in DMF and CH₃CN would give results comparable to those in DMSO. The MW distribution of the three polymerizations are reported in Figure 8.11:

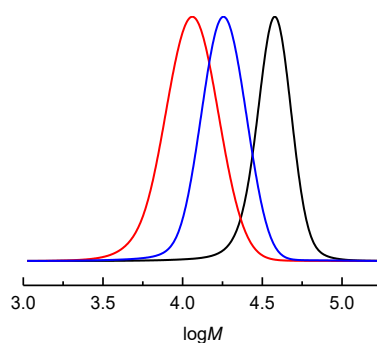


Figure 8.11. Galvanostatic *e*ATRP (program V) of 50% (v/v) MA catalyzed by $[\text{Cu}^{\text{II}}\text{TREN}]^{2+}$ at $T = 50\text{ }^{\circ}\text{C}$. MW distribution of PMA-Br produced in DMSO (—), CH₃CN (—) and DMF (—).

8.8 Chain extension

To verify the living character of the polymer, chain extension of a PMA-Br macroinitiator, synthesized according to the conditions reported in Table 8.7 (entry 1), was performed with methyl acrylate. It is noteworthy to highlight that chain-extension was triggered with the same current program V. Table 8.8 reports the results.

Table 8.8. Chain extension of PMA-Br with MA by *e*ATRP using $[\text{Cu}^{\text{II}}\text{TREN}]^{2+}$ as catalyst.^a

| Entry | <i>t</i> (h) | Conv. (%) | M_n^{th} | M_n^{app} | \bar{D} | I_{eff} |
|-----------------------|--------------|-----------|-------------------|--------------------|-----------|------------------|
| PMA-Br | 0.5 | 45 | 21600 | 22400 | 1.13 | 0.96 |
| PMA- <i>b</i> -PMA-Br | 1 | 42 | 61500 | 66800 | 1.13 | 0.92 |

^aSupporting electrolyte: 0.1 M Et_4NBF_4 ; electrolysis program V. Conditions for chain extension: $C_{\text{MA}}:C_{\text{TREN}}:C_{\text{Cu}}:C_{\text{EBIB}} = 552:0.2:0.05:0.5$. $V = 10$ mL; $C_{\text{CuBr}_2} = 5 \times 10^{-4}$ M; DP = 1104.

When PMA-Br was extended (Figure 8.12), a neat shift to higher MW without detectable dead chains are observed. The chain extension process was well-controlled and the new homopolymer exhibited $M_n > 6 \times 10^4$ Da and $\bar{D} = 1.13$, the same of the macroinitiator.

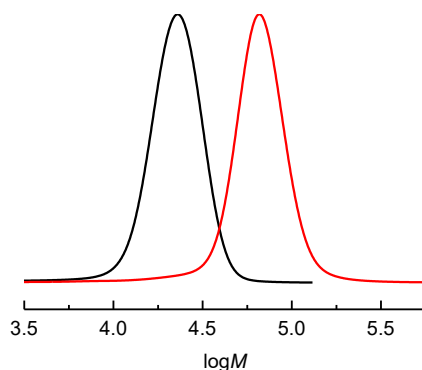


Figure 8.12. Chain extension of PMA-Br by galvanostatic *e*ATRP (program V) of 50% (v/v) MA catalyzed by $[\text{Cu}^{\text{II}}\text{TREN}]^{2+}$ in DMSO + 0.1 M Et_4NBF_4 at $T = 50$ °C. MW distribution of PMA-Br macroinitiator (—) and PMA-*b*-PMA-Br (—) after 1 h of chain extension.

Additionally, $^1\text{H-NMR}$ of PMA-Br confirmed the retention of chain-end functionality (Figure 8.13).

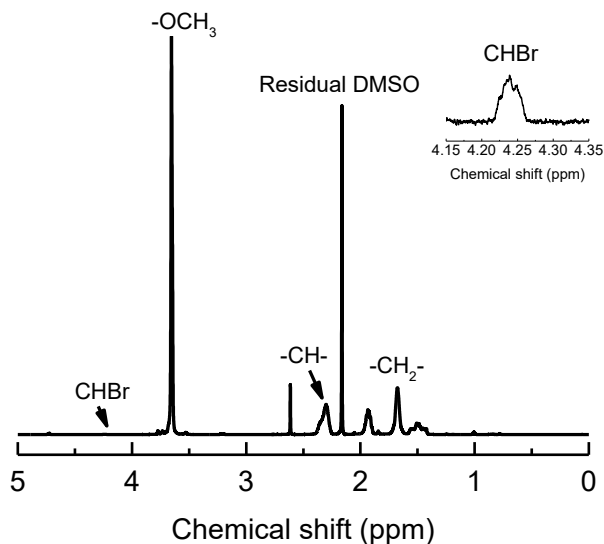


Figure 8.13. 600 MHz $^1\text{H-NMR}$ of PMA-Br produced by *e*ATRP in DMSO using program V. Spectrum was recorded in CDCl_3 .

8.9 ICP-MS analysis of the polymerization mixture

Undesired side reactions involving the electrode material may cause the release of metal ions into the solution. Trace metal analysis by inductively coupled plasma-mass spectrometry (ICP-MS), carried out at the end of a polymerization, showed a rather small presence of metal ions in solution (Table 8.9). Additionally, ICP-MS showed that Cu ions were preserved in solution after *e*ATRP, confirming that reduction of Cu^{I} to metallic Cu at the electrode did not occur. Therefore, the main role of the reactor is to act as a source of electrons for the reduction of Cu^{II} to Cu^{I} .

Table 8.9. ICP-MS analysis of the *e*ATRP mixture after polymerization (μg in 10 mL).

| Entry | Cathode | Ni (μg) | Cr (μg) | Fe (μg) |
|----------------|---------|----------------------|----------------------|----------------------|
| 1 ^a | - | 4.0 | 1.5 | 18.2 |
| 2 ^b | SS304 | 1.1 | 1.0 | 12.0 |

^aBlank sample: a solution containing all components of *e*ATRP, before the electrolysis.

^bGalvanostatic *e*ATRP of 50% (v/v) MA in CH_3CN + 0.1 M Et_4NBF_4 at $T = 50$ °C. $C_{\text{MA}}:C_{\text{TREN}}:C_{\text{Cu}}:C_{\text{EBiB}} = 552:0.2:0.1:1$ with initial $C_{\text{Cu(II)}} = 5 \times 10^{-4}$ M; $V_{\text{tot}} = 10$ mL.

ICP-MS results show that impurities of Ni, Cr and Fe are already present as contaminants in the components necessary for *e*ATRP (*i.e.* monomer, solvent, catalyst, *etc.*). Analysis before and after the polymerization shows clearly that SS304 is not chemically involved in ATRP process; it acts only as a source of electrons, excluding any SARA ATRP process, which otherwise would imply the oxidation of the surface and consequent release of metal ions into the solution.

8.10 *e*ATRP of other monomers in the reactor

The galvanostatic approach not only is useful for methyl acrylate but can also be applied to different polymerizations, with different catalysts and solvents. Indeed, the current stimulates the regeneration of the catalyst, which mediates the polymerization, leaving the activator/deactivator ratio free to drift with time. For this reason, an electrolysis program is a universal tool to drive a reaction, after choosing the proper catalyst and initiator for every monomer. To this purpose, electrolysis program V was applied to *e*ATRP of butyl acrylate (BA), methyl methacrylate (MMA) and Styrene (Sty) in appropriate catalyst/solvent systems.

Table 8.10. *e*ATRP of 50% (v/v) MA, BA, MMA or Sty, using program V at $T = 50\text{ }^{\circ}\text{C}$.^a

| Entry | Catalyst | Solvent | t (h) | Conv. (%) | M_n^{th} | M_n^{app} | \bar{D} | I_{eff} |
|-------|--|-------------|---------|-----------|-------------------|--------------------|-----------|------------------|
| MA | $[\text{Cu}^{\text{II}}\text{TREN}]^{2+}$ | DMSO | 1 | 85 | 40600 | 37400 | 1.10 | 1.09 |
| BA | $[\text{Cu}^{\text{II}}\text{Me}_6\text{TREN}]^{2+}$ | DMF | 1 | 73 | 32800 | 31100 | 1.08 | 1.05 |
| MMA | $[\text{Cu}^{\text{II}}\text{PMDETA}]^{2+}$ | [BMIm][OTf] | 3 | 53 | 24800 | 25400 | 1.43 | 0.98 |
| Sty | $[\text{Cu}^{\text{II}}\text{TPMA}]^{2+}$ | EtOH | 5 | 37 | 11200 | 12300 | 1.22 | 0.91 |

^aSupporting electrolyte: 0.1 M Et₄NBF₄; electrolysis program V. Conditions: $C_M:C_L:C_{Cu}:C_{RX} = x:0.1:0.2:y$, where $x = 552$ for MA, 349 for BA, 467 for MMA and 291 for Sty, $y = 1$ for MA, BA and MMA, and 1.5 for Sty. L = TREN for MA, Me₆TREN for BA, TPMA for Sty and PMDETA for MMA. RX = EBiB for MA, BA and Sty, and BPN for MMA. $V = 10\text{ mL}$; $C_{\text{CuBr}_2} = 10^{-3}\text{ M}$. DP = 552 for MA, 349 for BA, 467 for MMA and 291 for Sty.

All polymerizations were controlled ($\bar{D} < 1.5$) and produced polymers of narrow molecular weight distribution. It appears clearly that galvanostatic *e*ATRP using program V can be applied universally to different polymerization systems (Figures 8.14 and 8.15).

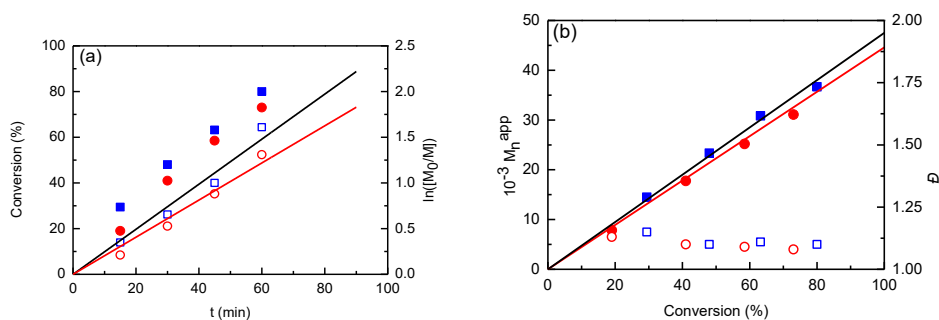


Figure 8.14. a) Kinetic plots and b) evolution of M_n and \bar{D} of *e*ATRP of 50% (v/v) MA in DMSO catalyzed by $[\text{Cu}^{\text{II}}\text{TREN}]^{2+}$ (■) or 50% BA (v/v) in DMF catalyzed by $[\text{Cu}^{\text{II}}\text{Me}_6\text{TREN}]^{2+}$ (●) at $T = 50\text{ }^{\circ}\text{C}$. Empty symbols refer to the right ordinate in the figures.

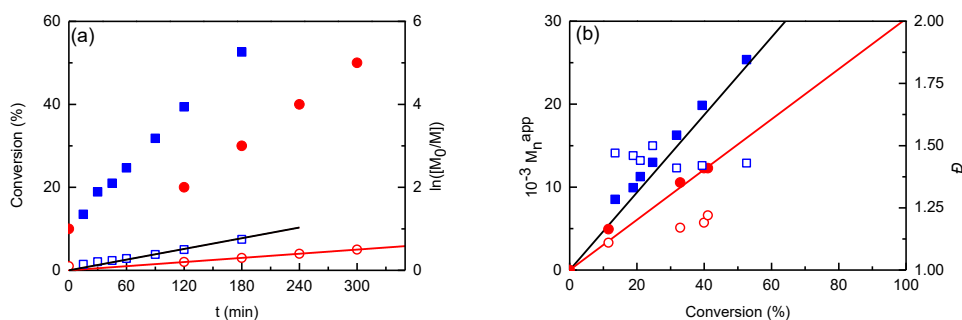


Figure 8.15. a) Kinetic plots and b) evolution of M_n and D of eATRP of 50% (v/v) MMA in [BMIm][OTf] catalyzed by $[Cu^{II}PMDETA]^{2+}$ (■) or 50% (v/v) STY in EtOH catalyzed by $[Cu^{II}TPMA]^{2+}$ (●) at $T = 50$ and 80 °C, respectively. Empty symbols refer to the right ordinate in the figures.

8.11 Toward the scale-up

Optimized conditions (Table 8.7, entry 1) were used as a starting point to scale-up eATRP of MA in the reactor, by increasing the solution volume from 10 mL to 40 mL. Because of volume increase, the geometrical surface of the reactor exposed to the solution increased from 22.6 cm^2 to 52.2 cm^2 . This has implications on the polymerization rate and some corrections of the electrolysis program (V) are needed to account for the geometrical modifications in the electrochemical cell. The applied current must consider the new surface/volume (S/V) ratio. In other words, currents must be changed to reflect into the scale-up the original optimized conditions. First, the currents were converted to current densities (j , mA/cm^2) and then, they were corrected by the $\left(\frac{S}{V}\right)$ ratio, according to Eq 1:

$$\frac{i_2}{S_2} = \frac{i_1}{S_1} \times \frac{\left(\frac{S}{V}\right)_2}{\left(\frac{S}{V}\right)_1} \quad (1)$$

where, i_1/S_1 and i_2/S_2 are the original initial and new current densities, respectively, and $(S/V)_1$ and $(S/V)_2$ are the original and new surface/volume ratios, respectively. Accounting for the new changes, new electrolysis programs (named program VII and VIII) were defined (Figure 8.16).

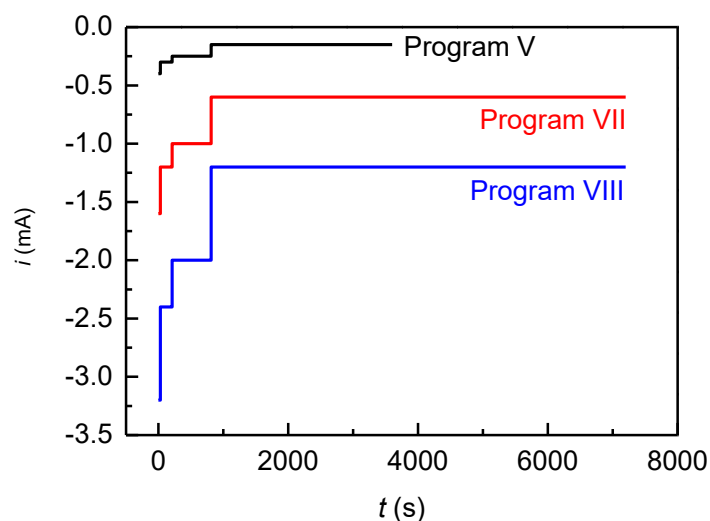


Figure 8.16. Electrolysis programs V (—), VII (—) and VIII (—) applied to *e*ATRP of methyl acrylate in DMSO at $T = 50\text{ }^{\circ}\text{C}$ during the scale-up.

Table 8.11 shows a comparison of the original polymerization with *e*ATRP with scale-up conditions.

Table 8.11. *e*ATRP of 50% (v/v) MA in the SS304 reactor with 10 mL or 40 mL reaction volume at $T = 50\text{ }^{\circ}\text{C}$.^a

| Entry | Program | V (mL) | t (h) | Conv. (%) | M_n^{th} | M_n^{app} | \bar{D} | I_{eff} | Q (C) |
|-------|---------|----------|---------|-----------|-------------------|--------------------|-----------|------------------|---------|
| 1 | V | 10 | 1 | 85 | 40600 | 37400 | 1.10 | 1.09 | 0.635 |
| 2 | VII | 40 | 2 | 80 | 38000 | 36700 | 1.10 | 1.04 | 4.70 |
| 3 | VIII | 40 | 2 | 82 | 38900 | 39500 | 1.16 | 0.98 | 9.40 |

^aSupporting electrolyte: 0.1 M Et_4NBF_4 ; electrolysis program V, VII and VIII. Conditions: $C_{\text{MA}}:C_{\text{TREN}}:C_{\text{Cu}}:C_{\text{EBIB}} = 552:0.2:0.1:1$; $C_{\text{CuBr}_2} = 10^{-3}$ M. $\text{DP} = 552$.

Polymerizations were overall similar, except that the reaction slower in the scale-up with program VII but afforded PMA-Br with the same dispersity. To increase the polymerization rate, a new electrolysis program (VIII) was tested, by increasing of 8 times currents of program V but maintaining the same time steps.

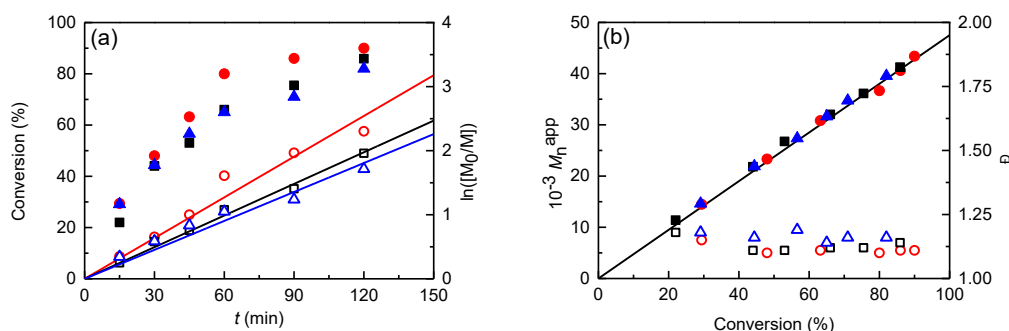


Figure 8.17. a) Kinetic plot and b) evolution of M_n and D of *e*ATRP of 50% MA (v/v) in DMSO catalyzed by $[Cu^{II}TREN]^{2+}$ with program V (■), program VII (●) and program VIII (▲) at $T = 50$ °C. Empty symbols refer to the right ordinate in the figures.

Program VIII was unsuccessful to improve the polymerization rate. Indeed, the feeding of a higher charge promoted side-reactions rather than the polymerization. Dispersity of produced PMA-Br deteriorated, slightly although evidently. It appears once again the intrinsic difficulty of scaling-up a chemical process, simply by passing from 10 to 40 mL. Despite this, the scale-up demonstrated its feasibility in the electrochemical reactor still affording very well-defined PMA-Br in short time and high conversions (Figure 8.18).

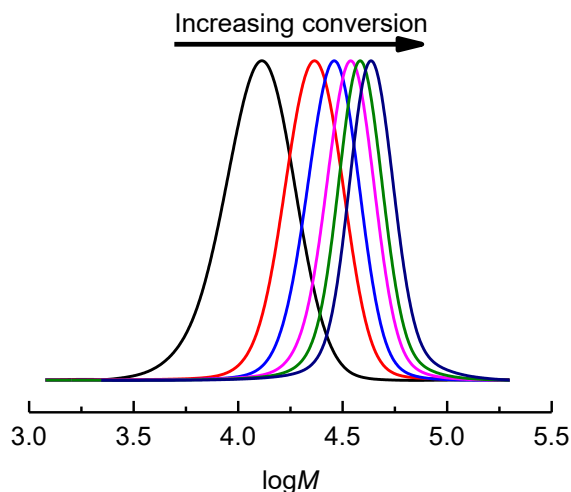


Figure 8.18. MW distribution of PMA-Br produced during galvanostatic *e*ATRP (program VII) of 50% (v/v) MA catalyzed by $[Cu^{II}TREN]^{2+}$ in DMSO + 0.1 M Et_4NBF_4 at $T = 50$ °C.

Fortunately, the possibilities given by electrochemical modulation of the polymerization rate, leave plenty of space to tune and adapt this small series of

electrolysis programs proposed in this chapter in the next future for bigger polymerizations in bigger reactors.

8.12 Conclusions

The extremely simplified electrochemical setup, consisting of an SS304 vessel and a sacrificial anode, makes this peculiar electrochemical setup suitable for scale-up. The SS304 vessel has the dual function of cathode and reactor and the whole electrochemical setup does not involve expensive, noble metals with a considerable money saving. The use of $[\text{Cu}^{\text{II}}\text{TREN}]^{2+}$ as catalyst, with concentrations as low as 55 ppm, makes this system inexpensive, user-friendly with improved cleanness of the polymer. Six electrolysis programs, single or multistep, showed that proper tuning of the electrolysis is necessary for a high conversion and low dispersity. However, almost all PMA-Br so obtained had a narrow MW distribution ($D \leq 1.4$). Livingness of the polymer was proved by chain extension with methyl acrylate, affording PMA-Br up to $M_n \sim 6 \times 10^4$ Da. Polymerizations of butyl acrylate with the same current program, but in different media and conditions (catalyst, initiators, solvents) were successfully achieved. A scale-up of the model MA polymerization was attempted. The rate of the polymerization was affected not only by the charge fed to the system but also by the surface-to-volume ratio. To maintain roughly the same rate of polymerization after increasing the solution volume from 10 mL to 40 mL, it was found necessary to increase *ca* 4 times both current and charge. Higher charges did not significantly affect the dispersity of the polymer but contributed instead to ensure a proper reaction time. We anticipate that at this stage of development, due to the galvanostatic mode, no dedicated electrochemical equipment is required: any source of electricity can be used, including electricity produced by renewable sources.

References

1. Matyjaszewski, K., Atom Transfer Radical Polymerization (ATRP): Current Status and Future Perspectives. *Macromolecules* **2012**, *45*, 4015-4039.
3. Park, S.; Chmielarz, P.; Gennaro, A.; Matyjaszewski, K., Simplified Electrochemically Mediated Atom Transfer Radical Polymerization using a

Sacrificial Anode. *Angewandte Chemie International Edition* **2015**, *54*, 2388-2392.

4. Gromada, J.; Spanswick, J.; Matyjaszewski, K., Synthesis and ATRP Activity of New TREN-Based Ligands. *Macromolecular Chemistry and Physics* **2004**, *205*, 551-566.

5. Tsarevsky, N. V.; Braunecker, W. A.; Vacca, A.; Gans, P.; Matyjaszewski, K., Competitive Equilibria in Atom Transfer Radical Polymerization. *Macromolecular Symposia* **2007**, *248*, 60-70.

6. Lorandi, F.; Fantin, M.; Isse, A. A.; Gennaro, A., Electrochemically mediated atom transfer radical polymerization of n-butyl acrylate on non-platinum cathodes. *Polymer Chemistry* **2016**, *7*, 5357-5365.

7. Matyjaszewski, K.; Jakubowski, W.; Min, K.; Tang, W.; Huang, J.; Braunecker, W. A.; Tsarevsky, N. V., Diminishing catalyst concentration in atom transfer radical polymerization with reducing agents. *Proceedings of the National Academy of Sciences* **2006**, *103*, 15309-15314.

8. Egorova, K. S.; Ananikov, V. P., Which Metals are Green for Catalysis? Comparison of the Toxicities of Ni, Cu, Fe, Pd, Pt, Rh, and Au Salts. *Angewandte Chemie International Edition* **2016**, *55*, 12150-12162.

9. Horn, M.; Matyjaszewski, K., Solvent Effects on the Activation Rate Constant in Atom Transfer Radical Polymerization. *Macromolecules* **2013**, *46*, 3350-3357.

Chapter 9

Electrochemically mediated Atom Transfer Radical Polymerization of Vinyl Chloride

9.1 Introduction

Poly(vinyl chloride) (PVC) is the second most consumed polymer worldwide, sharing the second place with high-density polyethylene (HDPE), according to estimations made in 2016 by analysis of stock markets. Despite the numerous discussions on the necessity to replace halogenated polymers for environmental and health reasons, its market underwent a long and consistent growth. PVC has important characteristics such as general versatility, flame retardant properties and inexpensiveness, which led to its vast use in many applications. Packaging, healthcare devices, toys, electrical wire insulation, clothes, furniture, interior decoration, building materials, automotive industry products, pipes, window frames, bottles, and credit cards are only some of the materials that contain PVC. The industrial production of PVC is fundamental because it incorporates chlorine (~57% of the VC mass), which is a by-product of chloralkaline industry. The polar C-Cl bond enhances the ability of the monomer to polymerize. To date, free radical polymerization (FRP) is the only method for the synthesis of PVC on an industrial scale. Such a polymerization is inevitably accompanied by the occurrence of side-reactions and structural defects. The latter are responsible for the low thermal stability of PVC and hence their presence is a limitation of the process. The use of stabilizers and plasticizers limits also the temperature range of PVC processability. These strong limitations exasperated the attempts to apply macromolecular engineering to achieve controlled PVC. To this end, RDRP methods provided a major contribution in controlling VC polymerization.

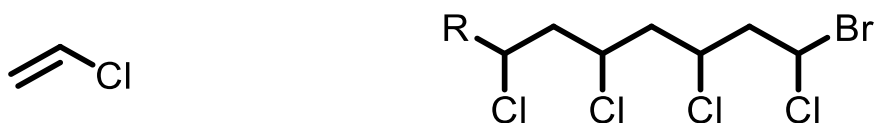


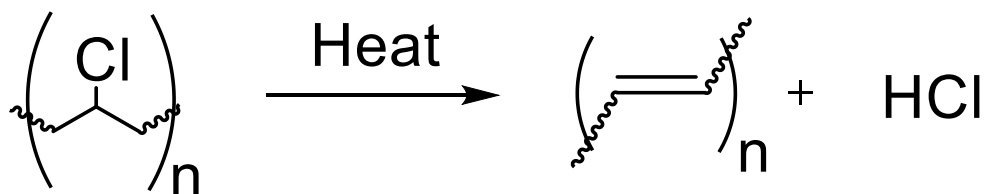
Figure 9.1. Structures of VC monomer and PVC polymer.

9.1.1 Vinyl chloride monomer

Vinyl chloride is a non-conjugated olefin ($\text{H}_2\text{C}=\text{CHCl}$) with a weak-electron-withdrawing substituent.¹ VC has one of the largest values of chain transfer rate constant (k_{tr}) in the portfolio of possible monomers for RDRP; its k_{tr} is two orders of magnitude higher than that of methyl methacrylate or styrene.^{1,2} Propagation and termination rate constants of VC are, in addition, two orders of magnitude larger than those of the above-mentioned monomers.^{1,3}

9.1.2 PVC polymer: the need for controlled polymerizations

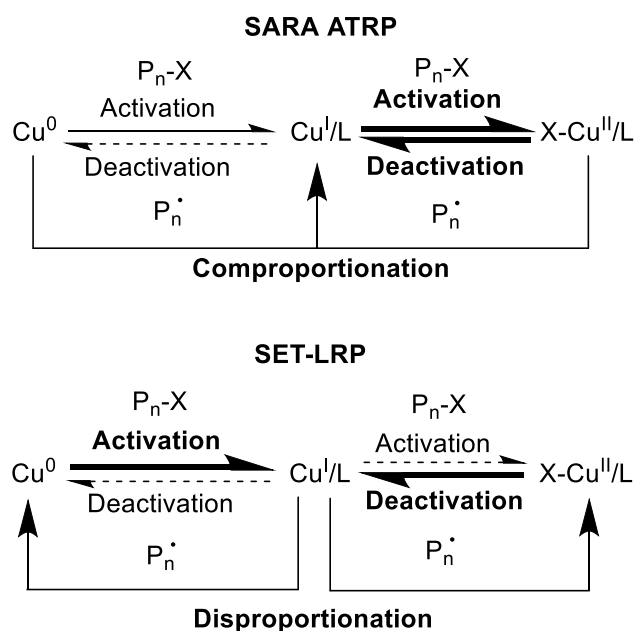
FRP has a very poor control over PVC molecular weight distribution, which is completely governed by the polymerization temperature.⁴ On increasing the temperature, chain transfer to monomer becomes competitive with propagation, impeding the growth of the macromolecule.⁴ This leads to the formation of low MW PVC with a reduced thermal stability.⁵ Since the polymerization is controlled by temperature (i.e. the final MW of PVC), low temperatures should be preferred, with an inevitable dilatation of reaction time. Previous attempts by FRP showed that PVC topped a maximum MW of 92000⁶⁻⁷ at near-ambient temperature; at 75 °C the maximum MW was only 28200.⁶⁻⁸ In addition, raising the polymerization temperature increases the number of structural defects in the final PVC. These defects include the presence of allylic centers and tertiary halogen atoms and it has been suggested that they are mainly responsible for zipper dehydrochlorination reactions that generate conjugated polyene sequences (Scheme 9.1).⁹



Scheme 9.1. Dehydrochlorination reaction induced by heating in PVC.

9.1.3 SARA ATRP vs. SET-LRP: (never) ending controversy?

Vinyl chloride polymerization is interesting also from a mechanistic point of view. To date, the only successful ATRP method for the polymerization of VC is SARA ATRP, also improperly known as SET-LRP, although direct ATRP was attempted, but with scarce results. In Cu⁰-mediated polymerizations, there are two models proposed in the literature: SARA ATRP^{10,11-13} and SET-LRP^{14,15}. The latter claims that Cu^I does not participate in the activation of alkyl halides but undergoes instantaneous disproportionation to Cu⁰ and Cu^{II} (with minimal comproportionation); therefore, Cu⁰ is the exclusive activator of alkyl halides, whereas Cu^{II} is the major deactivator.^{14,16,17,18} In contrast, SARA ATRP adheres to the traditional ATRP mechanism involving activation by Cu^I and deactivation by Cu^{II}, with Cu⁰ playing the role of a supplemental activator and regenerator of Cu^I by comproportionation with Cu^{II}. The competitive mechanisms are shown in Scheme 9.2:



Scheme 9.2. SARA ATRP (top) and SET-LRP (bottom) mechanisms. Bold arrows indicate major reactions, whereas solid arrows indicate supplemental or contributing reactions. Cu⁰, Cu^IX/L and Cu^{II}X₂/L represent a Cu⁰, Cu^I and Cu^{II} species without particular speciation. For clarity, radical products are omitted in activation reactions, and stoichiometric balance is neglected in comproportionation/disproportionation processes. Finally, all radicals can propagate with monomer or terminate.

SARA ATRP and SET-LRP mechanisms use the same components and are comprised of the same reactions, but with vastly different contributions to the

overall polymerization. The crucial question of the debate between SARA ATRP and SET-LRP can be summarized within the following: is Cu^{I} or metallic copper the major activator? Relevant mechanistic studies showed that Cu^{I} activates alkyl halides with a rate constant 3-5 orders of magnitude higher than disproportionation rate constants of Cu^{I} ; activation by Cu^{I} is also much faster than activation driven by Cu^0 , which is a supplemental activator and reducing agent and not the major activator of alkyl halides.¹⁰⁻¹³ The debate has been vigorous but most of the evidences show that the mechanism of the polymerization in the presence of Cu^0 is consistent with SARA ATRP in organic media and water. Thus, SET-LRP terminology should not be used. Moreover, one of the major claims of SET-LRP is that it is the only method to polymerize “inactive” monomers such as VC. With all the indicators supporting the SARA mechanism (*i.e.* activation by Cu^{I}) the polymerization is expected to proceed also by *e*ATRP, without Cu^0 , provided that a Cu^{I} catalyst capable of activating the dormant species (VC-X) is used. A successful electrochemical ATRP should be the definitive proof that the mechanism of SET-LRP is inconsistent.

9.1.4 SARA ATRP of Vinyl Chloride

Several studies have been published in the literature regarding SARA ATRP of VC. Sulfolane has been proposed as an efficient solvent for the SARA ATRP of acrylates, methacrylates, styrene and VC, with few ppm of copper catalyst added to the mixture.¹⁹ Fast (co)polymerizations of VC were obtained in sulfolane/water (90/10 (v/v)).²⁰ Moreover, solvent mixtures of cyclopentyl methyl ether (CPME)/DMSO (70/30)²¹ or sulfolane/1-butyl-3-methylimidazolium hexafluorophosphate ([BMIm][PF₆]) (75/25 (v/v))²² were successfully used. Block copolymers PSty-*b*-PVC-*b*-PSty with controlled structure were prepared by using SARA ATRP. Also, block copolymers of PMA-*b*-PVC-*b*-PMA were obtained by venting-off VC after the synthesis of homotelechelic PVC and the addition of MA. Applied polymerization conditions used by ATRP are attractive for a future industrial implementation.

9.2 Toward *e*ATRP of vinyl chloride

The experimental polymerization conditions selected for this work are based on previously reported results of SARA ATRP of VC: $[\text{Cu}^{\text{II}}\text{TREN}]^{2+}$ as catalyst, CHBr_3 as the initiator, DMSO as solvent and $T = 40\text{ }^\circ\text{C}$.^{19-20, 22} In contrast to the previously reported systems used for SARA ATRP of VC, here $[\text{Cu}^{\text{I}}\text{TREN}]^+$ is formed by application of an electrical stimulus to reduce $[\text{Cu}^{\text{II}}\text{TREN}]^{2+}$ at the electrode surface.

9.2.1 Kinetics of $[\text{Cu}^{\text{I}}\text{TREN}]^+$ disproportionation and activation

Detailed electrochemical investigation of $[\text{Cu}^{\text{II}}\text{TREN}]^{2+}$ was performed prior to electrochemically mediated ATRP. Although the stability constants of $[\text{Cu}^{\text{I}}\text{TREN}]^+$ and $[\text{XCu}^{\text{I}}\text{TREN}]^+$ in DMSO and VC/DMSO are not known, it is likely that $[\text{Cu}^{\text{I}}\text{TREN}]^+$ is the only species present in solution when TREN is the only ligand in solution, whereas both species will be formed in the presence of both TREN and X^- . Lack of knowledge on the stability constants precludes any possibility of calculations on Cu^{I} speciation and hence identification of predominant species that may be undergoing disproportionation. It is important to stress, however, that if different Cu^{I} species are present, for instance $[\text{Cu}^{\text{I}}\text{L}]^+$, $[\text{XCu}^{\text{I}}\text{L}]$ $[\text{Cu}^{\text{I}}\text{X}_2]$, etc, one must consider all possible reactions between these species. The overall disproportionation reaction will be made up of different contributions from a series of parallel reactions between Cu^{I} species. Thus, even if one were able to compute precise speciation of Cu^{I} , this would hardly be of any help to determine separate disproportionation rate constants for the various possible reactions. Faced with these difficulties, we decided to measure the overall rate constant of disproportionation. Additionally, we consider disproportionation to be principally occurring in solution, especially in the initial stages of the reaction where the surface of Cu^0 is very small. Although disproportionation can occur also by a heterogeneous process involving Cu^0 , the reaction kinetics was analyzed as a homogeneous process. The general disproportionation reaction of Cu^{I} species present in solution can be expressed as:



Investigations on the kinetics of disproportionation were performed by monitoring the concentration of Cu^{I} on a rotating disc electrode (RDE), operating at a fixed angular velocity (ω) and a constant applied potential. This value is significantly more positive than $E_{1/2}$ of all the relevant copper complexes present so that all Cu^{I} species undergo oxidation at the electrode. The oxidation process at this potential is under diffusion control and the measured limiting current, I_L , is correlated to the bulk concentration of Cu^{I} , $C_{\text{Cu}^{\text{I}}}$, through the Levich equation²³:

$$I_L = 0.62nFAD^{2/3}\omega^{1/2}\nu^{-1/6}C_{\text{Cu}^{\text{I}}} \quad (2)$$

where n is the number of exchanged electrons, F is the Faraday constant, D is the diffusion coefficient of Cu^{I} species undergoing oxidation, A is the area of the electrode and ν is the kinematic viscosity.

The reaction rate can be expressed as the rate of disappearance of Cu^{I} :

$$-\frac{dC_{\text{Cu}^{\text{I}}}(t)}{dt} = 2k_{\text{disp}} C_{\text{Cu}^{\text{I}}}(t)^2 \quad (3)$$

which upon integration gives the kinetic rate law:

$$\frac{1}{C_{\text{Cu}^{\text{I}}}(t)} - \frac{1}{C_{\text{Cu}^{\text{I}}}^0} = 2k_{\text{disp}}t \quad (4)$$

where $C_{\text{Cu}^{\text{I}}}^0$ is the initial concentration of Cu^{I} .

To determine k_{disp} a constant potential of -0.4 V vs. $\text{Fc}^+|\text{Fc}$ was applied to the RDE ($\omega = 2500$ rpm) in a solution containing the ligand but without copper. Cu^{I} was then introduced and immediately an anodic current was observed, which decayed with time owing to the disproportionation reaction. The limiting current, I_L , measured when Cu^{I} was introduced ($t = 0$) is related to the initial concentration of Cu^{I} , $C_{\text{Cu}^{\text{I}}}^0$ through the Levich equation (Eq. 2). The same equation can be applied to the decaying current measured during the disproportionation reaction. It follows then that the concentration of Cu^{I} as a function of time is given by

$$C_{\text{Cu}^{\text{I}}}(t) = \frac{I_L}{I_L^0} C_{\text{Cu}^{\text{I}}}^0 \quad (5)$$

Examples of current decay and kinetic analysis according to Eq. (2) are shown in Fig. 9.2. It is important to note that only the first 600 s of the reaction were

analyzed with the linear regression to determine k_{disp} . This short reaction time was chosen to avoid possible contribution of the inverse comproportionation reaction to the overall reaction rate and to prevent significant consumption of Cu^{I} by the oxidation process at the electrode. Both comproportionation and Cu^{I} consumption by electrooxidation become relevant at much longer times. The disproportionation rate constants determined for $[\text{Cu}^{\text{I}}\text{TREN}]^+$ in DMSO are summarized in Table 9.1. It is worth noting that in general these disproportionation experiments did not give highly reproducible results, therefore all reported k_{disp} values were obtained as the average of at least two replicas. According to the data reported in Table 9.1, disproportionation of $[\text{Cu}^{\text{I}}\text{TREN}]^+$ in DMSO is not a fast reaction. This is in contrast with the claims of SET-LRP.¹⁴⁻¹⁷

Table 9.1. Disproportionation rate constant, k_{disp} , for $[\text{Cu}^{\text{I}}\text{TREN}]^+$ in DMSO + 0.1 M Et_4NBF_4 at $T = 40\text{ }^\circ\text{C}$.^a

| Entry | TREN (mM) | C_{Br^-} ^b (mM) | C_{Cu} (mM) | k_{disp} ($\text{M}^{-1}\text{s}^{-1}$) |
|-------|--------------|--|-------------------------|---|
| 1 | 0.5 | 0 | 0.5 | 1.06 |
| 2 | 1 | 0 | 0.5 | 1.04 |
| 3 | 1 | 2 | 0.5 | 0.90 |

^a $C_{\text{Cu}(\text{I})} = 5 \times 10^{-4}$ M. Accuracy $\pm 1\%$.^bAdded as Et_4NBr .

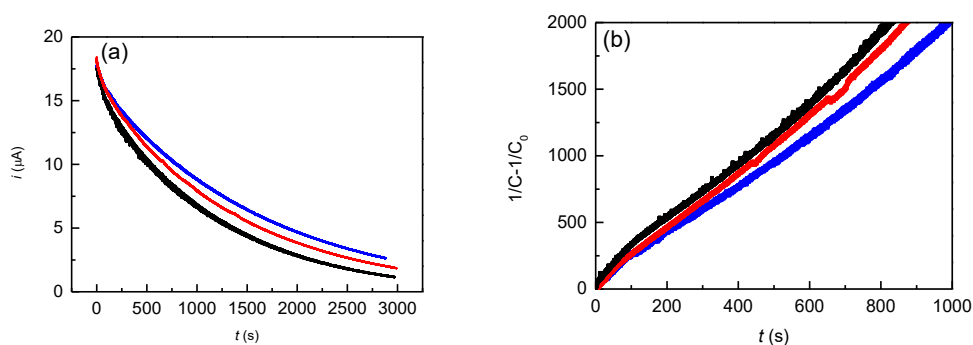


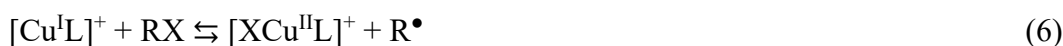
Figure 9.2. a) Decay of limiting current vs. time during disproportionation of $[\text{Cu}^{\text{I}}\text{TREN}]^+$ (—), $[\text{Cu}^{\text{I}}\text{TREN}]^+ + 1$ eq TREN (—), $[\text{Cu}^{\text{I}}\text{TREN}]^+ + 1$ eq TREN + 2 eq Et_4NBr (—), and (b) data elaboration according to Eq. (2) for k_{disp} determination in DMSO + 0.1 M Et_4NBF_4 : $C_{\text{CuI}/\text{TREN}} = 5 \times 10^{-4}$ M, $T = 40\text{ }^\circ\text{C}$, $\omega_{\text{RDE}} = 2500$ rpm. Analyzed interval time: 600 s. CV were recorded on GC electrode.

Once we established that disproportionation is not fast, kinetic analysis to determine k_{act} was performed. The model dormant species for VC is 1-bromo-1-chloroethane (CH_3CHClBr , VC-Br), a geminal alkyl dihalide that mimics the terminal unit (Fig. 9.3).



Figure 9.3. Structures of VC monomer and of CH_3CHClBr which mimics the PVC end-functionality.

The reactions between $[\text{Cu}^{\text{I}}\text{L}]^+$ and RX are fast, but the ATRP equilibrium is strongly shifted toward the reactants. In normal conditions the fraction of converted Cu^{I} is very low, preventing the possibility of obtaining any kinetic information by simply mixing Cu^{I} and RX . To overcome this difficulty, the radical scavenger 2,2,6,6-tetramethyl-1-piperidinyloxy (TEMPO) was used in a large excess with respect to Cu^{I} , allowing quantitative and irreversible trapping of R^\bullet . The rate constant of radical trapping by nitroxides is typically close to the diffusion controlled limit,²⁴ so that the overall process (Eqs. 6 and 7) can be irreversible and kinetically controlled by the activation reaction, due to $[\text{Cu}^{\text{I}}\text{TREN}]^+$.²⁵



Another important issue that should be considered is that besides activating RX , Cu^{I} is always engaged in a disproportionation reaction. Previous kinetic studies comparing the decay rates of Cu^{I} in the absence and presence of RX have shown that RX activation is much faster than disproportionation.²⁶ The lifetime of Cu^{I} is drastically reduced in the presence of RX ; disproportionation reactions require hours to approach equilibrium, whilst activation reactions last within few minutes. Therefore, activation kinetics can be studied by monitoring the disappearance of Cu^{I} at a rotating disc electrode (RDE), neglecting the contribution of disproportionation to the overall rate of Cu^{I} decay. Two kinetic regimes can be used to determine k_{act} . For relatively slow reactions, the activation kinetics can be

examined under pseudo-first-order conditions, that is, using $\frac{C_{RX}^0}{C_{[Cu^I L]^+}} \geq 20$. The rate of disappearance of $[Cu^I L]^+$ in this circumstance can be expressed as:

$$-\frac{dC_{Cu(I)}}{dt} = k_{act} C_{[Cu^I L]^+} C_{RX} = k' C_{[Cu^I L]^+} \quad (8)$$

which upon integration gives

$$\ln C_{[Cu^I L]^+} = \ln C_{[Cu^I L]^+}^0 - k' t \quad (9)$$

where $k' = k_{act} C_{RX}^0$

The results of the activation rate constant experiments are reported in Table 9.2, where C_{TREN} and C_{Br^-} are expressed with respect to $C_{Cu(I)}$, and Fig. 9.4.

Table 9.2. k_{act} for the reaction between $[Cu^I TREN]^+$ and $CH_3CHClBr$ in DMSO + 0.1 M Et_4NBF_4 at $T = 25$ °C.^a

| Entry | C_{TREN} (eq) | C_{Br^-} ^b (eq) | k_{act} ($M^{-1}s^{-1}$) |
|-------|--------------------|---------------------------------|---------------------------------|
| 1 | 1 | 0 | 519 |
| 2 | 2 | 0 | 794 |
| 3 | 1 | 2 | 596 |
| 4 | 2 | 2 | 457 |

^a $C_{Cu(I)} = 2 \times 10^{-4}$ M, $C_{Cu(I)}:C_{VC-Br}:C_{TEMPO} = 1:1:20$. Accuracy $\pm 5\%$. ^bAdded as Et_4NBr .

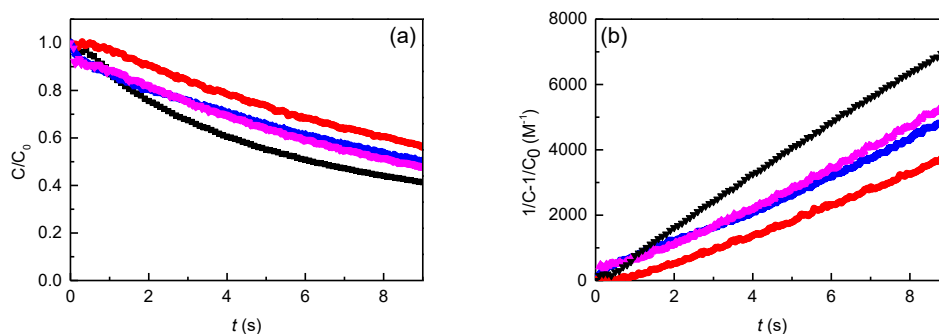


Figure 9.4. (a) Decay of 2×10^{-4} M $[Cu^I TREN]^+$ vs. time + 2×10^{-4} M VC-Br + 1×10^{-4} M TREN (—); or 2×10^{-4} M VC-Br + 4×10^{-4} M Et_4NBr (—); or 2×10^{-4} M VC-Br (—); or 2×10^{-4} M VC-Br + 4×10^{-4} M Et_4NBr (—); (b) data elaboration for k_{act} determination in DMSO + 0.1 M Et_4NBF_4 at 25 °C, according to second-order rate law; $\omega_{RDE} = 4000$ rpm, analyzed interval time: 9 s. Currents were recorded on GC electrode.

Surprisingly, the activation involved the cleavage of both C-X bonds, as confirmed by CV of the resulting mixture recorded at the end of the experiment, where both $[\text{Cu}^{\text{II}}\text{TRENBr}]^+$ and $[\text{Cu}^{\text{II}}\text{TRENCl}]^+$ redox couples are observed (Fig. 9.5).

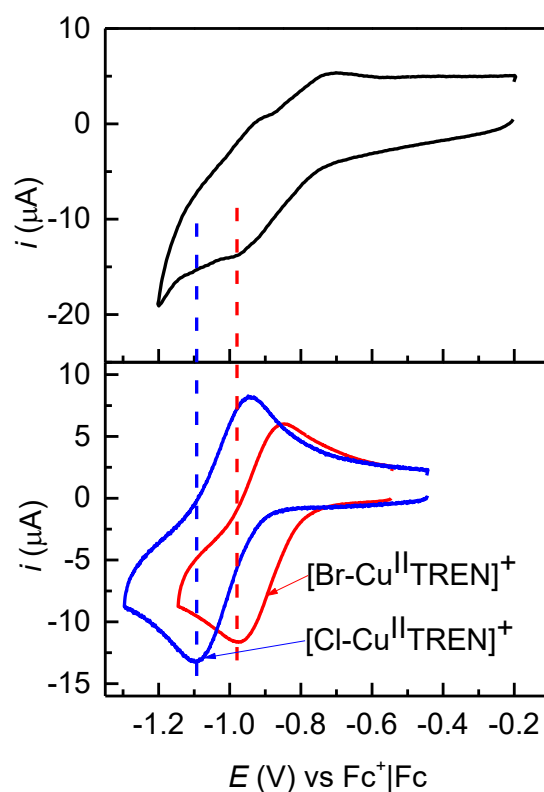


Figure 9.5. CV of the reaction mixture (—) in the potential window of the ATRP catalyst in DMSO + 0.1 M Et_4NBF_4 at 25 °C, recorded at the end of the activation experiment (Table 9.2, Entry 1). Both redox couple attributed to $[\text{Br-Cu}^{\text{II}}\text{TREN}]^+$ (—) and $[\text{Cl-Cu}^{\text{II}}\text{TREN}]^+$ (—) were identified. CV were recorded on GC electrode.

This anomalous behavior was never reported in the literature to the best of our knowledge. If a C-Cl bond is cleaved, the resulting deactivator $[\text{ClCu}^{\text{II}}\text{TREN}]^+$ would deactivate a growing macroradical as 1,1-dichloroethane rather than as 1,1-bromochloroethane. This can affect the polymerization: if two competing equilibria proceed simultaneously, according to their $k_{\text{act}}/k_{\text{deact}}$ values, the dispersity of the resulting polymer broadens.

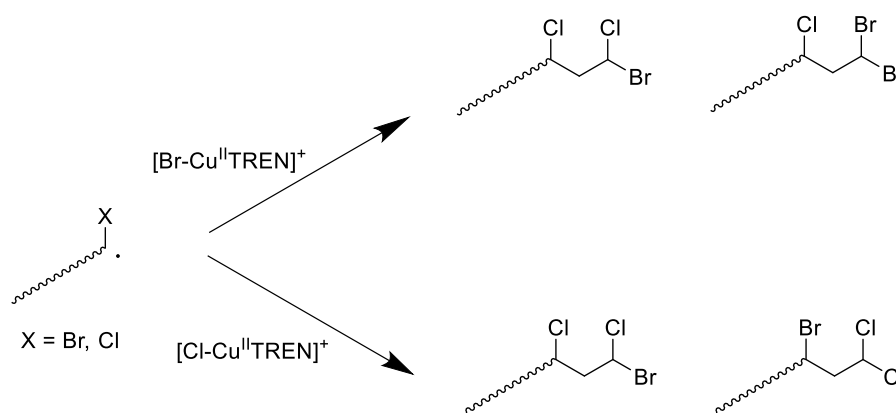
k_{act} was measured also for 1,1-dichloroethane, which as a dormant species mimics a PVC chain with *gem*-dichloride end-functionality. The activation rate constants measured for the different chain-end functionalities are summarized in Table 9.3.

Table 9.3. Activation rate constant, k_{act} , for the reaction between $[\text{Cu}^{\text{I}}\text{TREN}]^+$ and CH_3CHClBr or CH_3CHCl_2 , in DMSO + 0.1 M Et_4NBF_4 at $T = 25\text{ }^\circ\text{C}$.^a

| RX | k_{act} $\text{M}^{-1}\text{ s}^{-1}$ |
|----------------------------|---|
| CH_3CHClBr | 794 |
| CH_3CHCl_2 | 35 |

^a $C_{\text{Cu}(\text{I})} = 2 \times 10^{-4}\text{ M}$, $C_{\text{Cu}(\text{I})}:C_{\text{TREN}}:C_{\text{RX}}:C_{\text{TEMPO}} = 1:2:1:20$. Accuracy $\pm 5\%$.

Although k_{act} of C-Br is *ca* 23-fold higher than that of C-Cl, the effect of C-Cl activation on the polymerization must be considered. The slow activation of C-Cl chain-end builds up $[\text{ClCu}^{\text{II}}\text{TREN}]^+$, adding CHCl_2 -terminated PVC and C-Br structural defects along the macromolecule (Scheme 9.3). In this framework, it is not possible to conclude that ATRP of VC proceeds uniquely *via* C-Br activation.



Scheme 9.3. Possible paths and products of deactivation of a VC radical by $[\text{X-Cu}^{\text{II}}\text{TREN}]^+$: top, deactivation by Br; bottom, deactivation by Cl after anomalous activation of a C-Cl bond.

9.2.2 Blank test of SARA ATRP of VC in SS304 reactor

It is known that zerovalent metals, including iron (the main metal in SS304), may trigger SARA ATRP. However, as shown in Chapter 8, no SARA ATRP takes place if the ligand in solution is in a very small excess over Cu^{II} . To further exclude that the surface of the SS304 vessel may promote supplemental activation

of bromoform thus triggering polymerization, blank tests were performed with vinyl chloride as described in Chapter 8.

Table 9.4. Blank tests of SARA ATRP of VC at $T = 40\text{ }^{\circ}\text{C}$ performed in DMSO in an SS304 reactor.^a

| [Cu ^{II}] (mM) | TREN (mM) | t (h) | Conv. (%) | M_n^{th} | M_n^{app} | D | I_{eff} |
|-----------------------------|--------------|------------|--------------|-------------------|--------------------|-----|------------------|
| 1 | 1 | 6 | <1 | 200 | - | - | - |
| 1 | 2 | 6 | 1 | 400 | - | - | - |

^aOther experimental conditions: $C_{\text{VC}}:C_{\text{TREN}}:C_{\text{Cu}}:C_{\text{RX}} = 728:1.5:0.2:0.1$. $V = 10\text{ mL}$. VC = 50% v/v.

Two experiments were carried out: one without excess ligand and the other with a 2-fold excess of TREN over Cu^{II}. In both cases, negligible conversion was observed, while GPC analysis did not evidence any polymer. To trigger SARA ATRP, a considerable excess of ligand is required for the activation of the initiator by the metal surface.^{10,27}

9.2.3 Modeling of electrolysis programs

Electrochemically mediated ATRP can be successfully carried out in both divided and undivided cells under either potentiostatic or galvanostatic control.²⁸ In controlled potential electrolysis, a reference electrode (Ag|AgI, Ag|AgCl, Hg|Hg₂SO₄, saturated calomel electrode, etc.) is used so that one has always a precise knowledge of the potential at which the electrochemical process of interest is occurring. Instead, in galvanostatic electrolysis the current is controlled without necessarily using a reference electrode, which might be difficult to handle if drastic conditions (in terms of pressure and temperature) are to be used. It is important to note that although potentiostatic setup provides better defined experimental conditions than the galvanostatic mode, the latter is simpler and more appropriate for large scale preparations, especially at industrial level. Therefore, *e*ATRP of VC was exclusively studied under galvanostatic mode in an undivided cell with a sacrificial anode.

In galvanostatic *e*ATRP, polymerization is triggered by applying an appropriate fixed current or current program (multistep galvanostatic *e*ATRP). Therefore, a series of different electrolysis programs were evaluated in a preliminary study to define the best galvanostatic conditions. Usually multistep current *e*ATRP performs better than a fixed current electrolysis and the easiest way to choose appropriate values of current and number and length of steps is to use chronoamperometry recorded in an electrolysis at a constant potential (potentiostatic *e*ATRP, Figure 9.7). This was not possible with vinyl chloride. Thus, to model the programs of current, methyl acrylate was used as monomer and potentiostatic *e*ATRP was performed exactly in the same conditions of the polymerization of VC. Chronoamperometry was recorded during *e*ATRP at $E_{app} = E_{1/2} = -0.422$ V vs. SCE.

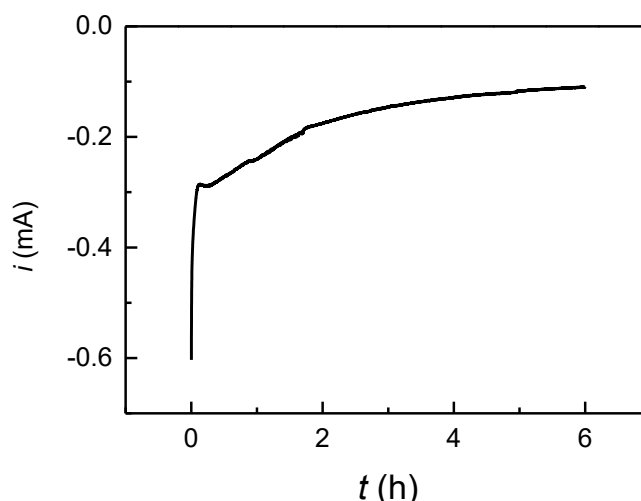


Figure 9.7. Chronoamperometry of *e*ATRP of methyl acrylate in DMSO catalyzed by 1×10^{-3} M $[\text{BrCu}^{\text{II}}\text{TREN}]^+$ in MA/DMSO (1:1, v/v) initiated by 1.5×10^{-2} M CHBr_3 , recorded at $T = 40$ °C on a Pt gauze electrode.

The selected electrolysis programs for galvanostatic *e*ATRP tests at a platinum electrode were:

- I. Single current step of 6 h at $I_{app} = 0.15$ mA;
- II. Single current step of 6 h at $I_{app} = 1$ mA;
- III. Multistep electrolysis of 6 h at variable $I_{app} = 0.4, 0.3, 0.25, 0.15$ and 0.1 mA for 300, 600, 2700, 3600 and 14400 s;

- IV. Multistep electrolysis of 3 h at variable $I_{app} = 0.4, 0.3, 0.25, 0.15$ and 0.1 mA for 30, 180, 600, 2790 and 7200 s;
- V. Long term multistep electrolysis of 9 h at variable $I_{app} = 0.4, 0.3, 0.25, 0.15$ and 0.1 mA for 100, 300, 1600, 5200 and 25200 s (vinyl chloride = 50%);
- VI. Multistep electrolysis of 3 h at variable $I_{app} = 0.4, 0.3, 0.25, 0.15$ and 0.1 mA for 300, 600, 2700, 3600 and 3600 s (vinyl chloride = 25%);
- VII. Multistep electrolysis of 6 h at variable $I_{app} = 0.3, 0.2, 0.15, 0.1$ and 0.075 mA for 300, 600, 2700, 3600 and 14400 s ($[Cu^{II}TREN]^{2+} = 0.5$ mM);

The electrolysis programs are shown in Figure 9.8:

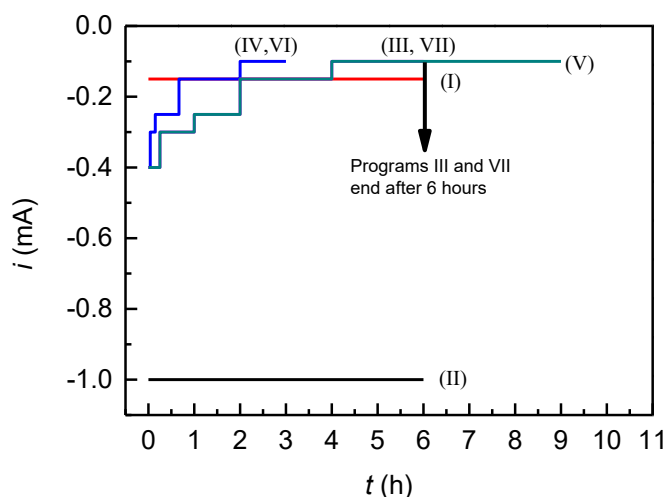


Figure 9.8. Electrolysis programs applied during galvanostatic *e*ATRP of vinyl chloride.

Five current steps, with progressively decreasing I_{app} , were applied to simulate the decay of i vs. t during a potentiostatic electrolysis. The current steps were chosen to produce $[Cu^I TREN]^+$ at a high rate at the beginning of the polymerization and then slowly in later stages of the process.

9.3 Electrochemically mediated ATRP of vinyl chloride

Different strategies to trigger the polymerization were applied by changing the electrolysis program. Thus, *e*ATRP was explored in multiple conditions, to

evaluate how the reaction responds to the external stimulus. Polymerization of VC was studied by *e*ATRP with a single stimulus (applied current, i_{app}). With the imposition of a constant current, the reaction is only marginally influenced by modifications of the polymerization media. Indeed, under galvanostatic conditions the potentiostat modifies the difference of potential between cathode and anode maintaining constant the desired value of current. The results are summarized in Table 9.5:

Table 9.5. Electrochemically mediated ATRP of 50% (v/v) VC in DMSO with different operational conditions at $T = 40$ °C. ^a

| Entry | DP | Program ^b | <i>t</i> (h) | Conv. (%) | M_n^{th} | M_n^{app} | \bar{D} | I_{eff} | Q (C) |
|----------------|------|----------------------|-----------------|--------------|------------|-------------|-----------|-----------|---------|
| 1 | 485 | I | 6 | 40 | 12100 | 15800 | 1.78 | 0.77 | 3.24 |
| 2 | 485 | II | 6 | 1 | 300 | 600 | 1.90 | 0.50 | 21.60 |
| 3 | 485 | III | 6 | 31 | 9400 | 10400 | 1.47 | 0.90 | 2.95 |
| 4 ^c | 1460 | III | 6 | 18 | 16400 | 24000 | 2.27 | 0.68 | 2.95 |
| 5 ^d | 485 | III | 6 | 58 | 20900 | 21700 | 1.38 | 0.96 | 2.95 |
| 6 ^e | 291 | IV | 3 | 30 | 5500 | 7500 | 1.67 | 0.73 | 1.35 |
| 7 | 485 | V | 9 | 28 | 8500 | 10200 | 1.92 | 0.83 | 4.19 |
| 8 | 485 | VI | 3 | 50 | 7600 | 8400 | 1.92 | 0.90 | 1.35 |
| 9 ^f | 485 | VII | 6 | 47 | 14200 | 16100 | 1.69 | 0.88 | 1.35 |

^aConversion was determined gravimetrically. Conditions $C_{VC}:C_{TREN}:C_{Cu}:C_{RX} = 728:0.2:0.1:1.5$; copper was added as $CuBr_2$ and unless otherwise stated $C_{CuBr_2} = 10^{-3}$ M; estimated geometrical surface of the Pt electrode = 6 cm²; $V = 10$ mL. ^bThe current/time electrolysis program. ^c $C_{CHBr_3} = 5 \cdot 10^{-3}$ M. ^dVC + MA (1:1 v/v) with overall 50% monomer. ^e $C_{CHBr_3} = 0.03$ M. ^f $C_{CuBr_2} = 5 \cdot 10^{-4}$ M.

When a constant current of $1.5 \cdot 10^{-4}$ A was applied for 6 h, moderate conversion was achieved with dispersity $\bar{D} > 1.5$, indicating poor control over chain growth (Entry 1). By contrast, when a single step of 10^{-3} A was applied for 6 h, only few oligomers of PVC with broad dispersity were obtained (Entry 2). Polymerization did not occur in this circumstance possibly because the high current caused the unwanted reduction of $[Cu^I TREN]^+$ to Cu^0 with the displacement of the ligand. In this framework, also the generated high concentration of $[Cu^I TREN]^+$, which in turn produced many radicals, may have accelerated termination reactions to the detriment of propagation.

To further improve the polymerization, we moved to a multistep current profile, based on a chronoamperometry recorded during potentiostatic *e*ATRP of methyl acrylate (see section 9.2.3). The polymerization greatly improved with program III, achieving a more controlled reaction but with lower conversion. The highly active bromoform (more active than P_n-Br) with an appropriate electrolysis program assured proper initiation and concurrent growth of all chains (Entry 3). Increasing the target DP of the polymerization to 1460, by modulating the amount of initiator, resulted in a poorly controlled reaction yielding PVC with $D > 2$ (Entry 4). In this case, excessive viscosity due to the higher molecular weight might have prompted radical coupling. Inefficient stirring may be also a limiting factor and could as well promote termination by coupling. A stunning improvement of control was achieved when VC was randomly copolymerized with methyl acrylate, using an equimolar ratio of the monomers (Entry 5). In this case, 58% conversion (calculated as the sum of VC and MA conversions) was achieved in 6 h yielding a copolymer with $D = 1.38$. Additionally, the reaction showed a very high initiation efficiency. ¹H-NMR spectrum of the produced material (Figure 9.9) showed that the copolymer is poly(methyl acrylate) with a low incorporation of VC. This is a consequence of the higher reactivity of MA, both in terms of activation (k_{act}) and propagation (k_{p}), than VC. Indeed, a PMA-Br end-functionality is reactivated faster than a PVC-Br one, and the polymerization of MA is largely favored over that of VC. The high k_{p} of methyl acrylate (2.4×10^4 L mol⁻¹s⁻¹ in bulk at 60 °C) also favors homopolymerization rather than copolymerization. In this scenario, a considerable improvement might be obtained if methyl acrylate is slowly fed to a VC polymerization.

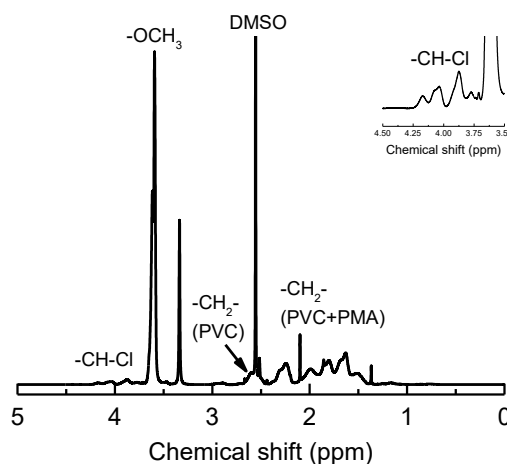


Figure 9.9. 600 MHz $^1\text{H-NMR}$ of PVC-*r*-PMA-Br produced by *e*ATRP. Inset: zoom of the 3.5-4.5 ppm region with -CHCl- signals. Spectrum was recorded in $\text{DMSO-}d_6$.

With the aim of targeting a lower degree of polymerization ($\text{DP} = 291$), program III was modified by reducing step durations so that the total reaction time becomes 3 h (Entry 6); this modified program was called program IV. This did not provide any significant improvement. In fact, if compared to the *e*ATRP with program III, although the same conversion was achieved in a much shorter time, the dispersity was considerably higher. PVC produced by this reaction was used as a macroinitiator for a chain-extension experiment. NMR of the macroinitiator is shown in Figure 9.10:

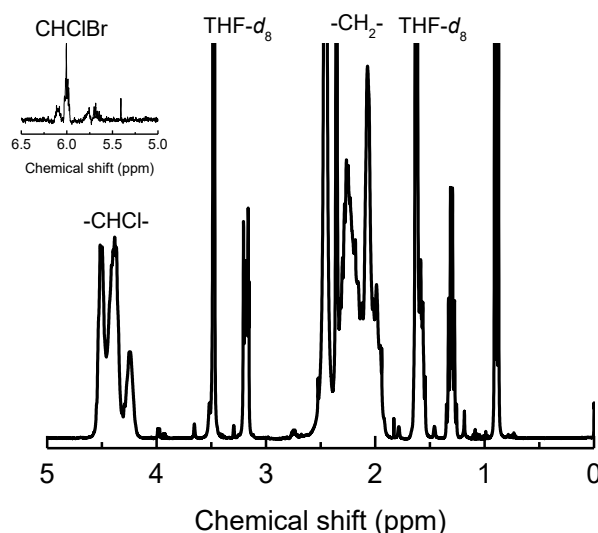


Figure 9.10. 600 MHz $^1\text{H-NMR}$ of PVC-Br produced by *e*ATRP (Table 9.5, entry 6). Inset: zoom of the 5.0-6.5 ppm region with -CHClBr end-functionality signals. The spectrum was recorded in $\text{THF-}d_8$.

Returning to target DP of 485, the program was again modified, as before acting only on the step times (program V, entry 7). Now the reaction time was extended to 9 h, but no improvements were obtained; instead, the results were worse in terms of both conversion and dispersity if compared to the reaction with program III (Entry 3). The monomer concentration was then reduced from 50% to 25% (v/v) and the electrolysis was repeated (Entry 8). This resulted in an improvement of conversion, but polymerization control was completely lost. When the catalyst concentration was reduced to 0.5 mM (70 ppm, entry 9) the polymerization was surprisingly improved, with a conversion of 47% and dispersity of 1.69. This may be an indication that the catalyst could be involved in some side reactions, including also catalytic radical termination (CRT), which becomes less pronounced at lower catalyst loads.

Although $D \sim 1.5-1.7$, the possibility of obtaining PVC by *e*ATRP confirms that the reaction is catalyzed by $[\text{Cu}^{\text{I}}\text{TREN}]^+$ in solution. Considering that the rate of disproportionation is markedly lower than the rate of activation of RX by $[\text{Cu}^{\text{I}}\text{TREN}]^+$ (more than 3 orders of magnitude) and since there is no metallic Cu^0 in the system the polymerization of VC occurs *via* atom transfer. The successful *e*ATRP of vinyl chloride is in contrast with the claims of SET-LRP mechanism. Appropriate modifications of the reactor design to allow performing potentiostatic *e*ATRP can open a wide range of possibilities to optimize various aspects of the process, including dispersity, conversion, rate of polymerization and obtaining different PVC macromolecular architectures.

9.4 Livingness of the polymerization: chain extension with methyl acrylate

To verify the living character of the process, chain-extension of a PVC macroinitiator with methyl acrylate was triggered by SARA ATRP. This was achieved by using $[\text{Cu}^{\text{II}}\text{TREN}]^{2+}$ as catalyst, which efficiently activates the dormant PVC-Br. If chain extension is done with a monomer more reactive than the macroinitiator, a mismatch in the reactivity order may cause an ill-defined block copolymerization. To avoid this problem a novel strategy combining catalytic halogen exchange (see Chapter 4) and ligand exchange was adopted. The

steps of the experiment and the outcome of each step are summarized in Table 9.6, whereas the mechanism of the reaction is shown in Scheme 9.3.

The reaction was carried out in different steps. First a PVC-Br macroinitiator was prepared with program IV (Table 9.5, entry 6). Chain extension of PVC-Br with MA was then carried out with $[\text{Cu}^{\text{II}}\text{TREN}]^{2+}$ as catalyst for 0.16 h, after which the reaction was stopped, and TPMA and Et_4NCl were added. The concentration of TPMA was 1.2-fold higher than that of TREN to favor full conversion of $[\text{Cu}^{\text{II}}\text{TREN}]^{2+}$ to $[\text{Cu}^{\text{II}}\text{TPMA}]^{2+}$, whereas 1.5-fold excess of Cl^- over Br^- was used to ensure that all C-Br end functionalities are changed to C-Cl. Polymerization was then continued for 1.5 h.

The sequence of reactions occurring in these conditions can be summarized as follows. First, $[\text{Cu}^{\text{I}}\text{TREN}]^+$ activates PVC-Br, which propagates adding methyl acrylate units (step 2 of Table 9.6 and reaction 1 of Scheme 9.3). In the second step, the introduction of TPMA causes an immediate ligand exchange. Copper binds stronger to TPMA than to TREN, which is displaced, and all the catalyst is converted to $[\text{Cu}^{\text{II}}\text{TPMA}]^{2+}$ (reaction 2, Scheme 9.3, Figure 9.11). Fresh $[\text{Cu}^{\text{I}}\text{TPMA}]^+$ activates the dormant PVC-*b*-PMA-Br and simultaneously the excess of chloride ions converts $[\text{Br-Cu}^{\text{II}}\text{TPMA}]^+$ to $[\text{Cl-Cu}^{\text{II}}\text{TPMA}]^+$ (reactions 3 and 4, Scheme 9.3). All chain-end functionalities are switched from C-Br to C-Cl and polymerization continues. *c*HE suppresses the activation rate mismatch between vinyl chloride and methyl acrylate and narrows the molecular weight distribution of the block copolymer from 1.59 to 1.38 (Figure 9.12).

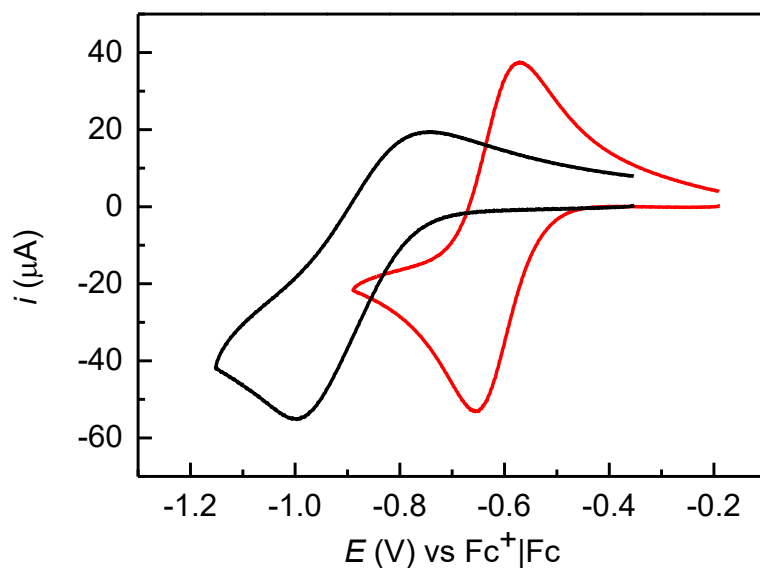
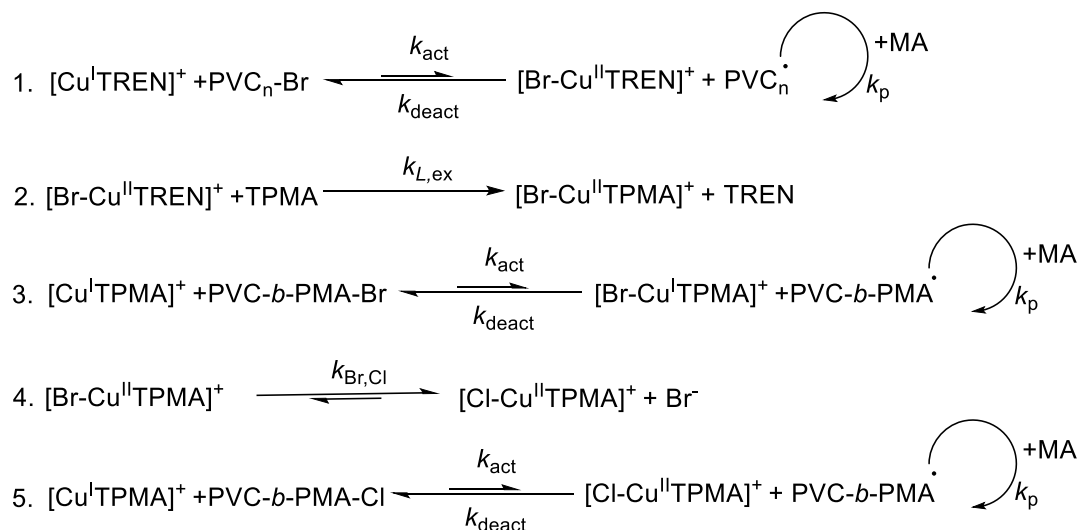


Figure 9.11. Cyclic Voltammetry of 10^{-3} M $[\text{BrCu}^{\text{II}}\text{TREN}]^+$ (—) and immediately after adding 1.2×10^{-3} M TPMA (—). CV are recorded in DMSO at 25°C on a GC disk electrode at 0.2 V/s.

Table 9.6. SARA ATRP of 50% v/v MA in DMSO using PVC-Br macroinitiator and catalytic halogen exchange at $T = 50^\circ\text{C}$.^a

| Entry | Step | (Co)polymer | t (h) | Conv. (%) | M_n^{th} | M_n^{app} | \mathcal{D} | I_{eff} |
|-------|----------------|-----------------------|---------|-----------|-------------------|--------------------|---------------|------------------|
| 1 | 1 | PVC-Br | 0 | - | 5500 | 7500 | 1.67 | - |
| | 2 | PVC- <i>b</i> -MA-Br | 0.16 | 23 | 32800 | 34700 | 1.59 | 0.94 |
| | 3 ^b | PVC- <i>b</i> -PMA-Cl | 1.5 | 29 | 40000 | 42100 | 1.38 | 0.95 |
| 2 | 1 | PVC-Br | 0 | - | 5500 | 7500 | 1.67 | - |
| | 2 | PVC- <i>b</i> -PMA-Br | 0.75 | 30 | 41100 | 42600 | 1.38 | 0.96 |

^a Conditions: $C_{\text{MA}}:C_{\text{L}}:C_{\text{Cu}}:C_{\text{PVC-Br}} = 552:0.5:0.1:0.4$; $V = 10$ mL; $C_{\text{CuBr}_2} = 10^{-3}$ M; $\text{DP} = 1380$. ^b In the presence of Et_4NCl and TPMA with $C_{\text{Et}_4\text{NCl}} = C_{\text{TPMA}} = 6 \times 10^{-3}$ M.



Scheme 9.3. Mechanism of catalytic halogen exchange and with ligand exchange.

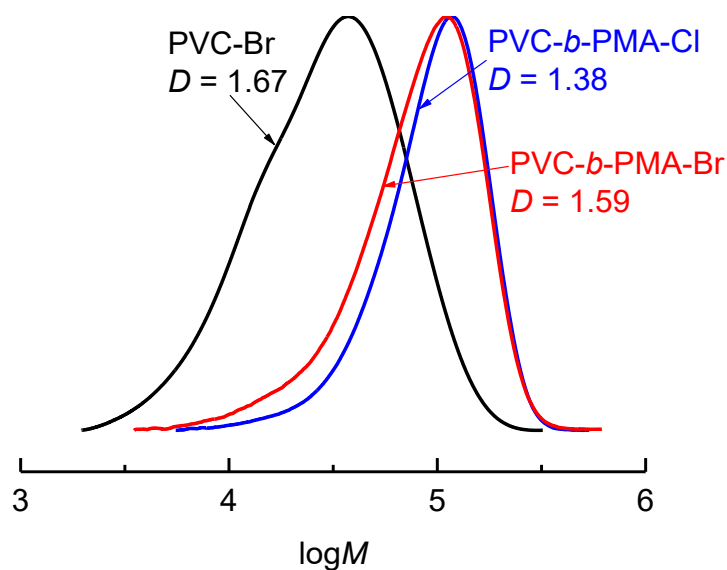


Figure 9.12. Evolution of the molecular weights during the chain extension of PVC-Br with methyl acrylate and catalytic halogen exchange.

By contrast, if *c*HE is not used and chain extension is accomplished with a brominated chain-end (Table 9.5, entry 2), the polymerization reaches almost the same conversion achieved with the *c*HE/ligand exchange method but, in a much shorter time, affording an equivalent PVC-*b*-PMA-Br block copolymer. In this case, *c*HE did not outperform SARA ATRP, probably because of the telechelic

macroinitiator (Br-PVC-BrCH-PVC-Br), which ensures a concurrent re-initiation on both sides of the macromolecule, virtually suppressing the reactivity mismatch between VC and MA terminal units.

9.5 A comparison between SARA ATRP and *e*ATRP: synthesis of 4-arm star PVC

To compare SARA ATRP and *e*ATRP, a SARA ATRP of VC was performed using the same experimental conditions of *e*ATRP (VC/DMSO: 1:1 v/v, $C_{VC}:C_{Cu}:C_{TREN}:C_{RX} = 728:0.1:0.2:1.5$, with $C_{Cu} = 10^{-3}$ M) with the only exception of 10-fold excess of ligand with respect to copper. The results are reported in Table 9.7.

Table 9.7. *e*ATRP vs SARA ATRP of VC at $T = 40$ °C in 50% (v/v) VC in DMSO.^a

| Entry | t (h) | M_n^{th} | M_n^{app} | D | Conv. (%) | I_{eff} | Q (C) |
|---------------|---------|------------|-------------|------|-----------|-----------|---------|
| SARA | 6 | 7300 | 7700 | 1.90 | 24 | 0.93 | - |
| <i>e</i> ATRP | 6 | 9400 | 10400 | 1.47 | 31 | 0.90 | 2.95 |

^aConversion was determined gravimetrically. Other experimental conditions: $C_{VC}:C_{TREN}:C_{Cu}:C_{RX} = 728:x:0.1:1.5$ ($x = 0.2$ for *e*ATRP or 1 for SARA). Cu^0 wire $l = 5$ cm, $d = 1$ mm. 0.1 M Bu_4NBF_4 was used as a supporting electrolyte in DMSO during *e*ATRP; estimated surface area of the Pt working electrode = 6 cm². $M_n^{th} = conv \times MW_{VC} + MW_{RX}$.

Polymerization of VC by SARA ATRP was considerably less controlled than *e*ATRP in DMSO with the same conditions; it also achieved lower conversion although the difference was not very high. This is consistent with the recognized ability of electrochemical methods to outperform other advanced ATRP techniques. The choice of an appropriate current/time program in conjunction with the stringent electrochemical control forced the polymerization to obey to the applied stimulus, reducing side reactions and promoting better control (Fig. 9.13).

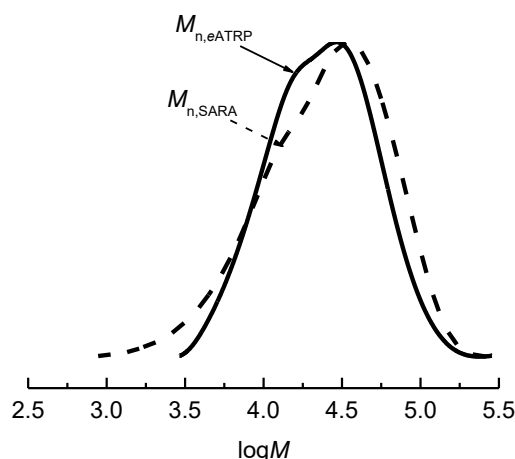


Figure 9.13. Molecular weight distribution of PVC obtained during *e*ATRP (solid line) or SARA ATRP (dashed line) at $T = 40\text{ }^{\circ}\text{C}$ after 6 h of reaction.

To further enrich the toolbox of materials based on PVC, a 4-star arm PVC was synthesized by using the tetra-functional initiator pentaerythritol tetrakis(2-bromoisobutyrate) (EBiB-4f) with both techniques to have an additional comparison. The results are summarized in Table 9.8.

Table 9.8. *e*ATRP and SARA ATRP of 50% (v/v) VC in DMSO using EBiB-4f initiator at $T = 40\text{ }^{\circ}\text{C}$.^a

| Technique | t (h) | Conv. (%) | M_n^{th} | M_n^{app} | \bar{D} | I_{eff} | n_{branch} |
|---------------|---------|-----------|-------------------|--------------------|-----------|------------------|---------------------|
| SARA | 3 | 3 | 5500 | 5700 | 2.79 | 0.99 | 3.8 |
| <i>e</i> ATRP | 3 | 21 | 47800 | 36600 | 1.55 | 1.31 | 3.3 |

^aConversion was determined gravimetrically. *e*ATRP conditions: $C_{\text{VC}}:C_{\text{TREN}}:C_{\text{Cu}}:C_{\text{RX}} = 728:0.2:0.1:0.2$, SARA ATRP conditions: $C_{\text{VC}}:C_{\text{TREN}}:C_{\text{Cu}}:C_{\text{RX}} = 728:1:0.1:0.2$. $V = 10\text{ mL}$; $C_{\text{CuBr}_2} = 10^{-3}\text{ M}$. $\text{DP} = 3664$. Cu^0 wire $l = 5\text{ cm}$, $d = 1\text{ mm}$. $M_n^{\text{th}} = \text{conv} \times \text{MW}_{\text{VC}} + \text{MW}_{\text{RX}}$.

Four arms stars of PVC were obtained by both SARA and *e*ATRP. The latter was faster and far better controlled in the same conditions (Fig. 9.14). Activation of the BriB functionality by $[\text{Cu}^{\text{I}}\text{TREN}]^+$ allowed the growth of a PVC macromolecule for every arm. The star structure was confirmed by both TriSEC and universal calibrations, which allowed determination of the number of branches (n_{branch}) as 3.3 and 3.8 for *e*ATRP and SARA, respectively.

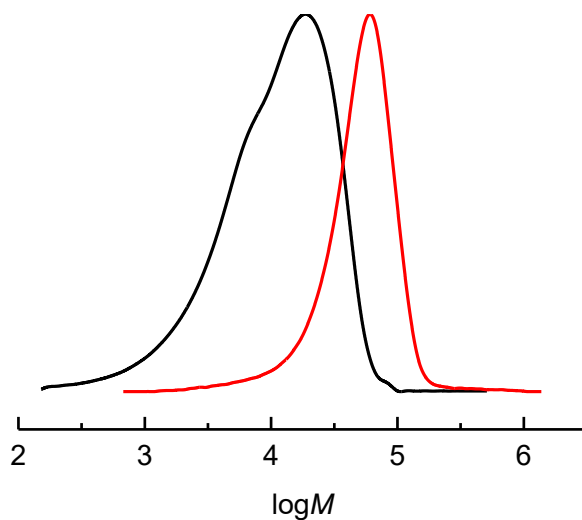


Figure 9.14. MW distribution of four-arm star PVC obtained by SARA (—) or *e*ATRP (—) after 3 h of reaction in DMSO at $T = 40\text{ }^{\circ}\text{C}$.

$^1\text{H-NMR}$ of PVC showed also chain-end functionality retention.

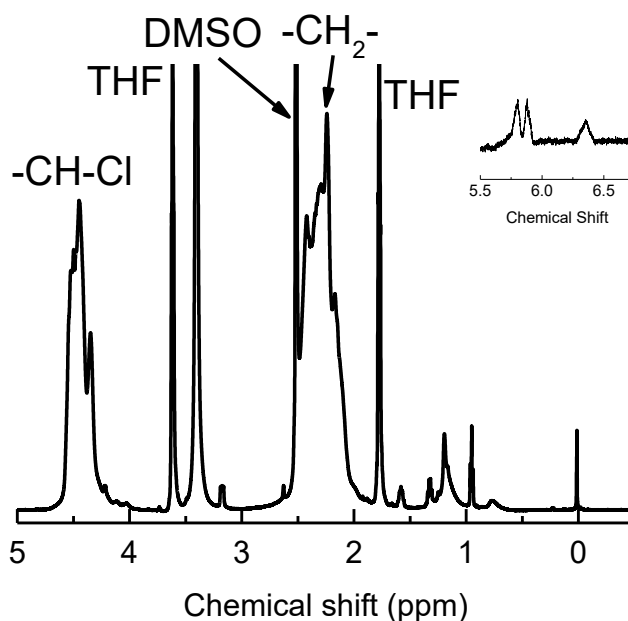


Figure 9.15. 600 MHz $^1\text{H-NMR}$ of PVC produced by *e*ATRP using EBiB-4*f* as initiator in $\text{DMSO-}d_6$. Inset: zoom of the 5.5-6.5 ppm region with CHClBr chain-end functionality detected.

9.6 Conclusions

The use of $[\text{Cu}^{\text{II}}\text{TREN}]^{2+}$ as an efficient catalyst for vinyl chloride polymerization resulted in the successful synthesis of PVC by an electrochemical stimulus. The

absence of any added metallic copper proves that $[\text{Cu}^{\text{I}}\text{TREN}]^+$ is the real activator and, if a sufficiently active catalyst is used, controlled ATRP of non-activated monomers can be achieved. This preliminary work demonstrates that *e*ATRP can afford a new and pioneering solution to the preparation of PVC. Vinyl chloride was polymerized by *e*ATRP using 70-140 ppm of a copper catalyst, yielding polymers with acceptable dispersity ($D \sim 1.47\text{-}1.78$) and M_n^{app} in agreement with theoretical values. The reaction was relatively fast (58% conversion in 3 h at $T = 40\text{ }^\circ\text{C}$) under appropriate operational conditions. The living/controlled nature of the process was demonstrated by the possibility to reactivate dormant PVC-Br through chain-extension with methyl acrylate, using SARA ATRP mediated by $[\text{Cu}^{\text{II}}\text{TREN}]^{2+}$. PVC-*b*-PMA block copolymer was obtained with the same dispersity also *via* catalytic halogen exchange (cHE) triggered by a simultaneous ligand and halogen exchange during chain extension, by adding TPMA and Et_4NCl to the polymerization mixture.

References

1. Odian, G., *Principles of polymerization*. John Wiley & Sons: 2004.
2. Brandrup, J.; Immergut, E. H.; Grulke, E. A.; Abe, A.; Bloch, D. R., *Polymer handbook*. Wiley New York etc: 1989; Vol. 7.
3. Asandei, A. D.; Percec, V., From metal-catalyzed radical telomerization to metal-catalyzed radical polymerization of vinyl chloride: Toward living radical polymerization of vinyl chloride. *Journal of Polymer Science, Part A: Polymer Chemistry* **2001**, *39*, 3392-3418.
4. Ugelstad, J.; Mork, P.; Hansen, F.; Kaggerud, K.; Ellingsen, T., Kinetics and mechanism of vinyl chloride polymerization. *Pure and Applied Chemistry* **1981**, *53*, 323-363.
5. Vogl, O.; Kwei, T. K.; Qin, M., Head to head polymers. 42. Head to head poly (vinyl halide) blends: Thermal and degradation behavior. *Journal of macromolecular science. Pure and applied chemistry* **1997**, *34*, 1747-1769.
6. Coelho, J. F. J.; Fonseca, A. C.; Gonçalves, P. M. O. F.; Popov, A. V.; Gil, M. H., Scaling-up of poly(vinyl chloride) prepared by single electron transfer-degenerative chain transfer mediated living radical polymerization in water media—II: High molecular weight-ultra stable PVC. *Chemical Engineering Science* **2012**, *69*, 122-128.
7. Coelho, J. F. J.; Gonçalves, P. M. F. O.; Miranda, D.; Gil, M. H., Characterization of suspension poly(vinyl chloride) resins and narrow polystyrene standards by size exclusion chromatography with multiple detectors: Online right angle laser-light scattering and differential viscometric detectors. *European Polymer Journal* **2006**, *42*, 751-763.

8. Coelho, J. F. J.; Fonseca, A. C.; Gois, J. R.; Gonçalves, P. M. O. F.; Popov, A. V.; Gil, M. H., Scaling-up of poly(vinyl chloride) prepared by single electron transfer degenerative chain transfer mediated living radical polymerization in water media: 1) Low molecular weight. Kinetic analysis. *Chemical Engineering Journal* **2011**, *169*, 399-413.
9. Iván, B., Thermal Stability, Degradation, and Stabilization Mechanisms of Poly(vinyl chloride). In *Polymer Durability*, American Chemical Society: 1996; Vol. 249, 19-32.
10. Konkolewicz, D.; Wang, Y.; Zhong, M.; Krys, P.; Isse, A. A.; Gennaro, A.; Matyjaszewski, K., Reversible-Deactivation Radical Polymerization in the Presence of Metallic Copper. A Critical Assessment of the SARA ATRP and SET-LRP Mechanisms. *Macromolecules* **2013**, *46*, 8749-8772.
11. Wang, Y.; Zhong, M.; Zhu, W.; Peng, C.-H.; Zhang, Y.; Konkolewicz, D.; Bortolamei, N.; Isse, A. A.; Gennaro, A.; Matyjaszewski, K., Reversible-Deactivation Radical Polymerization in the Presence of Metallic Copper. Comproportionation–Disproportionation Equilibria and Kinetics. *Macromolecules* **2013**, *46*, 3793-3802.
12. Peng, C.-H.; Zhong, M.; Wang, Y.; Kwak, Y.; Zhang, Y.; Zhu, W.; Tonge, M.; Buback, J.; Park, S.; Krys, P.; Konkolewicz, D.; Gennaro, A.; Matyjaszewski, K., Reversible-Deactivation Radical Polymerization in the Presence of Metallic Copper. Activation of Alkyl Halides by Cu⁰. *Macromolecules* **2013**, *46*, 3803-3815.
13. Zhong, M.; Wang, Y.; Krys, P.; Konkolewicz, D.; Matyjaszewski, K., Reversible-Deactivation Radical Polymerization in the Presence of Metallic Copper. Kinetic Simulation. *Macromolecules* **2013**, *46*, 3816-3827.
14. Percec, V.; Guliashvili, T.; Ladislav, J. S.; Wistrand, A.; Stjerndahl, A.; Sienkowska, M. J.; Monteiro, M. J.; Sahoo, S., Ultrafast synthesis of ultrahigh molar mass polymers by metal-catalyzed living radical polymerization of acrylates, methacrylates, and vinyl chloride mediated by SET at 25 degrees C. *Journal of the American Chemical Society* **2006**, *128*, 14156-65.
15. Percec, V.; Popov, A. V.; Ramirez-Castillo, E.; Monteiro, M.; Barboiu, B.; Weichold, O.; Asandei, A. D.; Mitchell, C. M., Aqueous room temperature metal-catalyzed living radical polymerization of vinyl chloride. *Journal of the American Chemical Society* **2002**, *124*, 4940-4941.
16. Rosen, B. M.; Percec, V., Single-electron transfer and single-electron transfer degenerative chain transfer living radical polymerization. *Chemical Reviews* **2009**, *109*, 5069-5119.
17. Levere, M. E.; Nguyen, N. H.; Leng, X.; Percec, V., Visualization of the crucial step in SET-LRP. *Polymer Chemistry* **2013**, *4*, 1635-1647.
18. Zhang, Q.; Wilson, P.; Li, Z.; McHale, R.; Godfrey, J.; Anastasaki, A.; Waldron, C.; Haddleton, D. M., Aqueous Copper-Mediated Living Polymerization: Exploiting Rapid Disproportionation of CuBr with Me₆TREN. *Journal of the American Chemical Society* **2013**, *135*, 7355-7363.
19. Mendes, J. P.; Branco, F.; Abreu, C. M. R.; Mendonça, P. V.; Serra, A. C.; Popov, A. V.; Guliashvili, T.; Coelho, J. F. J., Sulfolane: an Efficient and Universal Solvent for Copper-Mediated Atom Transfer Radical (co)Polymerization of Acrylates, Methacrylates, Styrene, and Vinyl Chloride. *ACS Macro Letters* **2014**, *3*, 858-861.

20. Mendes, J. P.; Mendonca, P. V.; Maximiano, P.; Abreu, C. M. R.; Guliashvili, T.; Serra, A. C.; Coelho, J. F. J., Getting faster: low temperature copper-mediated SARA ATRP of methacrylates, acrylates, styrene and vinyl chloride in polar media using sulfolane/water mixtures. *RSC Advances* **2016**, *6*, 9598-9603.
21. Maximiano, P.; Mendes, J. P.; Mendonça, P. V.; Abreu, C. M. R.; Guliashvili, T.; Serra, A. C.; Coelho, J. F. J., Cyclopentyl methyl ether: A new green co-solvent for supplemental activator and reducing agent atom transfer radical polymerization. *Journal of Polymer Science, Part A: Polymer Chemistry* **2015**, *53*, 2722-2729.
22. Mendes, J. P.; Góis, J. R.; Costa, J. R. C.; Maximiano, P.; Serra, A. C.; Guliashvili, T.; Coelho, J. F. J., Ambient temperature SARA ATRP for meth(acrylates), styrene, and vinyl chloride using sulfolane/1-butyl-3-methylimidazolium hexafluorophosphate-based mixtures. *Journal of Polymer Science, Part A: Polymer Chemistry* **2017**, *55*, 1322-1328.
23. Bard, A. J.; Faulkner, L. R.; Leddy, J.; Zoski, C. G., *Electrochemical methods: fundamentals and applications*. Wiley New York: 1980; Vol. 2.
24. Skene, W. G.; Scaiano, J. C.; Listigovers, N. A.; Kazmaier, P. M.; Georges, M. K., Rate Constants for the Trapping of Various Carbon-Centered Radicals by Nitroxides: Unimolecular Initiators for Living Free Radical Polymerization. *Macromolecules* **2000**, *33*, 5065-5072.
25. De Paoli, P.; Isse, A. A.; Bortolamei, N.; Gennaro, A., New Insights into the Mechanism of Activation of Atom Transfer Radical Polymerization by Cu(I) complexes. *Chemical Communications* **2011**, *47*, 3580-3582.
26. Lorandi, F.; Fantin, M.; Isse, A. A.; Gennaro, A., RDRP in the presence of Cu⁰: The fate of Cu(I) proves the inconsistency of SET-LRP mechanism. *Polymer* **2015**, *72*, 238-245.
27. Konkolewicz, D.; Krys, P.; Góis, J. R.; Mendonça, P. V.; Zhong, M.; Wang, Y.; Gennaro, A.; Isse, A. A.; Fantin, M.; Matyjaszewski, K., Aqueous RDRP in the Presence of Cu⁰: The Exceptional Activity of Cu^I Confirms the SARA ATRP Mechanism. *Macromolecules* **2014**, *47*, 560-570.
28. Chmielarz, P.; Fantin, M.; Park, S.; Isse, A. A.; Gennaro, A.; Magenau, A. J. D.; Sobkowiak, A.; Matyjaszewski, K., Electrochemically mediated Atom Transfer Radical Polymerization (*e*ATRP). *Progress in Polymer Science* **2017**, *69*, 47-78.

Conclusions and Future Perspectives

ATRP in green solvents possesses all features required for scale-up in a relatively near future. The investigation of the ATRP catalytic system in [BMIm][OTf], used as a model ionic liquid, showed that this solvent is similar to conventional organic solvents, in terms of speciation of the catalyst, redox potentials, reactivity of $[\text{Cu}^{\text{I}}\text{L}]^+$ and stability of $[\text{X-Cu}^{\text{II}}\text{L}]^+$. To obtain reliable electrochemical data and reproducible polymerizations, high purity [BMIm][OTf] was prepared by a novel purification procedure, designed to minimize typical impurities of the commercially available ionic liquid. In electrochemically mediated ATRP excellent control is achieved thanks to the possibility of easily modulating the rate of (re)generation of the active $[\text{Cu}^{\text{I}}\text{L}]^+$ complex and hence the ratio between Cu^{I} and Cu^{II} concentrations during polymerization.

*e*ATRP of methyl acrylate (a model acrylate) in [BMIm][OTf] proved to be fast, efficient and well-controlled in a wide range of conditions by varying several parameters, such as temperature, monomer and catalyst concentrations, degree of polymerization and applied potential. Galvanostatic *e*ATRP, which is triggered by applying a current rather than a fixed potential, performs very well and considerably simplifies the electrochemical setup. Application of an electrochemical switch (ON/OFF toggling) to trigger or stop polymerization proved the quantitative retention of C-Br end-functionality. Recycling of ionic liquids was obtained with simple procedures and polymerizations performed in recycled solvents yielded similar results as those in fresh solvents. All reagents employed during the recycling process, such as toluene or exhaust methyl acrylate, could be reused as well.

Catalytic Halogen Exchange (*c*HE) was introduced as an unprecedented tool for macromolecular engineering, allowing the preparation of very well-defined block copolymers (e.g., PMA-*b*-PAN-Cl). The method utilizes only a catalytic amount of a copper complex and a source of chloride ions and is highly efficient for the

rapid change of C-Br end functionality to C-Cl, with high retention of the latter and complete reactivation of the macroinitiator.

Block copolymers containing acrylonitrile are of wide interest in the energy sector as can be useful precursors for nanostructured carbon materials. Well-defined PAN was prepared via *e*ATRP, catalyzed by CuX₂/TPMA. The redox properties of Cu/TPMA were analyzed by cyclic voltammetry. Polymerizations were triggered by applying a potential more positive than the standard reduction potential of the catalyst, to ensure the presence of enough Cu^{II} species, which effectively deactivated the propagating chains. Yet, very reactive ATRP initiators showed better performances than less reactive ones. The catalyst concentration was successfully decreased from 327 to 41 ppm. PAN with very low dispersity, $D < 1.1$, was prepared even at high AN loading (up to 50% v/v). High-MW PAN ($M_n = 79$ kDa and 91 kDa) was prepared *via e*ATRP in ≤ 3 h. The good retention of chain end functionality was proved by extending a PAN-Br macroinitiator with butyl acrylate, thus forming a PAN-*b*-PBA copolymer, with $D = 1.11$. On the other hand, catalytic halogen exchange proved to be a very valuable tool to build well-defined block copolymers by extending bromine-capped macroinitiators from butyl acrylate, styrene, methyl acrylate and OEOA with more active monomers in the presence of chloride ions. *c*HE was shown to be independent of the mechanism of Cu^I regeneration, both *e*ATRP and SARA yielding excellent results. Different copolymers with high molecular weight and narrow dispersity were obtained in different solvents with different couples of monomers, showing that *c*HE is suitable for a wide range of polymerization mixtures. So far it is rather difficult to envisage which Cu(I) regeneration method is better for *c*HE, however, controlled potential electrolysis should be preferred as a unique and outstanding way to precisely modulate the amount of generated active catalyst and avoid side-reactions.

Thanks to *c*HE, *e*ATRP of the very active methyl methacrylate was successfully achieved in [BMIm][OTf] by (i) using very active initiators such as 2-bromopropionitrile or ethyl 2-bromophenylacetate and (ii) adding an excess of halide ions (chlorides) to the polymerization mixture, which changes the chain-end functionality from C-Br to C-Cl, suppressing the mismatch of reactivity. The

presence of Cl^- also disfavors the dissociation of $[\text{ClCu}^{\text{I}}\text{TPMA}]^+$ to $[\text{Cu}^{\text{I}}\text{TPMA}]^+$ and lowers the reactivation rate of PMMA-Cl . *e*ATRP of MMA can be performed also with an inexpensive catalyst such as $[\text{Cu}^{\text{II}}\text{PMDETA}]^{2+}$, which, combined with the extremely active initiator EBPA, provides a fast and very well-controlled polymerization in less than 90 min. Methyl methacrylate was polymerized also in an inexpensive and green solvent such as ethanol. This solvent allowed well controlled polymerizations, using *c*HE mechanism, in 4 h with higher conversion and comparable dispersity with respect to $[\text{BMIm}][\text{OTf}]$, due to the lower viscosity. Interestingly, PMMA precipitates upon cooling the alcoholic solution at the end of the reaction, thus facilitating polymer recovery and cleaning. Tacticity of PMMA obtained in an ionic liquid was very similar to that of PMMA obtained in ethanol, pointing out the absence stereoregularity induction by the bulky ionic liquid.

Mixtures of $[\text{BMIm}][\text{OTf}]$ and water are exceptionally benign for *e*ATRP of methyl acrylate. Despite some undesired side equilibria promoted by water, the typical precautions normally used in aqueous ATRP (excess of halide ions and application of a relatively positive potential) can be neglected/mitigated as all polymerizations are fast and very well-controlled. The presence of water deeply modifies the properties of the ionic liquid polarizing the solvent and enhancing the overall rate (R_p) of polymerization. This effect appears to be of general validity since addition of water to various traditional solvents was also found to enhance R_p . All polymerizations reached moderate-to-high conversion in 4 h and were well-controlled. The conjugation of aqueous and organic solvents allowed the polymerization of the hydrophobic methyl acrylate in $[\text{BMIm}][\text{OTf}]$ containing up to 60% (v/v) water. In this case the presence of the ionic liquid helped to solvate both monomer and polymer with moderate conversion in less than 2 h, by working at a high temperature (80 °C).

Poly(ionic liquids) are a class of polyelectrolytes gaining increasing relevance in the last years. The simple synthesis of ionic liquid monomers through aqueous neutralization of methacrylic acid with a base provided a plethora of ionic liquid monomers (ILMs). 1-Methylimidazolium methacrylate represents just one example of a much wider portfolio. *e*ATRP of ILMs was studied in water at

ambient temperature, by varying the chain-end structure, applied potential, temperature, degree of polymerization and monomer amount. Optimized conditions were very close to those of ATRP of methacrylic acid: i) large excess of chloride ions to convert all chain-end from C-Br to C-Cl, ii) high Cu^{I} regeneration rate and iii) acid conditions. Changing the cation showed the possibility of synthesizing different PILs with narrow dispersity, while the type of ILM showed minimal effects on the polymerization rate. ILMs with two or more polymerizable functionalities, based on alkyl amines, were polymerized with success, showing the robustness of *e*ATRP.

With the aim of developing *e*ATRP scale-up, a homemade reactor made of stainless steel (SS304) was tested with the dual function of reaction vessel and cathode, using as electrode the SS304 surface exposed to the solution. ICP-MS showed that the SS304 scaffold acts only as source of electrons and is not chemically involved in ATRP. The polymerization of methyl acrylate catalyzed by $[\text{Cu}^{\text{II}}\text{TREN}]^{2+}$ was studied with galvanostatic regeneration of $[\text{Cu}^{\text{I}}\text{TREN}]^+$. The polymerization exhibited best results when a multistep electrolysis program was applied with low charge feeding. The effects of the catalyst load and nature of the solvent were found to be in line with previous results. Other monomers such as butyl acrylate, methyl methacrylate and styrene were polymerized in the reactor with their own optimized setups; all reactions reached high conversions in a short time, yielding polymer of narrow dispersity. Attempts to scale-up the polymerization by passing from 10 mL to 40 mL were very promising. After correcting the applied current program to consider both the increased volume and the bigger electrode surface, well-controlled and very fast polymerizations, with high conversions, were achieved. These findings proved that the scale-up of *e*ATRP is feasible and may pave the way to industrial implementation of the technique.

A breakthrough obtained during this PhD program is the electrochemically mediated ATRP of vinyl chloride (VC). Until now ATRP of vinyl chloride, considered impossible and mined by the risk and the complexity of working with a carcinogenic monomer, it has never been investigated by *e*ATRP. Therefore, to carry out safely *e*ATRP of VC, the reactor used for the scale-up was meticulously

adapted as a gas-tight electrochemical reactor that operates in a galvanostatic mode. The effect of electrolysis program, as well as monomer loading and electrolysis time, was investigated. PVC of $D = 1.47$ was obtained in a reasonable time. It is important to stress that this value is one of the lowest D values reported in the literature for PVC by all CRP methods. SARA ATRP and *e*ATRP were compared in the synthesis of a complex PVC 4-arms star polymer. Electrochemical ATRP outperformed SARA ATRP in terms of both conversion and dispersity, showing that electrochemical (re)generation is the best method for PVC synthesis. These results proved that SET-LRP mechanism is inconsistent.

In conclusion, this Ph.D. thesis provides numerous steps forward *e*ATRP implementation and mechanistic understanding of very relevant aspects of polymer synthesis. However, these findings should be only considered starting points, as they answered to some questions, but gave birth to new challenges.

Appendix A

Experimental Section

A.1 Chemicals

Copper. Copper(II) trifluoromethanesulfonate ($\text{Cu}(\text{OTf})_2$, Alfa Aesar, 98%), copper(II) chloride (Acros Organics, 99%), copper(II) bromide (Sigma-Aldrich, 99.999% traces metal basis), were used without further purification. Metallic copper wire (Alfa Aesar, $d = 1$ mm, 99.9%) was washed with HCl/MeOH (1/3, v/v) and dried under nitrogen before the use.

Amine ligands. Tris(2-pyridylmethyl)amine (TPMA, Sigma-Aldrich, 97%), tris[2-(dimethylamino)ethyl]amine (Me_6TREN , Alfa Aesar, 99+%), tris(2-aminoethyl)amine (TREN, Alfa Aesar, 98%) and N,N,N',N'',N''' -pentamethyldiethylenetriamine (PMDETA, Sigma-Aldrich, 98%) were used as received.

Initiators. All initiators were purchased from Sigma-Aldrich or Alfa Aesar with good purity and used without further purification.

Ionic Liquid. 1-Butyl-3-methylimidazolium trifluoromethanesulfonate [BMIm][OTf] was purchased from Iolitec (Germany) and was purified as described later.

Supporting electrolytes and other salts. Tetraethylammonium chloride (Et_4NCl , Sigma-Aldrich, 99%), tetraethylammonium bromide (Et_4NBr , Sigma-Aldrich, 99%) and tetraethylammonium tetrafluoroborate (Et_4NBF_4 , Alfa Aesar, 99%) were purified by recrystallization from dichloromethane-acetone-hexane (2/2/1, v/v), ethanol-diethyl ether (1/2, v/v) and ethanol, respectively. They were then dried under vacuum for at least 48 h and stored over P_2O_5 . Tetrabutylammonium tetrafluoroborate (Bu_4NBF_4 , Sigma Aldrich, 98%), tetrabutylammonium chloride (Bu_4NCl , Sigma-Aldrich, 98%), NaBr (Aldrich, ACS reagent, 98%) and NaCl (Alfa Aesar, 99.99+%) were used as received.

Monomers. Methyl acrylate (MA), methyl methacrylate (MMA), butyl acrylate (BA), acrylonitrile (AN), oligoethyleneoxide methyl ether (meth)acrylate (OEO(M)A) and Styrene (Sty) (all Sigma Aldrich, 99%) were passed through a column filled with basic alumina to remove polymerization inhibitors.

Methacrylic acid (MAA, Sigma-Aldrich, 99%) was distilled through a 10 cm Vigreux column, under reduced pressure, to remove the polymerization inhibitors. Copper turnings were added in the distillation flask together with a copper wire inserted in the Vigreux column to prevent polymerization.

Vinyl Chloride (VC, Cires Ltd, Portugal, 99%) was supplied under pressure in a stainless-steel gas bottle and used as received, removing each time the head fractions.

Solvents. DMF for HPLC (VWR, 99.98%), DMSO (Sigma Aldrich anhydrous, 99.9%), absolute ethanol (Sigma Aldrich, 99.8%) were used as received. Before the polymerization, ethanol was kept over anhydrous sodium sulfate to remove traces of water. Ethyl acetate, acetonitrile, tetrahydrofuran (all Sigma-Aldrich) were all high purity and used without further purification.

Other chemicals. Double distilled water was obtained by distilling deionized water in a KMnO_4 bath to remove all organics. Perchloric acid (Sigma-Aldrich, >70%), sulfuric acid (Sigma Aldrich, 98%) and nitric acid (Sigma Aldrich, 65%) were used without further purification.

A.2 Instrumentation

Cyclic Voltammetry (CV) and chronoamperometry. CVs were performed either by an Autolab PGSTAT30 potentiostat (Metrohm AG, Utrecht, The Netherlands) interfaced to a PC running GPES 4.9 software, a PARC 173A potentiostat, interfaced with a computer running Echem software, or an Autolab 302N potentiostat (Metrohm AG, Utrecht, The Netherlands) interfaced with a computer running Nova 2.1 software. The experiments were carried out in a 5-electrode cell with a glassy carbon disc working electrode (GC electrode, 3 mm diameter, Metrohm) and a graphite or Pt counter electrode in a divided cell. The reference electrode was $\text{Ag}|\text{AgI}|0.1 \text{ M } n\text{-Bu}_4\text{NI}$ in DMF and was calibrated after each experiment against the ferrocenium/ferrocene couple ($\text{Fc}^+|\text{Fc}$). Chronoamperometry experiments were performed using a rotating disc electrode (RDE) with a glassy carbon (GC) tip of 3 mm diameter (Metrohm AG, The Netherlands). Prior to each experiment, the working electrode surface was cleaned by polishing with 0.25- μm diamond paste, followed by ultrasonic rinsing in

ethanol for 5 min. Bulk polymerizations were triggered by chronoamperometry, using as working electrode a Pt gauze (Alfa Aesar, 99.999% trace metal basis) of $\sim 6 \text{ cm}^2$ area. The platinum gauze, used in electrochemical polymerizations, was activated by cycling the potential between +0.7 and -1 V vs. $\text{Hg|Hg}_2\text{SO}_4$ at 0.2 V/s (60 cycles) in 0.5 M aqueous H_2SO_4 . The electrode was then rinsed with double distilled water and acetone. When the SS304 reactor was used, the walls of the vessel wet by the polymerization mixture acted as working electrode. After each polymerization, the reactor was washed with abundant acetone or chloroform to remove residual polymer. No specific cleaning or activation procedures of SS304 were adopted before each experiment.

Nuclear Magnetic Resonance. NMR was used to measure monomer conversion and M_n^{th} during polymerization reactions ($M_n = M_{\text{RX}} + (C_M/C_{\text{RX}}) \times \text{MW} \times \text{conversion}$). The signal of solvents was used as internal standard to determine monomer conversion, using a Bruker 200 or 300 MHz instrument. High resolution NMR spectrometer was a Bruker DMX 600 MHz.

Tacticity. PMMA was precipitated in cold methanol ($-20 \text{ }^\circ\text{C}$) and washed with cold methanol and diethyl ether. It was dissolved in THF and filtered over neutral alumina and a 200 nm polytetrafluoroethylene (PTFE) filter. THF was removed under reduced pressure. A small amount was dissolved in CDCl_3 and put in an NMR probe. Tacticity was measured using $^1\text{H-NMR}$, calculating the integral of the peaks corresponding to *mm*, *mr* and *rr* triads, generated by the α -methyl protons of the backbone.

Gel Permeation Chromatography (GPC). GPC was used to measure relative M_n , and D of the polymer samples. Polymer samples were filtered over neutral alumina and 200 nm PTFE filters prior to injection. Analysis was carried out at $35 \text{ }^\circ\text{C}$ on two Agilent PLgel $5 \mu\text{m}$ MIXED-C, $300 \times 7.5 \text{ mm}$ columns, connected in series; the mobile phase was THF (stabilized with butylated hydroxytoluene) for (meth)acrylic polymers and styrene, while DMF+LiBr (LiBr 10 mM) for poly(acrylonitrile) and PAN-containing copolymers. Calibrations were performed with either PMMA or PSty standards. Aqueous columns, instead, were PL Aquagel-OH columns (guard, 30, 50), thermostated at $30 \text{ }^\circ\text{C}$; the RID was set at $30 \text{ }^\circ\text{C}$. The mobile phase was aqueous 0.1 M Na_2HPO_4 at a flow rate of 1 mL/min .

Sodium methacrylate standards were used for the second order calibration. TriSEC analysis was used for poly(vinyl chloride) (PVC). The chromatographic parameters of the samples were determined using high performance size exclusion chromatography (HPSEC); Viscotek (Viscotek TDAmx) with a differential viscometer (DV); right-angle laser-light scattering (RALLS, Viscotek); low-angle laser-light scattering (LALLS, Viscotek) and refractive index (RI) detectors. The column set consisted of a PL 10 mm guard column ($50 \times 7.5 \text{ mm}^2$) followed by one Viscotek Tguard column (8 μm), one Viscotek T2000 column (6 μm), one Viscotek T3000 column (6 μm) and one Viscotek LT4000L column (7 μm). HPLC dual piston pump was set with a flow rate of 1 mL/min. The eluent (THF) was previously filtered through a 0.2 μm filter. The system was also equipped with an on-line degasser. The columns were thermostated at 30 °C using an Elder CH-150 heater. Before the injection (100 μL), the samples were filtered through a PTFE membrane with 200 nm pore. The system was calibrated with narrow PSty standards. The dn/dc was determined as 0.063 for PMA, 0.105 for PVC and 0.185 for polystyrene standards. Molecular weight (M_n^{app}) and D of the synthesized polymers were determined by multi-detectors calibration. All molecular weights in this thesis are expressed in Da.

A.3 General procedures

Ionic liquid purification. [BMIm][OTf] was first neutralized to pH = 7 with aqueous 0.2 M KOH (50 mL of [BMIm][OTf] were dissolved in 50 mL of double-distilled water and then titrated to pH = 7). Water was then removed at a rotary evaporator. The IL was vigorously stirred for 180 min with 50 mL of diethyl ether, after which the mixture could settle and then separated. After repeating this procedure once more, a third aliquot of 100 mL of diethyl ether was added to the IL, followed by intense stirring for 12 h and separation. Residual ether in the IL phase was removed at a rotary evaporator, then the ionic liquid was dried by high vacuum ($\sim 0.03 \text{ mbar}$) at 110 °C for at least 24 h. The yield was *ca.* 95%. Purified [BMIm][OTf] was stored under inert atmosphere.

General eATRP procedure. A five-neck, thermostated electrochemical cell was used for the polymerizations. In a typical experiment with $[\text{Cu}^{\text{II}}\text{TPMA}]^{2+}$ as

catalyst, 2.5 mL of [BMIm][OTf] (6.72 mmol), 2.5 mL MA (27.58 mmol), 1.5 mg TPMA (5 μmol) and 1.11 mg CuBr_2 (5 μmol) were added to the cell. 7.33 μL of ethyl 2-bromoisobutyrate (50 μmol) was added to this mixture. The cell was equipped with the Pt gauze working electrode, an Ag|AgI reference and a graphite rod counter electrode. The counter electrode was separated from the cathodic compartment by a glass frit and a methylcellulose gel saturated with Et_4NBF_4 . The solution was thermostated at 50 $^\circ\text{C}$ and degassed with Ar for at least 15 min, then the reaction was performed under vigorous stirring (~ 2 cm stirring bar at ~ 1000 rpm), by applying the appropriate potential to the working electrode. Cyclic voltammetry measurements were taken on a glassy carbon disc working electrode (area ~ 0.07 cm^2) before and after the polymerization.

General SARA ATRP procedure. 0.175 g of NaCl (3 mmol), 0.536 mL of MAA (0.547 g, 6.35 mmol), 11.6 mg TPMA (40 μmol), 3.61 mg of $\text{Cu}(\text{OTf})_2$ (10 μmol), 2.1 μL of 2,2-dichloropropionic acid (20 μmol), 0.5 mL of 1-methylimidazole (6.35 mmol) and 1.6 mL of perchloric acid (26.6 mmol) were added to 7.36 mL of H_2O . The solution was degassed for at least 30 min and then transferred to a previously degassed and sealed flask containing 5 cm Cu wire with diameter $d = 1$ mm.

General SARA ATRP of vinyl chloride procedure.

To an Aceglass® #9486 pressure tube ($V = 50$ mL) 2.23 mg of CuBr_2 (10 μmol), 15 μL of tris(2-aminoethyl)amine (0.1 mmol), 13.1 μL of bromoform (0.15 mmol) and 5 mL of DMSO were added. The solution was degassed for at least 30 min and then frozen in liquid nitrogen. Vinyl chloride (5 mL, 72.88 mmol) was pre-condensed in liquid nitrogen and added into the pressure tube. The stirring bar, with 5 cm Cu wire with diameter $d = 1$ mm wrapped around, was inserted and the pressure tube sealed with the valve. The tube was submitted to *ca.* 20 freeze-thaw-pump cycles to remove traces of oxygen, close to the temperature of liquid nitrogen, to avoid vinyl chloride evaporation. The exact amount of vinyl chloride was determined gravimetrically. The tube was placed in a thermostated water bath at 40 $^\circ\text{C}$ for the proper reaction time.

General *e*ATRP of vinyl chloride procedure.

To a round bottom flask 2.23 mg of CuBr₂ (10 μmol), 3 μL of tris(2-aminoethyl)amine (20 μmol), 13.1 μL of bromoform (0.15 mmol) and 5 mL of DMSO were added. The solution was degassed for at least 30 min. Vinyl chloride (5 mL, 72.88 mmol) was pre-condensed in liquid nitrogen. The body of the reactor was cooled in liquid nitrogen and pre-condensed VC was poured inside; the reactor was then closed and submitted to *ca.* 10 freeze-thaw-pump cycles to remove traces of oxygen, close to the temperature of liquid nitrogen, to avoid vinyl chloride evaporation. The solution containing the catalyst and initiator was injected under nitrogen flow into the reactor *via* a syringe. The reactor was submitted to *ca.* 10 new freeze-thaw-pump cycles, close to the temperature of liquid nitrogen, to avoid vinyl chloride evaporation. The exact amount of vinyl chloride was determined gravimetrically. Later it was placed in a thermostated water bath at 40 °C for the proper reaction time. Electrolysis was triggered by applying currents.

Appendix B

Publications

Articles

1. Lorandi, F.; **De Bon, F.**; Fantin, M.; Isse, A. A.; Gennaro, A., Electrochemical characterization of common catalysts and initiators for atom transfer radical polymerization in [BMIm][OTf]. *Electrochem. Commun.* **2017**, *77*, 116-119.
2. Costa, J.; Góis, J.; **De Bon, F.**; Serra, A. C.; Guliashvili, T.; Isse, A. A.; Gennaro, A.; Coelho, J., Addressing the role of triphenylphosphine in copper catalyzed ATRP. *Polymer Chemistry* **2018**.
3. **De Bon, F.**; Fantin, M.; Isse, A. A.; Gennaro, A., Electrochemically mediated ATRP in ionic liquids: controlled polymerization of methyl acrylate in [BMIm][OTf]. *Polymer Chemistry* **2018**, *9*, 646-655.
4. Lorandi, F.; Fantin, M.; **De Bon, F.**; Isse, A. A.; Gennaro, A., Electrochemical Procedures To Determine Thermodynamic and Kinetic Parameters of Atom Transfer Radical Polymerization. In *Reversible Deactivation Radical Polymerization: Mechanisms and Synthetic Methodologies*, American Chemical Society: **2018**; Vol. 1284, pp 161-189.
5. Trevisanello, E.; **De Bon, F.**; Daniel, G.; Lorandi, F.; Durante, C.; Isse, A. A.; Gennaro, A., Electrochemically mediated atom transfer radical polymerization of acrylonitrile and poly(acrylonitrile-*b*-butyl acrylate) copolymer as a precursor for N-doped mesoporous carbons. *Electrochim. Acta* **2018**, *285*, 344-354.
6. **De Bon, F.**; Isse, A.A.; Gennaro, A. Towards Scale-up of Electrochemically-Mediated Atom Transfer Radical Polymerization: Use of a Stainless-steel reactor as both Cathode and Reaction Vessel. *ACS Macro Letter*, submitted.

Conferences

1. *Macrogiovani 2016, 11-14 May 2016, Catania (Italy)*. Oral presentation: **De Bon, F.**; Isse, A.A.; Gennaro, A. Electrochemically mediated Atom Transfer Radical Polymerization of methyl acrylate in Ionic Liquids.
2. *67th Annual meeting of the International Society of Electrochemistry 21-26 August, 2016, Den Haag (The Netherlands)* De Bon, F.; Isse, A.A.; Gennaro, A. *e*ATRP of methyl acrylate in ionic liquids.
3. *GEI 2016 Giornate dell'Elettrochimica Italiana, 11-14 September 2016, Gargnano (Italy)*. Oral presentation: **De Bon, F.**; Isse, A.A.; Gennaro, A. Electrochemically mediated Atom Transfer Radical Polymerization of methyl acrylate in Ionic Liquids; Poster presentation: **De Bon, F.**; Isse, A.A.; Gennaro, A. Atom Transfer Radical Polymerization of Styrene.
4. *Macrogiovani 2017, 22-23 June 2017, Trento (Italy)*. Oral and poster presentation: **De Bon, F.**; Isse, A.A.; Gennaro, A. Electrochemically mediated ATRP in Ionic Liquids/Water mixtures;
5. *European Polymer Federation Congress, 2 – 7 July 2017, Lyon (Italy)*. Oral Presentation: **De Bon, F.**; Isse, A.A.; Gennaro, A. Electrochemically mediated ATRP in Ionic Liquids/Water mixtures;
6. *XXVI Congresso Nazionale della Società Chimica Italiana, 10 – 14 settembre 2017, Paestum, Salerno (Italy)*. Oral Presentation: **De Bon, F.**; Isse, A.A.; Gennaro, A. *Improvements of eATRP of styrene using ionic liquids as supporting electrolytes*;
Poster presentation: **De Bon, F.**; Isse, A.A.; Gennaro, A. *Electrochemically mediated Atom Transfer Radical Polymerization in Ionic Liquid/Water mixtures*.
7. *Giornate dell'Elettrochimica Italiana, 21-25 January 2018, Sestriere (Italy)*. Oral presentation: **De Bon, F.**; Isse, A.A.; Gennaro, A. Catalytic Halogen Exchange in Electrochemically mediated ATRP: the case of methyl methacrylate.

8. *Bordeaux Polymer Conference 28-31 May 2018, Bordeaux (France)*. Poster Presentation – Poster Prize winner: Góis, J.R.; Costa, J.R.; De Bon, F., Serra, A.C.; Gennaro, A.; Coelho, J.F.J, Triphenylphosphine – a SARA agent for Cu catalyzed SARA ATRP of MA?
9. *Macrogiovani 2018, 14-15 Giugno 2018, Salerno (Italy)*. Oral presentation: **De Bon, F.**; Isse, A.A.; Gennaro, A. A Stainless-Steel reactor for electrochemically mediated ATRP: toward the scale-up,
10. *69th Annual Meeting of the International Society of Electrochemistry, 2 – 7 September 2018, Bologna (Italy)*. Poster presentation: **De Bon, F.**; Isse, A.A.; Gennaro, A. Electrochemically mediated ATRP in a stainless-steel reactor: toward a scale-up of eATRP?

Awards

1. Concorso Manageranch'io! December 2015, *Padova*. Winner;
2. *Macrogiovani 2016, 11-14 May 2016, Catania*. Best oral presentation;
3. *Macrogiovani 2017, 22-23 June 2017, Trento*. Best oral and poster presentations;
4. *Macrogiovani 2018, 14-15 Giugno 2018, Salerno*. Best oral presentation.

De Bon, F. is written in bold in oral or poster presentations done by the author.